# UNIVERSITÉ DE STRASBOURG

*ÉCOLE DOCTORALE DES SCIENCES DE LA VIE ET DE LA SANTE*

**IGBMC – CNRS UMR 7104 – Inserm U 964**

# THÈSE présentée par :

## Yury ZGADZAY

soutenue le : **30 Novembre 2022**

pour obtenir le grade de : **Docteur de l'université de Strasbourg**

Discipline : Aspects moléculaires et cellulaires de la biologie

## Structural investigations of the protein synthesis apparatus of *Candida albicans* studied by cryo-EM

**THÈSE dirigée par :**

   **M. YUSUPOV Marat**         Directeur de recherche, Université de Strasbourg

**RAPPORTEURS :**

   **Mme. SCHMITT Emmanuelle**     Directeur de recherche, École Polytechnique (Paris)
   **M. RAK Alexey**                  Head of Biophysics Department at Sanofi (Paris)

**EXAMINATEUR :**

   **M. MASQUIDA Benoît**            Directeur de recherche, Université de Strasbourg

# Table of contents

# ACKNOWLEDGEMENTS

First of all, I thank you, dear **Marat** and **Gulnara**, for inviting me for an internship during your visit to Kazan. It was an invaluable experience that I gained during my first visit to Strasbourg. Thank you very much for inviting me later on to perform a Ph.D. in your lab and for your valuable advice and guiding, which allowed me to complete the tasks on time.

Also, I thank my jury members for agreeing to participate in my defense. Dear **Emmanuel**, **Alexey**, and **Benoit**, I am so grateful to you for coming to my defense, and I appreciate your helpful questions and comments.

Indeed, my defense would not have been possible without my lovely wife, **Olga**, who is an active participant in this project. Dear **Olga**, I thank you immensely for all your help and support during my graduate studies. Only through our joint efforts, we could move our projects in the right direction. I wish you a successful defense next year.

I would also like to acknowledge our collaborators, who have made significant contributions to this research. Dear **Albert** and **Artem**, thank you for always being willing to help us with cryo-EM experiments on short notice; your help has been indispensable. Dear **Matthew** and **Cheng**, thank you very much for your support with the cell-free experiments; you are true experts in this field.

I would also like to thank the members of my lab. Dear **Lasse**, thank you for your always valuable advice and help! Dear **Liliia**, thank you for your support and spending time together; I wish you good luck with your project! Dear **Nemanja** and **Salvatore**, thank you very much for your helpful hints; I hope you will have successful publications of your results! Dear **Bulat**, thank you for your support and help; I hope you will have a successful defense. Finally, dear **Muminjon** and **Alexey**, thank you for sharing your thoughts with me; they were constructive.

I would especially like to thank the former members of my lab. Dear **Simone**, thank you very much for teaching me the ribosome kitchen. During my first visit to Strasbourg, I had never held a pipette before; thanks to you, I was able to learn the basics of biochemistry and structural biology. Dear **Margarita**, thank you for your active participation in the beginning. You and I thawed out the Candida project in 2018 and found directions for a successful project. I wish you the best of luck in your scientific career! Finally, dear **Iskander**, **Justine**, **Melanie**, and **Alexander,** thank you very much for your support and help!

# LIST OF FIGURES

# LIST OF TABLES

# ABBREVIATIONS

| | |
|---|---|
| Aa | Amino acid |
| ANM | Anisomycin |
| ALS | Agglutinin-Like Sequence |
| A-site | Aminoacyl-tRNA binding site |
| AU | Absorbance Unit |
| BLS | Blasticidin S |
| CFTS | Cell-Free Translation System |
| CHX | Cycloheximide |
| CTD | C-Terminal Domain |
| CTF | Contrast Transfer Function |
| Cryo-EM | Cryogenic electron microscopy |
| Da | Dalton unit |
| DC | Decoding center |
| DLS | Dynamic Light Scattering |
| DTT | Dithiothreitol |
| EDTA | EthyleneDiamineTetraacetic Acid |
| E-site | Exit tRNA binding site |
| FSC | Fourier shell correlation |
| IAS | Isoaspartate |
| IC50 | Half-maximal inhibitory concentration |
| LSU | Large subunit |
| LUC | Luciferase |
| MIC | Minimum Inhibitory Concentration |
| MLZ | Monomethylated Lysine |
| mRNA | Messenger RNA |
| Nt | Nucleotide |
| NTD | N-Terminal Domain |
| OD | Optical Density |
| PAGE | Polyacrylamide Gel Electrophoresis |
| PDB | Protein Data Bank |
| PEG | Poly Ethylene Glycol |
| PIC | Protease Inhibitor Cocktail |

| | |
|---|---|
| PHY | Phyllanthoside |
| PSU, ψ | Pseudouridine |
| PTC | Peptidyl Transferase Center |
| P-site | Peptidyl-tRNA binding site |
| PUT | Putrescine |
| r-protein | Ribosomal protein |
| RNAsin | RiboNuclease inhibitor |
| RR | Rabbit Reticulocytes |
| RRL | Rabbit Reticulocytes Extract |
| rRNA | Ribosomal RNA |
| S | Svedberg |
| SDS | Sodium Dodecyl Sulfate |
| SPD | Spermidine |
| SPK | Spermine |
| spLUC | sea pansy Luciferase |
| SSU | Small Subunit |
| TR | Tandem Repeats |
| tRNA | Transport RNA |
| YPAD | Yeast Extract, Peptone, Adenine, D-Glucose |
| YPD | Yeast Extract, Peptone, D-Glucose |

# SUMMARY

Fungal infections still affect many patients, and the risk is exceptionally high for immunocompromised people. Candida species are one of the common causes of nosocomial fungal infections in Europe, with mortality rates of up to 50% [1]. Patients with oral candidiasis have a significantly higher risk of developing all cancers [2]. Of the at least 15 species of Candida yeast that can infect humans, *Candida albicans* (*C. albicans*) is the most common. Several effective antifungal drugs against *C. albicans* target the cell wall, plasma membrane, ergosterol, or RNA/DNA biosynthetic pathways. Unfortunately, many side effects occur due to the similarity of the target to the corresponding cellular components in humans. For example, one of the best-known antifungal molecules, amphotericin B, cross-reacts with human sterol and is, therefore, highly toxic [3]. Therefore, developing new inhibitors specific to new targets, such as the protein synthesis pathway, is essential. One of the most promising targets in this pathway is the ribosome.

The ribosome is cellular machinery responsible for the fundamental process of protein biosynthesis and is involved in the expression of genetic information. Over the last decade, numerous papers have been published describing small molecule inhibition of protein synthesis. Usually, these agents are attached to tRNA binding sites (A, P, E), the decoding center, and the peptidyl transferase (PTC) center. The main challenge is finding specific inhibitors that only act against the chosen target, such as the *C. albicans* ribosome. Unfortunately, despite the similarities and multiple conserved parts of eukaryotic ribosomes, there are chemical compounds that bind to yeast and human ribosomes but are not active against *C. albicans*.

For example, it has been empirically observed in hospitals that *C. albicans* is resistant to cycloheximide. This resistance was due to a mutation of the L42 protein in the E-site of the large subunit (LSU). Nevertheless, this resistance has never been proven by structural studies. Furthermore, this mutation of the L42 protein has not been found in human ribosomes, making the E-site of the *C. albicans* ribosome a fascinating target for synthesizing specific compounds. Finally, it is worth mentioning that there is evidence to suggest that modification of the L42 ribosomal protein in humans affects cellular processes such as cancer development [4].

All the above observations illustrate the importance of further structural studies, which would be impossible without obtaining the high-resolution structure of the *C. albicans* ribosome. For large macromolecules, such as the ribosome, obtaining a high-resolution structure is a significant challenge, as it is difficult to achieve due to many factors, such as sample purity and

stability. In this project, we obtained the structure of the *C. albicans* ribosome by high-resolution cryo-electron microscopy (2.3 A) and described its structural determinants.

The first chapter reviews the virulence mechanisms of *C. albicans*. The characteristic properties of *C. albicans* that determine its pathogenicity are the following. The attachment to the host cell, cell dimorphism (budding yeast-hyphae), damage to the cell wall by hyphae, genetic dimorphism (opaque-white cells), biofilm formation, and the response of candida to stress conditions. The combination of these properties allows candida to penetrate cell barriers actively and remain invisible to the host immune system, which determines its pathogenicity. To make a rapid transition from the non-hazardous form (budding yeast) to the hazardous form (hyphae), a cascade of processes occurs within the cell, including the regulation of translation for the synthesis of proteins required for hyphal formation.

The second chapter deals with the particularities of the translation process in *C. albicans*. One of the main characteristics of *C. albicans* is the duality of the leucine tRNA. In *C. albicans*, the CUG codon is mainly translated into Ser (95%) rather than Leu (5%), whereas in other eukaryotes, the CUG codon is translated only into leucine. The existence of signature motifs in the mRNA that determine whether the amino acid is inserted or whether a terminator tRNA binds to the mRNA instead leads to reassigned codons that, in turn, code for other amino acids or truncated proteins, respectively, is related to the duality of codons. The expression of genes related to cell adhesion and hyphal development is ultimately induced when stress conditions arise because a bigger proportion of tRNA begins to generate leucine. In addition, polyadenylation of ribosomal RNA at the 3' end is produced in response to stress conditions, thus triggering the process of rRNA degradation in response to stress.

Chapter three describes the protein synthesis apparatus of *C. albicans*, the ribosome, based on the available literature. A comparison was made with the yeast and human ribosomes based on ribosomal RNA and protein sequences. Significant differences were found in the expansion segments ES7 and ES27 and the eL40 protein, which is expected to be two times shorter in *C. albicans* than in yeast. Furthermore, no sequence data is available in existing databases for the eL41 protein that bridges the subunits. Based on the literature data, sites in the rRNA and ribosomal proteins may differ structurally and identify the specificity of the *C. albicans* ribosome.

Chapters 4 to 6 are devoted to the experimental part of my project. Chapter 4 describes the process of ribosome isolation. A detailed protocol for the isolation is given. Experimental results showing the purity and stability of our sample are also presented. Finally, a detailed plan

for preparing the cryo-EM experiment is presented as a data processing flowchart at the end of the chapter.

Chapter 5 describes the resulting high-resolution structure of *C. albicans*. This chapter focuses on the general description of the structure (rotation angles of the small subunit and the head of the small subunit) as well as on the found modifications of the ribosomal RNA and proteins. In addition, the quality of the cryo-EM map made it possible to search for the isomers of specific amino acids in the protein and locate polyamines (spermidine, spermine, putrescine) and ions, and water molecules. The information obtained enables the most accurate description of the three-dimensional structure of the *C. albicans* ribosome and serves as a starting point for the search for selective inhibitors.

Chapter 6 compares the functional centers of the ribosome by forming complexes with known inhibitors. Since almost all known E-site inhibitors have a glutarimide moiety, it is clear that, like CHX, they do not bind to the *C. albicans* ribosome. Using cell-free assays, we found only one inhibitor - phyllanthoside (PHY) - that exhibits translational inhibition efficiency. Using this fact, we obtained a complex with phyllanthoside at 2.56 Å proving its binding to the E-site. Due to the absence of the glutarimide moiety, it does not interact directly with the Q56 of the eL42 protein. The other functional sites are highly conserved. We made complexes with anisomycin and blasticidin S, which bind to the peptidyl transferase center. From our structure and cell-free assays, we see no difference in the binding mode of this compound, showing that the PTC is identical to those in *S. cerevisiae* and *H. sapiens*.

Our results explain the resistance of *C. albicans* to CHX and demonstrate specific characteristics of the *C. albicans* ribosome. Based on structural and cell-free data, we propose that CHX cannot bind to the *C. albicans* ribosome due to the clash of the glutarimide group of CHX with the Q56 side chain of eL42. In contrast to CHX, PHY binds to the E-site of *C. albicans* at a physiologically relevant concentration. Due to the absence of the glutarimide moiety, PHY adopts an entirely different interaction pattern and does not conflict with Q56. Our study provides a solid basis for the potential future development of anti-Candida drugs without a glutarimide moiety that could lead to specific binding to the *C. albicans* ribosome. Understanding ribosome inhibition will significantly improve the treatment of candidiasis and reduce associated mortality.

# RESUME EN FRANCAIS

Actuellement, les infections fongiques touchent encore de nombreux patients, et le risque est particulièrement élevé pour les personnes immunodéprimées. Les espèces de Candida sont l'une des causes fréquentes d'infections fongiques nosocomiales en Europe, avec des taux de mortalité pouvant atteindre 50 % [1]. Les patients atteints de candidose buccale présentent un risque significativement plus élevé de développer tous les cancers [2]. Parmi les 15 espèces au moins de levures Candida qui peuvent infecter l'homme, Candida albicans (*C. albicans*) est la plus répandue. Il existe actuellement plusieurs médicaments antifongiques efficaces contre *C. albicans*, qui ciblent la paroi cellulaire, la membrane plasmique, l'ergostérol ou les voies de biosynthèse ARN/ADN. Malheureusement, de nombreux effets secondaires se produisent en raison de la similitude de la cible avec les composants cellulaires correspondants chez l'homme. Par exemple, l'une des molécules antifongiques les plus connues, l'amphotéricine B, a une réaction croisée avec le stérol humain et est donc très toxique [3]. Sur cette base, il est important de développer de nouveaux inhibiteurs spécifiques à de nouvelles cibles, telles que la voie de synthèse des protéines. L'une des cibles les plus prometteuses de cette voie est le ribosome.

Le ribosome est une machinerie cellulaire responsable du processus fondamental de la biosynthèse des protéines et impliquée dans l'expression de l'information génétique. Au cours de la dernière décennie, de nombreux articles ont été publiés décrivant l'inhibition de la synthèse des protéines par de petites molécules. Habituellement, ces agents sont fixés aux sites de liaison des ARNt (A, P, E), au centre de décodage et au centre de la peptidyl transférase (CPT). Actuellement, le principal défi consiste à trouver des inhibiteurs spécifiques, qui n'agiront que contre la cible choisie, comme le ribosome de *C. albicans*. Malgré les similitudes et les multiples parties conservées des ribosomes eucaryotes, il existe des antibiotiques et des composés chimiques qui se lient aux ribosomes de la levure et de l'homme mais qui ne sont pas actifs contre *C. albicans*.

Par exemple, il a été observé empiriquement dans les hôpitaux que *C. albicans* est résistant au cycloheximide. On a découvert que cette résistance était due à une mutation de la protéine L42 dans le site E du CPT. Mais cette résistance n'a jamais été prouvée par des études structurelles. Cette mutation de la protéine L42 n'a pas été trouvée dans les ribosomes humains, ce qui fait du site E du ribosome de *C. albicans* une cible extrêmement intéressante pour la synthèse de composés spécifiques. Il convient de mentionner qu'il existe des données suggérant qu'une modification de la protéine ribosomale L42 chez l'homme affecte des processus cellulaires tels que le développement du cancer [4].

Toutes les observations susmentionnées illustrent l'importance d'études structurelles supplémentaires, qui seraient impossibles sans l'obtention de la structure à haute résolution du ribosome de *C. albicans*. Pour les grandes macromolécules, telles que le ribosome, l'obtention d'une structure à haute résolution est un défi majeur, car elle est difficile à réaliser en raison de nombreux facteurs, tels que la pureté et la stabilité de l'échantillon. Dans ce projet, nous avons obtenu la structure du ribosome de *C. albicans* par cryomicroscopie électronique à haute résolution (2.3 A) et déterminé ses déterminants structurels.

Le premier chapitre décrit les mécanismes de virulence de *C. albicans*. Les propriétés caractéristiques de *C. albicans* qui déterminent sa pathogénicité comprennent l'attachement à la cellule hôte, le dimorphisme cellulaire (levure bourgeonnante - hyphes), l'endommagement de la paroi cellulaire par les hyphes, le dimorphisme génétique (cellules blanches-opaques), la formation de biofilms et la réponse du candida aux conditions de stress. La combinaison de ces propriétés permet à la candidose de pénétrer activement les barrières cellulaires et de rester invisible pour le système immunitaire de l'hôte, ce qui détermine sa pathogénicité. Pour passer rapidement de la forme non dangereuse (levure bourgeonnante) à la forme dangereuse (hyphes), une cascade de processus se produit à l'intérieur de la cellule, notamment la régulation de la traduction pour la synthèse des protéines nécessaires à la formation des hyphes.

Le deuxième chapitre traite des particularités du processus de traduction chez *C. albicans*. L'une des principales caractéristiques de *C. albicans* est la dualité de l'ARNt leucine. Chez *C. albicans*, le codon CUG est principalement traduit en Ser (95%) plutôt qu'en Leu (5%), comme chez d'autres eucaryotes où le codon CUG est traduit uniquement en leucine. La dualité des codons est liée à la présence de motifs de signature dans l'ARNm qui définissent si l'acide aminé est inséré ou si un ARNt terminateur se lie à l'ARNm, ce qui entraîne des codons réassignés codant pour différents acides aminés ou pour des protéines tronquées, respectivement. Lorsque des conditions de stress se produisent, un pourcentage plus élevé d'ARNt commence à produire de la leucine, ce qui induit finalement l'expression de gènes impliqués dans l'adhésion cellulaire et la croissance des hyphes. En outre, la polyadénylation de l'ARN ribosomal à l'extrémité 3' se produit en réponse à des conditions de stress, déclenchant ainsi le processus de dégradation de l'ARNr en réponse au stress.

Le chapitre trois décrit l'appareil de synthèse des protéines de *C. albicans*, le ribosome, sur la base de la littérature disponible. Une comparaison a été faite avec les ribosomes de la levure et de l'homme sur la base des séquences de l'ARN ribosomal et des protéines. Des différences significatives ont été trouvées dans les segments d'expansion ES7 et ES27 ainsi que dans la protéine eL40, qui devrait être deux fois plus courte chez le *C. albicans* que chez la

levure. De plus, aucune donnée de séquence n'est disponible dans les bases de données existantes pour la protéine eL41 qui forme le pont entre les sous-unités. Sur la base des données de la littérature, les sites dans l'ARNr et les protéines ribosomales qui peuvent présenter des différences structurelles et déterminer la spécificité du ribosome de *C. albicans* sont identifiés.

Les chapitres 4 à 6 sont consacrés à la partie expérimentale de mon projet. Le chapitre 4 décrit le processus d'isolement des ribosomes. Un protocole détaillé pour l'isolement est donné, avec néanmoins des pertes au cours de l'isolement. Des résultats expérimentaux montrant la pureté et la stabilité de notre échantillon sont également présentés. À la fin du chapitre, un plan détaillé de la préparation de l'expérience cryo-EM est présenté, ainsi qu'un organigramme du traitement des données.

Le chapitre 5 décrit la structure haute résolution de *C. albicans* qui en résulte. Ce chapitre se concentre sur la description générale de la structure (angles de rotation de la petite sous-unité et de la tête de la petite sous-unité) ainsi que sur les modifications de l'ARN ribosomal et des protéines trouvées. Par ailleurs, la qualité de la structure a permis de rechercher les isomères de certains acides aminés dans la protéine et de localiser les polyamines (spermédine, spermine, putrescine) ainsi que les ions et molécules d'eau. Les informations obtenues permettent la description la plus précise de la structure tridimensionnelle du ribosome de *C. albicans* et servent de point de départ à la recherche d'inhibiteurs sélectifs.

Le chapitre 6 compare les centres fonctionnels du ribosome en formant des complexes avec des inhibiteurs connus. Étant donné que presque tous les inhibiteurs connus du site E ont une fraction glutarimide, il est clair que, comme la CHX, ils ne se lient pas au ribosome de *C. albicans*. En utilisant des essais en milieu acellulaire, nous avons trouvé un seul inhibiteur - le phyllanthoside - qui présente une efficacité d'inhibition de la traduction. En utilisant ce fait, nous avons obtenu un complexe avec le phyllanthoside à 2.56 Å prouvant sa liaison au site E. En raison de l'absence de la fraction glutarimide, il n'interagit pas directement avec le Q56 de la protéine eL42. Les autres sites fonctionnels sont hautement conservés. Nous avons fait des complexes avec l'anisomycine et la blasticidine S, qui se lient au centre de la peptidyl-transférase. D'après notre structure et les essais en milieu acellulaire, nous ne voyons aucune différence dans le mode de liaison de ce composé, ce qui montre que le CTP est identique à ceux de *S. cerevisiae* et de *H. sapiens*.

Nos résultats expliquent la résistance de *C. albicans* au CHX et démontrent des caractéristiques spécifiques du ribosome de *C. albicans*. Sur la base de données structurelles et acellulaires, nous proposons que la CHX ne peut pas se lier au ribosome de *C. albicans* en raison du clash du groupe glutarimide de la CHX avec la chaîne latérale Q56 de eL42. Contrairement à

la CHX, la PHY se lie au site E de *C. albicans* à une concentration physiologiquement pertinente. En raison de l'absence de la fraction glutarimide, PHY adopte un schéma d'interaction entièrement différent et n'entre pas en conflit avec Q56. Notre étude fournit une base solide pour le développement futur potentiel de médicaments anti-Candida sans fraction glutarimide qui pourraient conduire à une liaison spécifique au ribosome de *C. albicans*. La compréhension de l'inhibition du ribosome permettra d'améliorer considérablement le traitement de la candidose et de réduire la mortalité qui lui est associée.

# CANDIDA ALBICANS: VIRULENCE
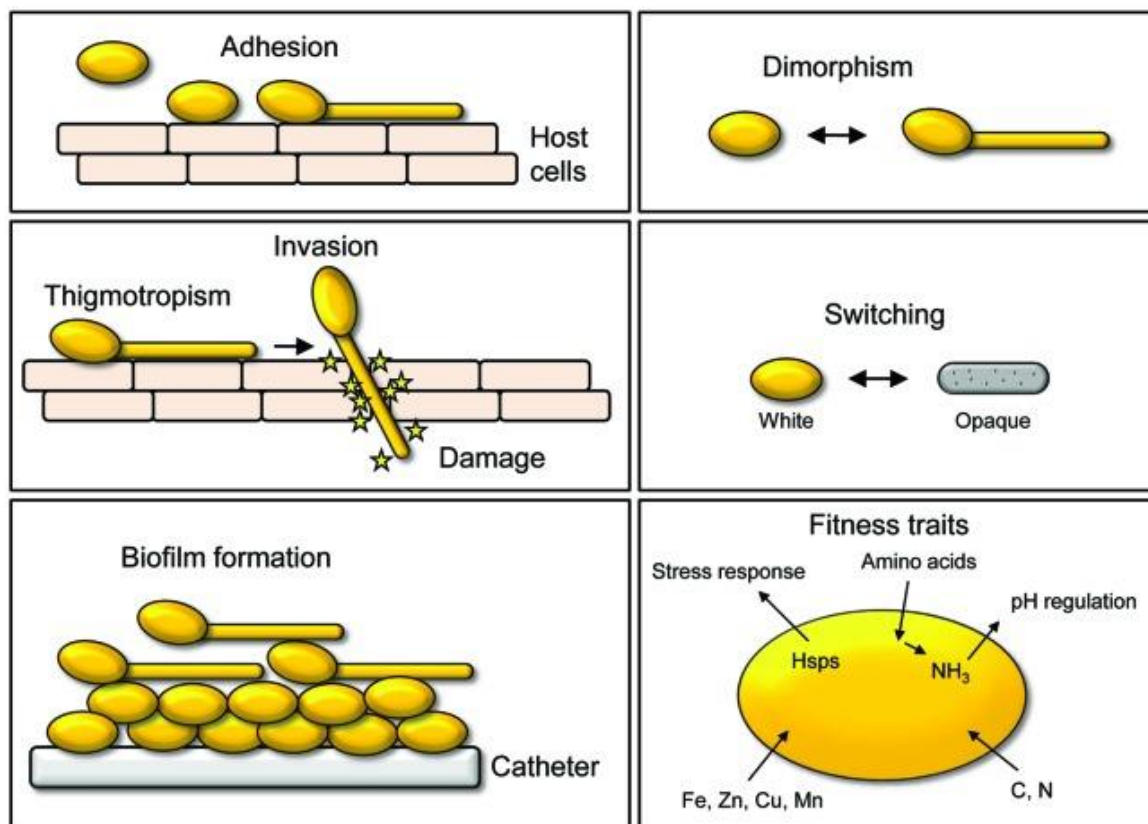


Figure 1 - Virulence factors of *C. albicans [5]*

*Candida albicans* – is an opportunistic yeast that is a typical member of the human gut flora. *C. albicans* belongs to the yeast family. The main difference between *C. albicans* and *S. cerevisiae* is that, under certain circumstances, it becomes pathogenic. Not considering how *C. albicans* switches from the "non-pathogenic" to "pathogenic" form, six main virulence factors follow the transition of *C. albicans* to the pathogenic form (Figure 1). The first factor is the adhesion to the host cells.

## Adhesion to the host cells

First, *C. albicans* must attach to the host cells, i.e., *H. sapiens*. Several families of proteins realize adherence of the pathogenic cells at the cell surface. The following classes of substances are defined adhesins and cadherins.

The first adhesin gene was discovered by Hoyer in 1995 *[6]*. It was named ALS due to its similarity with Saccharomyces cerevisiae's alpha-agglutinin protein, which promotes contact

between the cells during sexual reproduction *[7]*. Since then, 8 ALS proteins have been found (ALS 1-7, 9), which establish interaction between the pathogen and the host cells in the fungi (not only in *C. albicans*) *[8]*. ALS protein consists of 4 domains: N-terminal domain (NT), T-domain, tandem repeats (TR), and C-terminal domain (CT) (Figure 2) [9].
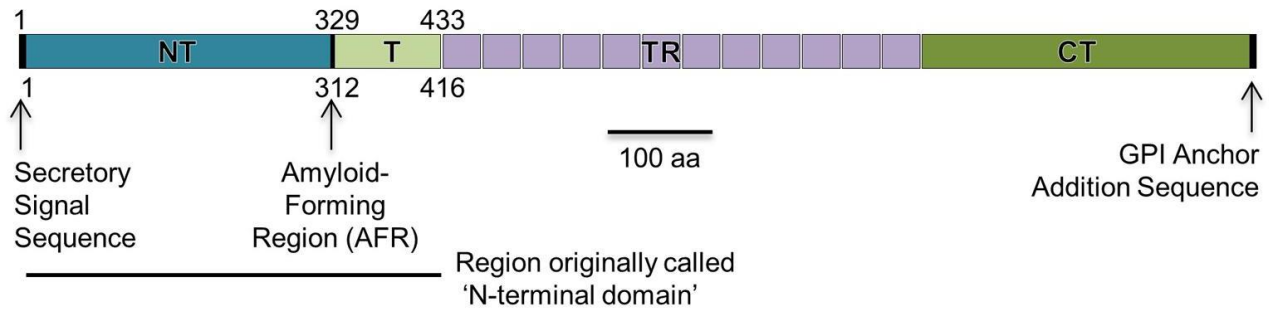


Figure 2 - Schematic representation of ALS domains [9]

The first extensively studied protein from the ALS family is ALS3. Depletion of ALS3 leads to the impaired adhesive ability of *C. albicans*. Using the molecular modeling method, it was established that the NT domain of ALS is responsible for the binding with the host cells *[10]*. Furthermore, the first X-ray structure of the NT domain of ALS revealed that there is a protein-binding cavity, which is capable of interacting with up to 6 amino acids (aa) from the C-terminal of host-cell protein (Figure 3) *[11]*.
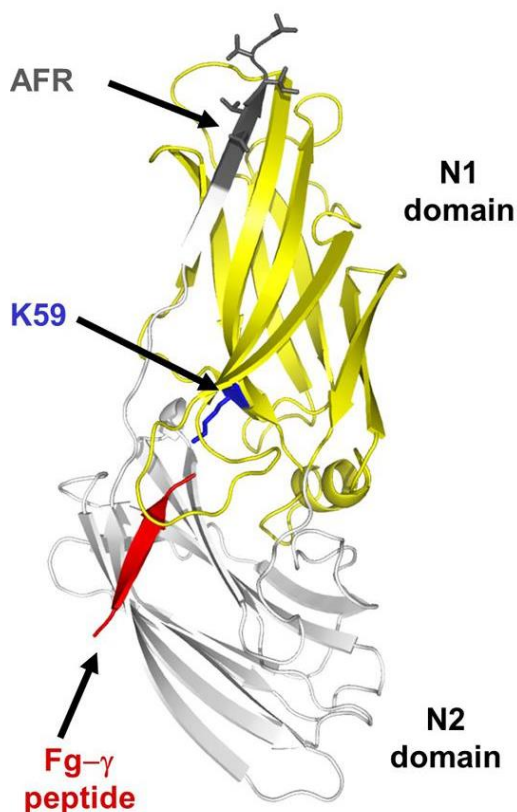
Figure 3 - X-ray structure of Als3 in complex with Fg-γ peptide [9]

The essential aa is the K59 which forms a salt bridge with the C-terminal carboxylic acid of the incoming peptide. Along with K59, other amino acids inhibit the binding activity of ALS: A116, S170, and Y301. Besides that, at the end of the N-terminal, the amyloid fibril region (AFR) was recognized, which plays a significant role in ALS protein association. In the absence of ligands, i.e., C-terminal, ALS mainly forms protein aggregates contacting by AFR region (311-313 aa). Aside from the interaction with the C-terminal of incoming peptide, ALS3 interacts with the human cadherins, forming a solid dimer that helps the C. albicans attach to the host cell *[12]*.

Apart from the ALS family, there are three cell-wall proteins whose deletion leads to adhesion loss of *C. albicans*. They are putative GPI-anchored protein 1 (PGA1), hypha-associated GPI-linked protein 1 (hwp1), and enhanced adherence to polystyrene protein 1 (Eap1). Hwp1 is a human transglutaminase substrate that helps covalently bind with the host cell wall *[5]*. The Eap1 was discovered by its ability to mediate the adhesion to polystyrene, but lately, the deletion of the gene coding Ea1p has led to the loss of adhesion of *C. albicans [13]*. Finally, PGA1 – is a small, 133 aa protein that is upregulated during cell wall regeneration and

mediates the adhesion to the host cell *[14]*. To summarize, there are 11 proteins in *C. albicans* responsible for adhesion to the host's cell wall.

# Genomic plasticity of *C. albicans* (phenotype switching)

Genetic plasticity is one of the factors which plays a vital role in the *Candida albicans* cells' diversity and pathogenicity. During the evolution period, *C. albicans* acquired specific genetic features such as ploidy, mating, loss-of-heterozygosity, the presence of short tandem repeats, etc. (Table 1) [15]. Compared with other candida species, *C. albicans* causes much more severe infections and have different ploidy: haploid, diploid, tetraploid, and aneuploid [16]. *Candida albicans* was considered a sexual species for a long time, but recent studies show that it has asexual and parasexual mating [17]. During sexual mating, *C. albicans* produce tetrasomic cells. During parasexual mating, cells return to the diploid state with a chromosome loss (Fig 4) [18]. These mating processes are possible only if the phenotype switch is observed. Without the conditions for phenotype switching (i.e., in the laboratory), cells exhibit asexual mating, leading to the cells with the phenotype being white or opaque. The phenotype switch is crucial to surviving the host cell immune response [19]. During the parasexual cycle, the volatile tetraploid cell loses a chromosome, which leads to a high diversity of the daughter cells (Fig 4) [18]. Such behavior helps the *C. albicans* during an immune response and leads to the high pathogenicity of *C. albicans*.
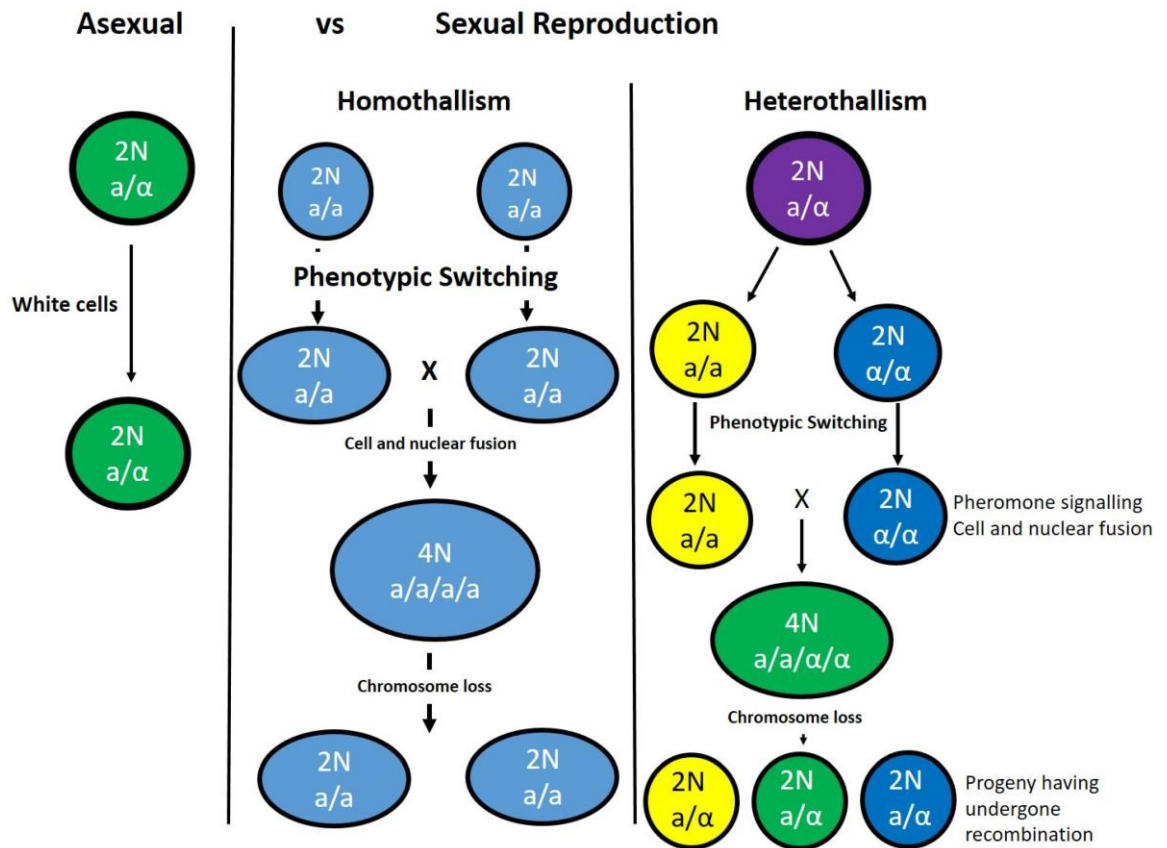
Figure 4 - 3 types of *C. albicans* cells mating [18].

The second important factor is the frequency of heterozygosity loss (LoH). Under non-stress conditions, *C. albicans* have eight heterozygous chromosomes. Nevertheless, LoH occurs when the information in one of the homologs is lost. It was shown that the high frequency of LoH, such as in *C. albicans* and *C. dubliniensis* (Table 1), leads to resistance to fluconazole and phenotype switching [20].

Also, one of the crucial parameters of genomic plasticity is the proportion of short tandem repeats (STRs) in the genome. STRs are short repeats of DNA fragments in the genome (usually 6-8 bp). A higher number of STRs in the genome leads to increased genomic plasticity, mutation rate, and adaptability to the host [21]. Amongst Candida species. The proportion of STRs is higher in *C. albicans* and *C. dubliniensis,* which corresponds to the high pathogenicity and difficulties in treating infections caused by *C. albicans.*

Table 1 - Genetic features of the *C. albicans* family [15]

| | *C. albicans* | *C. dubliniesis* | *C. glabrata* | *C. parapsilosis* | *C. tropicalis* | *C. krusei* |
|---|---|---|---|---|---|---|
| Pathogenicity (Intensity) | +++ | + | ++ | ++ | ++ | + |
| Ploidy | haploid, diploid, tetraploid, aneuploid | diploid | haploid | diploid | diploid | diploid, triploid |
| Mating | Sexual, parasexual | Parasexual | No | No | Parasexual | heterothallic |
| Haploid genome size (Mbp) | 14.5 | 14.6 | 12.3 | 13 | 14.5 | 10.9 |
| Number of chromosomes | 8 | 8 | 13 | 14 | 5-6 | 5 |
| Total coding genes | 6277 | 5860 | 5294 | 5837 | 6254 | 4949 |
| Pseudo-genes | 1 | 123 | 17 | 26 | 1 | none |
| SAP genes | 10 | 8 | none | 3 | 4 | none |
| ALS genes | 8 | 3 | none | 5 | 16 ALS-like | none |
| LoH frequency | high | low | none | low | low | common (one large region) |
| CTG glade | yes | no | no | yes | yes | no |
| Rate of SNPs | 0.3–1.1% | 0.008–0.2% | 0.01% | 0.01% | 0.17% | 0.30% |
| Proportion of STRs in the genome | 1–2% | 1–2% | none | none | none | none |
| Number of transposable elements | >250 kbp | >250 kbp | none | ~160 kbp | >250 kbp | none |

# Morphological plasticity of *C. albicans* (Dimorphism)

Despite the genomic plasticity of *Candida albicans*, it also has broad morphological plasticity. High morphological plasticity helps *C. albicans* to invade the host cells and be invisible to the host immune system. *C. albicans* distinguish three cell types: budding yeast, pseudohypha, and hypha.
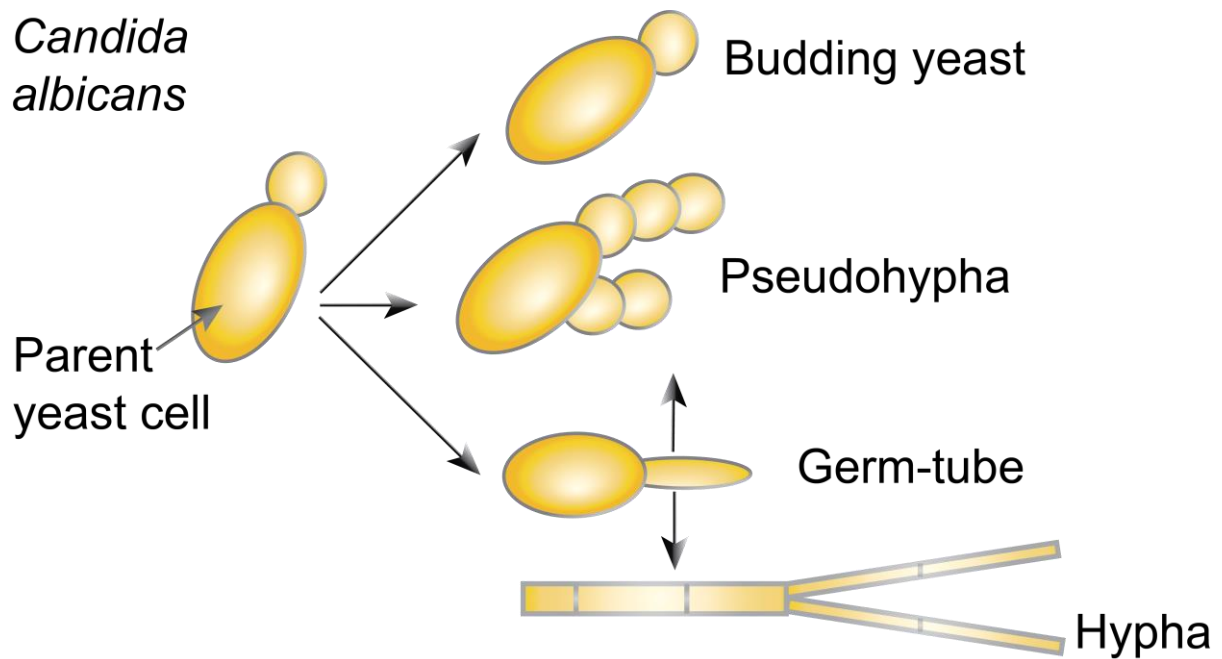
Figure 5 - Morphological plasticity of *C. albicans* cells [22]

The budding yeast colonies, such as *S. cerevisiae*, cannot invade the host cells. This cell type is primary in non-pathogenic cases when the candida cells are conquering with other microorganisms for the nutrient source. In this lag phase, candida does not damage the host's cell wall and remains visible to the host immune system and macrophages [23].

Another cell type is pseudohypha. Pseudohypha represents a group of cells connected in a chain. Such filamentous growth makes *C. albicans* invisible to the immune system, but pseudohypha cells are not producing factors responsible for cell wall damage [24]. In pseudohypha, elongated daughter cells are eligible to produce their elongated copies in contrast to budding cells. Pseudo hypha is considered an intermediate state between budding type colonies and hyphae – which is the most aggressive cell type of *C. albicans*.

The third cell type is hyphae. Hyphae, in strict contrast to other cell types, represent a highly pathogenic form. Hyphae is a pseudohypha from a cell chain, up to 10 times more in length than parent cells [25]. The main difference between pseudohypha and hypha is that filamentous assembling starts from a germ tube construction. These elongated germ tubes are further divided by septate–cell–wall components. The cell growth in hypha goes along a polarized axis. Furthermore, hyphae cells produce candidalysin, 31 aa toxins responsible for host cell lysis and following *C. albicans* invasion [26].

# Invasion and damage of the host cells
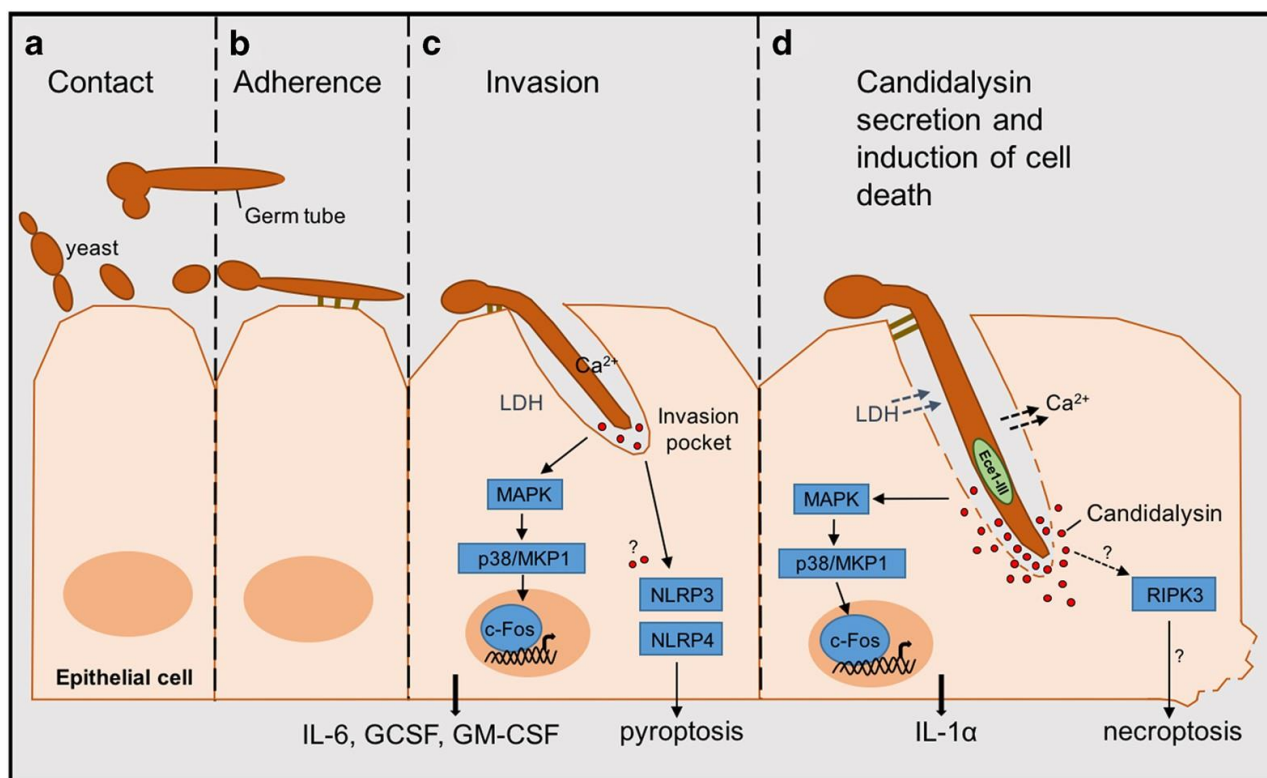


Figure 6 - Schematic interaction of adhesion and invasion of *C. albicans* to the epithelial cell [27]

After adhesion, *C. albicans* must overcome the cell barrier to invade the host cells. As written before, the necessary precondition is germ tube (hyphae) formation. Only hyphae produce toxins, namely candidalysins, which could destroy the cell membrane. The penetration process is usually divided into early and late invasions (Fig 6) [27].

In the early toxin secretion, *C. albicans* induces the host's immune response by activating MAPK phosphatase 1 (MKP1) and transcription factor c-Fos [28]. Occurred immune signaling events provoke a release of cytokines and their inductors: interleukine-6 (IL-6), granulocyte colony-stimulating factor (GCSF), and Granulocyte-macrophage colony-stimulating factor (GM-CSF) [29, 30]. There is a second pathway of cell death along with cytokine release – macrophage pyroptosis [31]. Cell damage leads to the activation of nucleotide-binding oligomerization domain and leucine-rich repeat-containing receptors family pyrin domains containing 3, 4 (NLRP3, NLRP4) [32, 33]. NLRP3 is expressed predominantly in macrophages and, as a component of the inflammasome, detects products of damaged cells such as extracellular ATP and crystalline uric acid. Activated NLRP3 and NLRP4, in turn, trigger an immune response.

Here the one question that remains unclear is whether candidalysins directly trigger NLRPs activation or not.

The expression level of candidalysin is significantly increasing the more profound penetration into the cell, along with the secretion of hydrolytic enzymes such as secreted aspartic proteinases, phospholipase, and other lipases digesting the cell membrane and its components (Fig 7) [34]. All of them facilitate the penetration of hyphae into epithelial cells. In addition, secreted aspartic proteinases play a significant role in suppressing immune responses by degrading IgG and other proteins produced during the immune response. All these factors provide a rapid invasion of hyphae into the host's epithelial cells following cell death and penetration into the bloodstream.
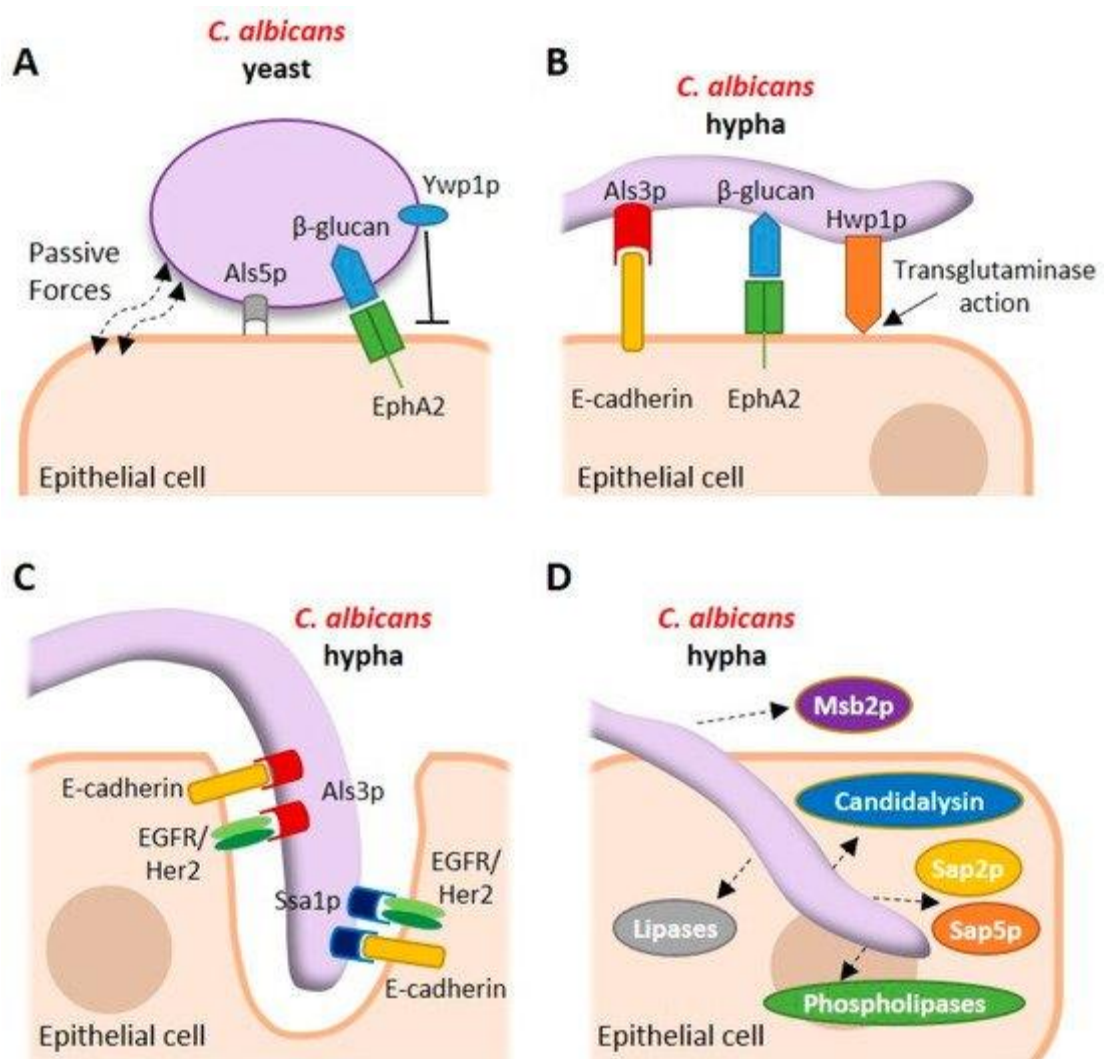


Figure 7 - Schematic representation of *C. albicans* adhesion and invasion indicates enzymes and proteins participating [34].

# Biofilm formation
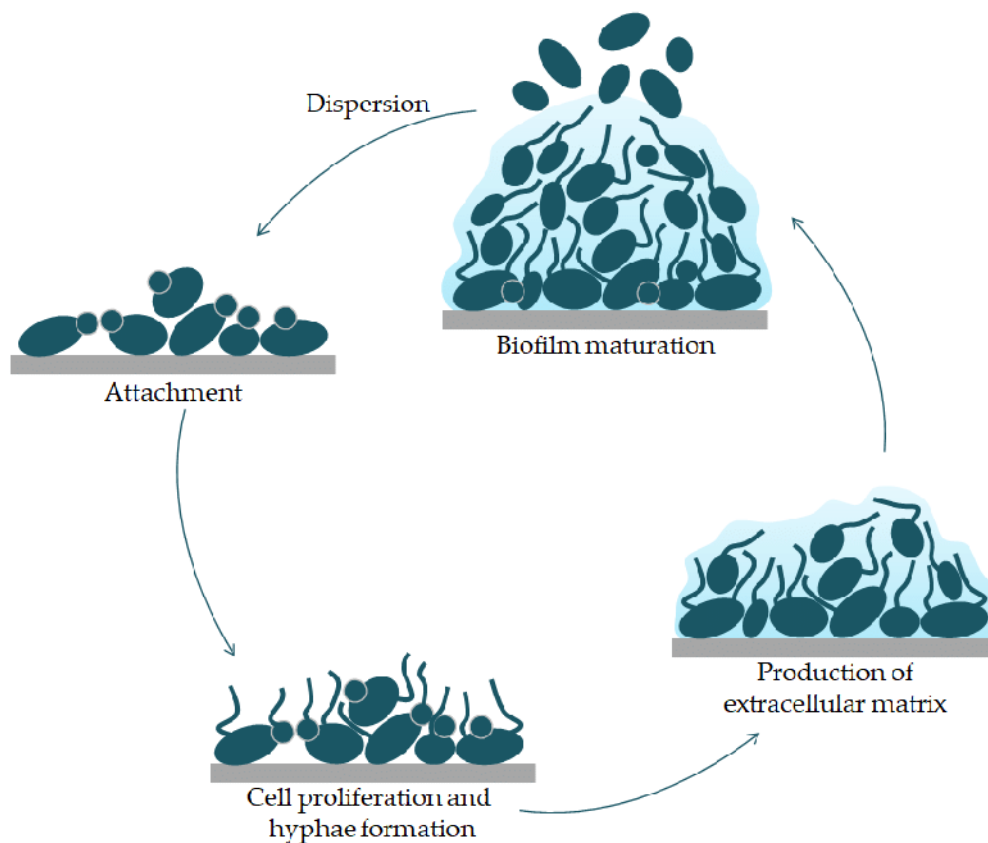


Figure 8 - Stages of biofilm formation in *C. albicans [35]*

Biofilm formation is one of the major virulence factors of the Candida family. Due to the restricted diffusion, biofilm formation makes the candida cells almost invisible to the current drugs [36]. The lethal dose kills only the cells on the surface of the biofilm, leaving other cells untreated. Several studies show that, in distinct contrast to the cells inside the biofilms, the floating cells are susceptible to the same drug dose [37]. The second problem is the possibility of biofilm formation not only on the host cell surface but also on inorganic surfaces, such as catheters. Biofilm formation on the catheters represents a significant challenge in hospitals because it frequently leads to disseminated forms of candidiasis once cells are detached from the surface of the catheter [38].

Biofilm formation is not a specific feature of Candida but all fungi. Biofilm is the first colonization type that appeared in fungi during evolution. Its formation gives the main advantage of evading the cell's immune response. The mechanism of evading was not known for a while, but nowadays, there are three main theories [39]:

1) Biofilms silence the immune system by impairing immune sensing mechanisms;
2) Biofilms deviate the immune system by driving it to non-productive avenues;

3) The immune system cannot dissolve the biofilms, so it creates immune resistance to the cells inside the biofilms

Apart from the immune evading, biofilms facilitate the nutrient supply and cooperate with other fungi/bacteria making mixed biofilms even more resistant to the immune system.

There are four main stages of biofilm formation (Fig 8) [35]:

1) Attachment to a surface. Budding candida cells attach to the cell surface of the host

2) Microcolony formation. *C. albicans* cells are starting to proliferate and form hyphae.

3) Extracellular matrix production. The matrix is made up of a wide variety of extracellular polymeric components (EPS, polysaccharides, nucleic acids, proteins, lipids, and lipoproteins) that are responsible for the distinctive characteristics of the virulence and lifecycle of biofilms.

4) Biofilm maturation. The biofilm reaches a critical mass and disperses the *C. albicans* cells, ready to colonize other surfaces.

To sum up, the ability of Candida species to form biofilms is crucial for its pathogenicity.

# Fitness traits (Stress response)
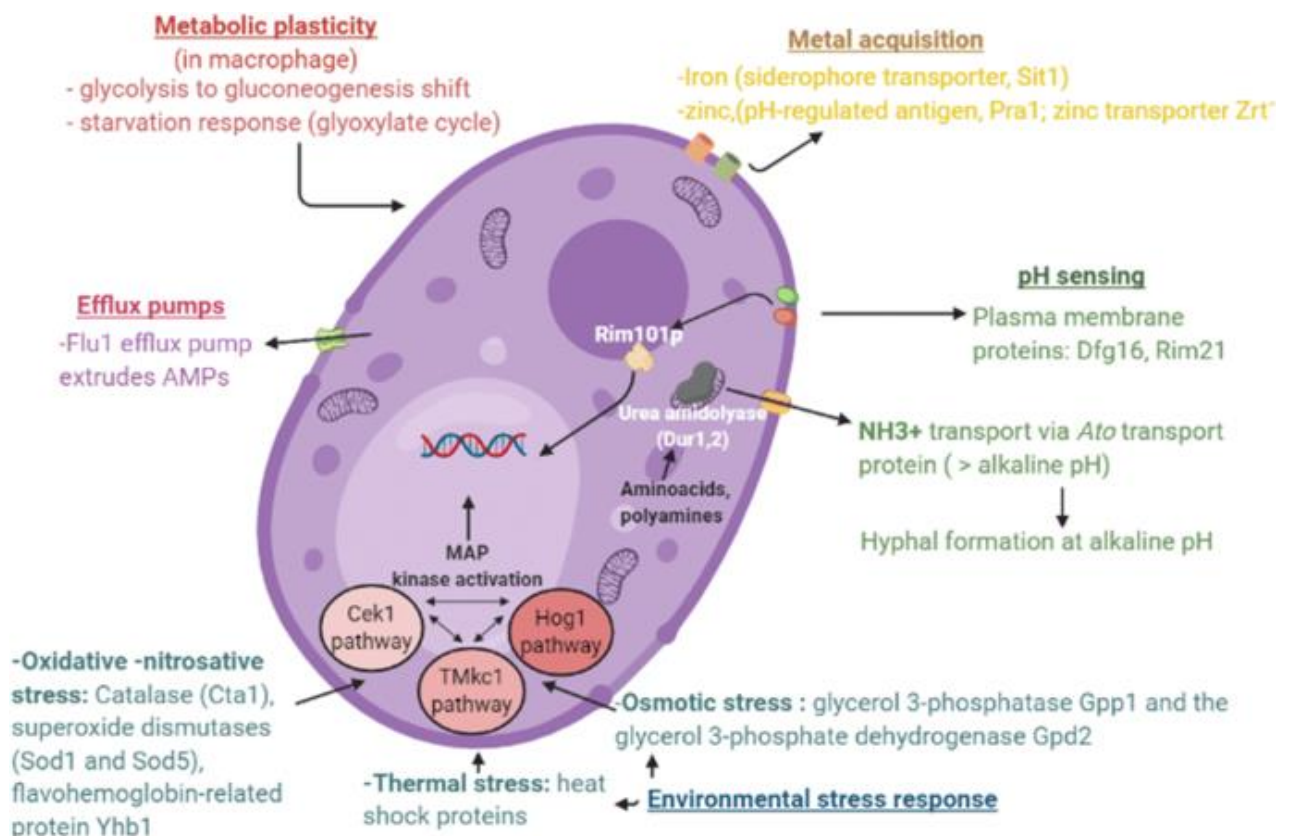


Figure 9 - Regulation mechanisms of *C. albicans* on the environmental stress response. [40]

To adopt the host variability and stress response, *C. albicans* have multiple survival mechanisms depending on the origin of the stress (Figure 9) [40].

1) Metabolic (nutrition) stress. In non-stress conditions, *C. albicans* is predominantly located in a gastrointestinal microbiome [5, 41]. In the presence of other microorganisms, *C. albicans* has restricted access to the nutrients which control their proliferation. During the pathogenic switch, *C. albicans* penetrate the bloodstream where glucose concentration – the main fungal nutrient is rather high (6-8 mM) [42]. However, at the same time, *C. albicans* cells can be phagocyted by macrophages and neutrophils. To survive inside the phagocytes, where nutrient access is limited, *C. albicans* switches from glycolysis to gluconeogenesis. *C. albicans* is starting to produce the secretases which hydrolyze the host-cell proteins, nucleic acids, and phospholipids to produce glucose from them. Also, as a response to starvation to keep the carbon level inside the cells, *C. albicans* switches to the glyoxylate cycle, which allows using the two carbon compounds, such as acetate, as a carbon source.

2) pH variability stress. *C. albicans* possess high plasticity to adopt to a high pH range of the surrounding environment. Fungi cells are present in the host niches, where pH ranges from acidic (pH 2) in the digestive system to slightly alkaline (pH 8) in the bloodstream. Recently, two cell wall proteins (β-glycosidases) were found, which allow survival in a broad pH range, namely PHR1 and PHR2 [43, 44]. PHR1 is expressed at neutral-alkaline pH, and PHR2 – at acidic pH. To modulate the level of these proteins, *C. albicans* senses a pH via the Rim101 signal transduction pathway. In this pathway, pH is monitored by two plasma membrane receptors, Dfg16 and Rim21 [45]. Activation of these receptors leads to the induction of a signaling cascade, upregulating a PHR1 and PHR2 synthesis via activating the Rim101 factor.

   Along with pH sensing, it was found that *C. albicans* can modulate the surrounding pH by alkalizing the surrounding space. The mechanism of pH modulation is not known yet, but there is a presumption that in the absence of glucose. *C. albicans* cleaves the amino acids and polyamines intracellularly with the urea amidolyase Dur1,2 and exports the resulting ammonia via external transport proteins (Ato) [46] so that the extra ammonium atoms located outside of the cell alkalize the outer environment and promote hyphal growth.

3) Thermal stress. In response to the temperature fluctuation, *C. albicans* produces heat-shock proteins, which act as chaperons preventing a protein from unfolding and degrading. Along with the heat-shock proteins, it was recently found that there is an accumulation of trehalose, which acts as a 'chemical chaperon' by stabilizing the proteins inclined to unfold [47, 48].

4) Osmotic stress. To counteract the osmotic stress, which leads to the loss of water molecules, *C. albicans* accumulate glycerol inside the cell. The glycerol production is mediated by the glycerol 3-phosphatase Gpp1 and the glycerol 3-phosphate dehydrogenase Gpd2.

5) Oxidative (nitrogen) stress. Phagocytic cells produce reactive oxygen species (ROS) [49], such as peroxide and hydroxyl radicals which lead to the oxidative stress of *C. albicans*. To prevent its toxic effects, *C. albicans* produces catalase Cta1 and superoxide dismutases, Sod1 and Sod5 [50]. Neutrophils also produce reactive nitrogen species (RNS), which are highly toxic to *C. albicans*. It was found that there is only one protein, Yhb1, which neutralizes RNS in *C. albicans* [51].

6) Metal acquisition. Acquisition of the metal ions plays a substantial role in *C. albican's* invasion and proliferation. To date, the most widely investigated translation metal is iron. In *C. albicans,* iron plays a vital role during invasion serving as substrate for the ALS3 protein. A study shows that the ALS3 mutant unable to bind iron prevents *C. albicans* host invasion [52]. The second most abundant metal ion is Zinc. *C. albicans* secretes the zinc-binding protein Pra1 (pH-regulated antigen 1), whose deletion strongly decreases the pathogenicity of *C. albicans* [53].

# CANDIDA ALBICANS: PROTEIN TRANSLATION

The following virulence factors describe the plasticity of *C. albicans* to survive in different conditions and reflect on the stress factors attack. Such high plasticity of the *C. albicans* would not be possible without the characteristic features of the translation machinery. The translation system can quickly change to stress response and possesses characteristic features that drastically differentiate them from other eukaryotes. The following characteristic features of the translational apparatus of *C. albicans* are CUG-clade, rRNA polyadenylation, and point mutations in ribosomal functional sites.

## CUG clade (Ser/Leu t-RNA dualism)

In 1968, Crick introduced a universal genetic code doctrine. In 1989 the first evidence of the decoding ambiguity was discovered in *C. albicans*. In *C. albicans* CUG codon is translated to Ser and not the Leu as in other eukaryotes. Several switches were identified: CUG-Leu to CUG-Ser switch and CUG-Leu to CUG-Ala (Figure 10) [54].



Figure 10 - Genetic code matrix. CUG codon is a unique codon translated differently across the species [54].

The existence of signature motifs in the mRNA determines whether the amino acid is inserted or whether a terminator tRNA binds to the mRNA, leading, accordingly, to reassigned codons encoding various amino acids or in truncated proteins. [55]. Such codon dualism led to significant rearrangements in the genetic code of *C. albicans*. The CUG codon is presented in >50% of the decoding genes of *C. albicans*, especially in the plasma membrane, DNA repair, etc. [56].

A mutation evolutionally created such CUG ambiguity in the serine CUG-tRNA, where the adenine insertion in the tRNA's anti-codon loop resulted in the serine CAG-tRNA. Further changes in the Ser-CAG-tRNA resulted in recognizing this tRNA both by seryl and leucyl synthetase in a competitive manner (Figure 11) [57]. Such CUG-dualisms significantly extend the proteome of CUG-clade species, mainly the microorganisms responsible for severe diseases.
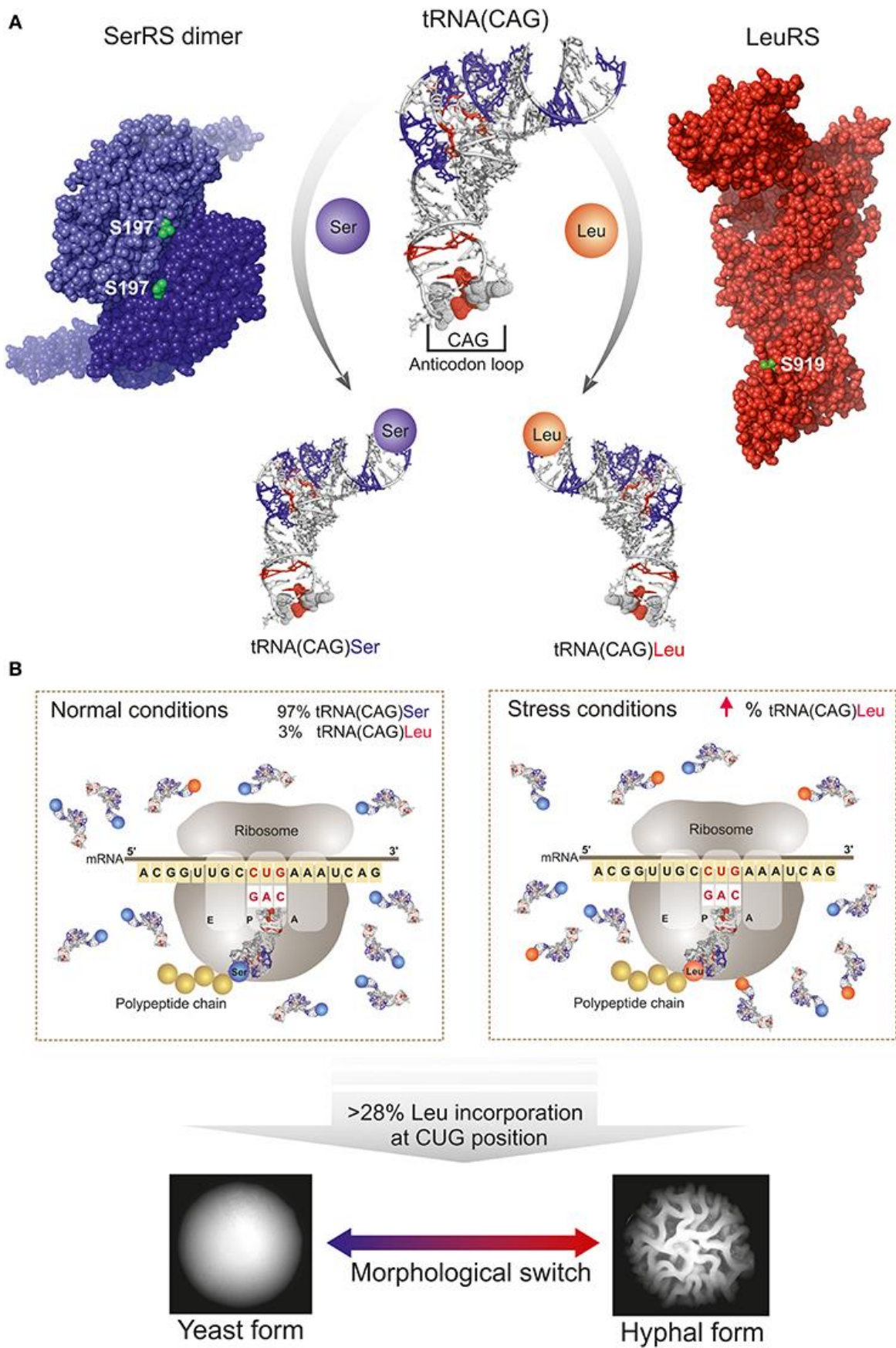
Figure 11 - Schematic representation of CUG codon translation ambiguity mechanism in *C. albicans* [57].

To prevent the misfunction and unfolding of the protein due to the Leu/Ser dualism, most of the CUG sequences coding the serine were replaced by leucine during the evolution process. Overall, 90% of the CUGs were relocated, mainly in the areas exposed to the solvent or in the α-helices (rich in Leu) and β-strands (rich in Ser). The resulting position of the CUG-residues seems to be optimally suited to prevent the massive protein misfolding that would result from incorporating polar serine residues in the proteins' hydrophobic cores, where generally, leucine residues are favored.

It's interesting that a number of pieces of evidence support the idea that, barring unavoidable structural repercussions, inserting a serine or leucine into a specific position is unlikely to have a completely neutral impact on the overall function of the protein with implications for *C. albican's* homeostasis. This is underscored by the frequently observed inability to complement *S. cerevisiae* deletion strains with *C. albicans* CUG functionally- codon-containing genes [58]. Leucine incorporation is increased when *C. albicans* is genetically altered, and this causes morphological traits that are connected to the expression of genes for cell attachment and hyphal development. (Figure, 11B) [59].

However, it is unknown how these variations in the biology and virulence of *C. albicans* will affect the translation. SerRS is the primary tRNA$_{CAG}$ charging enzyme under physiological circumstances, despite the fact that the comparative values for the affinities of *C. albicans* recognition both by seryl- (SerRS) and leucyl-tRNA (LeuRS) synthetases isoforms toward the tRNA$_{CAG}$ are yet unknown. Given that the majority of CUG- residues are translated as serine, LeuRS seems to be a weak rival. *C. albicans's* growth rates were unaffected by the genetic manipulation that increased leucine incorporation levels to 28%, but the altered cell morphology (Figure 11B) and induced expression of genes involved in cell adhesion and hyphal growth were simultaneously accompanied by a decreased susceptibility to phagocytosis by murine macrophages [59].

Taking a closer look at the differences between CAG-Ser/Leu-tRNA in *C. albicans* and CAG-Leu-tRNA in *S. cerevisiae,* several differences in the sequence could be responsible for translation ambiguity. For example, it was found that guanidine in position 33 (next to anticodon triplet) is highly conserved in the Ser-Clade family and is different from that found in higher eukaryotes, such as *S. cerevisiae* (Figure 12). Moreover, the substitution of G33 to A, U, or C significantly increases the level of Leu incorporation in the peptide chain during translation. This finding also discovers the impact of the single mutation in the tRNA, significantly changing the translation ambiguity in *C. albicans.* Another example is methylated-G37 (m$^1$G37), which is also highly conserved in the CTG-clade species, except for *Candida cylindracea* tRNA, in which

adenosine is found at position 37 (A37) [56]. Replacing the m$^1$G37 with another nucleotide was shown to suppress leucylation. This indicates a balancing effect of G33 and m$^1$G37 as leucylation suppressors and enhancers, respectively, leading to low-level mischarging of CTG-clade Ser-tRNA$_{CAG}$ with leucine. Structural investigations of functional complexes should be performed to understand better the impact of G33, m1G37, and other sequence differences. To date, there is no robust explanation of the impact of Leu/Ser-tRNA dualism on the structural level.
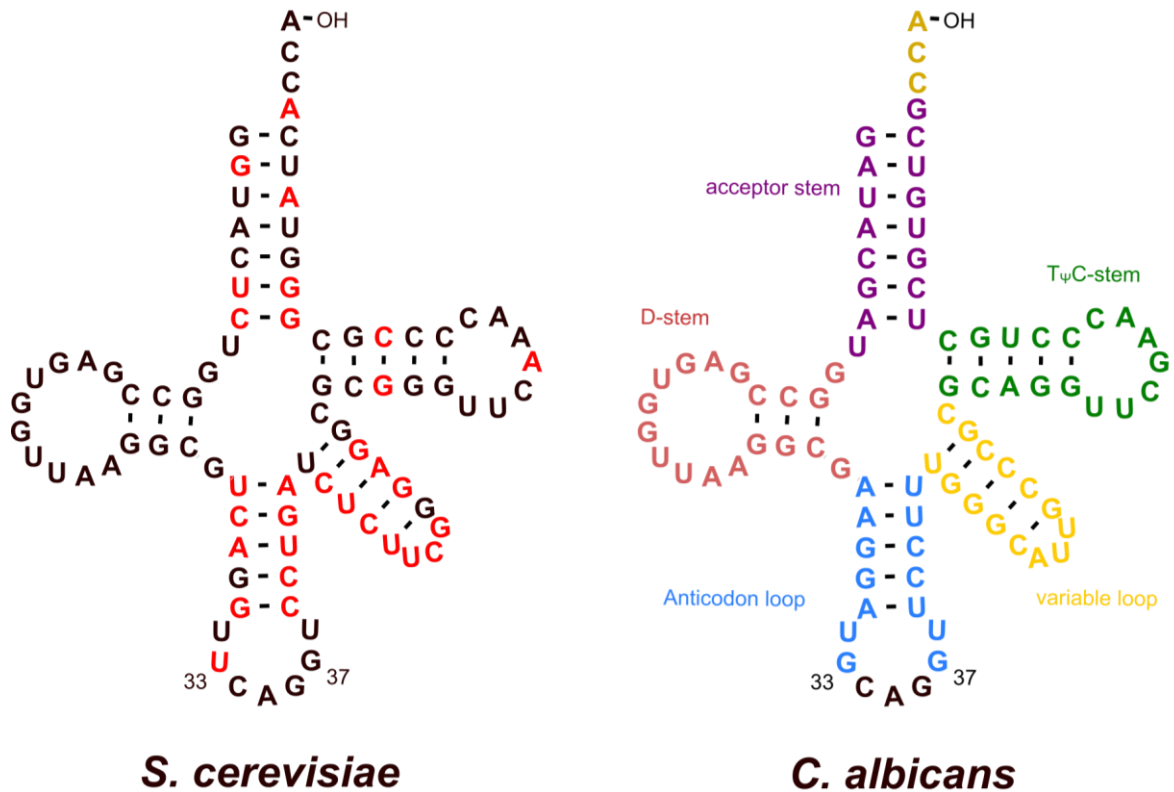


Figure 12 - Schematic representation of Leu-tRNA (CAG) in *S. cerevisiae* and Ser/Leu-tRNA (CAG) in *C. albicans*.

## rRNA Polyadenylation

Along with the CUG-codon dualism in *C. albicans* which gives a higher degree of plasticity during the host invasion, it was found that there are changes in the sequence of ribosomal RNA (rRNA). The changes in rRNA occur in reply to the stress conditions. Visualizing the stress conditions in *C. albicans* is a well-established protocol of serum exposure [60]. Upon serum exposure, *C. albicans* start to form hyphae. Using the differential display method, the modification in 25S rRNA was found for the first time. After sequencing the modified rRNA, it was found that modifications are polyadenylation (polyA) of the 25S rRNA.

Polyadenylation occurs in the 3'-end of the rRNA. The length of the polyA tails is different, but they all occurred one of two pyrimidine bases apart (Figure 13) [61]. The tail location suggests that the polyadenylation occurred at the cleavage site of the maturation process.

```
CTTGTTGTCTGATTTGTAAAAAAAAAAAAAAAAAAAAAAAAAAAAA
AAAAAAAAAAAAAAAAAAAAAAAAAACTCGAGTG

CTTGTTGTCTGATTTGTAAAAAAAAAAAAAAAAAAAAAAAAAAAA
AAAAAAAAAAAAAAAAACTCGAGTG

CTTGTTGTCTGATTTGTCTAAAAAAAAAAAAAAAAAAAAAAAA
AAAAAAAAAAAAAAAAAAAAAAAAAAAAAAAAAAAAAAAATAA
AAAAAAAAAAACTCGAGTG

CTTGTTGTCTGATTTGTCTAAAAAAAAAAAAAAAAAAAAAAAA
AAAAAAAAAAACTCGAGTA

CTTGTTGTCTGATTTGTCTAAAAAAAAAAAAAAAAAAAAAAAAACA
AAAAAAAAAAAAAAAAAAAAAAAAAAAAAAAACGCGGCCGCG
GAGCTCGCCGAATT
```

Figure 13 - PolyA tails in 3'-end of *C. albicans* 25S rRNA [61].

Later, polyadenylation of 18S rRNA was also found. Unlike the large 25S subunit, polyadenylation sites near the 3' end are more variable, and no polyadenylation was found at the reported maturation site of 18S. PolyA tails occur downstream and upstream from the 3' end of 18S rRNA (Figure 14) [62]. There is an assumption that the 3'-end of the 18S rRNA plays an essential role in the recognition of start sites on mRNA, which is why it could be vigorously protected from modifications. The transient increase in polyadenylation of both the large and the small subunits of ribosomal RNA just before the appearance of hypha raises the possibility of a role in this process.

```
      Y¹            S¹      Y⁴Y¹
1624-CCGCCCGTCGCTACTACCGATTGAATGGCTTAGTGAGGCCTCCGGATTG

GTTTAGGAAAGGGGGCAACCTCATTCTGGAACCGAGAAGCTGGTCAAACTTGGT

CATTTAGAGGAAGTAAAAGTCGTAACAAGGTTTCCGTAGTGAACCTGCGGAAGG
                                              S²
ATCATTA (reported 3'end) CTGATTTGCTTAATTGCACCACATGTGTT
                            Y¹                      S¹
TTTCTTTGAAACAAACTTGCTTTGGCGGTGGGCCCAGCTGCCGCCAGAGGTCTA

AACTTACAACCAATTTTTTTATCAACTTGTCACACCAGATTATTACTAATAGTCA

AAA
```

Figure 14 - PolyA tails of *C. albicans* 18S rRNA [62].

Moreover, during the experiments aimed at finding polyadenylation tails of rRNA, an overall decrease in the rRNA was observed [60]. Therefore, it was proposed that, most probably, as a response to the stress (serum exposure), *C. albicans* started deleting the rRNA by inserting polyA tails. These mechanisms were previously described for *S. cerevisiae*. In *S. cerevisiae*, rRNA degradation is performed via polyadenylation by TRAMP complexes, followed by nuclear exosome degradation [63]. Such a mechanism is not yet described for *C. albicans,* but it is most likely a reason for the observed polyA tales and rRNA decrease.

Nevertheless, it is unclear if the decrease in rRNA abundance plays a vital role in hypha formation. However, the current data do not directly link hypha formation and rRNA decrease. Furthermore, the rRNA decrease was also observed in *C. glabrata*, which does not form the hypha, suggesting that rRNA decrease is not connected with hypha formation after serum exposure.

Furthermore, rRNA processing was thoroughly investigated in the past decades, revealing the overall similarity in rRNA processing to higher eukaryotes. However, in *C. albicans,* specific RNA enzymes participate in rRNA processing, such as CaDCR1 [64]. CaDCR1 dicer is required to cleavage the 3′ external transcribed spacer from unprocessed pre-rRNA of *C. albicans*.

# Cell-free translation

The first cell-free system in fungi was established to understand better the genomic features of C. albicans, such as translation and initiation. The cell-free system in *C. albicans* was created based on a well-established system in *S. cerevisiae*. Both systems have very similar physiological conditions for successfully translating synthetic PolyU mRNA templates. For example, the optimum Mg concentration in *S. cerevisiae* is 12 mM, and in *C. albicans* – 15mM. The overall comparison of the optimal condition for cell-free translation in *C. albicans* and *S. cerevisiae* is presented in Table 2 [65].

Table 2 - Optimal condition of cell-free synthesis of the synthetic PolyU mRNA template in *C. albicans* and *S. cerevisiae*

| Parameter | Optimal conditions | |
|---|---|---|
| | *C. albicans* lysate | *S. cerevisiae* lysate |
| Time of incubation | 20-30 min | 20-30 min |
| $Mg^{2+}$ concentration | 15 mM | 12 mM |
| KOAc concentration | 180 mM | 150 mM |
| Temperature | 30-37 °C | 30-37 °C |
| Protein concentration | 1.2-1.6 mg/ml | - |
| Poly(U) concentration | 500 μg/ml | 400 μg/ml |

The cell-free translation in *C. albicans* strictly requires the presence of ATP in the sample. The ATP saturation in *C. albicans* reached 100 μM and could not be increased by adding GTP. So, the cell-free extract of *C. albicans* is as ATP-dependent as *S. cerevisiae*. However, at the same time, in *C. albicans*, adding GTP does not increase the translation efficiency as it was found for *S. cerevisiae*. This phenomenon was found in the translation of not only synthetic PolyU mRNA templates but also natural mRNAs.

The elongation step of translation was examined by testing the known translation inhibitors, such as cycloheximide, puromycin, tetracycline, etc. *C. albicans* were observed to be sensitive at the same level as *S. cerevisiae* to most compounds except for cycloheximide (Table 3). *C. albicans* was approximately 200 times less sensitive to CHX than *S. cerevisiae*. Moreover, there are slight differences in sensitivity to Puromycin and fusidic acid: *C. albicans* is four times more sensitive to Puromycin and 3-fold less sensitive to Fusidic acid. At that time, such strong resistance to CHX was not explained at the molecular level. There were the assumptions that its due to natural variation in the protein of the LSU. Only ten years later, the first functional data

found an essential mutation in the eL42 protein of *C. albicans*, but the molecular mechanism of the CHX resistance still was not known [66, 67].

Table 3 - Inhibition of translation elongation in cell-free systems from *C. albicans* and *S. cerevisiae*

| Inhibitor | MIC$_{50}$ (µg/ml) | |
|---|---|---|
| | *S. cerevisiae* lysate | *C. albicans* lysate |
| Tetracycline | 110 | 75 |
| Fusidic acid | 85 | 200 |
| Puromycin | 19 | 4.5 |
| Cycloheximide | 0.2 | 200 |
| Emetine | 65 | 65 |
| Diphtheria toxin | 1 | 1 |

# CANDIDA ALBICANS: RIBOSOME

## Bacteria/eukaryote-specific structural features of the ribosome

To get further details on the translation machinery and its role in *C. albicans* virulence, structural studies of the *C. albicans* ribosome are needed. The ribosome is the cellular machinery responsible for the fundamental process of protein biosynthesis and is involved in the expression of genetic information. According to the current structural and functional data, the ribosomes are highly conserved across the species. Nevertheless, comparing the bacterial and eukaryotic ribosomes, there are many differences in rRNA and ribosomal proteins. First, the bacterial ribosome is much smaller than its eukaryotic counterpart.

The bacterial ribosome consists of 2 subunits – the 30S and 50S, with a protein / rRNA ratio of 1:2 (Figure 15) [68]. The 30S subunit consists of 16S rRNA (app 1540 nts) and 21 ribosomal proteins. The 50S subunit consists of 23S rRNA and 5S rRNA, and 33 ribosomal proteins. The molecular weight of the bacterial ribosomes is app. 2.3 MDa.
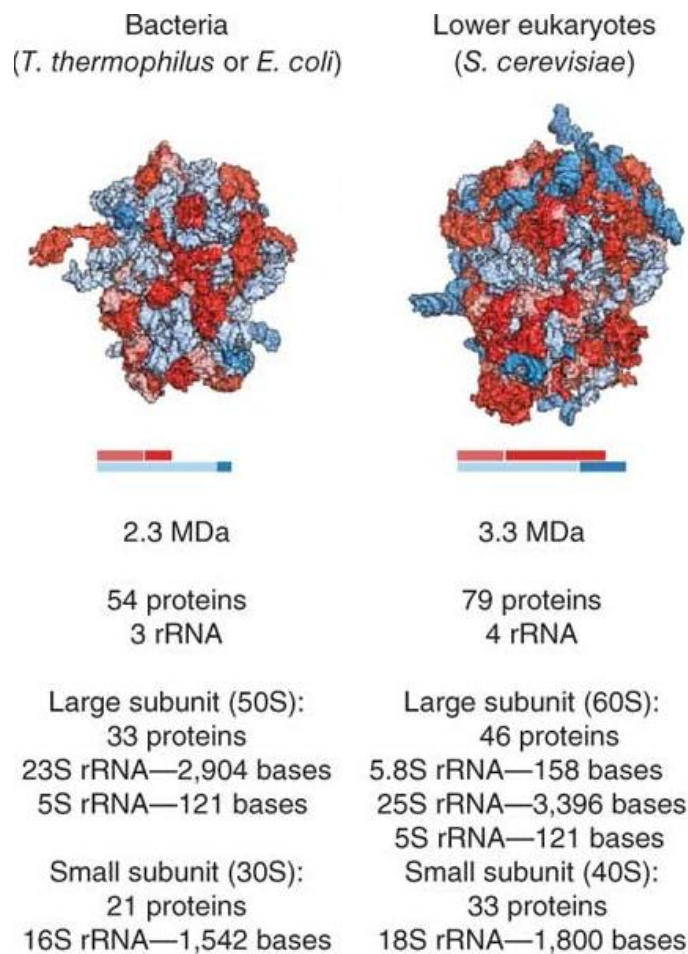


Figure 15 - Composition of the bacterial and eukaryotic ribosomes [68].

The eukaryotic ribosome also consists of two subunits, much bigger than in bacteria – 40S and 60S, with a protein / rRNA ratio of 2:1. The 40S subunit consists of 18S rRNA (app 1800 nts) and 33 ribosomal proteins. The 60S subunit consists of 25S rRNA (app 3300 nts), 5.8S (app 150 nts) and 5S rRNA (app 120 nts), and 46 ribosomal proteins. The molecular weight of the eukaryotic ribosomes averages 3.3 MDa.

Despite the different numbers of proteins and rRNA, bacterial and eukaryotic ribosomes share a common structural core, consisting of 15 ribosomal proteins in the SSU and 19 in the LSU. According to the new nomenclature [69], the proteins in the core have the same acronyms in bacteria and eukaryotes, except for the P stalk proteins P1/P2 (L7/L12). The list of the conserved proteins is presented in Table 4 for LSU and Table 5 for SSU.

Table 4 - Ribosomal proteins of the LSU conserved in bacteria and eukaryotes.

| New nomenclature | Bacterial name | Yeast name |
| --- | --- | --- |
| uL1 | L1 | L1 |
| uL2 | L2 | L2 |
| uL3 | L3 | L3 |
| uL4 | L4 | L4 |
| uL5 | L5 | L11 |
| uL6 | L6 | L9 |
| uL10 | L10 | P0 |
| uL11 | L11 | L12 |
| uL13 | L13 | L16 |
| uL14 | L14 | L23 |
| uL15 | L15 | L28 |
| uL16 | L16 | L10 |
| uL18 | L18 | L5 |
| uL22 | L22 | L17 |
| uL23 | L23 | L25 |
| uL24 | L24 | L26 |
| uL29 | L29 | L35 |
| uL30 | L30 | L7 |
| bL12 / (P1/P2) | L7/L12 | P1/P2 |

Table 5 - Ribosomal proteins of the SSU conserved in bacteria and eukaryotes.

| New nomenclature | Bacterial name | Yeast name |
|---|---|---|
| uS2 | S2 | S0 |
| uS3 | S3 | S3 |
| uS4 | S4 | S9 |
| uS5 | S5 | S2 |
| uS7 | S7 | S5 |
| uS8 | S8 | S22 |
| uS9 | S9 | S16 |
| uS10 | S10 | S20 |
| uS11 | S11 | S14 |
| uS12 | S12 | S23 |
| uS13 | S13 | S18 |
| uS14 | S14 | S29 |
| uS15 | S15 | S13 |
| uS17 | S17 | S11 |
| uS19 | S19 | S15 |

Nevertheless, some ribosomal proteins are specific for bacteria and eukaryotes in the conserved common core. For example, there are 6 bacterial specific proteins in SSU (bS1, bS6, bS16, bS18, bS20, bS21) and 14 in LSU (bL9, bL17, bL19, bL20, bL21, bL25, bL27, bL28, bL31, bL32, bL33, bL35, bL36). Eukaryotes, in comparison, have much more specific proteins: 18 in the 40S subunit and 28 in the 60S subunit.

Apart from the ribosomal proteins, there are drastic changes in the ribosomal RNA. The eukaryotic rRNA is more than 900 nts longer than the bacterial one. These differences mainly occurred in the regions exposed to the solvent, thus accessible for potential interactions with molecular partners, such as translation factors and chaperones. These differences primarily represent the extension of the bacterial rRNA and are thus called expansion segments. There are theories that these expansion segments were introduced during the evolution process by elongation/insertion of the rRNA helixes. Most expansion segments present in *E. coli* consistently expanded during evolution, i.e., Helix 38, 52, and 101 (Figure 16) [70].

Nevertheless, the most appealing example is the expansion segment №7 (ES7). ES 7 originates with a short 22-nucleotide stem-loop in the last universal common ancestor, which is approximated here by *E. coli*. This stem-loop grows to an 80-nucleotide bent helix in the common ancestor of Archaea and Eukarya. The common ancestor of Archaea and Eukarya is approximated by the archaeon *Haloarcula marismortui*. In the next step, ES7 grows to a branched 210-nucleotide structure in the common ancestor of eukaryotes, which is approximated by *S. cerevisiae.* In the next step, ES7 grows to a 342-nucleotide structure in the common ancestor of metazoans (approximated by the arthropod *D. melanogaster*). Mammalian rRNA grows further, exemplified by the 876 nucleotides ES 7 domain in *H. sapiens*.
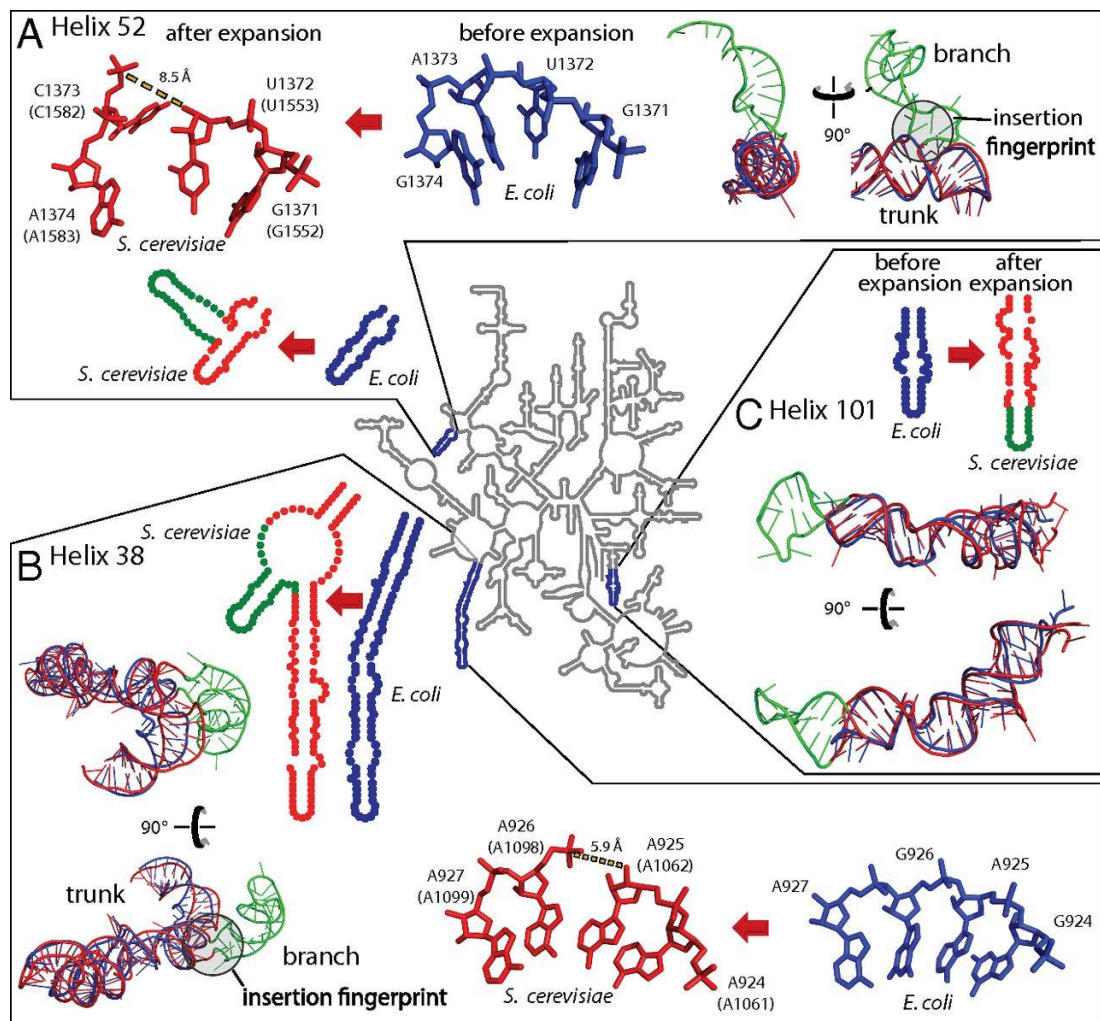


Figure 16 - rRNA expansion elements evolution [70]

# Specific features of *C. albicans* ribosome

## rRNA

*C. albicans* 80S ribosome, like any eukaryotic ribosome, consists of the 60S and 40S subunits. The 60S subunit has crown-like shapes, which include the 'central protuberance,' 'L1-stalk', and the 'P-stalk.' The 60S subunit of *C. albicans* consists of three rRNA (25S, 5.8S, 5S) and 44 ribosomal proteins. Even though the overall similarity to *S. cerevisiae* and other higher eukaryotes, the rRNA and ribosomal protein sequences are not identical to *S. cerevisiae* ones. *C. albicans* 25S rRNA consists of 3,361 nts (3396 nts in *S. cerevisiae*), 5.8S of 157 nts (158 nts in *S. cerevisiae*), and 5S of 121 nts. (Table 6). The overall identity of the rRNA ranges from 89.74% in 5S to 94.94% in 5.8S.

Table 6 - rRNA comparison in *C. albicans* and *S. cerevisiae*.

| rRNA | rRNA length | | Identity |
|---|---|---|---|
| | *C. albicans* | *S. cerevisiae* | |
| 25S | 3361 | 3396 | 91.76% |
| 5.8S | 157 | 158 | 94.94% |
| 5S | 121 | 121 | 89.74% |
| 18S | 1787 | 1800 | 93.80% |

The main differences in the rRNA between *C. albicans* and higher eukaryotes are in the expansion segments, namely ES7, ES27, and ES31. In *C. albicans* ES7 is 208 nts long. First, in comparison with *S. cerevisiae* ES7, there is the deletion of 2 bp in the a-helix (ES7a) and one bp insertion in the b-helix (ES7b) (Figure 17). So, overall, *C. albicans* ES7 is two nts shorter than *S. cerevisiae*. Moreover, the second crucial parameter is the GC content in the rRNA. GC pairs increase thermal stability because three hydrogen bonds hold the GC base pair together. In *C. albicans,* the GC content in ES7 is 55%, much higher than in *S. cerevisiae* (49% GC) [71].
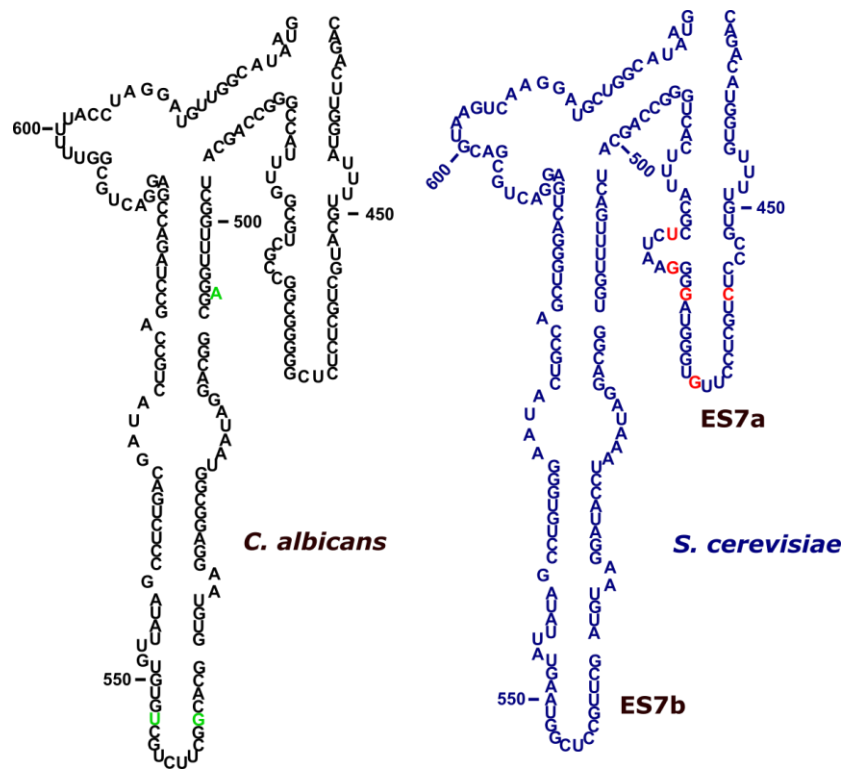
Figure 17 - ES7 comparison in *C. albicans* and *S. cerevisiae*. Deletions are shown in red, and insertion in green

The ES27L expansion segment performs a surprising role in translation fidelity. Increased readthrough, frameshifting, and amino acid misincorporation mistakes are observed in ribosomes with a loss in the distal region of ES27L. In order to promote the binding of a conserved enzyme, methionine aminopeptidase, ES27L functions as an RNA scaffold (MetAP) [72]. Translation starts with the initiator methionine throughout all kingdoms of life (met). It is cleaved off co-translationally from almost one-third of all proteins in eukaryotes and prokaryotes by MetAPs [73]. These results are consistent with the N-terminal processing roles of MetAPs and suggest that ES27L may be holding the MetAP family of proteins close to the exit tunnel, specifically in the eukaryotic ribosome. Through its association with ES27L, MetAP unexpectedly regulates the precision of ribosome decoding along with an improvement in its enzymatic performance. These results show that the ribosome's varied ESs play important functional roles and serve as platforms for binding proteins that regulate translation during evolution. ES27 in *C. albicans* is 18 nts shorter than in *S.cerevisiae* (figure 18). Previously it was found that truncation in ES27a of *S. cerevisiae* leads to higher sensitivity to paromomycin and lower translation fidelity. Such truncation in *C. albicans* could reflect the differences in translation modulation between *S. cerevisiae* and *C. albicans*.
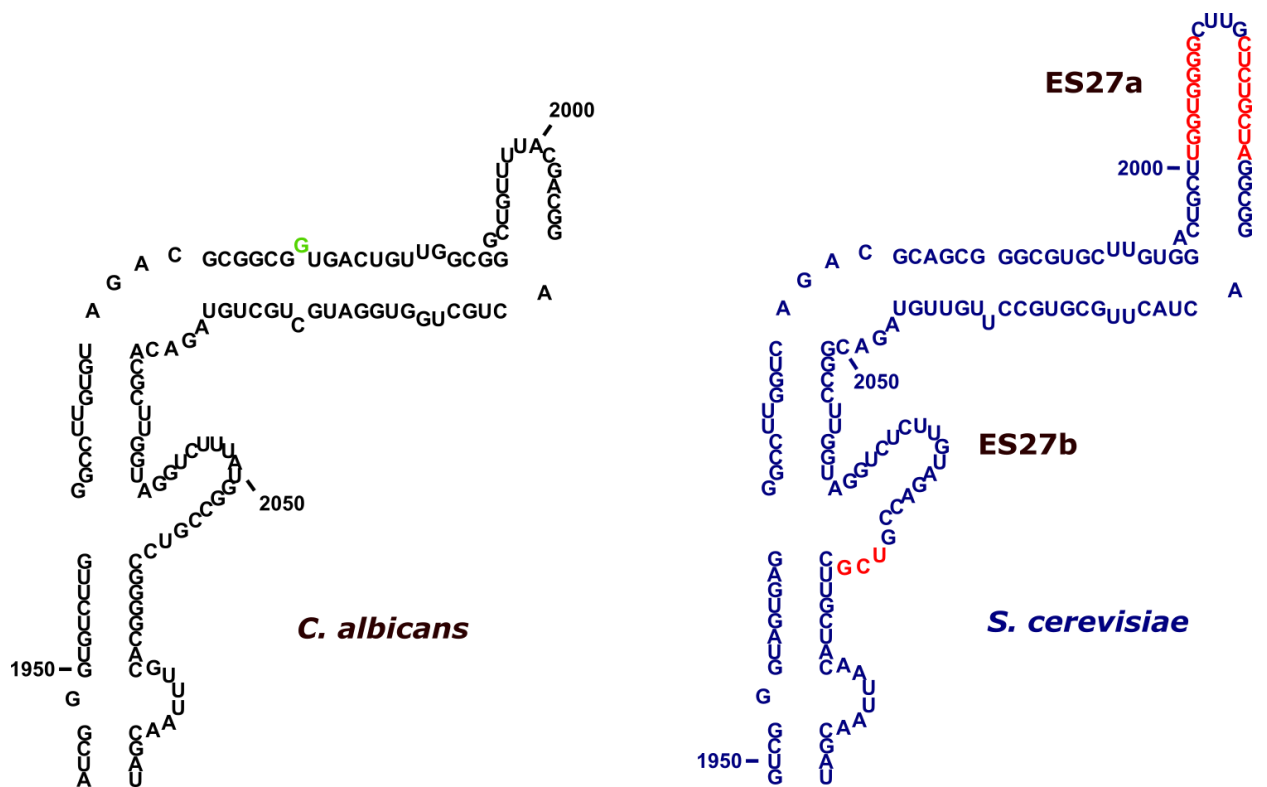
Figure 18 - ES27 comparison in *C. albicans* and *S. cerevisiae*. Deletions are shown in red, and insertion is in green.

Expansion segment ES9L is located on the back of the large subunit between ES7L and below the central protuberance. ES9L is the extension of the bacterial H31 and part of domain II of the 25S rRNA. Helices H28 and H30 have slightly different secondary structures compared to the bacterial template. In *C. albicans* H30 loop is one bp shorter than in *S. cerevisiae*. In the *S. cerevisiae*, the H30 loop is stabilized by eL18 and eL21 protein, so it is interesting how the one bp truncation can affect interaction with eL18 and eL21 (figure 19).
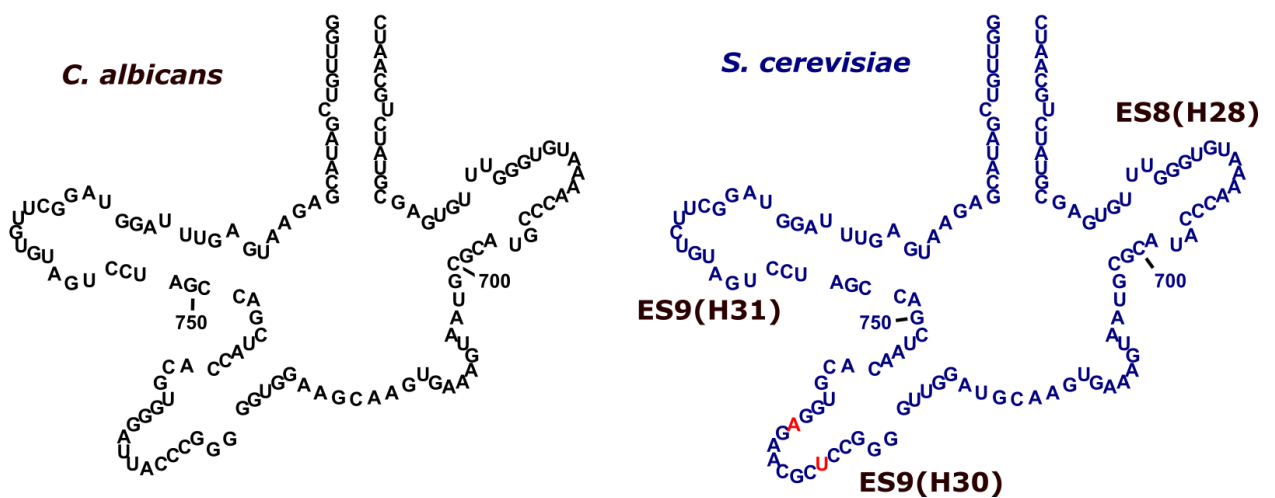


Figure 19 - ES9 comparison in *C. albicans* and *S. cerevisiae*. Deletions are shown in red.

Expansion segment ES31L is located on the side of the 60S subunit and close to ES4L, ES19L, and ES20L. ES31L emerges from H79 and is part of domain V of the 25S rRNA. In both species, *S. cerevisiae* ES31L consists of three helices, ES31La, ES31Lb, and ES31Lc, forming an RNA three-way junction. In *C. albicans,* the ES31b is five nts shorter than the yeast counterpart, and there is a one nt deletion in the linker between ES31a and ES31b loops (figure 20). In *S. cerevisiae,* this loop interacts with the eukaryotic-specific protein eL34. So three bp truncations in the ES31b could reflect the differences in the interaction pattern between the expansion segment and the protein.
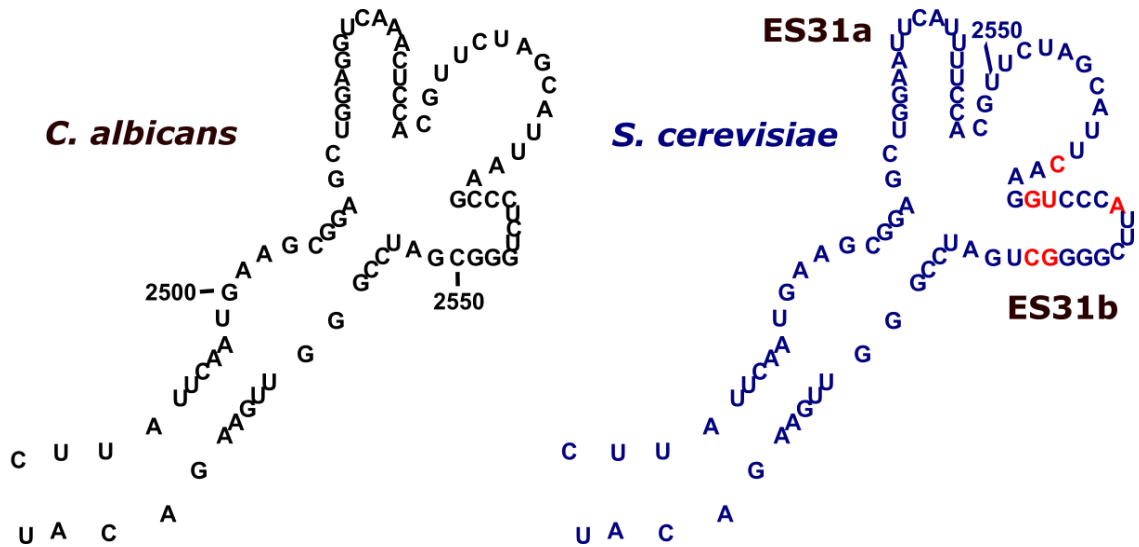


Figure 20 - ES31 comparison in *C. albicans* and *S. cerevisiae*. Deletions are shown in red.

Expansion segment ES39L is located on the back of the large subunit (Figure 9.2.43 A). ES39L emerges from H98 and is part of domain VI of the 25S RNA (Figure 9.2.43 B). ES39L consists of four helices ES39La, ES39Lb, ES39Lc, and ES39Ld. ES39L is the counterpart of the bacterial H98, which is not present in *H. marismortui* [74]. The single-stranded region between ES39La and ES39Lb is closely intertwined with r-proteins. In *C. albicans,* the a-loop is five nts shorter than in *S. cerevisiae* (figure 21). In *S. cerevisiae*, the tetraloop of ES39La interacts with the α-helix of the eukaryote-specific r-protein L6e. So, the five nts truncation in *C. albicans* could lead to losing contact with the eL6 or drastic changes in the interaction pattern.
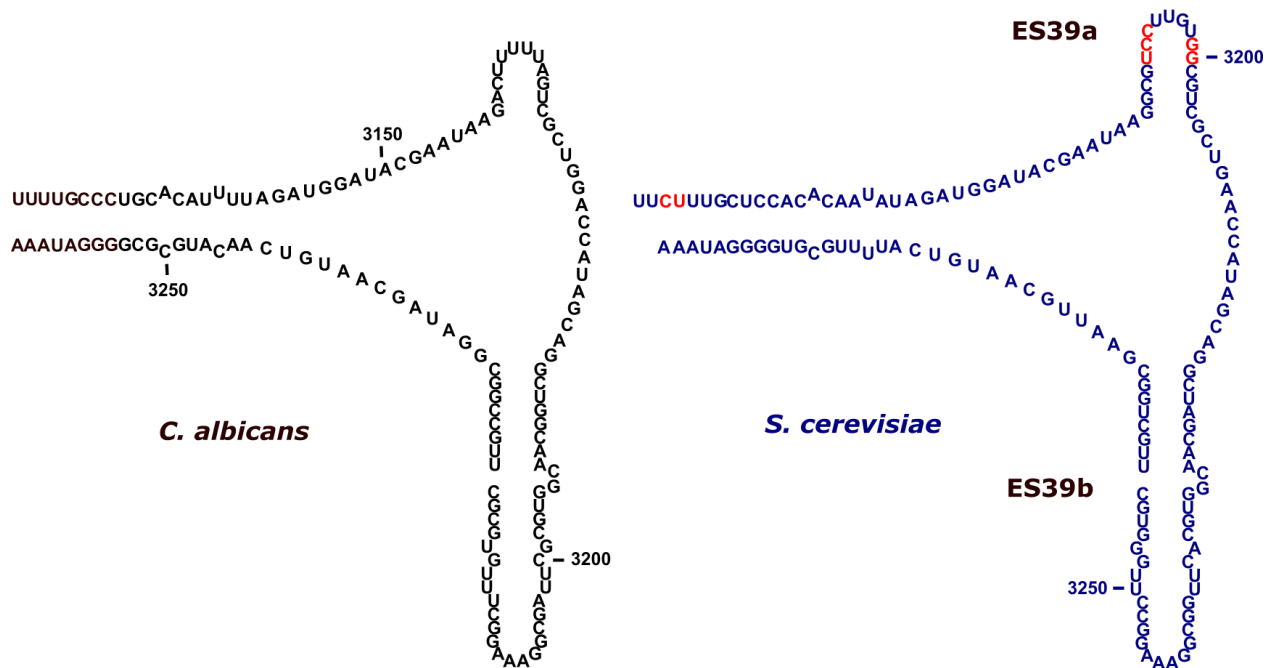
Figure 21 - ES39 comparison in *C. albicans* and *S. cerevisiae*. Deletions are shown in red.

Expansion segment es3 is located on the foot of the small subunit close to expansion segment es6. Es3 is part of the 5' domain of the 18S rRNA. In *S. cerevisiae,* the es3 helix substitutes h9 in bacteria and keeps es3a and es3c c in a close spatial arrangement. The 14-nt-long internal loop between helices es3a and es3b c was modeled to interact with the loop of es6, forming a 9-mer interhelical pseudoknot. es3 interacts with the ribosomal protein S17p and the eukaryote-specific r-protein S4e. In *C. albicans,* there is a 1 bp deletion in the es2 expansion segment followed by es3 (figure 22). The es2a loop is located towards the solvent in *S. cerevisiae* and is usually poorly visible in the available maps. The one bp truncation could lead to the more rigid structure of the a-loop of the es2, but structural approaches should verify it.
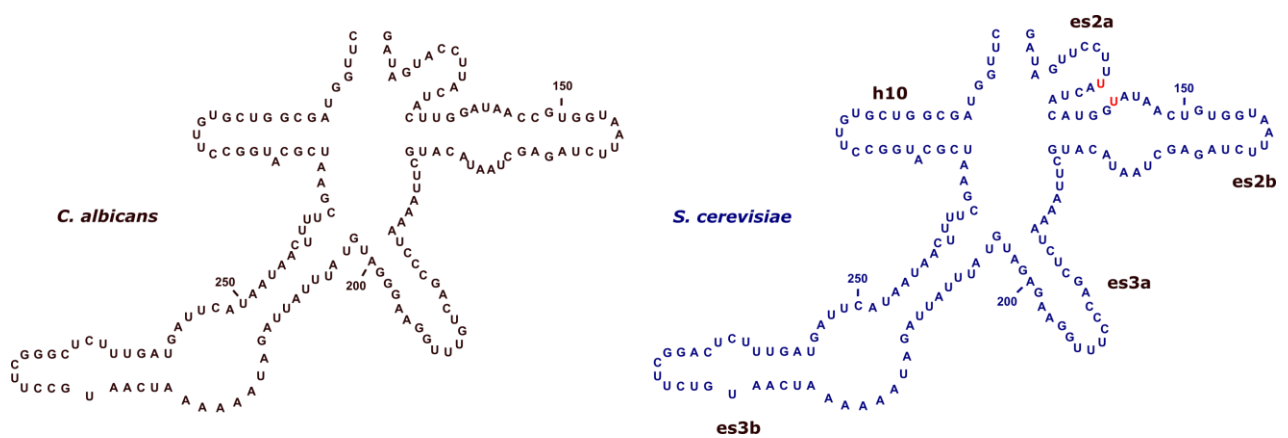


Figure 22 - es3 comparison in *C. albicans* and *S. cerevisiae*. Deletions are shown in red.

Expansion segment es6 is the largest ES on the small subunit located on the platform. es6 is part of the C-domain of the 18S rRNA. In the electron density for *S. cerevisiae*, four helices are visible. Sequence alignments of the bacterial helix 21 with the sequences of es6 of *S. cerevisiae* suggest that the first predicted a-helix es6 could be a eukaryotic counterpart. In *S. cerevisiae*, the eukaryote-specific r-protein eS4 stabilizes es6c. Helix es6b interacts with uS8 and the extension of uS5. In *C. albicans,* there are drastic differences in the length and organization of es6 (figure 23). In the es6c, two uracils are deleted in the single-stranded part of es6c, and one bp insertion is in the helix's tip. The b-loop of the es6 is six bp shorter than the yeast counterpart. All these differences could be a specific feature of *C. albican's* ribosome in interaction with ribosomal and non-ribosomal proteins.
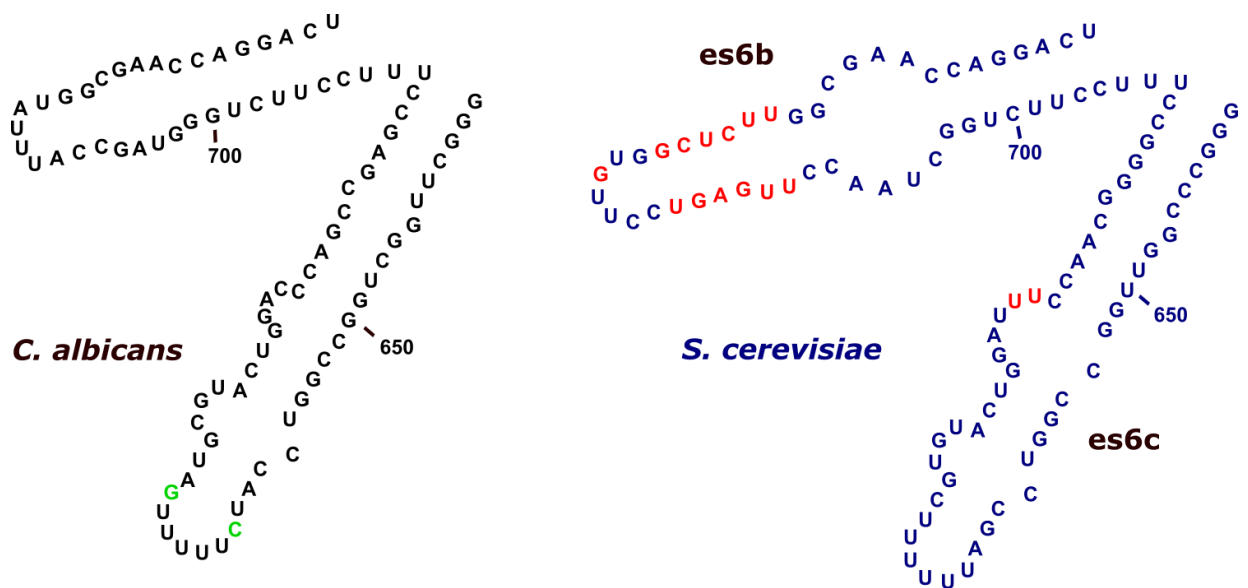


Figure 23 - es6 comparison in *C. albicans* and *S. cerevisiae*. Deletions are shown in red, and insertion in green.

Expansion segment es9s is the extension of helix 39 (h39) located next to h41 on the head of the small subunit. Es9 is part of the 3'M domain of the 18S rRNA. Although the secondary structure is predicted to be helical, h39 is bent like its bacterial counterpart. Two eukaryote-specific r-proteins interact with es9, namely RACK1 with the stem region and an a-helix of eS19 with the minor groove of the es9 loop. The N-terminal extension of uS10 contacts the backbone and minor groove of es9s. In *C. albicans,* there is one nt insertion close to the tip of the es9 loop. This difference could affect the interaction with the uS10 protein (figure 24).

The variable region helix 41 (h41) is denoted as es10. It is located next to es9 on the head of the small subunit. Helix 41 is part of the 3'M domain of the 18S rRNA. In *S. cerevisiae,* a similar kink-turn-fold as in *T. thermophilus* is observed. Helix 41 is closely intertwined with

several proteins. The newly identified eukaryote-specific r-proteins eS19 and eS25 interact with the lower stem region of h41 via the backbone and minor groove. Further, uS7, uS9, and the N-terminal extension of uS10, uS3, and uS13 interacted closely with h41. Such results in tight packing and stabilization of the kink-turn structure. In *C. albicans,* there is a one nt insertion in es10 which closely interacts with the eS19, which could lead to a specific interaction pattern (figure 24).
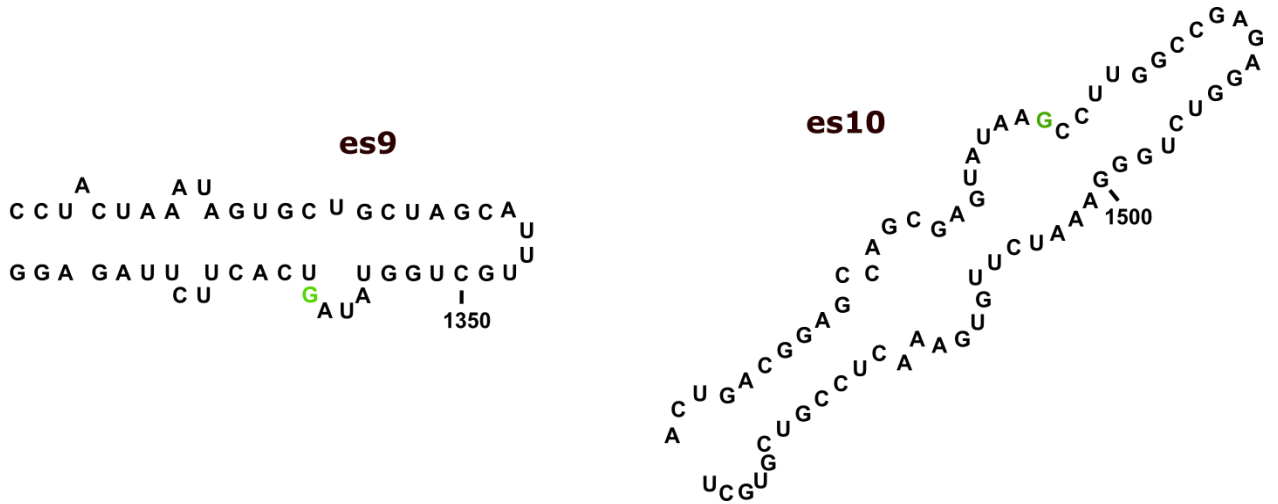


Figure 24 - 1-nucleotide insertion in the es9 and es10 of *C. albicans* 18S rRNA. Insertions are shown in green.

# Ribosomal proteins

The 40S subunit of *C. albicans* consists of 32 ribosomal proteins, and the 60S subunit - 45. All the ribosomal proteins of *C. albicans and the previously described rRNA* have many similarities with the higher eukaryotes. The main difference in *C. albicans* is a missing sequence for the eL41 protein and the truncated by half eL40 protein (Table 7).

eL41 protein is a small 21 aa α-helix protein located on the 60S subunit. In the first high-resolution structure of *S. cerevisiae*, it was established that eL41 forms a bridge between subunits. The sequence for the eL41 protein of *C. albicans* is not presented in all available protein databases. To check whether the sequence of the eL41 protein is missing in the databases or this protein is absent in *C. albicans,* the structure of the *C. albicans* ribosome should be solved.

The second example is the eL40 protein. eL40 is twice as short (52 aa instead of 128 aa in *S. cerevisiae*). eL40 is a ubiquitin-binding protein; the first 74 aa corresponds precisely to the ubiquitin-binding moiety in *S. cerevisiae*. Furthermore, several data show that the ubiquitin-binding moiety is cleaved during ribosome assembling. As proof, in *S. cerevisiae*, the starting part of the protein is not visible, assuming it is cleaved during ribosome assembly. In this sense, we can consider that the eL40 consists of 52 aa in *S. cerevisiae* and *C. albicans*, and there are no drastic differences between the species.

Table 7 - Ribosomal proteins comparison in LSU in *C. albicans* and *S. cerevisiae*.

| Protein | Length (aas) | | Identity |
|---------|--------------|--------------|----------|
| | *C. albicans* | *S. cerevisiae* | |
| uL1 | 217 | 217 | 88.48% |
| uL2 | 254 | 254 | 90.94% |
| uL3 | 389 | 387 | 85.01% |
| uL4 | 363 | 362 | 76.18% |
| uL5 (L11) | 174 | 174 | 87.36% |
| uL6 (L9) | 191 | 191 | 71.73% |
| eL6 | 176 | 176 | 81.14% |
| eL8 | 262 | 256 | 77.43% |
| uL10 (P0) | 312 | 312 | 76.28% |
| uL11 (L12) | 165 | 165 | 87.88% |
| uL13 (L16) | 200 | 199 | 80.81% |
| eL13 | 202 | 199 | 69.19% |

| | | | |
|---|---|---|---|
| uL14 | 137 | 137 | 86.13% |
| eL14 | 131 | 138 | 65.93% |
| uL15 (L28) | 149 | 149 | 81.21% |
| eL15 | 204 | 204 | 89.66% |
| uL16 (L10) | 220 | 221 | 86.57% |
| uL18 (L5) | 298 | 297 | 78.11% |
| eL18 | 186 | 186 | 86.02% |
| eL19 | 190 | 189 | 79.37% |
| eL20 | 172 | 172 | 81.40% |
| eL21 | 160 | 160 | 82.50% |
| uL22 (L17) | 185 | 184 | 79.35% |
| eL22 | 124 | 121 | 63.48% |
| uL23 (L25) | 142 | 142 | 78.17% |
| uL24 (L26) | 127 | 127 | 81.89% |
| eL24 | 155 | 155 | 76.77% |
| eL27 | 136 | 136 | 80.88% |
| uL29 (L35) | 120 | 120 | 80.00% |
| eL29 | 63 | 59 | 92.00% |
| uL30 (L7) | 241 | 244 | 76.89% |
| eL30 | 106 | 105 | 81.13% |
| eL31 | 112 | 113 | 81.82% |
| eL32 | 131 | 130 | 76.56% |
| eL33 | 107 | 107 | 84.11% |
| eL34 | 122 | 121 | 88.89% |
| eL36 | 99 | 100 | 69.07% |
| eL37 | 90 | 88 | 89.16% |
| eL38 | 78 | 78 | 69.23% |
| eL39 | 51 | 51 | 80.39% |
| eL40 | **52** | **128** | 94.23% |
| eL41 | **-** | **25** | - |
| eL42 | 106 | 106 | 92.45% |
| eL43 | 92 | 92 | 85.87% |
| P1/P2 | 106 / 108 | 106 / 106 | 67.92% / 64.21% |

The ribosomal proteins in the 80S subunit of *C. albicans* are similar to those in *S. cerevisiae*. The overall identity of proteins between the two species is 80,53%, with the lowest score (63,48%) for the eL22 protein and the highest identity (92.45%) for the eL42 protein. Despite the numerous difference in the amino acid composition of the protein, the overall length does not differ much between species. Nevertheless, several proteins have shorter/longer α-helix and β-strand regions.

Using the BLAST program, it is possible to identify the regions that could have some insertions/deletions while comparing several species [75]. In the large subunit, 21 proteins out of 45 have lengths different from *S. cerevisiae*. Most of these length variations are located in the terminal part of the protein. According to the alignment statistic, in the LSU, there are seven proteins with insertions/deletions in the N-terminal part and ten proteins with variations in the C-terminal part. Moreover, there are seven proteins with substantial changes in the body part of the protein, so it was interesting to identify how these variations could change the structure of the protein and its interaction with rRNAs and other ribosomal proteins.

To understand whether it is possible to interpret these differences from a structural point of view, the parts with variable lengths were inspected in the *S. cerevisiae* vacant ribosome structure (PDB 4V88, Table 8) [76]. Most changes have occurred in the eukaryotic-specific proteins (7 variations in universally conserved r-proteins, 12 in eukaryotic-specific r-proteins).

Among all these variations, only a few are placed in proximity to other proteins or rRNA; most are located in the periphery of the ribosome. There are several examples of meaningful length variations:

1) The C-terminal of uL4 interacts with eL21. One aa insertion could strengthen the interaction between uL4 and eL21

2) The N-terminal of eL6 interacts with eL32 and H46. The one aa deletion in the N-terminal could lead to more flexibility in this region.

3) In the eL8, there is a five aas insertion in the C-terminal. In *S. cerevisiae,* this part does not interact with other proteins or rRNA, but in *C. albicans,* it could interact with the eS1 protein, making an additional bridge between subunits.

4) In the uL13 variable, part interacts with uL33. One aa insertion in the N-terminal could strengthen the interaction between uL13 and uL33.

5) The eL13 protein has three insertions between 135-136 aas (*S. cerevisiae* numeration). According to the secondary structure prediction and 4V88 structure, this part has a helical structure but does not interact with other parties. So, it is unclear how the helix extension in the body of the protein could affect the structure and function of the eL13 protein.

Table 8 - Location of the insertion and deletion in LSU proteins of *C. albicans* compared to *S. cerevisiae*

| Protein | Location / number of insertion (I) / deletion (D) | | | Visibility in 4V88 |
|---------|------------|------------|------|--------------------|
|         | N-terminal | C-terminal | Body |                    |
| uL3  | -   | **2 I** | -   | Not visible |
| uL4  | 1 **I** | - | -   | Visible |
| eL6  | 1 D | -   | 1 D | Not visible |
| eL8  | 1 I | 5 I | -   | Visible |
| uL13 | 1 I | -   | -   | Visible |
| eL13 | -   | 1 I | 2 I | Visible |
| eL14 | 2 D | -   | 5 I | Visible |
| uL16 | -   | 1 D | -   | Visible |
| uL18 | -   | 1 I | -   | Visible |
| eL19 | -   | 1 I | -   | Visible |
| uL22 | -   | 1 I | -   | Visible |
| eL22 | -   | -   | 3 I | Visible |
| eL29 | -   | 4I  | -   | Visible |
| uL30 | 2 D | -   | 1 D | Not visible |
| eL30 | 2 I | 1 D | -   | Not visible |
| eL31 | 1 D | -   | -   | Not visible |
| eL32 | 1 I | -   | -   | Visible |
| eL34 | -   | 1 I | -   | Not visible |
| eL36 | 1 D | -   | -   | Visible |
| eL37 | -   | 2 I | -   | Visible |
| P2   | -   | -   | 2 I | Not visible |

6) In the eL14, there is a two aa deletion in the N-terminal. The N-terminal is visible in 4V88 but does not interact with the environment. Also, there are four aas deletions between 26-27 (*S. cerevisiae* numeration) and two aas deletions in the 45-46 range. These two parts correspond to the β-strand part of the *S. cerevisiae*, but they are not located near other proteins or rRNA. By aligning the two structures of *C. albicans* and *S. cerevisiae*, it is visible that the two β-strands are shorter in *C. albicans* (Figure 25). It could indicate that this

protein has a more compact 3D structure, and it could change the interaction with the extracellular proteins because this protein is located on the surface of the ribosome.
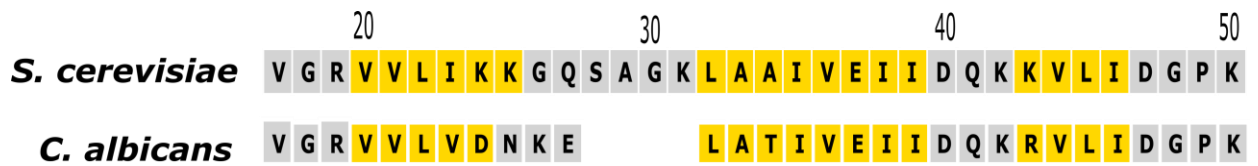


Figure 25 - β-strand truncation in the eL14 of the *C. albicans* (β-strand is colored in yellow)

7) In the eL22, there are three insertions in the protein body. eL22 is located between H58 and H96 of the 25S rRNA. The first two aas insertion is located between 58-59 residues, corresponding to the β-strand region directed to the outer part. Also, there is a one aa insertion between 70-71 residue. In *S. cerevisiae,* this region interacts with H57 of the 25S rRNA. In *C. albicans*, one aa insertion in this part could create an additional interaction with H57 making it more stable.

8) In the eL32 protein, there is one insertion in the N-terminal part of the protein. This part is visible in the available structure of the vacant *S. cerevisiae* structure (4V88) and is located quite close to the ES7. Short insertion in the N-terminal in *C. albicans* could create a direct interaction with ES7, which is drastically different in the *C. albicans*

In the other 13 proteins, all the segments with variable lengths are exposed to the solvent and do not interact with rRNAs and ribosomal proteins. No data shows these segments' interaction with the proteins outside the ribosome. However, it is interesting if these changes could regulate the translation in *C. albicans*.

In the small subunits, ribosomal proteins are more identical to those in *S. cerevisiae* (Table 9). The overall identity of the ribosomal proteins in the SSU is 83,02%, which is more than 2% higher than the LSU. The most identical protein is uS12 (95.86% identity), and RACK1 (63. 48%) is the most different protein. At the same time, the variation in protein length is much higher in the SSU. For example, the uS2 protein is 9 aas longer in *C. albicans*, uS3 is 11 aas longer, and eS10 is 13 aas longer.

In strict opposition to the LSU, where the number of insertions is higher for the eukaryotic-specific proteins, in the SSU, universally conserved proteins differ more drastically than eukaryote-specific ones compared to *S. cerevisiae*. Moreover, the length of these insertions is higher in SSU. In LSU, the average deviation is app. two aas, with a maximum value of 7 aas. On the contrary, in the SSU, the mean value is two times higher, 4 aas insertion/deletion, with the higher insertion of 13 aas in the eS10 protein.

Table 9 - Ribosomal proteins comparison in SSU in *C. albicans* and *S. cerevisiae*

| Protein | Length (aas) | | Identity |
|---|---|---|---|
| | *C. albicans* | *S. cerevisiae* | |
| eS1 | 256 | 255 | 79.30% |
| uS2 (S0) | 261 | 252 | 83.09% |
| uS3 | 251 | 240 | 69.17% |
| uS4 (S9) | 189 | 197 | 86.26% |
| eS4 | 262 | 261 | 86.64% |
| uS5 (S2) | 249 | 254 | 79.91% |
| eS6 | 236 | 236 | 78.72% |
| uS7 (S5) | 225 | 225 | 78.67% |
| eS7 | 186 | 190 | 80.00% |
| uS8 (S22) | 130 | 130 | 95.38% |
| eS8 | 206 | 200 | 80.58% |
| uS9 (S16) | 142 | 143 | 89.13% |
| uS10 (S20) | 119 | 121 | 81.63% |
| eS10 | 118 | 105 | 77.45% |
| uS11 (S14) | 132 | 138 | 94.92% |
| uS12 (S23) | 145 | 145 | 95.86% |
| eS12 | 143 | 143 | 73.77% |
| uS13 (S18) | 145 | 146 | 86.21% |
| uS14 (S29) | 56 | 56 | 85.71% |
| uS15 (S13) | 151 | 151 | 90.67% |
| uS17 (S11) | 155 | 156 | 82.69% |
| eS17 | 137 | 136 | 80.88% |
| uS19 (S15) | 142 | 142 | 68.31% |
| eS19 | 145 | 144 | 86.11% |
| eS21 | 87 | 87 | 88.51% |
| eS24 | 135 | 135 | 88.89% |
| eS25 | 105 | 108 | 80.77% |
| eS26 | 119 | 119 | 83.90% |
| eS27 | 82 | 82 | 69.51% |
| eS28 | 67 | 67 | 95.52% |
| eS30 | 63 | 63 | 85.71% |
| eS31 | 193 | 152 | 88.74% |
| RACK1 | 317 | 319 | 66.98% |

Table 10 - Location of the insertions and deletions in SSU of *C. albicans* compared to *S. cerevisiae*. * - not included in the statistics

| Protein | Location / number of insertion (I) / deletion (D) | | | Visibility in 4V88 |
|---|---|---|---|---|
| | N-terminal | C-terminal | Body | |
| eS1 | - | 1 I | - | Not visible |
| uS2 | - | 9 I | - | Not visible |
| uS3 | 1 I | 8I | 2I | Visible |
| uS4 | - | 8 D | - | Not visible |
| eS4 | - | - | 1 I | Visible |
| uS5 | 5 D | - | - | Not visible |
| eS7 | 3 D | - | 1 D | Visible |
| eS8 | - | - | 6 I | Not visible |
| uS9 | 1 D | - | - | Visible |
| uS10 | 1 D | 1 D | - | Not visible |
| eS10 | - | 13 I | - | Not visible |
| uS11 | 6 D | - | - | Not visible |
| uS13 | - | 1 D | - | Visible |
| uS17 | - | 1 D | - | Visible |
| eS17 | - | 1 I | - | Not visible |
| eS19 | - | 1 I | - | Visible |
| eS25 | - | 3 D | - | Visible |
| eS31* | 42 I | - | - | Not visible |
| RACK1 | - | - | 4 D | Visible |

In contrast to LSU, in the SSU, most modified proteins are truncated and not extended. Concerning the location of these variations, only a few are placed in proximity to other proteins or rRNA; most are located in the periphery of the ribosome, as in LSU. There are several examples of meaningful length variations (Table 10):

1) In the uS3 protein, there are modifications in the N and C-terminals and the body. There is a one aa insertion in the N-terminal compared to *S. cerevisiae*. In *S. cerevisiae,* the N-terminal interacts with the es10 expansion segment (h41). Therefore, the one aa truncation in the N-terminal could weaken the interaction with the 18s rRNA. In the body of the us3, there is a truncation between 216 and 218 residues (*S. cerevisiae* numeration).

This part of the body interacts with the 196th residue of the guanine nucleotide-binding protein RACK1. So, one aa deletion could change the interaction pattern between 2 proteins. The C-terminal protein, where there is an eight aas insertion in *C. albicans,* is not visible in the 4V88 map.

2) In the eS7 protein of the *C. albicans* ribosome, there are three aa deletions in the N-terminal and one aa deletion in the body of the protein (figure 26). Both parts suggested forming the α-helix based on the secondary structure and alpha fold predictions. The N-terminal of the eS7 protein interacts with the C-terminal of the eL19 protein. It is worth mentioning that the C-terminal of the eL19 is extended by one aa in the *C. albicans*. Along with the 3aa truncation in the N-terminal of the eS7 protein, it could create a different environment and interaction between the proteins. Also, the deletion in the body of the eS7 could reflect the change in the interaction between eS7 and eL19 because the α-helix at the beginning of the protein is located close to the C-terminal of eL19.



Figure 26 - Deletions in the eS7 protein of the *C. albicans* (α-helix is colored in pink)

3) In the eS10 protein, there is a 13 aas insertion in the C-terminal part of the protein. The C-terminal part in *S. cerevisiae* is located near the uS3 protein (residues 87-95). The C-terminal extension in *C. albicans* could create a specific interaction with the uS3 protein, and it will probably become visible (the C-terminal of the uS3 protein is not visible in 4v88).

4) The uS13 protein has a one aa deletion in the C-terminal. Even though it is an unstructured part of the protein, it is visible in the vacant *S. cerevisiae* structure and directly interacts with the Stm1 protein and h32 helix of the 18S rRNA. The one aa truncation of the C-terminal in *C. albicans* could lead to a loss of direct interaction followed by increased pocket flexibility.

5) Another example is the uS17 protein. Despite the high similarity with the *S. cerevisiae* counterpart, there is a one aa deletion in the C-terminal part in *C. albicans*. In *S. cerevisiae,* this part interacts with the h21 of the es6 expansion segment. Therefore, losing one aa could lead to a weakened interaction between the uS17 protein and the h21 helix in *C. albicans*.

6) The last example of significant modification is a RACK1 protein. RACK1 protein is also known as guanine nucleotide-binding protein and is located close to the mRNA tunnel exit. It was treated as a non-ribosomal protein for several decades, but according to the last nomenclature, it now corresponds to the family of SSU proteins. The RACK1 protein has two deletions in the so-called region "loop." It is not yet clear how this loop functions, but in the available crystal structure, this loop is disorganized and solvent-exposed. Nevertheless, proximity to the mRNA tunnel could mean the possible interaction of this protein with the mRNA coming out from the tunnel.

Despite the presented differences, all of them are based on the available high-resolution structure of the vacant *S. cerevisiae* ribosome and the secondary structure prediction tool. To verify this suggestion, the structure of the *C. albicans* ribosome is necessary.

Apart from the ribosomal proteins in the *S. cerevisiae* vacant ribosome, only one non-ribosomal protein was found – Stm1. This is a stress protein that binds to the ribosome upon glucose starvation when the majority of polysomes are switched to monosomes. In our lab, the body of the Stm1 (90-120 residues) was previously found in the entry of the mRNA tunnel. This part of the protein mimics the mRNA, so incoming mRNA cannot enter the ribosome.

According to the protein databases, in the *C. albicans* genome, the presence of the Stm1 protein is confirmed. Surprisingly, the Stm1 protein in *C. albicans* is the most dissimilar, with only 39,74% of identity. Because this protein is indispensable for ribosome preservation, the 3D structure of this protein needs to be solved. By aligning *C. albicans* stm1 protein with *S. cerevisiae,* there are many insertions/deletions, such as:

1) 4 aa insertion in the N-terminal part. In *S. cerevisiae*, this part interacts with the uS13 so that the short extension of the N-terminal could strengthen the contact between them.

2) There is a one aa deletion between 56-57 residues (*S. cerevisiae* numeration). This part is directly contacting with the uS19 protein.

3) There is a six aa deletion in the 68-75 range. In *S. cerevisiae*, this part is located near the uS13 protein and the h32 helix. Therefore, six aa deletions in this part could completely change the interaction in this region.

4) A 1 aa insertion is proposed to occur in the 108-110 range. This part is located in the mRNA entry tunnel and interacts with the 18S rRNA (h18 helix). This is the only difference in the part of the protein located in the mRNA tunnel, so even a minor change in the sequence should not affect its binding mechanism in *C. albicans*.

5) The eight aas insertion is located between 152-163 residues. In *S. cerevisiae*, it is an α-helical part located on the head of the 40S subunit. Based on the secondary structure prediction, this helix should be longer in *C. albicans* to create new contacts with the 40S subunit.

To sum up, even though the stm1 is the most different protein in the ribosome, the segment with the variable length is not located on its functional site – in the 85-105 region, which is located in the mRNA tunnel entry where it blocks mRNA binding and prevents binding of tRNAs in the A and P sites due to steric hindrance. So, we can consider that the interaction pattern in the mRNA tunnel should be the same as in *S. cerevisiae*. However, the other parts could interact differently with the 40S compared to other eukaryotes.

## Functional sites

Despite the differences in sequence in the core and the periphery of the *C. albicans* ribosome, the main interest represents the functional sites of the ribosome. Several functional sites are distinguished: peptidyl transferase center, E-tRNA binding site, decoding center, mRNA, and protein tunnels. Usually, functional sites are highly conserved in eukaryotes, but in *C. albicans,* there are several crucial differences.

### Peptidyl transferase center

The ribosomal peptidyl transferase center (PTC) resides in the large ribosomal subunit and catalyzes the two principal chemical reactions of protein synthesis: peptide bond formation and peptide release. PTC comprises only 25S rRNA nucleotides and is located adjacent to the CCA ends of the A-tRNA binding site (A-site) and the P-tRNA binding site. Therefore, the nucleotides, which are directly interacting with the CCA-tail of the tRNAs (aminoacylated tRNA), are of utmost interest to us because they represent the primary target for current eukaryotic-specific inhibitors.

The A-site on the 60S subunit of the *C. albicans* ribosome is formed by the following nucleotides: C2793, U2845, U2847, G2894, U2895, G2924, U2926, and A2943 (Figure 27). G2894 directly forms a canonical base pair with C75 of the A-tRNA, whereas U2895 and G2924 directly interact with C74 and A76, respectively. Other mentioned nucleotides directly interact with the incoming amino acid attached to the end of the CCA tail. The conformation of U2847 in the A-site is structurally different between bacteria and eukaryotes. The conformation of the U2847 highly depends on the 2375 nucleotide, which in the case of bacteria is a cytosine, but in eukaryotes is adenine. This finding made it possible to create the A-site binding eukaryotic-specific inhibitors.

The P-site on the 60S subunit of the *C. albicans* ribosome is formed by the G2591, G2592, A2791, and A2792 (Figure 27). G2591 forms a canonical base pair with the C75, whereas G2592 forms a base pair with the C74. In turn, A76 of the P-tRNA CCA tail is not forming a base pair and just directly interacts with the A2791 and A2792. The P-site is highly conserved between bacteria and eukaryotes, so there are not yet specific inhibitors targeting the P-site.
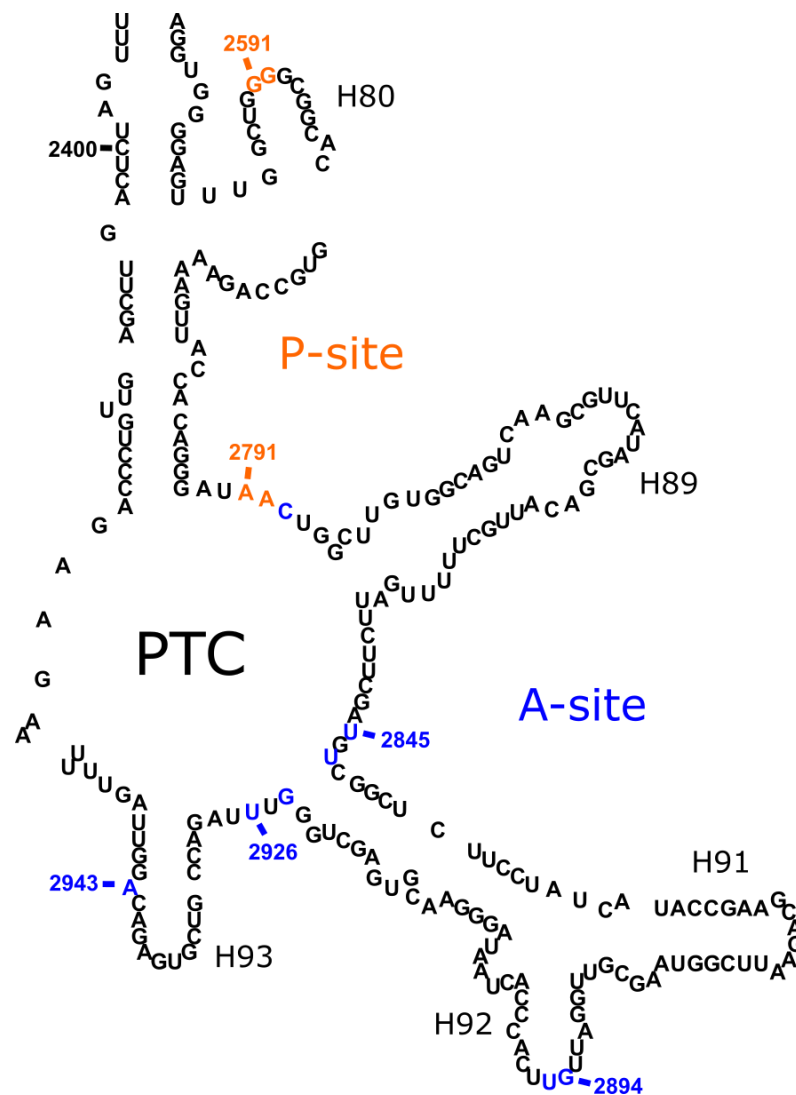
Figure 27 - Peptidyl transferase center (PTC) loop on the 25S rRNA of *C. albicans*. A-site nucleotides are colored in blue, and P-site in orange [77].

If we compare *C. albicans* with other eukaryotes, the catalytic nucleotides of PTC are 100% sequence-identical. This fact suggests that the catalytic center is highly similar across the eukaryotic domain, and there should be no difference during the reaction of peptide bond formation.

E-tRNA binding site

The E-tRNA binding site on the 60S subunit is the only binding site that composes not only the rRNA. H88 encounters the E-site from one side, H13 from another, and two ribosomal proteins, uL15 and eL42. The deacylated tRNA binds into the E-site in the following manner: A76 forms a stacking interaction with 2765 and C75 stacks on the Y43 of the eL42 protein.

Among all three tRNA binding sites on the large subunit, the E-site is the most diverse across species, showing different nucleotide and protein content in bacteria, archaea, and

eukaryotes. The part of the eL42 protein located in the E-site replaces the 23S rRNA in bacteria so that the binding pocket is drastically different across the species.

Compared to other eukaryotic species, the *C. albicans* ribosome has two crucial alterations in the E-site (Table 11). In the ribosomal protein eL42, proline 56 is substituted for glutamine and valine 57 for isoleucine. We have found only two differences in the organization of the E-tRNA binding site of the large subunit between *S. cerevisiae* and *C. albicans* ribosome.

Table 11 - E-site composition variations across the eukaryotic domain

| Site | Molecule name | Residue | | |
|---|---|---|---|---|
| | | *C. albicans* | *S. cerevisiae* | *H. sapiens* |
| E | 25S rRNA | G91 | G92 | G91 |
| | | U2735 | U2763 | U4340 |
| | | C2736 | C2764 | C4341 |
| | | G2765 | G2793 | G4370 |
| | | G2766 | C2794 | G4371 |
| | eL42 protein | Y43 | Y43 | Y41 |
| | | K55 | K55 | K53 |
| | | **Q56** | **P56** | **P54** |
| | | **I57** | **V57** | **I55** |
| | uL15 protein | Q38 | Q38 | Q38 |
| | | H39 | H39 | H39 |

Some data indicate that mutation of the 56th aa in eL42 could lead to changes from weak to high inhibition of E-site inhibitors, such as CHX [78]. Indeed, in the case of replacing proline with glutamine, resistivity is relatively high. Several functional studies prove this hypothesis, but it has never been demonstrated structurally.

The V57I mutation occurs not only in *C. albicans* but also in *H. sapiens*. However, based on the functional and structural data, this mutation does not lead to resistance to CHX. *H. sapiens* are sensitive to glutarimide-based compounds on the same level as *S. cerevisiae*. This fact indicates that the V57I mutation does not significantly change the E-site binding pocket but could change the interaction between the E-site tRNA and the 57th residue due to the higher hydrophobicity of the isoleucine residue.

Decoding center

The decoding center of the ribosome forms a geometrically restricted pocket that accurately selects aminoacyl-tRNA by mRNA codons positioned in the A-site. In addition, the decoding center contains the universally conserved adenines (A1755 and A1756 in *S. cerevisiae*), which are part of the helix 44 of 18S rRNA.

In *C. albicans,* these two adenines (A1742 and A1743) are also conserved. Considering the whole of helix 44, with the two conserved adenines (A1742 and A1743 in *C. albicans* numbering), there are no insertions/deletions compared with *S. cerevisiae*. However, there are differences in the sequence between them. For example, there are 13 bps which are different from those in *C. albicans*, so the overall identity between h44 in the two species is 86% (Figure 28). The GC content in the h44 of *C. albicans* is 49%, slightly lower than in *S. cerevisiae* (50%). This means that the stability and the secondary structure of the h44 should not be significantly different between the two species. The closest bp substitution is in the three bps (C1636-G1738). In *S. cerevisiae,* these pairs have identical nucleotides, but the C is inverted to G and vice versa. (G1649-C1751). It is unclear if this inversion affects the position of the decoding nucleotide, and it could be checked only after obtaining the high-resolution structure of the *C. albicans* ribosome.
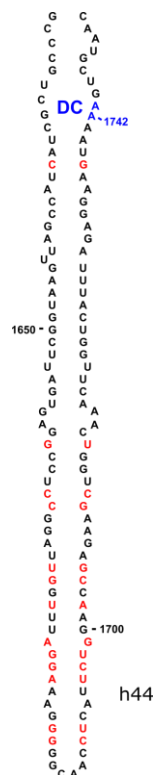


Figure 28 - Decoding center (DC) location on the h44 of the 18S rRNA of *C. albicans*. DC nucleotides are colored in blue, and bps different from *S. cerevisiae* are red.

In addition to the decoding nucleotides, another nucleotide (A2234, 25S rRNA) is located on H69 and contributes to the interaction between the ribosome and the substrates. Structural studies of tRNA and release factors bound to the ribosome reveal that H69 of the large subunit rRNA makes extensive contact with all of these factors. This universally conserved helix forms an intersubunit bridge B2A that is proximal to the substrate-binding cleft and directly contacts the functionally critical h44 of 18S rRNA, which contains two of the three nucleotides known to directly interact with the decoding helix (codon-anticodon) during tRNA selection (A1742 and A1743).

In *C. albicans*, the H69 is identical to that in *S. cerevisiae*; therefore, the substrate binding and pre-post accommodation are conserved in the higher eukaryotes. In bacteria, H69 contacts incoming tRNA in both the pre-and post-accommodation steps near positions 25/26 of the D stem and position 38, located near the anticodon stem; so, due to the similarity between bacteria and eukaryotes, we can assume the exact mechanism in *C. albicans*.

Peptide exit tunnel

During the translation process, the growing peptide passes through the peptide exit tunnel. In *S. cerevisiae,* this tunnel is ~65Å in length (from the PTC till the exit from the tunnel) and ~12-13Å in diameter. The channel wall in eukaryotes consists of the 25S rRNA (H63, H35, and PTC loop) and ribosomal proteins uL4, uL22, and eL39.

The significant difference between eukaryotes and bacteria is the narrower width of the tunnel due to insertions in the uL4 protein. The second difference between them is a mutation of A2081 (in *T. thermophilus*) to G2400 (in *S. cerevisiae*). These two main differences between bacteria and eukaryotes lead to the insensitivity of eukaryotes to macrolides. Macrolides bind to the protein tunnel with direct interaction with A2081. Hence, A to G substitution and narrowing of the tunnel leads to the absence of inhibitors that bind to the protein tunnel of eukaryotes.

The sequence of the protein tunnel in *C. albicans*, *S. cerevisiae*, and *H. sapiens* has several differences between the species (Table 12). There is a G83H mutation in the uL4 protein of *C. albicans* compared to *S. cerevisiae*. The G83H mutation is located in the vicinity of the tunnel, and in principle, it could be used for the specific compound search. Also, there is a T34K mutation in the eL39 protein, limiting the free volume in the tunnel. However, there is no significant difference between *C. albicans* and *H. sapiens so* it could be a bottleneck in the search for the specific anti-Candida compound targeting the peptide exit tunnel.

Table 12 - Peptide exit tunnel composition variations across the eukaryotic domain.

| Site | Molecule name | Residue | | |
|---|---|---|---|---|
| | | *C. albicans* | *S. cerevisiae* | *H. sapiens* |
| **Peptide exit tunnel** | 25S rRNA (H63, H35, PTC loop) | G2378 | G2400 | G3889 |
| | | A2095 | A2117 | A3606 |
| | | A878 | A882 | A1594 |
| | | U2950 | U2978 | U4540 |
| | uL4 protein (65-69, 76-86) | W66 | W65 | W67 |
| | | **G79** | **G78** | **R80** |
| | | **H84** | **G83** | **H85** |
| | uL22 protein (126-130, 133-137) | R128 | R128 | R128 |
| | | I136 | I136 | I136 |
| | eL39 protein (22-28, 34-39, 46-47) | **L23** | **L23** | **I23** |
| | | **K34** | **T34** | **K34** |
| | | R46 | R46 | R46 |

mRNA-tunnel

The last functional site of the 80S ribosome is the mRNA tunnel. Usually, the mRNA tunnel is divided into two parts: the entry and exit parts. The mRNA enters the ribosome through a channel that wraps around the neck of the 40S subunit. The 5′ end of the mRNA enters the groove between the head and platform at the back of the platform, wraps around the subunit's neck, and exits on the opposite side, between the head and shoulder.

The entry part of the tunnel consists mainly of the 18S rRNA and two ribosomal proteins: eS30 and eS4 (Table 13). The tunnel's entry part composition is similar to *S. cerevisiae* and *C. albicans*. There are only 3 single-point mutations in the 116 residues of the eS4 protein, alanine in *C. albicans*, aspartic acid in *S. cerevisiae*, and proline in *H. sapiens*. Even though the side chain is placed toward the channel vicinity, it should not change the charge distribution in the vicinity of the tunnel due to the small changes in the side-chain nature. Also, there is the substitution of the 59th residue of the eS30 protein (Table 13), but as for the eS4 protein, the side-chain length and nature are almost the same in all three species. The rRNA composition of the mRNA entry tunnel is highly conserved between species.

The tunnel's exit comprises the 18S rRNA and several small subunit ribosomal proteins: eS1, uS2, uS7, uS11, eS17, eS26, and eS28. The 18S rRNA part of the mRNA tunnel comprises helices h28, h23, h40, and h44. The nucleotide composition of the loops exposed to the tunnel is

identical between the species (Table 13). However, in the ribosomal proteins, which form the mRNA exit tunnel, there are single mutations in the proteins eS1, eS17, and es26. Some of this substitution could be interesting in terms of the specific interaction between mRNA and the tunnel walls, but it needs to be studied thoroughly in the presence of the long mRNA sequence.

The main interest here is the uS7 protein. The 150-156 residues range is exposed in the vicinity of the mRNA of the tunnel. In *S. cerevisiae,* this region adopts a b-strand secondary structure (loop region of the strand), and the sequence of this loop is highly dissimilar among the eukaryotic species. In *C. albicans*, compared to *S. cerevisiae*, there are four substitutions (G151S, G152S, A154T, A155V). Compared to the *H. sapiens* sequence, there are two differences: R151S and A152S. Since this loop region is responsible for the narrowing of the polypeptide tunnel, it could be used as a promising drug target. To date, there are no small-molecule compounds targeting this region, but they could become a potential target for inhibitors in the future.

To sum up all the functional sites of the *C. albicans* ribosome, the utmost interest is the E-site on the 60S subunit due to the known resistivity of the *C. albicans* to the cycloheximide, as well as the mRNA tunnel due to several differences in the sequences of the proteins forming the walls of the mRNA tunnel. These two sites could be further used as promising targets for specific anti-Candida inhibitors. To get in-depth details of these regions, the high-resolution structure of the *C. albicans* ribosome should be determined.

Table 13 - mRNA tunnel composition variations across the eukaryotic domain.

| Site | Molecule name | Residue | | |
|---|---|---|---|---|
| | | *C. albicans* | *S. cerevisiae* | *H. sapiens* |
| **mRNA tunnel (entry)** | 18S rRNA (h18, h34) | G575 | G585 | G626 |
| | | A577 | A587 | A628 |
| | | C1259 | C1282 | C1331 |
| | | A1413 | A1435 | A1489 |
| | eS4 protein (108-117, 142-146) | **K108** | **R108** | **R108** |
| | | **S115** | **T115** | **T115** |
| | | **A116** | **D116** | **P116** |
| | eS30 protein (48-60) | **T50** | **V50** | **T50** |
| | | **K55** | **R55** | **K55** |
| | | **S59** | **G59** | **A59** |
| **mRNA tunnel (exit)** | 18S rRNA (h28, h23, h40, h44) | G889 | G904 | G961 |
| | | A1137 | A1152 | A1209 |
| | | C1385 | C1399 | C1464 |
| | | G1625 | G1638 | G1702 |
| | eS1 protein (114-117, 145-152) | **R145** | **K145** | **K145** |
| | | **P147** | **A147** | **N147** |
| | | **K152** | **R152** | **K152** |
| | uS2 protein | R79 | R79 | R80 |
| | | R127 | R127 | R128 |
| | uS7 protein (150-156) | **S151** | **G151** | **R151** |
| | | **S152** | **G152** | **A152** |
| | | **T154** | **A154** | **T154** |
| | | **V155** | **A155** | **V155** |
| | uS11 protein (47-53, 137) | Y53 | Y58 | Y72 |
| | | L137 | L142 | L156 |
| | eS17 protein (124-126) | **I124** | **V124** | **G120** |
| | | **S125** | **S125** | **M121** |
| | eS26 protein (40-47, 80-85, 95-98) | **T40** | **A40** | **V40** |
| | | **R82** | **R82** | **K82** |
| | | **T96** | **A96** | **T96** |
| | eS28 protein (64-67) | R65 | R65 | R67 |

# CANDIDA ALBICANS: RIBOSOME PURIFICATION

## *Candida albicans* cell growth

*C. albicans* strain SC5314 was provided by Dr. Saidi Znadri and afterward transferred to the IGBMC by Dr. David Bruchlen [79]. This strain was isolated from a generalized infection (candidemia) patient.

According to the safety restrictions, *Candida albicans* correspond to the pathogen species, so specific requirements are applied. All the manipulations with the cell, cell growth, and harvesting should be performed in the L2 safety room. A particular room was installed in the IGBMC to work with the pathogenic cells of *C. albicans* and *S. aureus.*

First, the growth curve of the *C. albicans* SC5314 strains was measured after receiving the strain. After taking a single colony from the YPAD petri dish, they were dissolved in 100 µl of YPAD media and transferred to 50 ml flasks filled with 10 ml of YPAD media. Since the SC5314 strain is insensitive to kanamycin, it was added to the flasks at 50 µg/ml to prevent bacterial contamination. Then the cells were left to grow in the shaker at 30ºC at 180 rpm. The cell culture density was monitored each hour by measuring the optical density at 600 nm. The resulting growth curve is presented in figure 29.
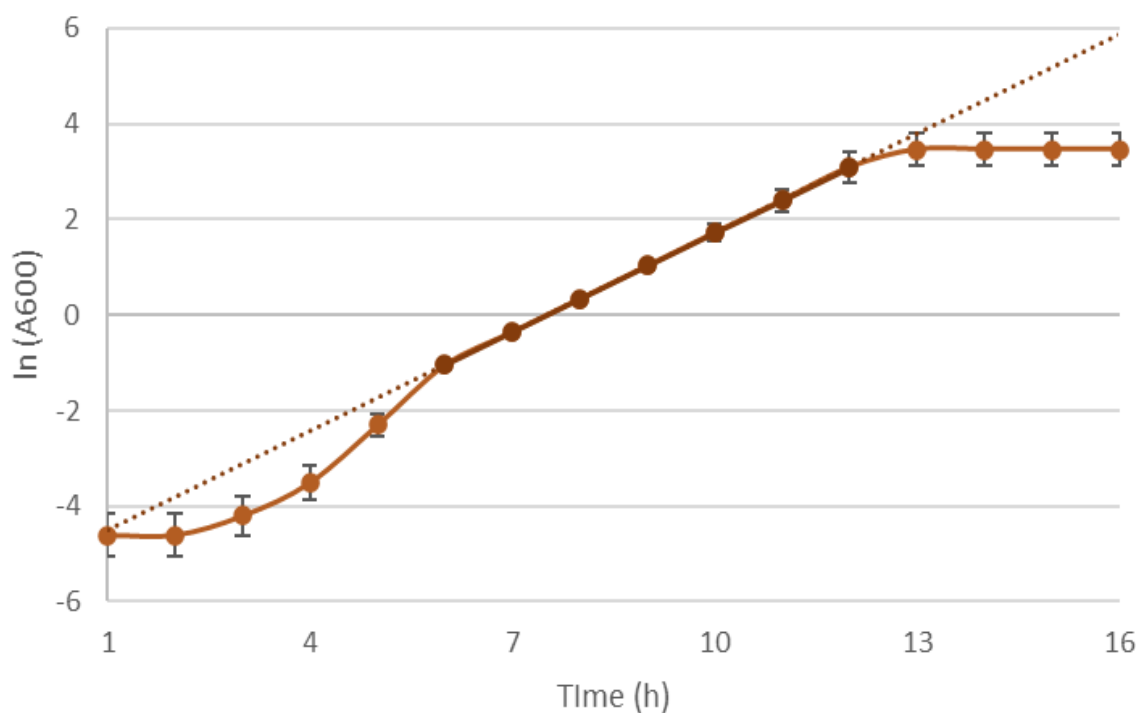


Figure 29 - The growth curve of the *C. albicans* SC5314 strain on the YPAD media.

There are several specific characteristics of the *C. albicans* cell growth on the YPAD media:

1) The doubling time of the cell growth is ≈ 54 min. It is more than 1.5 times shorter than is *S. cerevisiae* ribosome.

2) The Plato value (saturation) of the *C. albicans* SC5314 on the YPAD media is 32 OD/ml. It is two times higher than in the *S. cerevisiae* S288C strain.

After the growing curve of the *C. albicans* had been established, the next step was to prepare the cell stock for further use for purification.

## *Candida albicans* cell stock preparation

The cell growth of *C. albicans* was performed in YPAD media. The YPAD media comprises yeast extract, bacto peptone, adenine sulfate, and D-glucose (Table 14). Yeast extract (BD) is an autolyzed water-soluble cell extract of *S. cerevisiae* that provides nitrogenous compounds, carbon, sulfur, trace nutrients, and vitamin B complex. Bacto peptone (protein hydrolysates, Gibco) is widely used as a protein source in culture media. They are soluble mixtures of polypeptides and amino acids formed from the hydrolysis of animal and plant proteins. The adenine sulfate (Sigma) is added to the cell culture media since the yeast extract-based rich medium contains a low level of adenine. Adenine serves as a high-potential phosphate transfer compound in energy metabolism. D-glucose (Euromedex) is a primary fuel source in cell culture. The energy contained in its chemical bonds is used to synthesize adenosine triphosphate (ATP).

To prepare a cell stock, the C. albicans SC5314 cells were spread onto the YPAD agar plate with kanamycin (Kan, Sigma) 50 µg/ml. First, the agar plate is incubated for two days at 30 degrees. After the incubation, the single colony was taken and dissolved in 100 µl of YPAD media. Then the different amounts of the cells (25, 50, and 1 colony) were seeded in the 50 ml flasks filled with 10 ml of YPAD + Kan. These flasks were further incubated at 30 ºC at 180 rpm agitation. In 9-10 hours, the cell density reaches 6-8 OD/ml (ln(A600) = 1.8-2.1), which corresponds to the linear phase of the growth curve (Figure 29). After the desirable density was reached, the cell was mixed in a 1:1 ratio with the sterile 50% glycerol solution (Sigma). After mixing with the glycerol solution, cells were flash-frozen in the liquid nitrogen (N2) and stored at -80 ºC. Adding glycerol (25% final concentration) prevents cell damage during flash-freezing in N2.

Table 14 - YPAD-agar plate composition

| | |
|---|---|
| **Yeast extract** | 1% |
| **Bacto peptone** | 2% |
| **Adenine sulfate** | 0.04% |
| **Agar** | 2% |
| **D-glucose** | 2% |
| **Kanamycin** | 50 µg/ml |

## *Candida albicans* ribosome purification

The protocol for *C. albicans* ribosome is based on the protocol for *S. cerevisiae* ribosome with several changes [76, 79].

The ribosome purification starts with seeding from the cell stock onto the agar plate. The YPAD agar plate is incubated at 30 ºC for 40-48h (≈ 2 days) until the single colonies are visible on the plate. Once the single colonies have appeared, we pick a medium-size one and dissolve it in 100 µl of YPAD media. Then the different amounts of the cells (25 µl, 50 µl, and one colony) were seeded in the 50 ml flasks filled with the 10 ml of YPAD + Kan. The 50 ml flasks are incubated at 30 ºC, 180 rpm agitation for eight hours. After eight hours, cells are in the linear phase of cell growth: 25 µl flask – ≈ 2 OD/ml, 50 µl flask – ≈ 4 OD/ml, and one colony flask – ≈ 8 OD/ml. According to the cell culture's optical density, the amount of cells needed to be added to the big culture is calculated. For example, 15 µl of cells from the culture at 4.08 OD/ml is taken and added to the 1L flasks. This amount is used to have OD600 at 1 OD/ml after the big culture's overnight growth (14-15h).  The big culture (4 * 1L bottles) is incubated in the same manner as at the previous step (30 ºC, 180 rpm).

The next day, once the cell density in a big culture reaches 1 OD/ml (middle of the log phase), cells are ready to be harvested for further starvation. First, cells are transferred to 1L centrifuge bottles and spun for 15 min at 8300 g, 26 ºC. This step is performed to get rid of the glucose. Then, the cell pellet is resuspended in the YPA media (without glucose) and incubated for 10.5 minutes. The translation polysomes are transferred to monosomes during this starvation step due to the lack of energy supply. The incubation was optimized for *S. cerevisiae* since, during 10.5 minutes, the number of monosomes reached the maximum value after starvation cells were again precipitated for 15 min at 8300 g and cooled down to 4 ºC.

The next step is lysis. Before lysis, cells must be transferred to the buffer, which consists of components preventing osmotic stress during the lysis. In the case of *S. cerevisiae* and *C. albicans*, it is a buffer M. It is called 'M' due to the presence of the mannitol in the solution, which prevents the osmotic stress once the cell membrane is damaged (there is a vast difference in the pressure inside and outside the cell). The entire buffer composition is presented in table 15. Hepes / KOH (Sigma) buffer is one of the standard buffers in the ribosomal field due to its high pH stability, low metal chelating capability, and low UV absorbance. The concentration of monovalent K+ and bivalent Mg2+ ions has been picked to maintain the stability of the ribosome. EDTA (Euromedex) provides inhibition for metalloproteases; DTT (Sigma) - is a reducing agent that reduces disulfide bonds and protects from oxidation damage. The pH of the solution is optimal for the ribosomes (7.5 pH) to keep the optimal rate of peptide transfer.

Table 15 - Lysis buffer composition (Buffer M)

| Hepes / KOH pH 7.5 at RT | 30 mM |
|---|---|
| KCl | 50 mM |
| MgCl$_2$ | 10 mM |
| Mannitol | 8.5% (w/V) |
| EDTA | 0.5 mM |
| DTT | 2 mM |

The cell pellet, after starvation, was dissolved in 12 ml of butter M, and after resuspension, it was transferred to the 50 ml falcon tubes. The resuspension is followed by cell mass pelleting at 4400 rpm, 4ºC for 10 min. This step, called washing, was repeated three times to remove media traces and prepare the cells for lysis. Typically, from 4L of culture, we got ≈5.5g of cells.

Before cell lysis, the protein and RNA inhibitors cocktails were added to the system (Table 16). These inhibitors are indispensable for blocking the RNases and proteases, which could lyse the ribosomal proteins and rRNA. The concentration of the inhibitors was increased compared to the *S. cerevisiae* because we are using a non-modified clinical strain of *C. albicans*. There are two types of RNAse and protease inhibitors used in our experiment. Among RNAse inhibitors, we are using RNAsin (Promega) and Heparin (Alfa aesar). RNasin is effective against RNase A, RNase B, RNase C, and human placental RNase; it does not inhibit RNase T1, S1 nuclease, RNase H, or RNase from Aspergillus. Heparin is a non-specific RNase inhibitor to protect the RNA from degradation.

Moreover, for *S. cerevisiae,* it was found that heparin concentration affects the following PEG precipitation; that is why we kept the concentration of Heparin at 0.5 mg/ml. Pefablock (Roche) and PIC (Roche) have been used among protease inhibitors. PIC inhibits serine and cysteine proteases but is not active against aspartic and metalloproteases. Pefabloc belongs to the family of sulfonyl fluorides which irreversibly block serine proteases. The presence of EDTA inhibits metalloproteases.

Table 16 - Protease and RNAse inhibitors used in purification

| Inhibitor | Final concentration | Working range |
|---|---|---|
| RNAsin | 750 U/ml | 250-1000 U/ml |
| Pefablock | 2.3 mM | 1-5 mM |
| PIC | 2.8 X | 1-3 X |
| Heparin | 0.5 mg/ml | < 1 mg/ml |

The cell lysis is performed using glass beads vortex of cells. The obtained cell mass is dissolved in buffer M + inhibitors (1.45 ml of buffer M per gram of cell) and added to the prechilled Nalgene tube filled with acid-washed glass beads (425-600 μm in diameter, Sigma). The amount of glass beads is calculated according to the cell mass (3 grams of the beads per 1 gram of cells). Next, the KCl (Sigma) is added with inhibitors to reach the 130 mM concentration. An increase in the KCl concentration is required to precipitate the lipids during the S30 step. In *S. cerevisiae* KCl was added after the first PEG precipitation; however, in *C. albicans,* the lipid layer is poorly visible, so it was decided to precipitate the lipids right after the breaking of cells.

Next, cell lysis is performed. Cells were mechanically disrupted on a vortex at a frequency of 40 Hz for 1 min with 1-min breaks on ice between each shake. The number of cycles increases compared to *S. cerevisiae* (9 cycles instead of 5 in *S. cerevisiae*). This difference occurred since the cell wall of *C. albicans* is thicker than *S. cerevisiae* ones. Only after the seventh cycle does the solution become more viscous – an indication of successful cells breaking. Beads were removed by short centrifugation (20,000g for 2 min), and the lysate was further clarified by longer centrifugation (30,000g for 9 min). The supernatant (S30 fraction) is transferred to a new Nalgene tube before the polyethylene glycol (PEG) precipitation steps. Starting from here, all the manipulations have been performed in a cold room (4 ºC)

Polyethylene glycol is a nondenaturing water-soluble polymer whose ability to precipitate biological macromolecules and proteins from an aqueous solution can be qualitatively

understood in terms of an excluded volume mechanism. The increment in PEG concentration required to effect a given reduction in solubility is unique for a given macromolecule-polymer pair and primarily dependent on the size/solubility of the macromolecule/protein and polymer. The standard type of polyethylene glycol in the ribosome field is PEG 20000. For the first PEG precipitation (PEG1), Polyethylene glycol (PEG) 20,000 was added from a 30% (w/v) stock (Hampton Research) to a final concentration of 4.5% (w/v), and the solution was left to stand for 5 min on ice (to get a homogenized sample). The PEG1 step is needed to precipitate the cell debris and the cell parts with a lower solubility (higher molecular weight) than the ribosome. The solution was clarified by centrifugation (20,000g for 5 min), and the supernatant was transferred to a new tube. Then, the second PEG precipitation is performed. The PEG2 step aims to precipitate the ribosomal fraction (the 80S, 60S, 40S), leaving the more soluble molecules, such as proteins, in the soluble state. To do so, PEG 20,000 concentrations were adjusted to 8.5%, and the solution was left to homogenize for 10 min on ice. Next, ribosomes were precipitated (17,500g for 10 min), the supernatant was discarded, and a quick spin of the pellet eliminated any remaining solvent (14,500g for 1 min). After the PEG2 step, ribosomes were washed two times in buffer M+ to get rid of PEG 20k excess and resuspended in 500 µl of the same buffer. Buffer M+ consists of buffer M with KCl concentration adjusted to 150 mM and supplemented with protease inhibitors and heparin.  The increased KCL concentration + inhibitors eliminate unspecifically bound factors and RNases/proteases during the sucrose gradient step.

The next step is sucrose gradients. The resuspended ribosome pellet was measured on the spectrophotometer (A260) and layered on the 10-30% sucrose gradient (Table 17). 1 Absorption unit (A260) corresponds to 12.5 mg of the *C. albicans* ribosome. Before loading onto the gradients, we usually have 25-30 mg of the ribosome at a 13-15 mg/ml concentration. To not overload the gradient, not more than 7.5 mg of the ribosome per gradient were loaded. The sucrose gradients (SW28 rotor) were spun at 18,000 rpm, 4ºC for 15 hours (overnight).

Table 17 - Sucrose gradient composition

| | |
|---|---|
| **Hepes / KOH pH 7.5 at RT** | 20 mM |
| **KCl** | 120 mM |
| **MgCl$_2$** | 8.3 mM |
| **Sucrose** | 10/30% (w/V) |
| **EDTA** | 0.3 mM |
| **DTT** | 2 mM |

The next day, the sucrose gradients were fractionated (1ml volume), and each fraction's absorption (A260) was measured. The resulting sucrose gradient profile verifies the purity of the sample (if the subunits/oligomers are present or not). The typical sucrose gradient profile of the *C. albicans* ribosome is presented in figure 30.
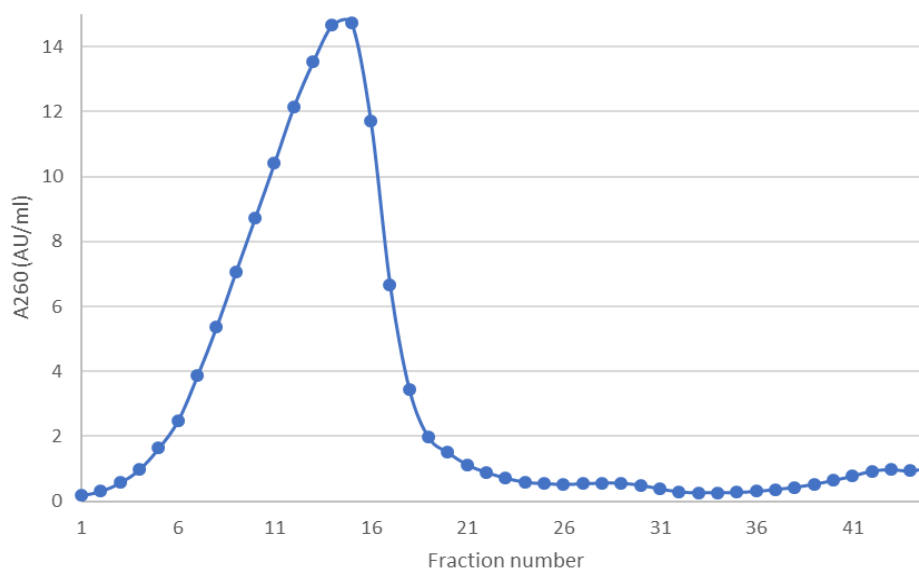


Figure 30 - The sucrose gradient profile of the *C. albicans* ribosome.

Usually, 5-6 fractions around peak value are chosen and pooled together in the Nalgene tube before the last PEG precipitation (PEG 3 step). After pooling the fractions, the magnesium and potassium concentration is increased (up to 10 mM and 150 mM, respectively), and the absorbance of the sample is measured. Usually, after the gradients, we get 15-17 mg of the ribosome at ≈ 10 AU/ml concentration. Further, the PEG3 precipitation is performed. PEG 20,000 was added to a final concentration of 7% (w/v), and the solution was left to stand for 10 min on ice. Ribosomes were precipitated (17,500g for 10 min), the supernatant was discarded, and the residual solution was removed by a short spin of the pellet (17,500g for 1 min). Ribosomes were suspended (25 mg/ml) in storage buffer G (10 mM Hepes-K (pH 7.5), 50 mM KOAc, 10 mM $NH_4OAc$, 2 mM DTT, and 5 mM $Mg(OAc)_2$]. After resuspension ribosome sample was split into 30 µl aliquots, flash-frozen in N2, and stored at -80ºC. Approximately 14 to 16 mg of pure ribosomes were obtained from 5.5 g of cells. Typical losses during the purification process are presented in table 18.

Table 18 - Typical losses during *C. albicans* ribosome purification

| Step | Yield | Loses |
|---|---|---|
| S30 | 85-90 mg | |
| PEG1 | 51-56 mg | 35-40% |
| PEG2 | 25-30 mg | 45-50% |
| WASH1 | 25-30 mg | 1-2% |
| Sucrose gradients | 15-17 mg | 45-50% |
| PEG3 | 14-16 mg | 6-10% |
| WASH2 | 14-16 mg | 1-2% |

## *Candida albicans* ribosome quality checking

### Protein polyacrylamide gel at denaturation conditions.

Protein polyacrylamide gel (PAGE) is indispensable for checking the presence of high-molecular-weight non-ribosomal proteins and separate proteins based on size [80]. For ribosomal proteins, 5-15% of acrylamide is usually used (5% – for stacking gel, 15% - for resolving). Before loading onto the gel, the sample is incubated for 3 min at 90°C (for protein denaturation). Denaturation conditions in the gel are maintained by the presence of 0.5% of SDS. The optimal amount to load into the slot for the ribosomal proteins is 0.05 AU, 0.1 AU, and 0.2 AU. After the sample is loaded into the slots, the gel runs for 10-15 min (120V, 110 mA, 2W) to be concentrated on the border between stacking/resolving gels. Once the sample is concentrated on the border, the gel is further launched until the dye goes out from the gel (180V 170mA 5W). The typical PAGE gel of the *C. albicans* ribosome is presented in figure 31. The resulting PAGE gel demonstrates the absence of high-molecular-weight non-ribosomal proteins.
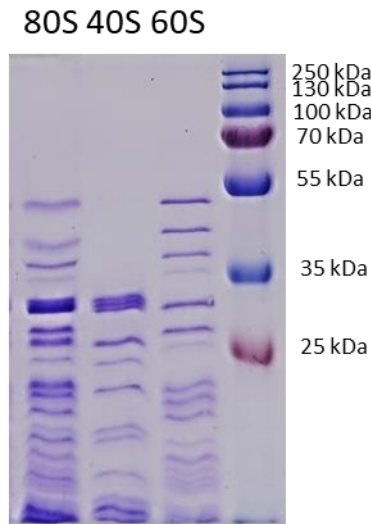
Figure 31 - 15% PAGE of the 80S *C. albicans* ribosome, as well as 40S and 60S subunits

## RNA agarose gel

An rRNA gel in denaturation conditions is the most common method to check rRNA integrity [81]. To get a high-quality gel of rRNA, the first rRNA should be separated from the ribosomal proteins. The most common way to get rid of ribosomal protein is phenol/chloroform extraction. Since phenol is a non-polar solvent, high-polar nucleic acids are not soluble in phenol; conversely, proteins are soluble in phenol. Moreover, phenol has a higher density than water, so there is a clear phase separation between them that facilities the supernatant taking. Two phases form when phenol is added to the solution and centrifuged. The aqueous, polar phase is at the top of the solution and contains nucleic acids and water. The organic phase containing denatured proteins and other cell components is at the bottom of the solution. After the first round of centrifugation, phenol is mixed with the chloroform. Chloroform is denser than phenol, so the phase separation meniscus is more visible. There is less cross-contamination from the organic phase in the aqueous phase, allowing a pure nucleic acid sample to obtain. After the phenol/chloroform extraction, rRNA is precipitated by 100% ethanol + sodium chloride (NaCl). The positive charge of sodium ions neutralizes the negative charge of a phosphate group, while 100% ethanol is less polar than water; it disrupts the shielding of the charges by water. If enough ethanol is added to the system (>70%), the electrical attraction occurs between the phosphate groups of rRNA and any positive atoms in the solution, leading to rRNA precipitation. After precipitation, the pellet is washed in 70% ethanol to get rid of salts, which decrease the gel quality, and then lyophilized for 2-3 h on a speed vac. The resulting rRNA powder is dissolved

in MQ and measured before loading onto the 0.8% denaturation agarose gel. Before loading onto the gel, the sample is incubated for 3 min at 95°C in the presence of 8M urea (RNA denaturation). The denaturation conditions on the gel are maintained by the presence of 10 mM of guanidine thiocyanate. The optimal amount to load into the slot for the ribosomal RNA is 0.015 AU, 0.03 AU, and 0.06 AU. After the sample is loaded into the slots, the gel runs for 45 min (150- 180V, 20W). The typical rRNA agarose gel of the *C. albicans* ribosome is presented in figure 32. Two sharp lines are visible, which correspond to the 25S and 18S rRNA. No smears on the gel prove the rRNA integrity and absence of degradation.
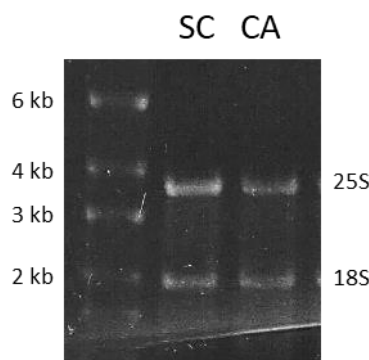


Figure 32 - 0.8% agarose gel of the *C. albicans* (CA) and *S. cerevisiae* (SC) ribosomal RNA

## Analytical ultracentrifuge

Analytical centrifugation studies the hydrodynamic properties of a molecule as it moves through a fluid medium. By accelerating a sample preparation in a centrifugal field, one can analyze a molecule's hydrodynamic properties, which rely on mass, density, and shape. The analytical ultracentrifuge has an integrated optical system that makes it possible to watch a sample move while it is being spun in a centrifuge rotor [82]. The centrifuge enables the study of molecules in their natural condition. The sample requirements are relatively low: the sample volume is 5-10 µl, and the sample amount is 1-3 AU. In our case, we loaded 1 AU of *C. albicans* ribosome onto the quartz cuvette. Analytical centrifugation was performed in the Beckman XL-I centrifuge at 4°C with monitoring of A260 absorption every 4 minutes. The SEDNTERP program was used for the interpretation of sedimentation velocity experiments. The resulting sedimentation profile of *C. albicans* ribosome is presented in figure 33. As presented in the picture, the purity of our sample is high. It consists mainly of 80S subunits (>95%) with minor contamination of subunits and their aggregates. All these findings show that our sample is a pure 80S *C. albicans* ribosome sample; there is no rRNA degradation, and there are no high-

molecular-weight non-ribosomal proteins in our solution. Having such quality control, we can move to the next step, sample preparation for cryo-EM experiments.
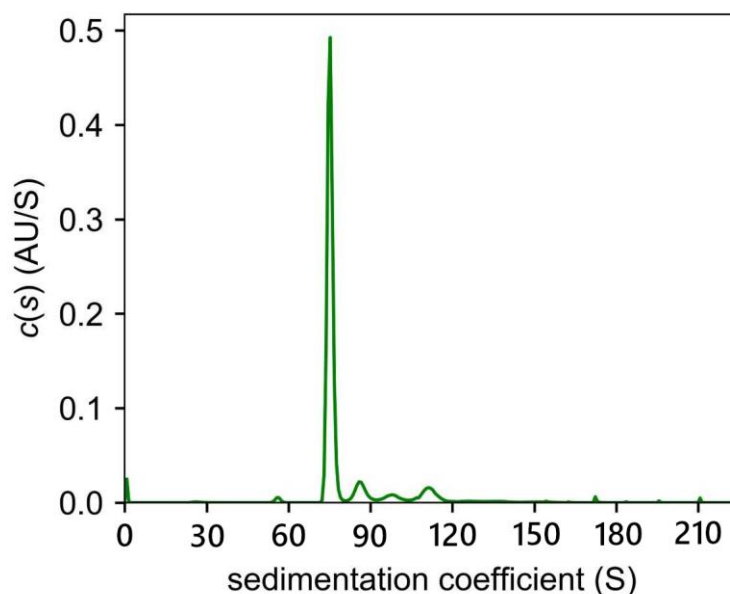


Figure 33 - Sedimentation coefficient distribution in the *C. albicans* ribosome sample

.

## *Candida albicans* ribosome sample preparation for cryo-EM experiments

### Dynamic light scattering (DLS)

Before putting the sample on the grid, the dispersity of the defrosted sample should be checked for ribosome oligomerization/aggregation [83]. The fastest way to check the polydispersity of the sample and the presence of oligomers is dynamic light scattering. DLS is an optical technique for analyzing various systems' dynamic properties and size distribution, such as biological macromolecules. A laser beam illuminates the sample, and the fluctuations of the scattered light are detected at a known scattering angle by a fast photon detector. By analyzing the intensity fluctuations in the sample, the spectra of diffusion coefficients can be analyzed and further transformed to the hydrodynamic radius of the molecule.

Before the DLS experiment, our ribosome sample (in buffer G) was filtered (0.22-µm centrifugal filters, Millipore) and diluted to 1 mg/ml. This concentration is an optimal concentration for the DLS experiments of the ribosome. Our sample was then transferred to a 50 µl disposable cuvette and equilibrated for 5-10 min inside the DLS machine. The experiments

were performed at different temperatures (4ºC, 30ºC, 37ºC) with time evolution. The obtained distribution of the *C. albicans* ribosomes proves the absence of oligomers in our system. The calculated hydrodynamic of the ribosome was ≈14 nm. However, it is an approximate value because the viscosity of the solution was not measured. Moreover, it was found that the lowest value of sample dispersion occurred after 15 min incubation at 30ºC (Figure 34). Therefore, these incubation conditions were a reference point for the 80S *C. albicans* ribosome sample preparation for cryo-EM.
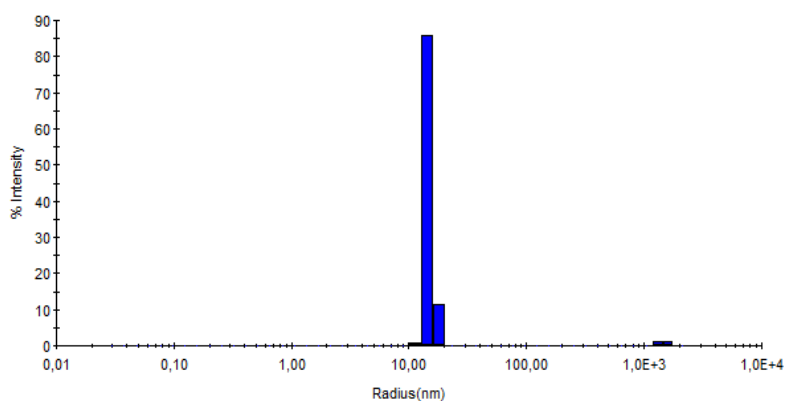


Figure 34 - Hydrodynamic radius distribution (DLS spectrum) in *C. albicans* ribosome sample

.

## Grid preparation for cryo-EM

The frozen ribosome sample (in buffer G) was thawed on ice for 1h. Then the sample is transferred to 0.22-µm centrifugal filters and spun at 11 000g, 4°C for 10 min. After the sample is recovered and diluted to 1-2 mg/ml concentration before incubation. As was written above, the optimal conditions for the incubation are the following: 10 min at 37°C. After incubation, the sample is maintained at room temperature before grid preparation. Aliquots of 2.7 µl were applied to freshly glow-discharged holey carbon grids (Quantifoil Cu R1.2/1.3 with ultrathin carbon support, 200 mesh). The excess liquid was blotted away for 3 to 5 s using an FEI Vitrobot Mark IV (Thermo Fisher Scientific), and the samples were plunge-frozen in liquid ethane. The optimal time of blotting is 4s. The typical cryo-EM grid of the 80S *C. albicans* ribosome is presented in figure 35.
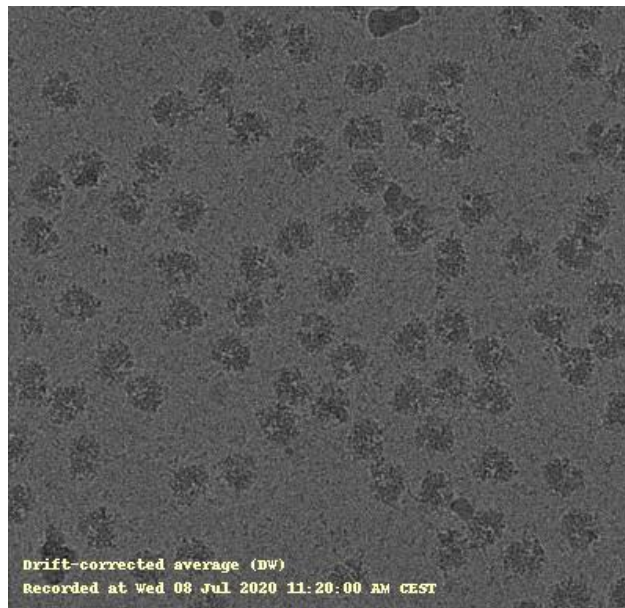
Figure 35 - Cryo-EM grids of the 80S *C. albicans* ribosome.

## *Candida albicans* ribosome single-particle cryo-EM data collection

After grids have been frozen, the next step is to screen the quality of the grids and start a data collection from chosen holes. Our colleagues from Groningen University, the Netherlands (Dr. Albert Guskov and Dr. Artem Stetsenko) performed the data collection. First, grids were collected in the NeCen microscope Center (Leiden, the Netherlands). Then, data collection was performed on a Titan Krios 300-keV microscope (Thermo Fisher Scientific) equipped with a K3 direct electron detector.

The frozen grids are stored unclipped to facilitate their transport to a facility in the specifically-designed pucks. Once arrive at microscope facilities, grids are visually inspected for the presence of crystalline ice, clipped, and further transferred to a microscope sample cassette. In the Titan Krios microscope, there is a possibility to load 12 grids in a row (1 calibration grid and up to 11 grids with the sample of interest). Before starting data collection, the microscope setup is performed. Using the calibration grid to beam alignment and resolution limits are tested and refined if needed. The calibration grid is exchanged for the cryo-EM specimen if the tests meet performance standards.

An "atlas" (low magnification) is generally recorded to outline the grid's explorable areas before the data collection session really begins. To choose the holes for the data collection, the areas are first thoroughly examined at a higher magnification. There are dozens to hundreds of individual holes suitable for data gathering inside each grid square. A typical data gathering session often records thousands of holes.

The process for gathering data employs a so-called "low dosage" strategy that alternates between the three modes of search, focus, and record. The "search" mode step places the microscope stage in the middle of a low-magnification imaging region. Following the area's centering, the target defocus of the image is set during the focusing process. To prevent radiation damage to the particles, the focussing is done far from the hole. A brief movie is made after a multi-second exposure is taken over the target hole after the defocus has been set. (figure 36). Each movie contains several frames processed and summed into a single image. Finally, the search-focus-record process is repeated for the next hole until all target holes have been recorded.
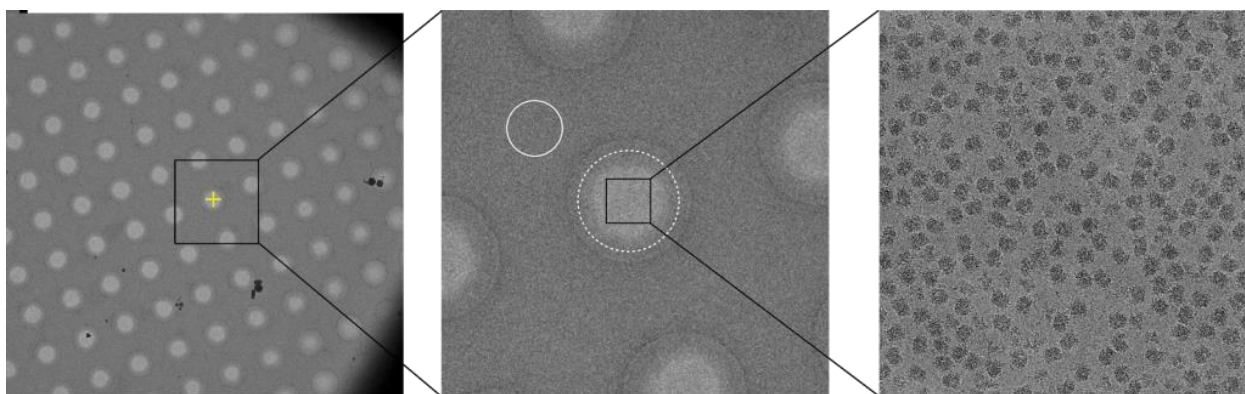


Figure 36 - Workflow of low dose approach (search – focus – record) [84].

To collect a successful dataset following parameters need to be optimized:

1) **Pixel size**. Pixel size is directly connected with the magnification level, which balances the number of particles per field of view and the achievable resolution. The physical distance that each pixel represents is known as the pixel size. The achievable resolution of the EM map is restricted by a pixel size (Nyquist limit). The Nyquist limit refers to twice the pixel size; e.g., images recorded at 1.0 Å per pixel have a physical limit of achieving a 2.0 Å resolution

2) **Nominal defocuses range**. The optimal defocus range compromises a high-resolution limit and sufficient contrast to enhance particle visibility. Particles might not be visible if the micrograph is focused too closely. The common minimum and maximum defocus ranges for cryo-EM datasets are -0.5 to -1.0 μm and -2.0 μm, respectively. A nominal defocus range is used to accomplish the information across the Fourier space.

3) **Total electron exposure.** The right quantity of electron exposure, or dose, will strike a compromise between producing enough signal for each frame of a video and reducing radiation damage while exposed to electron beams. If the dose is too low, there could not be enough information in each movie frame to adjust for motion. High dosages, on the

other hand, may cause severe radiation damage. An average electron dose is between 40 and 60 electrons per $\mathring{A}^2$.

All listed parameters have been optimized for the 80S C. albicans ribosomes (Table 19). Zero-loss images were recorded semi-automatically using the UCSF Image script [85]. The GIF Quantum energy filter was adjusted to a slit width of 20 eV. We collected more than 9800 images from one grid to obtain a high-resolution structure of the vacant *C. albicans* ribosome.

Table 19 - Grid freezing and data collection parameters for the 80S *C. albicans* ribosome

| *Grid freeing* | |
| --- | --- |
| *Grid type* | *Quantifoil Cu R1.2/1.3 with ultrathin carbon support, 200 mesh* |
| *Blotting time* | *3-5 s* |
| *Ribosome concentration (mg/ml)* | *0.5* |
| *Data collection* | |
| *Microscope* | *Titan KRIOS with K3-detector* |
| *Voltage* | *300 kV* |
| *Pixel size ($\mathring{A}$)* | *0.836* |
| *Defocus range (µm)* | *-0.5 to -2* |
| *Dose (electrons per $\mathring{A}^2$)* | *50* |
| *Micrographs collected (#)* | *9807* |

# *Candida albicans* ribosome cryo-EM data processing

Once micrographs have been collected, the next question is data processing. Nowadays, programs for cryo-EM data processing are highly developed, allowing one to get an electronic map shortly. For our data, all the data processing has been performed in cryoSPARC [85]. To get a high-resolution structure, first of all, some corrections should be applied to the micrographs: motion correction, dose-weighting, and Contrast Transfer Function (CTF) estimation [84]:

1) **Motion correction.** During data collection, the movement of particles occurs due to the electron beam's thermal heating of the grid. Particle movement would create a blurred image if the subsequent images were not correctly aligned. Modern algorithms have been developed to align individual movie frames accurately against each other [86]. Following this realignment, which eliminates beam-induced motion, aligned frames are added together to create a single, de-blurred micrograph.

2) **Dose weighting.** Exposure to the electron beam causes biological specimens harm. As a result, the electron dose in the Cryo-EM video frames increases. Although the radiation damage in the initial frames is quite minimal, there is little contrast in the images due to the low electron content of these frames. Later frames' images had better contrast as a result of the electron buildup, but high-resolution data quickly suffered from radiation damage. In modern algorithms, high-resolution content from video frames is downweighted as a function of their cumulative dosages. As a result, information in earlier frames is still high-resolution, whereas information in later frames is just low-resolution. The final micrograph is composed of the sum of individual dose-weighted frames.

3) **CTF estimation.** The image recorded in cryo-EM is a corrupted 2D projection of the real object. As a function of spatial frequency, the corruptions lead to an uneven transfer of information content. The contrast transfer function, or CTF, is a mathematical representation of this transfer as a sinusoidal wave. The electron wavelength, which is controlled by the microscope's accelerating voltage, spherical aberration, and picture defocus are only a few of the variables that affect the CTF. Within a cryo-EM dataset, the electron wavelength remain constant, but the defocus will change.Therefore, the most critical task in CTF estimation is determining each image's true defocus. Once CTF is estimated, the authentic version of the image can be restored.

From the motion-corrected micrographs, individual particle images are identified and extracted in the subsequent data processing stage. Particle selection can be done in a variety of

ways, from totally manual to fully automated. We adopted a semi-automated strategy in our circumstance. In this method, a few typical micrographs that span the dataset's defocus range are manually used to select a few hundred particles. The selected particles act as models for the complete dataset's autonomous particle selection. After selecting particles, they are extracted from the micrographs to generate a particle stack. In total, more than 440000 particles were extracted from 9807 micrographs. The extracted particles should have square dimensions and a sizable solvent space. In general, box sizes should be roughly 50% larger than the particle's most expanded perspective. In our case, the box size was 480 Å, which is approximately 50% larger than the longest dimension of the ribosome ($\approx$ 300 Å).

The stack of retrieved images is utilized for 2D classification after the particle selection process. Particles within a dataset are compared to one another in 2D classification, and then comparable particles are clustered together into groups. Differences in x and y translation, in-plane rotation, and CTFs are taken into account throughout the classification process. Since the resulting "class averages" have higher signal-to-noise ratios than raw images, they exhibit improved details. In other words, the impacts of noise are averaged out and the consistent properties of the particles are strengthened. In this step, particles sorted into well-resolved classes are separated into a refined stack from other particles sorted into poorly resolved or "junk" classes. In our cases, three cycles of 2D classification have been performed to eliminate junk particles. As a result, 267215 particles have been divided into 38 2D classes (figure 34).

The original 3D image is projected into 2D in particle pictures. Because it is difficult to determine the relative orientations of the particle pictures, which is typically the rate-limiting phase in the reconstruction process, 3D reconstruction poses a problem. By comparing cryo-EM images to projections of a reference 3D model, "projection matching" algorithms are the most used method for determining particle orientation [84]. Reference models are typically created using ab initio approaches or drawn from related structures. Notably, in order to reduce the unexpected consequences of model bias, the reference models employed should preferably be low-resolution. Each particle picture is back-projected into a fresh 3D reconstruction once relative orientations have been assigned.

The process of 3D reconstruction is iterative, with each new reconstruction acting as the base model for the subsequent cycle. The accuracy of orientation assignments is improved with each successive cycle, and higher-precision orientations will result in higher-resolution maps. The reconstruction project reaches a stage where subsequent iterations do not significantly alter the orientation assignments or the reconstruction resolution after a number of cycles [84]. The job is described as 'converged' and completed upon the generation of the final map. After the

first 3D reconstruction, the map resolution reached 2.57 Å resolution (90% of particles from 2D classes have been selected). The map's resolution is calculated according to the golden standard: FSC Fourier shell correlation (FSC) = 0.143. The FSC=0.143 threshold is based on an X-ray crystallography standard for map interpretability [84].

Several refinement sets have been performed to improve the map quality: global and local CTF refinements and non-uniform refinement [87, 88]. Global CTF Refinement adjusts the higher-order CTF terms (beam-tilt, trefoil, spherical aberration, tetrafoil) across an entire group of images to find the optimum values, accounting for misalignment or aberrations in the microscope itself. In local CTF refinement, experimental particle images are compared against the 3D reference from their half-set, from the best-known pose, at various defocus levels, and the best defocus is selected. Non-uniform refinement iteratively accounts for regions of a structure with disordered or flexible density causing local loss of resolution. Finally, by applying all these refinement schemes, we got a 2.32 Å resolution for the vacant *C. albicans* ribosome. The workflow of cryo-EM processing is presented in figure 37.

9807 micrographs

Particle picking,
particles inspection and export

444 158 particles

2D classification
(3 rounds)

267 215 particles



*Ab initio* volume generation

243 386 particles
(91.6%)

22 418 particles
(8.4%)

Non-uniform refinement

2.57 Å

Global and local CTF refinements,
Non-uniform refinement



Post-processing, local
refinements with masks,
structure building
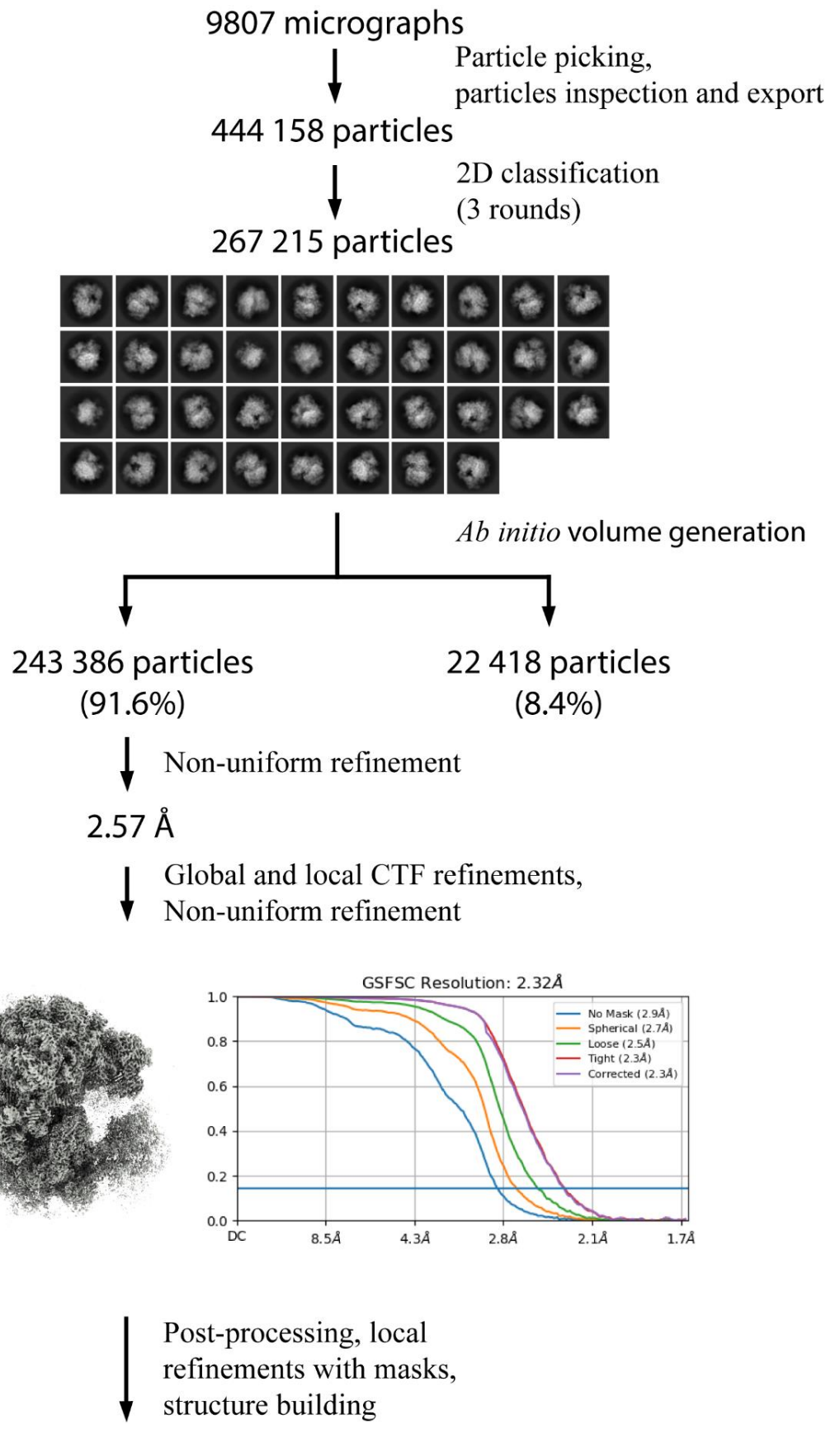
Figure 37 - Cryo-EM data processing scheme for the vacant *C. albicans* ribosome

# CANDIDA ALBICANS: HIGH-RESOLUTION VACANT RIBOSOME STRUCTURE

## *Candida albicans* ribosome model building

The structure of the *S. cerevisiae* 80S ribosome [76, 89] was used as a template for further model building. Model to map alignment was performed in Chimera [90]. The 60S and 40S subunits were refined separately into their respective focused maps using the Phenix real-space refinement [91]. The protein and rRNA chains were visually checked in Coot [92] and manually fit and adjusted where necessary.

During the initial map-to-model correlation, it was found that the density for the small subunit is much weaker than for the LSU. It indicates that the 40S subunit is highly flexible in contrast to the X-ray crystallography, with less difference in the electron density maps for LSU and SSU. To overcome this issue, we made two focused maps: one on the body of the SSU and the other on the head of the SSU. This approach allowed us to increase the local resolution of the SSU and look into the structural details of the SSU. The main problem is how to combine the three different maps: 1 unfocused and two focused maps. This feature available in the Phenix software package allows one to get a combined map without losing map quality and not creating a bias. The whole 80S ribosome of *C. albicans* was built using this combined map.

After the initial model building, several refinement steps followed by manual model revision allowed us to obtain a high correlation between the model and the map and appropriate statistics for geometry constraints, such as Ramachandran outliers, clash scores, and RMS deviation for bonds and angles. The overall statistics for the model quality are presented in table 20. The absence of Ramachandran outliers (0.02%) and the number of angles in a favored zone (>97%) indicate the proper geometry of ribosomal proteins. The clash score number reflects the number of severe clashes per 1000 atoms. In our case, the clash score is 7.59, showing that the rRNAs', proteins,' and ions' overall placement do not create severe clashes. All these parameters, along with the RMS deviations for the side chains and angles, prove the model's quality. Finally, the model-to-map fit quality is reflected by a correlation coefficient of 0.83 in our case, proving the absence of the model region for which there is no strong density.

Table 20 - Model refinement statistics of the vacant *C. albicans* ribosome

| *Refinement* | |
|---|---|
| *Particles (#)* | *243 386* |
| *Resolution (Å; at FSC = 0.143)* | *2.32* |
| *CC (model to map fit)* | *0.83* |
| ***RMS deviations*** | |
| *Bonds (Å)* | *0.004* |
| *Angles ($^0$)* | *0.779* |
| *Chirality ($^0$)* | *0.039* |
| *Planarity ($^0$)* | *0.005* |
| ***Validation*** | |
| *Clashscore* | *7.59* |
| *MolProbity score* | *1.54* |
| *RNA backbone* | *0.55* |
| *Favored rotamers (%)* | *99.61* |
| *Ramachandran favored (%)* | *97.33* |
| *Ramachandran allowed (%)* | *2.65* |
| *Ramachandran outliers (%)* | *0.02* |
| *CaBLAM outliers (%)* | *1.4* |
| *CA geometry outliers (%)* | *0.46* |

# *Candida albicans* 80S ribosome structure overview

Over the last 20 years, revolutionary advances in structure determination have identified a range of ribosomal subunit orientations. In early studies, cryogenic electron microscopy (cryo-EM) reconstructions visualized rotation ("ratcheting") of the small subunit (SSU; Fig. 38B) relative to the LSU [93]. More than a decade later, studies of eukaryotic ribosomes showed that the SSU might also undergo tilt-like rotation (i.e., "rolling"; Fig. 38D). Other studies have found that the head domain of the SSU (Fig. 38A) rotates relative to the SSU body in prokaryotic and eukaryotic ribosomes, a motion referred to as "swiveling." The range of accessible domain motions is further highlighted by structures of the tmRNA complex and subsequent simulations of tRNA-mRNA translocation, where tilt-like rotations of the SSU head are also apparent. To complement structural studies, a range of single-molecule measurements have also provided insights into the relationship between subunit rotations and tRNA rearrangement during translation. Together, this rapidly growing body of data demonstrates the various ways that rotary-like rearrangements of the SSU are integral to the dynamics of protein synthesis.
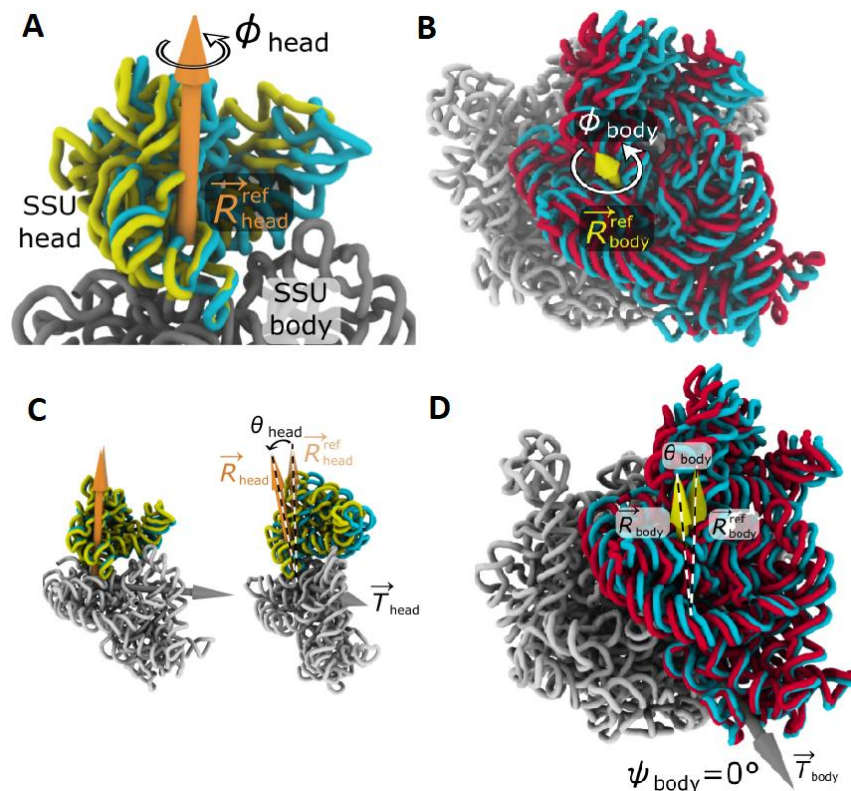


Figure 38 - Rotational motion of the body and the head of the SSU. **A**. Head swiveling. **B**. Body ratcheting **C**. SSU head tilt-like rotation **D**. SSU body rolling (tilt-like) [93]

To fully describe the six orthogonal degrees of freedom of each rigid body (i.e., SSU body or head), each orientation is described in terms of rotation about a fixed axis ($\phi$), a tilt-like

rotation (θ) about an orthogonal axis (in the direction ψ) and a translation vector (Δx). For the ribosome, this allows us to decompose each SSU head. Body orientation in terms of a rotation of magnitude - about an internal rotation axis R and a tilt-like rotation of magnitude θ that is about the axis T. T lies in the plane perpendicular to R, where the direction is given in terms of an angle (the direction of ψ= 0 is arbitrarily defined).

The rotation angles were calculated in a RADtool package [94]. In this package, a structure alignment step is first applied to identify the "cores" of the LSU, SSU body, and SSU head that are structurally similar to the reference *E. coli* structure. Next, a rigid-body approximation is applied, where the least-squares alignment of the cores is performed. These rigid-body descriptions are then used to decompose the orientation of the SSU body and SSU head in terms of Euler angles and translations.

We calculated the rotation angles in our *Candida albicans* structure using this approach. We found during model building that our vacant 80S *C. albicans* ribosome structure contains endogenous tRNA bound in the E-site and stm1 protein in the mRNA tunnel. Firstly, we measured the body's rotation of the SSU relative to the 60S subunit. The 40S subunit is in an almost non-rotated state; the SSU body is rotated only by 1.3° counterclockwise relative to the 60S. In addition, there is a 15° swiveling of the 30S head toward the E-site of the 60S subunit. Next, we measured the rotation of the head of the SSU relative to the body. The *C. albicans* most swiveled (13.5°) toward the E-site of the 60S subunit. In addition, the tilt-like rotation is present in the *C. albicans* ribosome: the 40S body is tilted by 2.8°, and the head is tilted by 6.0°. The 80S vacant *Candida albicans* ribosome consists of an almost non-rotated 40S and the most rotated SSU head.

While comparing our angles with other structures, it turned out that our structures have a unique set of angles. The closest structures are 5JUT and 6MTD. The first structure is one of the intermediates of *Saccharomyces cerevisiae* ribosome in complex with elongation factor eEF2-GDP-sordarin and Taura Syndrome Virus internal ribosome entry sites (IRES) [95]. The second structure represents translationally inactive mammalian ribosomes stalled by SERPINE mRNA binding protein 1 (SERBP1) occupying the ribosomal mRNA entrance channel [96]. If we compare only the body rotation, the closes structures are yeast disome (di-ribosome) stalled on poly(A) tract (6T83) [97], cryo-em reconstruction of the *Plasmodium falciparum* 80S ribosome bound to P-tRNA (3JBN) [98] and yeast 80S ribosome bound to eEF3 and A/A- and P/P-tRNAs (7B7D). If we compare only the head rotation, our structure is similar to the crystal structure of geneticin (G418) bound to the *S.cerevisiae* 80S ribosome [99] and Thermophilic eukaryotic 80S ribosome at the pe/E (TI)-POST state [100].

If we compare the available vacant ribosome structure, our structure is somewhat dissimilar to *S. cerevisiae* (4V88) and *H. sapiens* (6QZP) [76, 101]. The angles are presented in table 21. In *H. sapiens,* the ribosome is found in a non-rotated state, while in *S. cerevisiae* 80S, both body and head are rotated. *C. albicans* represents a hybrid state where the body is non-rotated while the head is highly rotated (maximum value across eukaryotes), giving a unique feature to our structure.

Table 21 - SSU body and head rotation angle comparison between vacant structures of eukaryotes

| Organism | body rot. | body tilt | body tilt dir. | head rot. | head tilt | head tilt dir. |
|---|---|---|---|---|---|---|
| *C. albicans* | -1.3 | 2.8 | 17.8 | 13.5 | 6.0 | 71.7 |
| *S. cerevisiae* | 4.1 | 2.8 | 88.4 | 14.0 | 8.7 | 63.4 |
| | 7.7 | 4.8 | 52.8 | 9.9 | 3.0 | 33.9 |
| *H. sapiens* | -1.9 | 3.0 | 22.2 | -0.1 | 1.4 | -65.9 |

To compare how these differences in the angle values can affect the interaction between subunits, we compared the intersubunit bridges described previously for bacteria end eukaryotes. Moreover, we inspected our map on the presence of the non-ribosomal protein, endogenous tRNAs, EF2, and the eL41 protein. eL41 protein forms a bridge between subunits, and it was interesting to see if it is present in our structure or not.

## Presence of non-ribosomal proteins and endogenous tRNAs

First, during the model inspection, we found a strong density for the stm1 protein in the mRNA entry tunnel. As written before, the stm1 protein in *C. albicans* is the most dissimilar to those in *S. cerevisiae*; there is only 39,74% of identity between them. Despite this low similarity, the protein core in the mRNA entry channel is highly conserved. However, the other parts are different, and the spatial arrangement of secondary structure parts differs from *S. cerevisiae*. In our map, we do not see the density of the whole protein. The N-terminal is partially invisible (1-21 is not present), while the C-terminal is absent; starting from 147 aa, there is no density for the protein (as previously found in *S. cerevisiae* 4V88). The most exciting thing is that the location of region 40-81 is different from the *S. cerevisiae*. The main question here is if this rearrangement reflects the difference in the body ratcheting between *S. cerevisiae* and *C. albicans* or two these features are independent of each other.

Moreover, during the inspection of the functional sites, in the E-tRNA binding site on the 60S subunit, we found a firm density that corresponds to the CCA-tail of the tRNA (figure 39). The E-tRNA was not introduced to our system from outside, so we can conclude that this density corresponds to the mixture of the endogenous E-tRNAs. Moreover, the density is only evident for the CCA-tail of tRNA, which is identical to the whole tRNA family. This fact also proves the hypothesis that the found density corresponds to the mixture of endogenous E-tRNAs. Due to the sequence variabilities (general flexibility/occupancy), the only visible part of the tRNA is the CCA-tail.
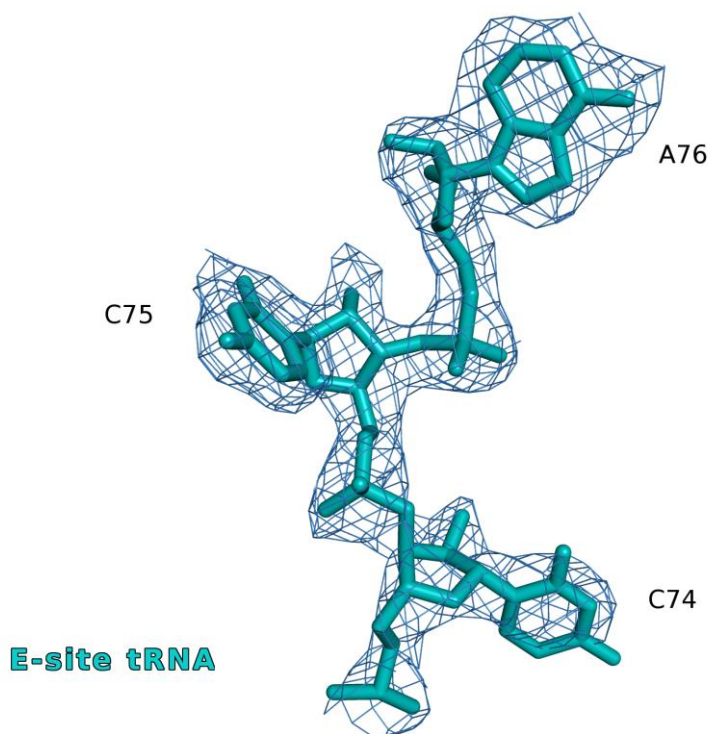


Figure 39 - Density map for CCA tail of *C. albicans* E-tRNA

Furthermore, we inspected if there was a density for the eL41 protein for which there is no sequence in the available databases. During the inspection, we found that the eL41 protein was evident in the experimental density of other eukaryotes. To identify the sequence of the eL41 protein, we first docked the one from *S. cerevisiae* and examined the side chain fit. We found that some of the AAs were not matching to the density. To get the sequence, we asked for the help of curators at the Candida Genome Database [102], who found a conserved DNA sequence in the genome of *C. albicans* SC5314 between orf19.1676 and orf19.1677. This sequence specifies a 25-residue polypeptide similar to *S. cerevisiae* eL41 that fits into the density and therefore appears to be the eL41 protein of the *C. albicans* ribosome (figure 40). eL41

protein from *C. albicans* has two substitutions in positions 2 and 10 and 1 aa insertion in the C-terminal.



Figure 40 - Identification of eL41 protein sequence. (**A**) Density map for the ribosomal protein eL41 of *C. albicans*. Amino acids that differ in *C. albicans* from *S. cerevisiae* are labeled red. (**B**) Sequence logos of eL41 of *S. cerevisiae* and newly identified *C. albicans* eL41.

Apart from the listed proteins and RNA, we did not find any evidence of the presence of other proteins and RNAs, such as EF2, found in the vacant structure of porcine (3J7P) and rabbit ribosomes. It is still unclear if these features can explain the angle of rotation of the body and the head of SSU. For example, the almost non-rotated state of the body of the SSU could be explained by the presence of stm1 and connected to the structure of the stalled disomes [97] because both ribosomes are inactive at this state. At the same time, the rotation angle of the SSU body is far from that in the *S. cerevisiae* vacant structure (4V88), where the stm1 protein is also present. The significant rotation of the head of the SSU could be brought about by the presence of the E-site tRNA as seen for the Thermophilic eukaryotic 80S ribosome at the (TI)-POST state (7OLD), where the tRNA is present in the pe/E state [100], what could be a reason in our case. However, in 7OLD, there is a density for the EF2 protein, which is not the case for *C. albicans*. All these observations lead us to conclude that we have a unique hybrid state for *C. albicans*, and we cannot explain the rotation angle just by the presence/absence of non-ribosomal proteins and RNAs.

# Intersubunit bridges in *C. albicans* ribosome

Based on the specific angles of rotation of the body and head of the SSU, we aimed to compare the intersubunit bridges in *C. albicans* ribosome with those in *S. cerevisiae* (4V88) and *H. sapiens* (6PZY) [76, 101]. In the eukaryotic ribosome, 17 intersubunit bridges were found, while in the bacterial ribosome, there are only 12. All these bridges are formed either by rRNAs or by ribosomal proteins. (rRNA – rRNA, rRNA – rprot, rprot – rprot). Here we describe the intersubunit bridges using the generally accepted nomenclature [76, 103]. The complete list of the bridges with participating residues is included in table S1.

1) **B1a**. The B1a bridge is universally conserved along species, but the interaction pattern differs. In *S. cerevisiae* and *H. sapiens*, the direct interaction between 25S (H38a) and 18S (h33) rRNA was reported, as well as between 25S and uS19 protein. In *C. albicans,* we do not observe direct interaction between rRNAs, and there is an interaction between 25S and uS19 protein (Figure 41). R72 from the uS19 protein is located in 3.1 Å to A1022 from 25S, forming a hydrogen bond between the R72 sidechain and the 1022 base (Figure 41).
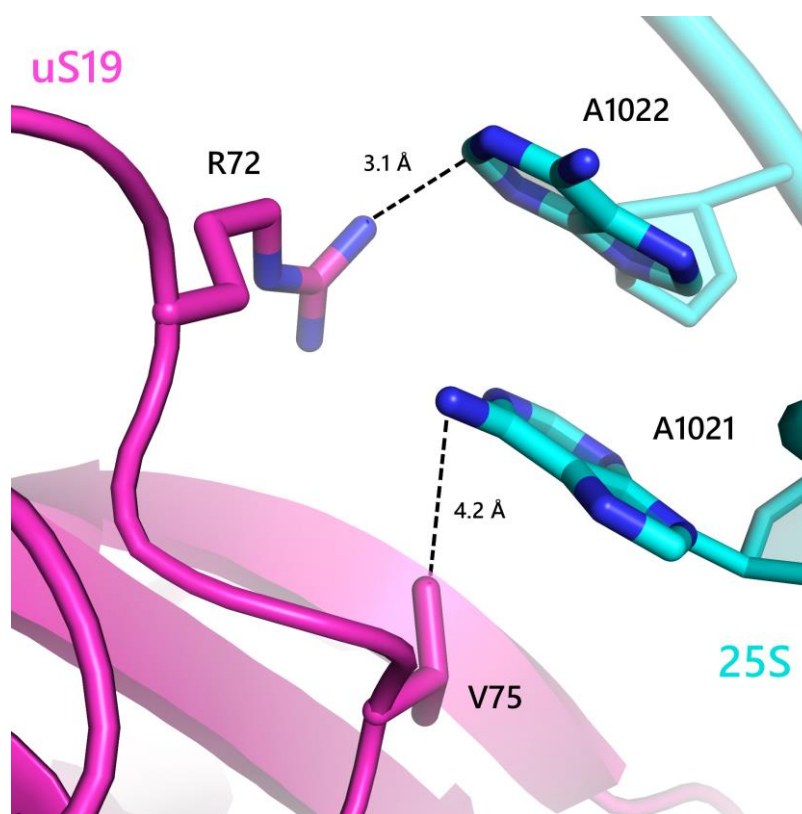


Figure 41 - Detail of bridge B1a highlighting protein-RNA interaction

2) **B1b/c.** This bridge is located between the central protuberance of the 60S and the 40S head and involves ribosomal proteins uL5, uS13, and uS19 (Figure 42A). The main feature

of this bridge is that the interaction pattern between proteins is different and depends on the elongation step. In the vacant human ribosome, the ribosome is found in the pre-translocation state, where the I113 and K118 (uL5) contact the side chains of R14 and Q10 (uS13) [104]. In the post-translocation state, previously found for the yeast and porcine ribosomes, the B1b/c bridge is formed by Y119 of uL5 and R108 of uS13 [105]. In the *C. albicans* ribosome, the interaction pattern is close to the yeast and porcine ribosome, showing that the head of the 40S of the *C. albicans* is in the post-translocation state. The B1b/c bridge in *C. albicans* is formed by the contact of E108 from uL5 and R110 from uS13 (Figure 42B). Moreover, there is an interaction between the N-terminal of uS19 and the uL5 protein (F12 of uS19 and E88 of uL5, figure 42C)
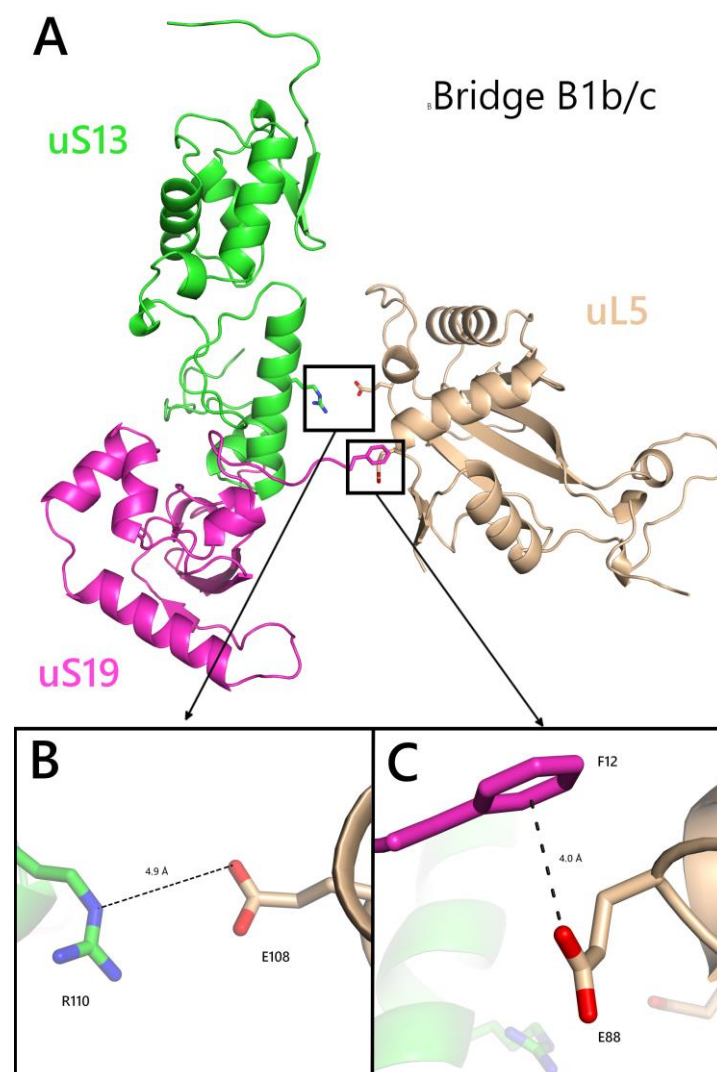


Figure 42 - Close up view of the B1b/c bridge of *C. albicans* ribosome. **A**. Overall view on B1b/c bridge. **B**. uS13-uL5 interaction **C**. uS19-uL5 interaction.

3) **B2a.** B2a bridge spans a large interface area of the 40S platform. It is located close to the decoding center on the 40S platform and is formed by helices h44 (18S) and H69. Bridge B2a/d undergoes a significant conformational change during tRNA selection. When aa-tRNA binds, the ribosome, A1742, and A1743 of h44 flip out of the helix and dock into the minor groove of the codon-anticodon helix. This rearrangement disrupts the interaction between A1442 of h44 and A2234 of H69. In the *C. albicans* ribosome, the B2a bridge is stabilized by the hydrogen bond formation between bases of A2234 (H69) and A1742 (h44) (Figure 43). Moreover, their bridge is stabilized by the contacts between A2233 and A2241 with G1744 and U1746, respectively. The functional sites paragraph presents a detailed description of the decoding center (DC).
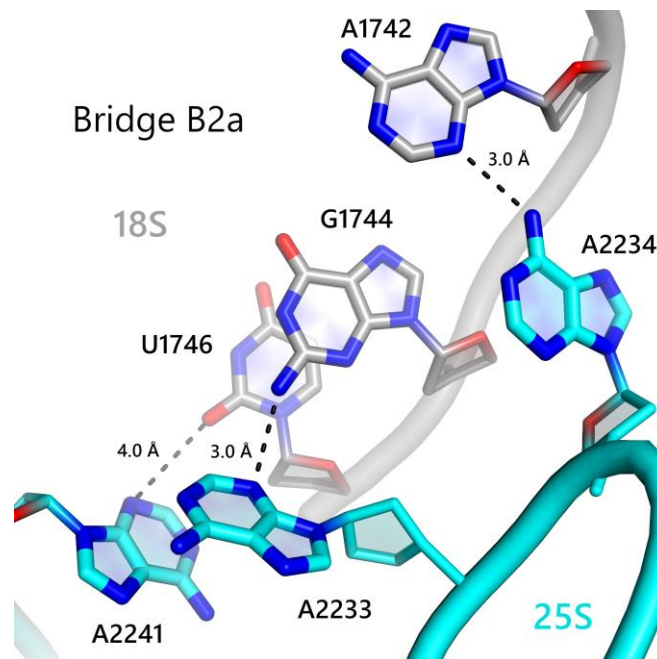


Figure 43 - Detail of bridge B2a highlighting RNA-RNA interaction

4) **B2b**. Bridge B2b is formed by hydrogen bonding between the ribose of A980 of helix h24 and the phosphate backbone of C2174 at the base of helix H68. B2b bridge the hydrogen bonds (OH-H) formed between 2-OH atoms of the ribose of 18S and the phosphate group of the 25S (figure 44). In *C. albicans,* there is also an interaction between C2173 (25S) and G979 (18S).
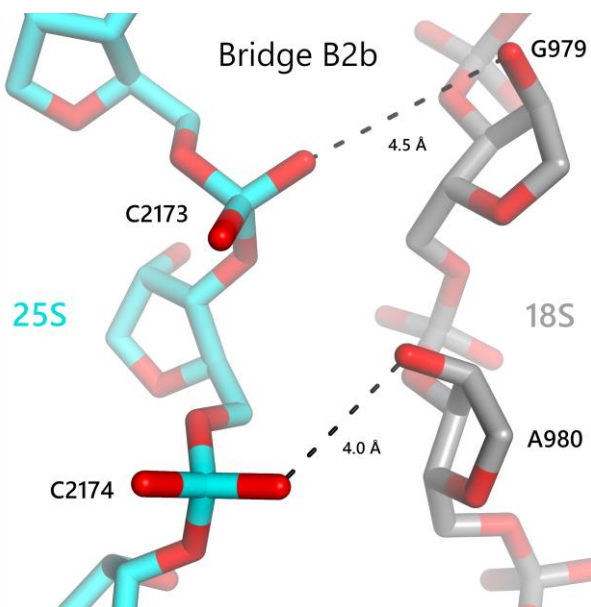
Figure 44 - Detail of bridge B2b highlighting ribose-phosphate backbone interaction

5) **B2c.** In this bridge, the phosphate backbone of C2129 of helix H67 interacts with G969 at the loop region of helix h24, which forms tertiary interaction with the base of helix h27 (figure 45A). In strict contrast to previously annotated bonds of *C. albicans*, the B2c bridge is coordinated by the presence of Mg ions between the backbone of H67 and h24/h27 (figure 45B).

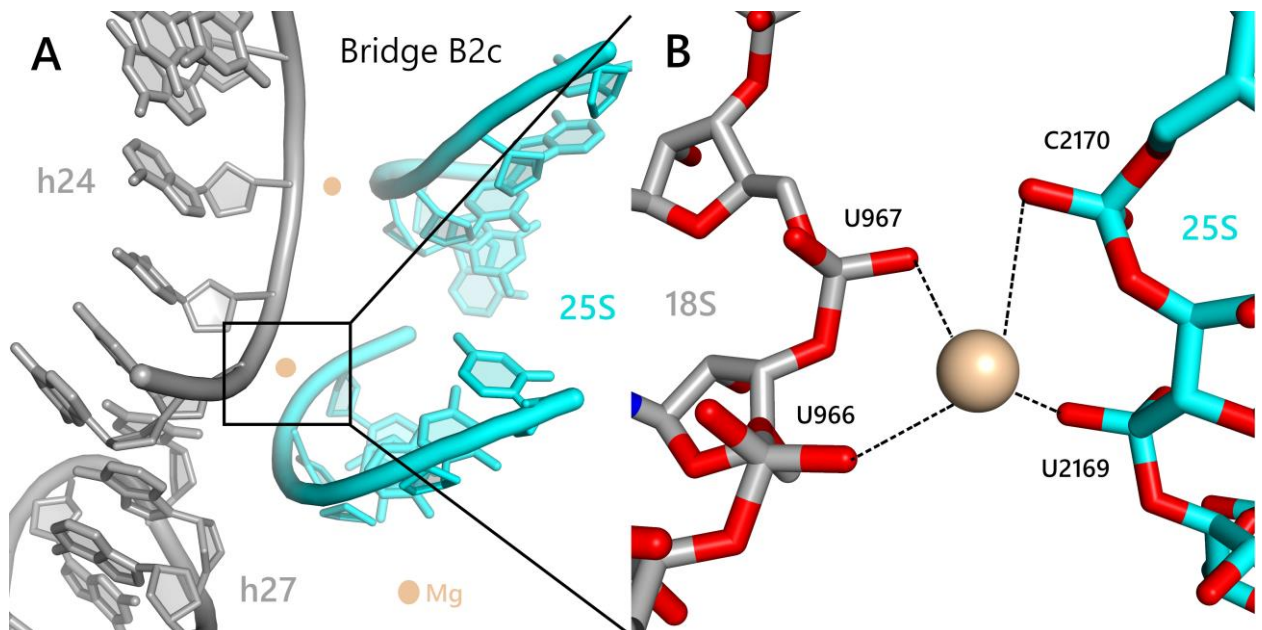

Figure 45 - Detail of bridge B2c highlighting Mg-mediated backbone interaction

6) **B3.** The B3 bridge is formed uniquely by rRNA between the tip of the helix H71 of the 25S rRNA (2268-2270, 2279-2283, and 2103) and the body of the helix h44 (1642-1643, 1732-1735 and 1657). The hydrogen bond formation between backbones mainly forms

this bridge, but there are sugar edge base pairs between G2280 (25S) – A1733 (18S) and A2269 (25S) – A1642 (18S). Moreover, we found the stacking interaction between the ribose of A2103 (25S) and the base of U1657 (18S).

7) **B4.** The B4 bridge is the interaction between helix H34 and eL30 protein from LSU and helix h20 and uS15 protein from SSU. It was discovered in low-resolution crystallography and hydroxyl radical probing in bacteria and was described as the interaction between H34 and uS15. In eukaryotes and mammals interaction pattern extends by the presence of eL30 protein and the closer location of the h20 helix. For example, in *C. albicans,* nt 842-844 from H34 interacts with the 626-627 and 956-959 of h20. In addition, there is an interaction between nts 843-844 of H34 and H123 and K140 of the uS15 protein. Also, there is a direct interaction between eL30 (81-86 aas) and uS15 (145-151 aas).

8) **B5.** Further from the decoding center, the B5 bridge forms between h44 (nt 1647 –1655, 1667 –1669) and helix H62 of 23S rRNA (nt 1931-1932). Besides the interaction between rRNAs, there is an interaction between uL14 (R32, P67 aas) and h44 (nt A1647, U1722). Also, there is an interaction between helix h14 of the 18S rRNA (nts 409-410) and the uL14 protein (S112, N128). In contrast to B2a/d and B3, the tertiary interaction at B5 lacks base-specific minor-groove interactions, and the nucleotide sequence is much less conserved.

9) **B6.** The last bridge contributed by h44 is formed mainly through electrostatic interactions between its phosphate backbone (stem part) and basic residues from large subunit protein eL24, with very little sequence conservation. In the *C. albicans*, we do not see any evidence of bridge formation because all listed interactions in *S. cerevisiae* are broken in *C. albicans*; there is a 6 Å distance between them.

10) **B7a.** Bridge B7 links the 40S platform domain and the base of the 60S L1 stalk, close to the E site. B7a bridge is formed only by RNA-RNA interaction between H68 of the 25S rRNA and h23 of the 18S rRNA. In *C. albicans,* B7a is mainly stabilized by stacking interaction. G898 flips out of helix h23 and stacks with an A2186 at the stem region of helix H68. In contrast to the *S. cerevisiae,* we do not see any evidence of the direct interaction between C895 of h23 and G2239 of H68. In *C. albicans,* these nts are located 6 Å apart from each other and there in density for ions/water molecules.

11) **B7b/c.** This B7b/c bridge is formed between the stem region of helix h23 of 18S rRNA and the ribosomal protein uL2. The C-terminal part of uL2 (residues 247-249) interacts with the phosphate backbone of h23 (nt 972-973). The N-terminal of the uL2 protein

consists mostly of the polar/positively charged amino acids explaining the interaction with the negatively charged and hydrophilic phosphate backbone. Apart from the uL2 proteins, there is also the interaction between the eL43 protein and h23. R24 and K28 interact with the backbone of A967 and A1005 (h23). This bridge also proves the presence of the E-site tRNA bound to *C. albicans* ribosome because, in the structure with no tRNA in the E-site, there is a loss of interaction between subunits.

12) **B8.** In this bridge, ribosomal protein uL14 contact the loop and stem regions of helix h14 of 18S rRNA, mainly through electrostatic interactions with the phosphate backbone. In bacteria, an $Mg2+$ ion coordinates additional interactions between the peptide backbone at the C-terminal region of uL14 and the non-bridging phosphate oxygen of the h14 loop. In *C. albicans,* this bridge is broken; the ul14 protein and h14 loop are located 8 Å apart from each other. The loss of this bridge was previously reported for *H. sapiens* and *Thermus thermophilus*, suggesting that the bridge typically separates during GTPase activation of EF-Tu /EF1a.

13) **eB8.** The eB8 intersubunit bridge is formed by contacts between eS1 and 25S rRNA ES31L and is located proximal to the mRNA exit tunnel. In *C. albicans* eB8 bridge adopts an entirely different pattern; there is no interaction between eS1 and ES31L. Instead, there is an interaction between eL43 and the h22 helix of SSU. The C-terminal of eL43 interacts with the phosphate backbone of the h23 stem (nt 865-869). In other vacant eukaryotic ribosomes, this interaction was not observed. In *H. sapiens,* there is an interaction between eS1 and eL8 proteins; in *S. cerevisiae,* there is an interaction between eL43 and ES31L with eS1.

14) **eB11.** The eB11 bridge is mainly formed by interactions between eS8 and the helix H101 of the 25S rRNA (ES41L). In the *C. albicans,* there is an interaction between the loop of the ES41L (nt 3316-3318) and the C-terminal domain of the eS8 protein (110, 124-132, 168-170). The interaction network differs from that of *H. sapiens* and *S. cerevisiae*. In *S. cerevisiae* ES41L interacts with the following residues: 92, 107-110, 161, 199. In *H. sapiens,* there is an interaction between H101 and residues 77-92; 105; 167-170; 200-205. So, the interaction of ES41L with the residues 124-132 is the specific feature of *C. albicans*.

15) **eB12.** The eB12 bridge is formed by the long C-terminal α-helix of the eL19, and that extends from the E-site of the 60S subunit. This bridge's main feature is that the helix conformation differs during the elongation step. A kink occurs in the pre-translocation state, while the helix is straight in the post-translocation state [104]. Based on this

102

hypothesis, we looked at the interaction pattern of the *C. albicans* ribosome. We found the C-terminal helix of the eL19 protein, proving that our 80S ribosome is in the post-translocation step. The interaction pattern is like those found in *S. cerevisiae*. The middle part of the C-terminal helix of the eL19 protein (middle part, residues 163-176) interacts with the helix h21 of the 18S rRNA (backbone + bases). The end of the helix (L184) interacts with the N-terminal domain of the eS7 protein (residues 35-36).

16) **eB13.** Similar to the eB12 bridge, the eB12 bridge is formed by the long C-terminal α-helix of the eL24 and extends from the A-site of the 60S subunit. However, the conformation of the C-terminal domain of eL24 completely changes during the transition from the pre- to post-translocation state. In the post-translocation step, the linker between N-terminal and C-terminal domains is located close to the eS6 protein, making direct contact between eS6 and eL24. In contrast, in the post-translocation step, the linker has no interaction with eS6. In our *C. albicans* structure, the linker between domains was not visible. Also, the density for the C-terminal helix was insufficient to build. To determine the state of the helix, we aligned all available structures of the mammalian ribosome. Indeed, the conformation of the C-terminal of eL24 shows that, in contrast to other bridges, the eB13 bridge is found in the pre-translocation state.

17) **eB14**. The eB14 bridge is the only eukaryote-specific bridge in the ribosome's center close to the decoding center. This bridge is formed by eL41 and 18S rRNA helices h44 and h45. The 25 amino acids long eL41 are positively charged and form a single α-helix. In *C. albicans,* the interaction pattern is primarily identical to *S. cerevisiae* and *H. sapiens* despite the minor substitutions in the sequence. Several studies suggest that eL41 is a nonessential ribosomal protein, indicating that eB14 is not vital. However, its deletion results in changes in peptidyl-transferase activity and translational fidelity.

## Post-translational modifications of ribosomal RNA

The chemical modification of ribosomal RNA and proteins is critical for ribosome assembly, for protein synthesis and may drive ribosome specialization in development and disease. However, the inability to accurately visualize these modifications has limited mechanistic understanding of the role of these modifications in ribosome function. Post-transcriptional modifications are mainly incorporated early in the process of ribosome biogenesis. These modifications stabilize rRNA structure and participate in binding functional ligands during ribosome biogenesis and translation. Along the different species, the number of

modifications is different. Moreover, the number of modifications is higher in eukaryotes; the highest number is found in *H. sapiens* (table 22) [106].

Table 22 - Comparison of ribosomal RNA modifications between the species

| Specie | Base Methyls | 2'-O-ribose Methyls | Pseudouridines | Total |
|---|---|---|---|---|
| *C. albicans* | 12 | 49 | 19 | 80 |
| *H. sapiens* | 10 | 107 | 95 | 212 |
| *S. cerevisiae* | 10 | 55 | 44 | 112 |
| *E. coli* | 22 | 4 | 10 | 36 |

Since *C. albicans* corresponds to the yeast family, we expected many modifications similar to *S. cerevisiae*. The quality of the map (2.32 Å) allowed us to search for the ribose/base methylations and pseudouridines. During the model building, we manually inspected each nucleotide on the presence of mutations/alterations where there was a strong density for the residue ($I/\sigma \geq 4$). In total, we found 80 rRNA modifications in *C. albican's* ribosome: 62 in LSU and 18 in SSU. This number of modifications in *C. albicans* is approximate due to the absence/weak density for some parts of the rRNA, such as expansion segments. To get the entirely correct list of modifications, other experiments, such as mass-spectrometry and reverse transcription, should be performed [107]. All known modifications can be divided into base modifications, ribose methylation, and pseudouridines. Only ~2% of the whole pool of nt is modified. Among them, ~50% are ribose methylations, ~40% - are pseudouridines, and ~10% - are base modifications.

In the 60S subunit of *C. albicans,* most modifications are like those in *S. cerevisiae*. Nevertheless, we found nine modifications (~10%) unique for *C. albican's* ribosome and not present in other species. Among them, we found five base modifications and four ribose methylations, all rRNA modifications of the 25S specific for *C. albicans* are present in figure 43. Specific base modifications are present in figure 46. In addition, we found two adenines methylated at the seventh position (M7A, fig. 46B, C), two guanines methylated at the seventh position (7MG, fig. 46D, E), and an unusual modification of C1702 (JMH, fig. 46A). In C1702 there is methylation in the third position, which was only found in humans [101], but in another position. The main question is the role of this base methylation and why it is specific for *C. albicans*. It is unclear whether these modifications can affect ribosome stability and translation fidelity and should be thoroughly investigated to elucidate their function.
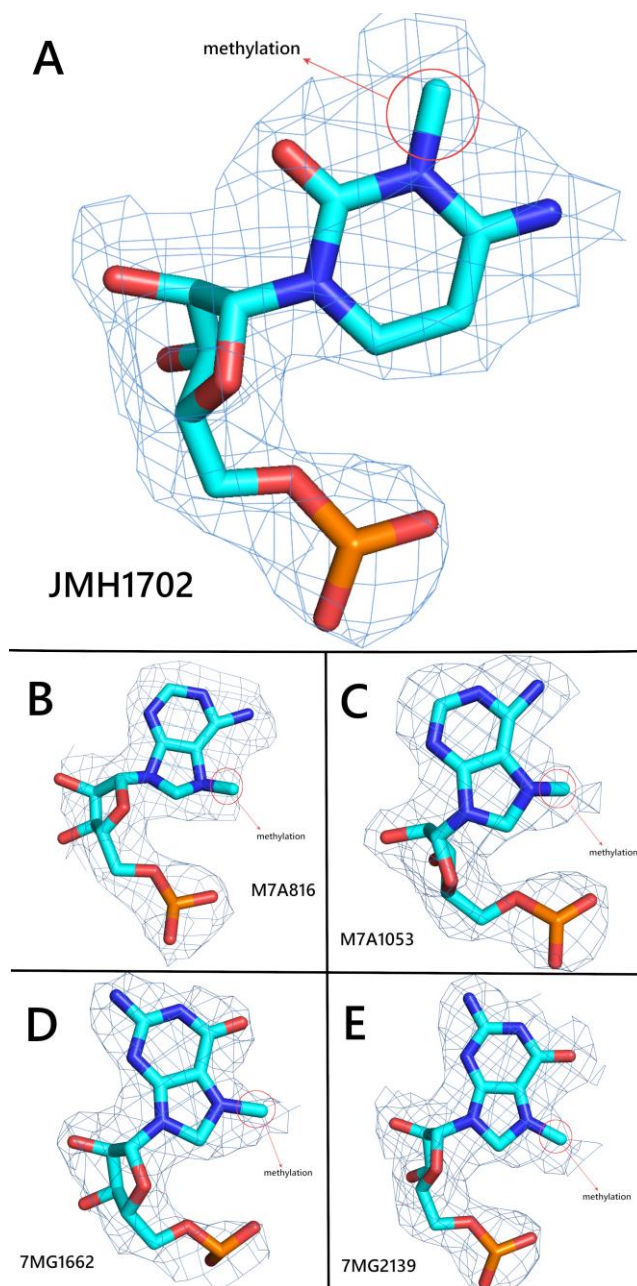
Figure 46 - Specific base-methylation of the 25S rRNA of *C. albicans*

Along with the ribose modification of the 25S rRNA, we found 4 of them present only in *C. albicans*: OMG1430, A2M2304, OMC2808, and OMG2919 (Figure 47). Ribose methylation is required to fold and stabilize rRNAs, thereby contributing to ribosome function. Along with a new specific modification of *C. albicans* 25S rRNA, we found several modifications present in *S. cerevisiae* ribosome but absent in *C. albicans*. A2M803, A2M813, OMU952, OMU2325, etc. All these observations could suggest that the 25S rRNA of *C. albicans* has slightly different physicochemical features, which could affect the thermal stability of rRNA and its function.
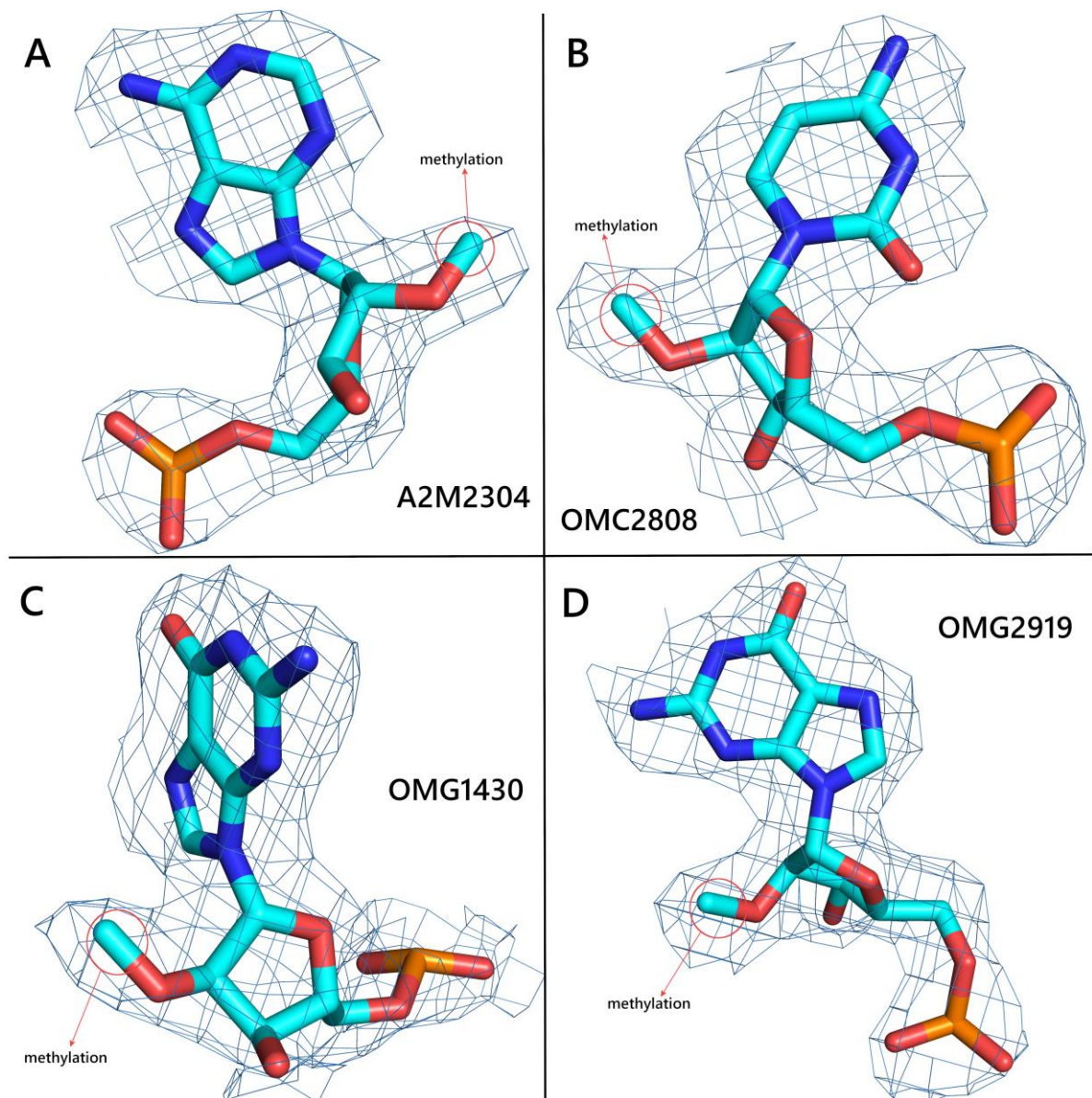
Figure 47 - Specific ribose-methylation of the 25S rRNA of *C. albicans*

The third type of modification is pseudouridines. Ribose pseudo uridylation in eukaryotes is introduced in the rRNA site specifically by small nucleolar ribonucleoprotein particles (snRNPs); H/ACA snRNPs catalyze the conversion of uridine to $\Psi$. According to recent data, pseudouridines mainly stabilize the structure of rRNAs by forming hydrogen bonds with the phosphate backbone via a water molecule. In *C. albicans,* we found three types of interaction of pseudouridines with rRNA. The first type, the most common, is the interaction of the pseudouridine base with the phosphate backbone via a water molecule (figure 48). The water molecule is located between the N5 atom of pseudouridine, the phosphate group of the pseudouridine, and the phosphate from the precedent nt. In total, three bonds keep the stability of rRNA. The main issue in identifying this type of interaction of the pseudouridine is that there are many places where the water molecule could be assigned close to uridine. The typical distance

between them ranges from 2.8 Å to 3.5 Å, and not all of them are pseudouridines according to other methods, so all probable pseudouridines should be double-checked not to create misleading information.
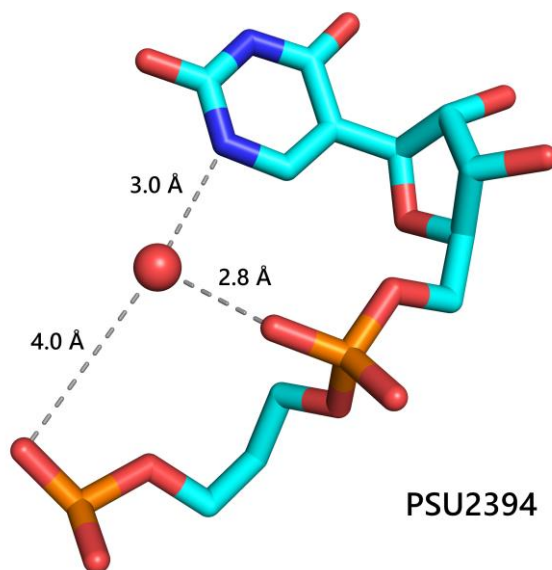


Figure 48 - Water mediated pseudouridine interaction with the rRNA backbone

The second type of pseudouridine interaction is a direct base-base interaction with hydrogen bond formation. For example, there is a base-base interaction between pseudouridine (PSU, Ψ) 772 and uridine 2691 (figure 49). This interaction stabilizes the rRNA by two hydrogen bonds formed between the bases. This type of modification is not prevalent in the rRNA; there are several interactions in the whole ribosome, but, interestingly, pseudouridine molecule could form not only Ψ-U pair but as well Ψ-A, Ψ-G, and Ψ-C pairs.



Figure 49 - Pseudouridine (Ψ) stabilizes RNA duplexes by Ψ-U pair formation

The third type of pseudouridine interaction found in the *C. albicans* rRNA is a direct interaction of the PSU base with the phosphate group of the precedent nucleotide. This type of interaction is somehow close to the first type. However, in this type, there is no more density for the water molecule, and the rRNA conformation allows the pseudouridine base adopts a conformation close to the phosphate group. One of the examples found in the 25S rRNA is PSU2327 interaction with oxygen OP2 of the 2326 (figure 50). The third and the second type of pseudouridine interactions are assigned only by proximity (<3.0 Å) of the probable PSU to the other bases/phosphate groups.
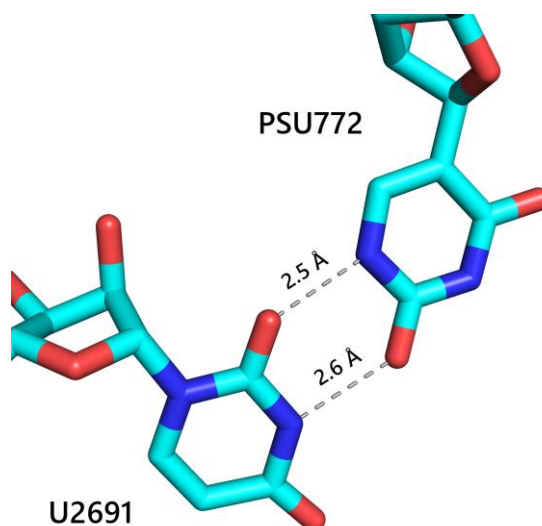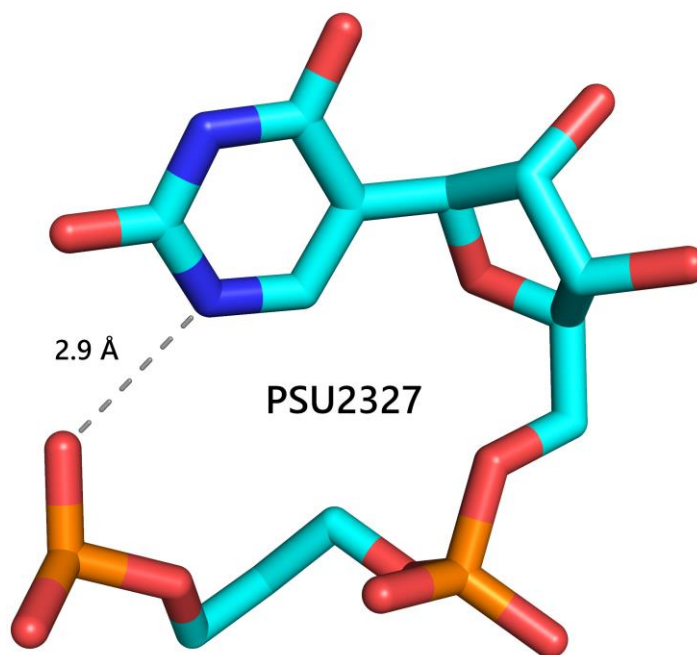


Figure 50 - Direct interaction of pseudouridine (Ψ) with the phosphate backbone of previous nt.

In contrast to the 25S rRNA, we do not see any specific rRNA modification in the 18S rRNA. In total, we found 18 rRNA modifications in the 18S which correspond to those found in *S. cerevisiae*, namely 13 nt with ribose methylation, three nt with base modification, and two pseudouridines. Typical modifications of the 18S rRNA of *C. albicans* are present in figure 51. The most interesting is – the base-acetylation of C1760 at position 4, located in the h45 of the 18S rRNA (N4-acetylcytidine). This modification is vital for protein translation and ribosome assembly.

Moreover, in addition to MA6 modification of nt 1768, 1769 in the SSU, this modification is directly contacted by the ribosomal protein eL41, which forms a bridge between the LSU and the decoding center in the SSU and conducts structural information between the subunits. eL41 protein also acts as a pivot for 40S subunit rotation during translation, suggesting

a mechanism by which monitoring for the presence of rRNA modifications is coupled with translation efficiency via ribosomal protein interactions [108]. In the 5S and 5.8S rRNA, we do not see any evidence for rRNA modification as it was found in *S. cerevisiae* previously. All found rRNA modifications are presented in table S2.
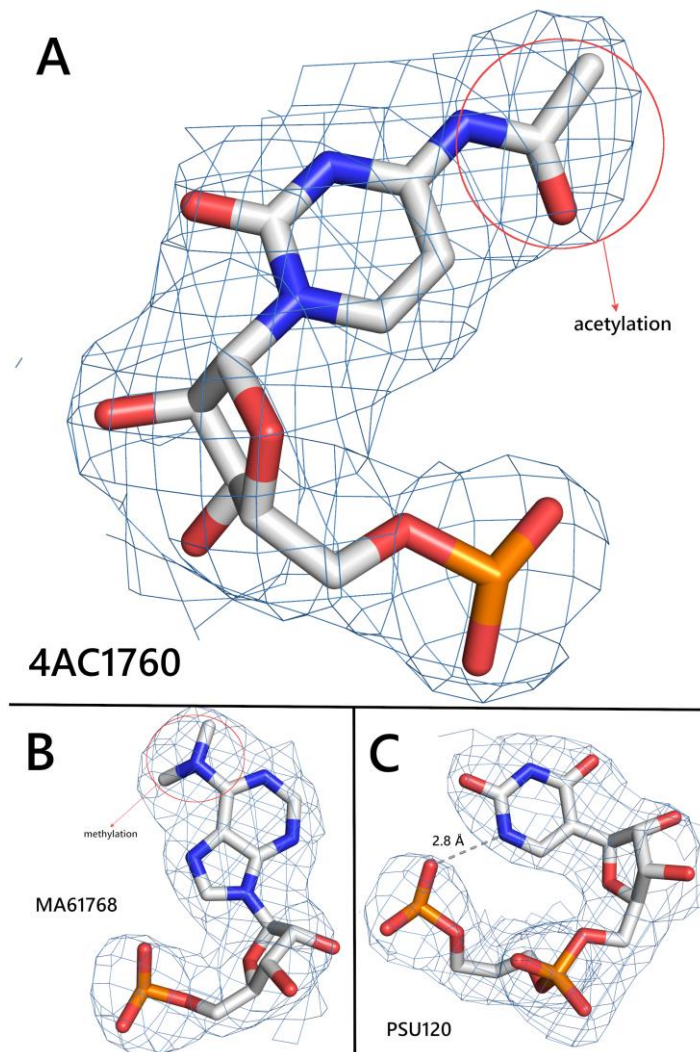


Figure 51 - Typical modifications of the 18S rRNA of *C. albicans*

## Post-translational modifications of ribosomal proteins

In contrast to ribosomal RNA modification, there is little data on ribosomal protein modification, especially in eukaryotes. The main obstacle here is that the cryo-em map could not be used as only the instance to prove them, especially in the case of the side chain modification, such as methylation. The only obvious modification of the ribosomal protein is N-terminal acetylation. A recent study of Pellegrino found 2 N-terminal acetylations of the proteins uS2 and eS21 in the *H. sapiens* ribosome [109]. In *Candida albicans,* we also see these modifications

according to our density (Figure 52). In the same study, these modifications were proven by mass-spectrometry analysis. They also identified N-terminal acetylation of uS7, eS6, eS12, uS13, and eS19; however, the N-termini of these ribosomal proteins were disordered. Similar to *H. sapiens,* in *C. albicans,* we also do not see the N-terminus of these proteins due to their high flexibility. In *S. cerevisiae*, the two proteins uL13 and uL14 were N-terminal acetylated [110]. However, since we do not have the strong density for these N-terminals, we cannot determine if they are equally modified in *C. albicans.*

The main restriction for detecting N-termini acetylation is that density should be strong enough and, at the same time, stable; otherwise, it is invisible on the cryo-em map.
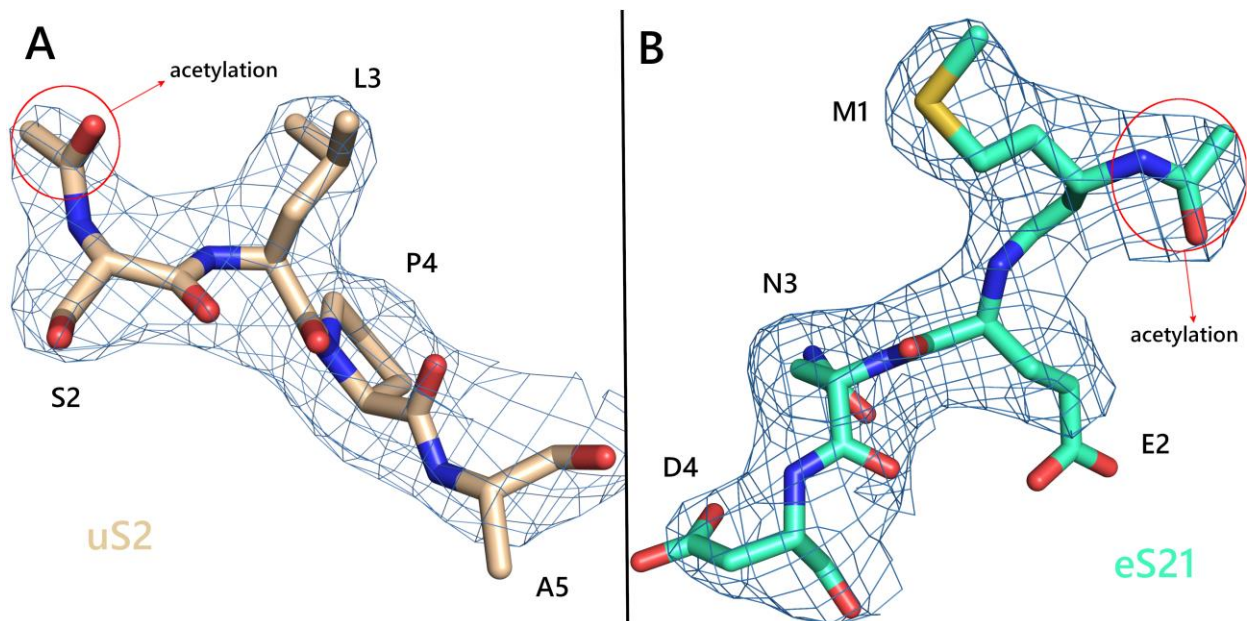


Figure 52 - N-terminal acetylation of the proteins uS2 (A) and eS21(B) in *C. albicans* ribosome

Another type of ribosomal protein is the methylation of the protein side chain. It was mainly found in arginines (R) and lysines (K), but there is also data on the modification of histidine and glutamic acid. Unfortunately, there is not much data on the side-chain methylation of the ribosomal proteins, only for uL11, uL14, uL3, and eL42. The most thorough study using mass-spectrometry and analytical method find-mode identified 18 aas with K/R side chain monomethylation [111]. In the *C. albicans* ribosome, we used literature data as a starting point for searching for side-chain modifications. We found a strong density indicating the methylation of K110 in the L14 protein and K40 and K55 in the L42 protein (figure 53). Even though these findings have to be proved by other methods, the quality of the cryo-EM map allowed us to make such assumptions.
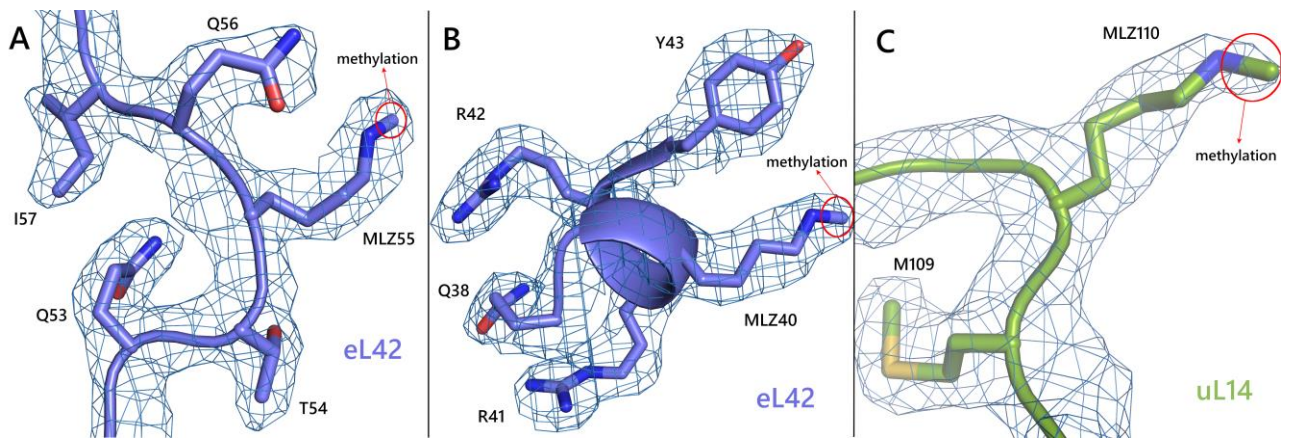
Figure 53 - Monomethylation of K40 (A) and K55 (B) of the eL42 protein and K110 (C) of the eL22 protein

In addition, it was proposed that in *E. coli* uS11, D119 is modified to an isoaspartyl residue [112]. Our results suggest that this can also take place in eukaryotes. We observe that the corresponding residue in *C. albicans* is moved to the backbone, indicating the isomeric form of aspartate. Without applying a modification to the residue, it cannot fully fit the observed density leading to the violation in a backbone position. The isoaspartyl modification found in the *C. albicans* ribosome is present in figure 54. The role of these modifications is not yet clear if they affect ribosome function. Making an analogy with histones suggests that side-chain methylation controls the interaction with other proteins.
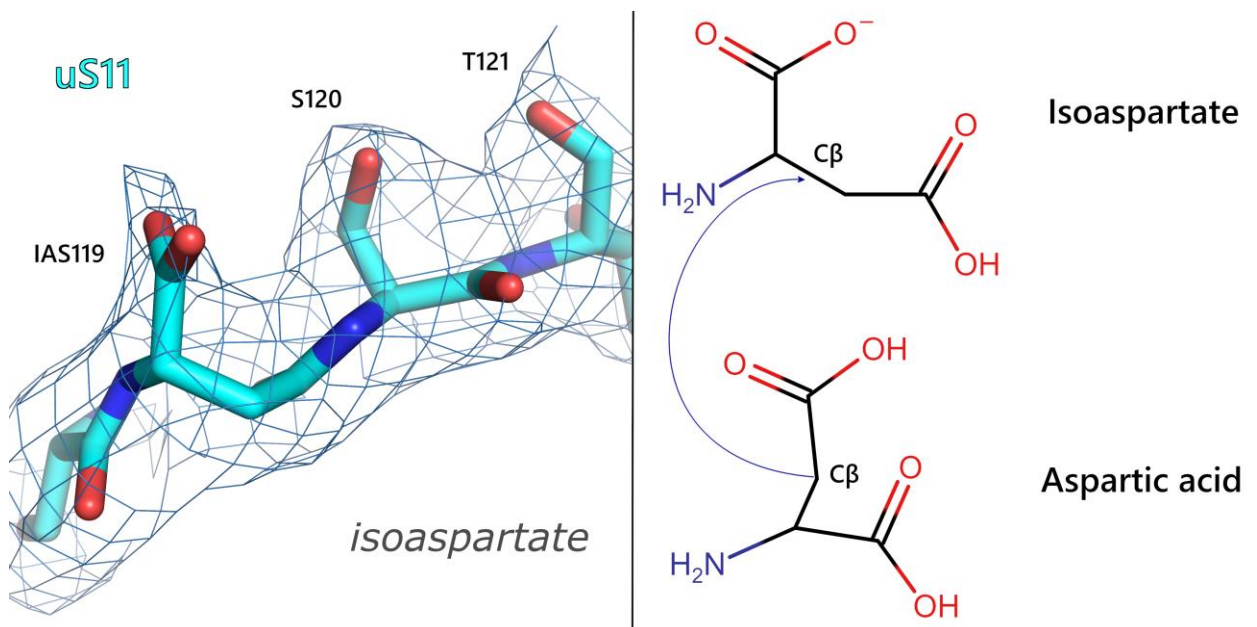


Figure 54 - Isoaspartate modification in uS11 protein

# Side chain isomers of the ribosomal proteins

Alternative conformations of ribosomal proteins might play an essential role in the assembly and functioning of ribosomes (34). However, the exact role of each conformation is still unclear. In our work, 32 AAs with multiple side-chain conformations were found, most of them in proteins eL18, eL33, and eL34 (figure 55). The complete list of the isomers is presented in table S3. Among all the conformations found, alternative lysine, glutamine, and arginine rotamers are the most frequent. However, we observe only two different isomers for the selected side chain. Therefore, it is not clear whether it is a factual representation of multiple side chain conformation of the side chain, and the selected side chain switches from "on to off" conformation, or whether the side chain is flexible. The visible conformation reflects the slow exchange between the bunch of the conformations.

Moreover, the multiple isomers do not affect other residues in proximity, so we can conclude that there is no influence of side-chain isomers on the overall stability of the pocket. To sum up, there are no answers to these questions, and other methods should thoroughly analyze them and the function of these isomers, which is not clear yet. Considering not only ribosomal proteins but protein side-chain conformations have also been shown to be closely related to protein mutations. Side-chain contacts mainly mediate the protein interactions with proteins, RNA/DNA, or ligands. During these functional steps, some critical side-chains may change their conformations to adapt to the shape and character of their interaction partner [113]. That is why side-chain conformational changes, or side-chain polymorphism, could be closely related to protein functions. Nevertheless, the side-chain variations have not yet been quantitatively analyzed [113], and understanding side-chain conformational variation is still intuitive and not systematic.
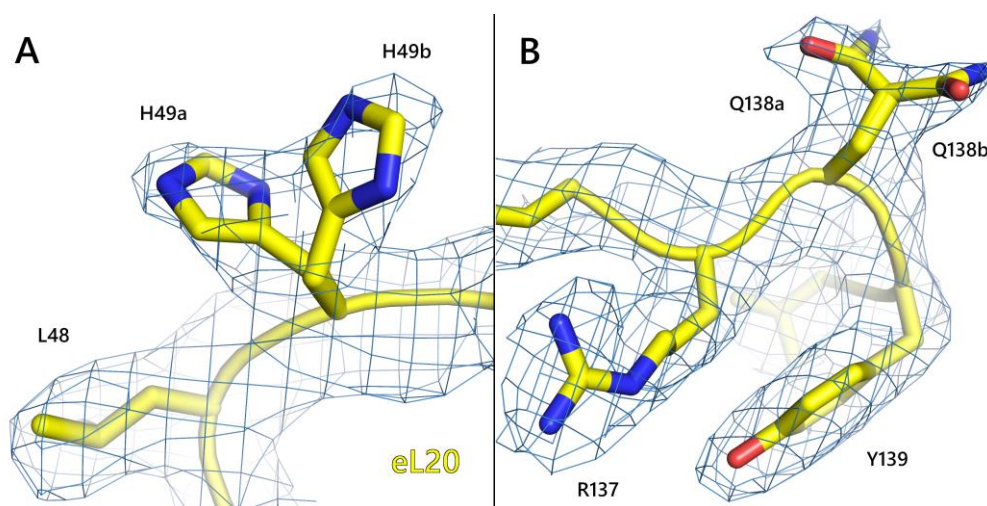
Figure 55 - Multiple side chain conformations of ribosomal proteins. Isomers of H49 and Q138 of eL20 protein

## Location of polyamines in the ribosome and their role

During the last decades, it became clear that polyamines play an essential role in ribosome stability and assembly. Nevertheless, for a long time, it was unclear where the binding site of the polyamines on the ribosome is and what mechanism keeps the stability of the rRNA. The first mentions of the polyamine binding site were made on the *S. cerevisiae* ribosome and later on the *N. crassa* ribosome, where they found an unambiguous density for the spermidine in the E-tRNA binding site [114, 115]. The same work was performed for *E. coli*; in the work of Cate, they identified 17 polyamines in the 70S ribosome [112]. In our work, we identified 10 spermidine molecules and two putrescine molecules (Table S5). The main point here is that we did not add the polyamines to our system from the outside; all of them were naturally synthesized by *C. albicans*. Therefore, we could only identify the polyamine binding site on the large subunit since we can assign the density for them at a resolution better than 2.5 Å, which is not the case for LSU. The polyamines' binding sites can be divided into two groups: interaction only with 25S rRNA and interaction with rRNA and ribosomal proteins. We observe that the polyamines, like metal ions, stabilize the tertiary structure of the rRNA and protein-rRNA interactions.

The first example, other groups previously identified, is the E-site stabilization by the spermidine located close to the uL15 protein (figure 56). SPD molecule directly interacts with the side chains of the Q38 and H39 of the uL15 protein and the phosphate group of G93 of 25S rRNA. In the available functional studies, mutation of Q38 by other amino acids led to strong resistance to the cycloheximide (CHX), which binds to the E-site on the 60S subunit [116, 117].

It was unclear how this mutation could affect the binding of CHX. Here we propose the mechanism that could explain CHX resistance in the Q38 mutation. If we measure the direct distance between the glutarimide group of CHX and the Q38 side chain, there is ≈8 Å between them. We suggest that the SPD molecule is mediating the interaction between them: it is located 3.4 Å apart from Q38 and 4.3 Å from CHX (figure 56B). In the case of the Q38 mutation, we guess that the SPD molecule leaves the binding pocket, leading to the considerable rearrangement of the E-site. So, we suggest that the SPD molecule plays an essential role in the E-site pocket stability.
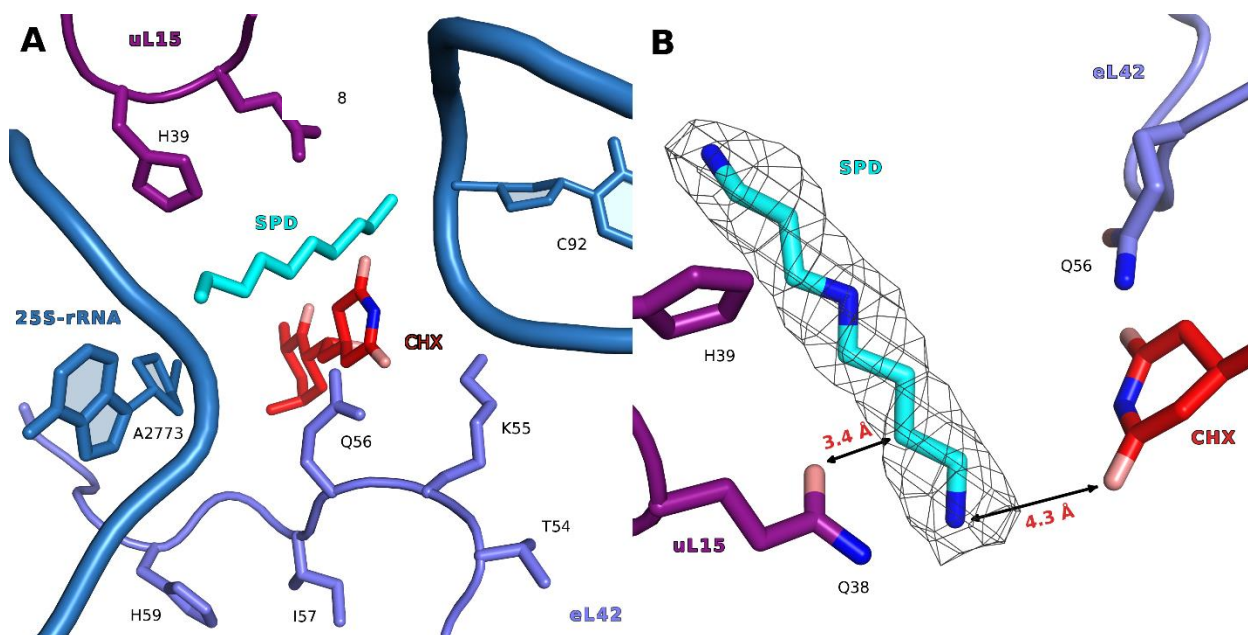


Figure 56 - Spermidine stabilizes the E-site binding pocket. (A) Overview of the E-site. (B) Close-up view of SPD with its density.

Another example is the spermine molecule (SPK) located close to the E-site and the putrescine (PUT) molecule near the protein tunnel. In both cases, we suggest that the role of the polyamines is to stabilize the pocket between the distinct parts of the rRNA and proteins. In the first case, SPK acts like a bridge between H13 and H21 of the 25S rRNA. Four hydrogen bonds formed between SPK and phosphate groups of the rRNA (figure 57A). From the one end with G282 (H21) and U45 and A48 (H13) from the other end. The PUT molecule is located near the peptide tunnel, interacting with the uL22 protein and the helix H26a of 25S rRNA. It is located along the base G2333, and one end (N2) interacts with the phosphate groups of C2332 and G2333 while the other end (N1) makes contact with the side-chain of R82 of the uL22 protein (figure 57B). The whole list of the polyamine's location with their interaction is presented in table S4. All our findings suggest that despite a few polyamines in the ribosome, they play an

indispensable role in supporting the stability of the ribosome and the rRNA-rRNA/rRNA-rprot contacts.
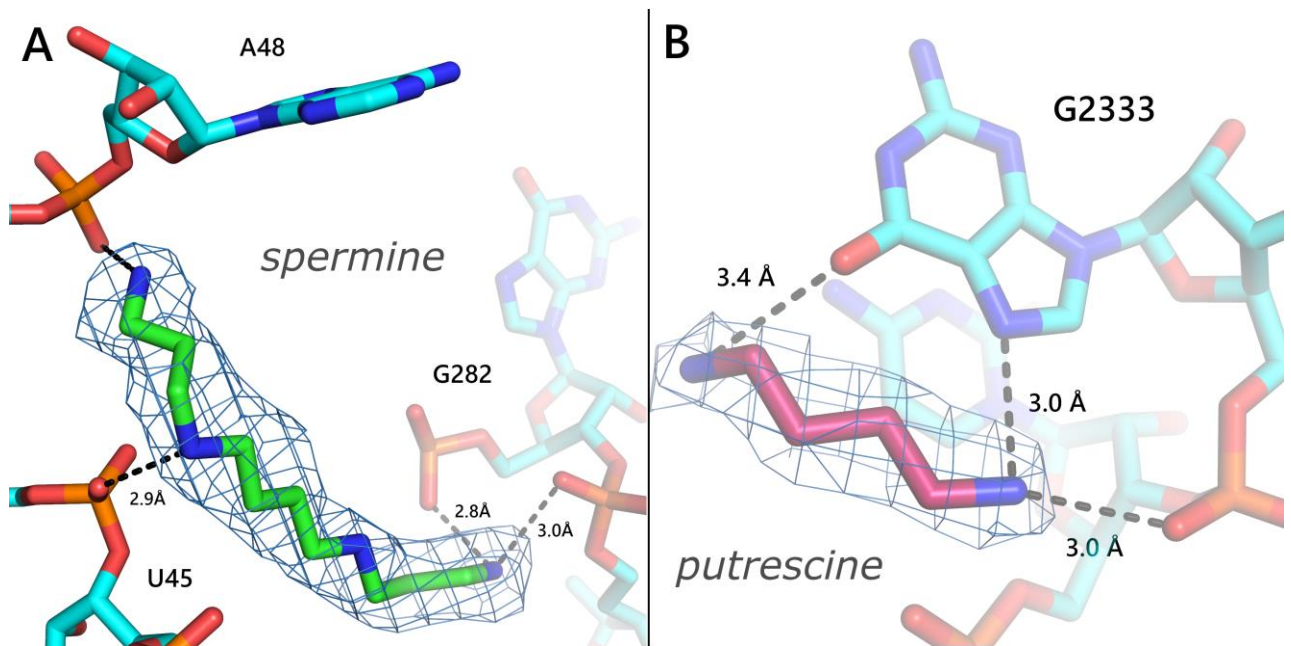


Figure 57 - Polyamines stabilize rRNA-rprot contacts. (A) SPK molecule between H13 and H21 helices. (B) PUT along the G2333.

## Location of metal ions and water molecules

By interacting with nucleic acids, especially RNA, metal ions like magnesium ($Mg^{2+}$), sodium (Na+), and potassium (K+) perform important biological purposes. For two reasons, magnesium is particularly well-suited to reducing the negative charge density linked to the RNA phosphate backbone. First, it is the most prevalent intracellular multivalent cation. Due to its comparatively modest ionic radius (0.6 Å), it possesses the highest charge density of all ions that are readily available for biological use. A "site binding" mode, which involves the specific coordination of anionic ligands to partially dehydrated $Mg^{2+}$, and a "diffuse binding" mode, which involves nonspecific long-range electrostatic interactions with $Mg^{2+}$ hexahydrate, have both been described as two general modes of $Mg^{2+}$ ion binding to RNA. Both are crucial for the stabilization of RNA's structural integrity. Less is known about the structural functions of monovalent cations like $Na^+$ and $K^+$ in maintaining RNA structure. However, the physiological abundance of $K^+$ and the fact that at least two RNA molecules require it specifically for structural purposes imply that it may also be crucial for stabilizing the tertiary structure in giant RNA molecules. The growth of Escherichia coli cells under $Mg^{2+}$ shortage results in ribosome depletion, indicating that $Mg^{2+}$ is necessary for the ribosome's structural integrity and assembly. The permanent loss of poly-phenylalanine polymerizing activity and the considerable unfolding

when mammalian ribosomes are moved to K+-free buffers demonstrate the importance of $K^+$ ions for ribosome structure and function [118]. In the *C. albicans* ribosome, we found 444 round-like densities assigned to $Mg^{2+}$. Most of them are close to the phosphate group of the rRNA, showing their role in rRNA integrity. We decided not to put monovalent ions in our structure since the density does not allow us to put them unambiguously. They must be inserted using a more robust method, such as an X-ray with anomalous scattering. This work was already performed for the *T. thermophilus* ribosome showing its vast possibilities [118].

Another ion that plays a crucial role in ribosome biogenesis is Zn. Zn ion binds to so-called zinc finger regions of the proteins composed of four cysteines. In our *C. albicans* structure we identified 8 zinc ions located in between 4 cysteines in following proteins: eL37, eL40, eL42, eL43, eS26, eS31, eS27 and uS14. The zinc finger motifs are highly conserved across the species. According to the available literature data, the eL37 protein is the only protein that has undergone a thorough genetic, biochemical, and structural analysis. In this study, the effect of cysteine by serine substitution was investigated. It was discovered that all four cysteines are necessary for zinc binding. Despite this, cells with mutations in three of the four cysteines do not significantly suffer from growth impairment, nor is the binding to rRNA of the mutant proteins materially affected. Although ribosomal proteins have evolved to employ different amino acid sequences or structures to bind to rRNA, as has been demonstrated to be the case with eL37, it is still feasible that the zinc finger motif in ribosomal proteins represents the leftovers, or biological fossils, of a primary function.

Apart from the metal ions, water molecules play an integral part in ribosome stability and biogenesis. Using a Phenix.douse utility, we identified 1367 blobs as water. To sum up, our structure reveals more than a thousand water molecules and around 500 metal ions that help keep the ribosome together as it produces proteins.

## Structural insights on the functional sites of the *C. albicans* ribosome

### E-tRNA binding site (E-site)

Previously, the structural organization of the E-site of the 60S subunit of *S. cerevisiae* ribosome was studied by determining complexes with a CCA-end analog of tRNA and E-site inhibitors [116]. It was shown that the rRNA in this pocket is highly conserved between yeasts and humans and is responsible for most interactions with inhibitors. Along with rRNA in the E-site, eukaryote-specific ribosomal protein eL42 interacts with some inhibitors and stabilizes them

in the binding pocket [119]. As was written before, we revealed that in the E-site of the sequence from the vacant *C. albicans* ribosome with the ribosomes from *S. cerevisiae* and *H. sapiens,* we revealed that in the E-site of *C. albicans* ribosome, there is a P56Q alteration in ribosomal protein eL42. The high-resolution structure of the vacant *C. albicans* ribosome allowed us to get structural information on this mutation. The quality of the map allowed us to unambiguously assign the density for the glutamine side and make a direct comparison with other eukaryotes (Figure 58)
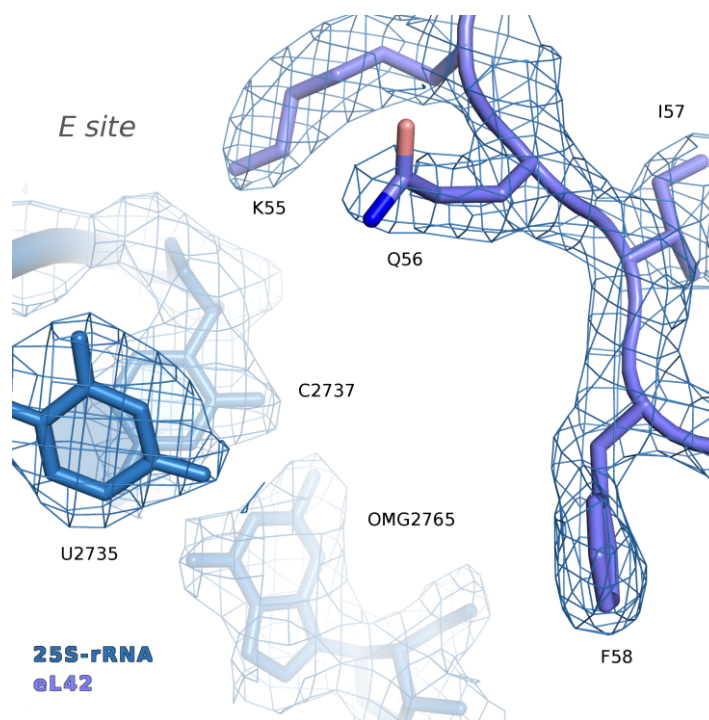


Figure 58 - Density map of 25S rRNA and eL42 protein in the E-site of 60S subunit.

The eL42 P56Q substitution decreases the volume of the binding pocket. To establish whether the reduction of the pocket volume affects the binding of inhibitors, we compared the *S. cerevisiae* ribosome (PDB 4U3U) and *H. sapiens* (PDB 5LKS) ribosome in a complex with CHX to the vacant *C. albicans* ribosome (at 2.3 Å) with a superimposed CHX molecule. CHX binds to the 60S subunit in the E-site, preventing translocation of tRNA from the P to the E site. In *S. cerevisiae*, CHX forms five hydrogen bonds with 25S rRNA: specifically with G92, C93, U2763, and C2764 (*C. albicans* G91, C92, U2735, and C2736). The main difference between the two species concerning CHX binding is the lack of interaction of CHX with P56 of eL42 in *S. cerevisiae,* where the CHX molecule is 3.1 Å distant from the proline side chain (Figure 59). Superimposing CHX into the vacant *C. albicans* ribosome creates a clash between the Q56 side chain and the glutarimide group of CHX (Figure 59). Our findings suggest that electrostatic

repulsion between Oε oxygen of the glutamine side chain and O6 oxygen of CHX occludes its binding to the *C. albicans* ribosome.
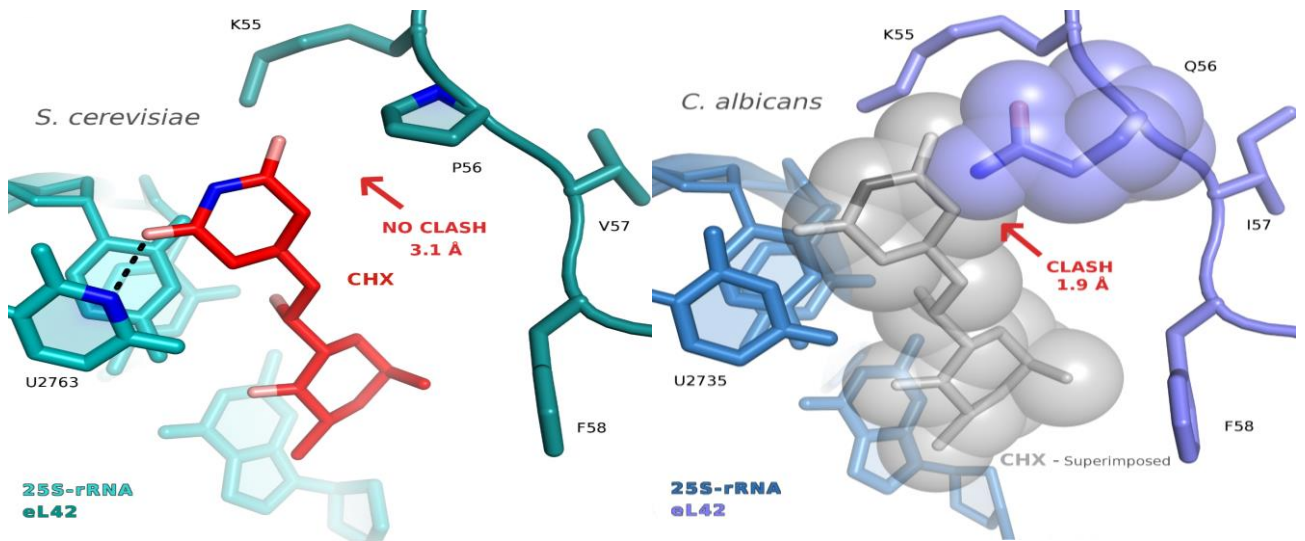


Figure 59 - Q56 prevents the binding of CHX to the *C. albicans* ribosome.

## Peptidyl transferase center

Aminoacyl-tRNA and peptidyl-tRNA sites (A-site and P-site, respectively) of the ribosome peptidyl-transferase center are highly conserved among eukaryotes. The PTC nucleotide composition of *C. albicans*, *S. cerevisiae*, and *H. sapiens* is identical. The PTC is a highly stable part of the ribosome, so the high-quality cryo-EM map allowed us to unambiguously assign the backbone and bases of the nts (Figure 60).
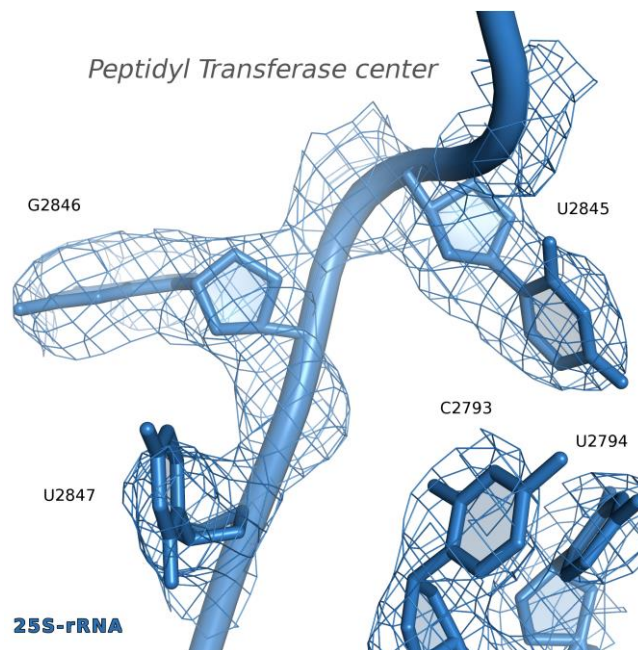
Figure 60 - Density map of 25S rRNA in the A-site of peptidyl transferase center.

The next step was to compare the position of nucleotides in other eukaryotes. We compared the *S. cerevisiae* ribosome (PDB ID 4v88) in the A-site of PTC, C2793, and U2847 adopting different conformations (figure 61A). Previously, in comparison of the eukaryotic and bacterial ribosomes, it was shown that the conformation of the U2847 plays a vital role in the insensitivity of the bacterial ribosome to A-site inhibitors, such as anisomycin (ANM). Anisomycin blocks the translation in eukaryotes but is not active against bacteria. Regarding the structural differences in U2847 conformation, we decided to understand whether these differences play any physiological role or just reflect the differences in sample preparation (single particles vs. a crystal). Based on these observations, we decided to make a complex with anisomycin and check whether it binds to *C. albicans* or not. Concerning the P-site of the ribosome, a different conformation of A2780 was recognized compared to the *S. cerevisiae* vacant ribosome (figure 61B). As previously described, this nt plays one of the significant roles in P-site inhibitors binding (18). To further characterize the binding of inhibitors to the P-site in *C. albicans* ribosome, we aimed to resolve its structure with blasticidin S (BLS), known P-site inhibitors active against bacteria and eukaryotes.
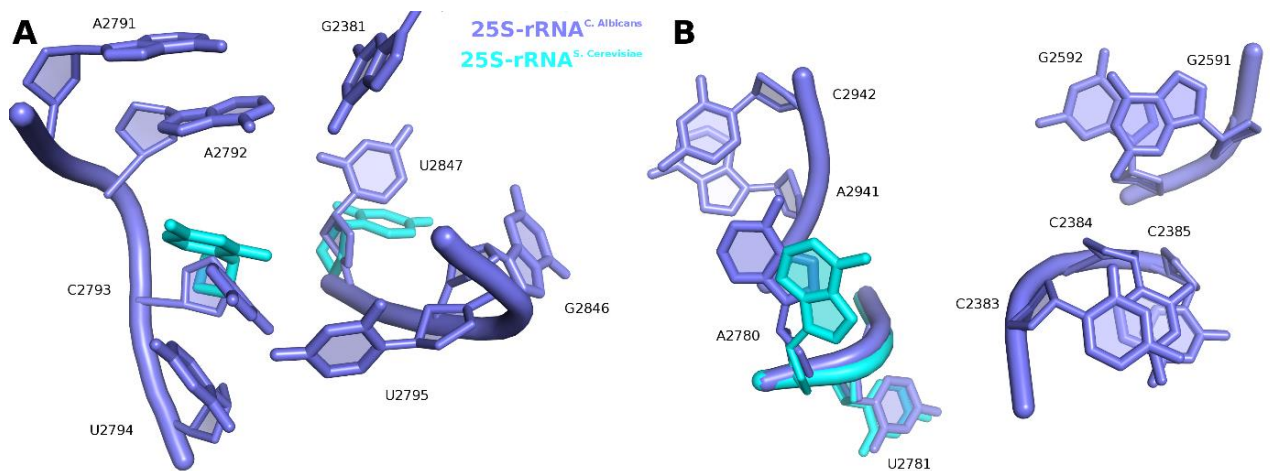


Figure 61 - Comparison of peptidyl transferase center. (A) A-site comparison. Compared to *S. cerevisiae* 2793C and U2847 adopt different conformations. (B) P-site comparison. A2780 position is shift-ed compared to the *S. cerevisiae* ribosome.

## Decoding center

Along with the PTC, the composition of the DC is identical between *S. cerevisiae*, *H. sapiens*, and *C. albicans*. Nevertheless, a difference in backbone position was observed between them in the cryo-EM map. Such a steric disposition can affect the translation process and the binding of

specific inhibitors, such as gentamycin (21). In *C. albicans,* decoding nucleotides A1742 and A1743 are in the so-called "in" position, while in *S. cerevisiae* (PDB ID 4v88)*,* A1743 is in the "out" position.  The base of the A1742 is slightly turned compared with *S. cerevisiae* (PDB ID 4v88), but the most crucial changes are observed in the position of A1743. Even though the density of the base is relatively weak for this residue, the positions of the phosphate bomb and the ribose suggest a 60° turn of the A1743 base (figure 62B).

Along with this observation, the position of A2234 of 25S rRNA is drastically changed; in our case, there is a direct interaction between the base of A2234 and the ribose of A1742, which is entirely different from the *S. cerevisiae* ribosome structure (PDB). Compared with the structure of the *H. sapiens* ribosome (PDB ID 6z6n), the difference is not so significant. *H. sapiens* are in the "out-in" position as in *S. cerevisiae*. The only difference is the conformation of A1743; in *C. albicans,* it is turned by 180° (figure 62A). Due to the high flexibility of the decoding center without the presence of mRNA and tRNA, we cannot make any assumptions about its specific features and inhibitors' sensitivity.
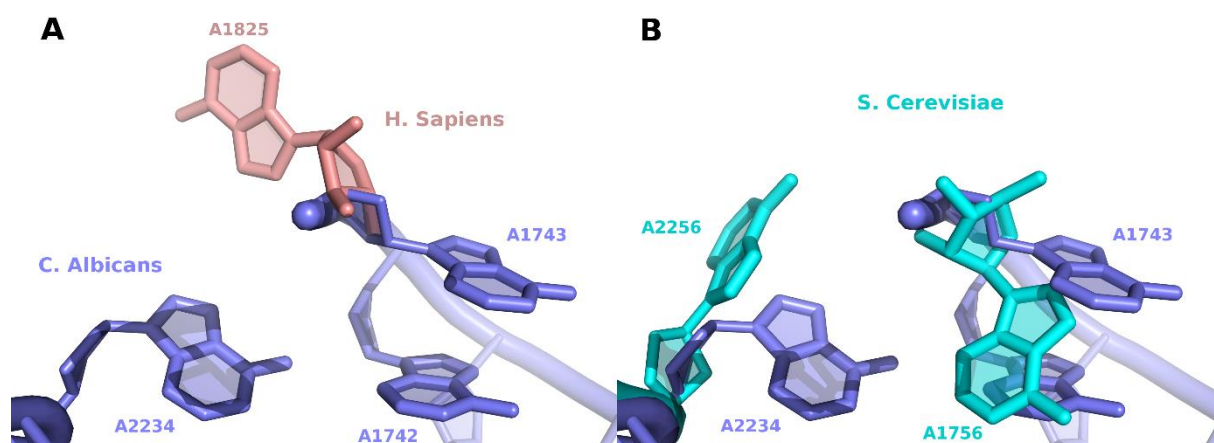


Figure 62 - Structure of the decoding center (DC). Comparison of DC of *C. albicans* (dark blue) with *S. cerevisiae* (cyan) (B) and *H. sapiens* (light red) (A).

## Structural insights on sequence difference of the *C. albicans* ribosome with other eukaryotes (expansion segments and protein deletions/insertions)

During the model inspection, we also look at footprinting parts of *C. albicans*, namely the expansion segments ES7 and ES27, which are highly different in *C. albicans*, and ribosomal proteins, which have differences in the secondary structure. The expansion segments ES7 and ES27 were not visible due to their high flexibility, so we cannot conclude any structural distance for them. On the other hand, most of the ribosomal proteins with several insertions/deletions

were visible on the map, allowing us to build them correctly and guess their role. The following differences have been observed:

1) The eL13 protein has a three aa insertion in the region 135-137. In the map, we observed that this region does not possess a secondary structure; in *C. albicans,* this region is folded in α-helix. This helix is located on the surface of the ribosome.

2) In the eL14 protein, there are several deletions in the body. For example, in the 25-28 region, there is a 4aas deletion, so there is an α-helix instead of a β-sheet. Also, the β-sheet (44-46 residues) is two aa shorter, and the backbone extension is in the 64th position.

3) In the eL22 protein, which is also located on the surface, two β-strands are longer, which are visible on the map (58-61 and 67-70 aas).

4) In the eL30 protein, there is a one aa insertion in the region 102-106 which leads to a bit different direction of the helix.

5) In the eS7 protein, there is a four aa truncation, which is visible in the cryo-EM, but this part is disordered as in *S. cerevisiae*.

6) The eS8 protein has six aa insertions in the β-strand region 125-146. This extension leads to a new intersubunit contact between the eS8 and the H100 helix of the 25S rRNA. There is a direct interaction between K124 and U3316, which is not present in *S. cerevisiae* and *H. sapiens.*

7) In the RACK protein, located at the exit of the mRNA tunnel, there is a 4aa deletion in the β-sheet, which is exposed to the solvent and forms a tip outside in *S. cerevisiae*.

We think all the mentioned structural differences are essential in interacting with the enzymes that bind to the ribosome surface. Unique insertions/deletions in some ribosomal proteins of *C. albicans* can interact with the non-ribosomal proteins, which can control ribosome assembly and functioning.

# CANDIDA ALBICANS: SENSITIVITY TO INHIBITORS

## Cell-free assays

Based on the vacant C. albicans ribosome results, we aimed to check how the differences in the functional sites affect the binding of the inhibitors. Therefore, to not only rely on structural data; in collaboration with Texas A&M University (C. Wu and M. Sachs), we performed cell-free assays in *C. albicans*, *S. cerevisiae*, and mammalian ribosome (Rabbit reticulocytes, RRL) to compare the activity of the known inhibitors on these three species. The cell-free assays were performed using the following protocol.

The cell-free translation extracts (CFTSs) were programmed with luciferase mRNA, and then their capacity to produce the enzyme in the presence of increasing concentrations of inhibitors was examined. *C. albicans* belongs to a subclade in which the "universal" genetic code is altered; in this "CTG-clade," the CUG codon is translated as Ser, not Leu [120, 121]. Therefore, sea pansy luciferase was used (spLUC) as the translational reporter because the coding region for this enzyme lacks CUG codons and functions as a reporter in *C. albicans* [122]. Translation of spLUC RNA using CFTSs from these yeasts can thus be directly compared without concern for using different genetic codes.

*C. albicans* and *S. cerevisiae* CFTSs were prepared using the Method 1 protocol for *S. cerevisiae*, and translation reactions were assayed for LUC activity, as described in [123]. Rabbit reticulocyte lysate (RRL) was obtained from Promega (L4960). Capped and polyadenylated sea pansy luciferase (spLUC) mRNA was prepared by T7 transcription of EcoRI-linearized plasmid pQQ101 encoding spLUC [124]. For quantification, triplicate independent CFTSs (10 µl each) programmed with 60 ng of spLUC RNA and RRLs programmed with 6 ng of spLUC RNA were incubated at 26°C in the absence or presence of different concentrations of inhibitors for 30 min, and the activity of sea pansy LUC then measured by luminometry.

## Complex with anisomycin

First, we attempted to make a complex with anisomycin, a known eukaryotic inhibitor that binds to the A-site of the PTC. However, most A-site inhibitors do not bind to the bacterial ribosome due to the different conformation of the U2847 (U2504 in bacteria). In bacteria, the different conformation was assigned to the influence of the nucleotide 2375 (2055 in bacteria). In bacteria, this nt is cytosine; in eukaryotes, it is adenine in 96% of cases. In *C. albicans,* 2375 nt is also adenine, and it adopts the same conformation as in *S. cerevisiae* and *H. sapiens;*

nevertheless, U2847 in *C. albicans* adopts a different conformation in comparison with other species. That is why we decided to check if this conformation affects the binding of the A-site inhibitors making the complex with anisomycin (ANM).

First, we decided to perform cell-free experiments using lysates from *C. albicans*, *S. cerevisiae*, and rabbit reticulocytes (RR). The results of cell-free assays are present in figure 63. The inhibition of ANM across the three species is similar but not at the same level. The IC50 values are ≈0.25 μM for RR, ≈0.5 μM for *S. cerevisiae*, and ≈1.0 μM for *C. albicans*. It is still unclear if this difference is directly connected with the conformation of U2847. However, we can speculate that it plays a role in the inhibitory activity of the A-site compounds.



Figure 63 - Inhibition of translation by ANM tested in cell-free systems from *C. albicans*, *S. cerevisiae*, and RR.

Using the results of the cell-free assays, we formed a complex with ANM. First, we incubated the 80S ribosomes of the *C. albicans* ribosome with the 250 μM of ANM at 30 ºC for 15 min. After it, we applied the same protocol for the vacant C. albicans ribosome, resulting in a 2.77 Å cryo-EM map (Fig. S1, S5C, Table S6). Despite the map quality being lower than the vacant C. albicans ribosome (2.3 Å), we could still distinguish rRNA bases and protein side chains. Furthermore, after the map analysis, we found a strong density in the A-site of the PTC, perfectly mimicking the ANM molecule (figure 64).
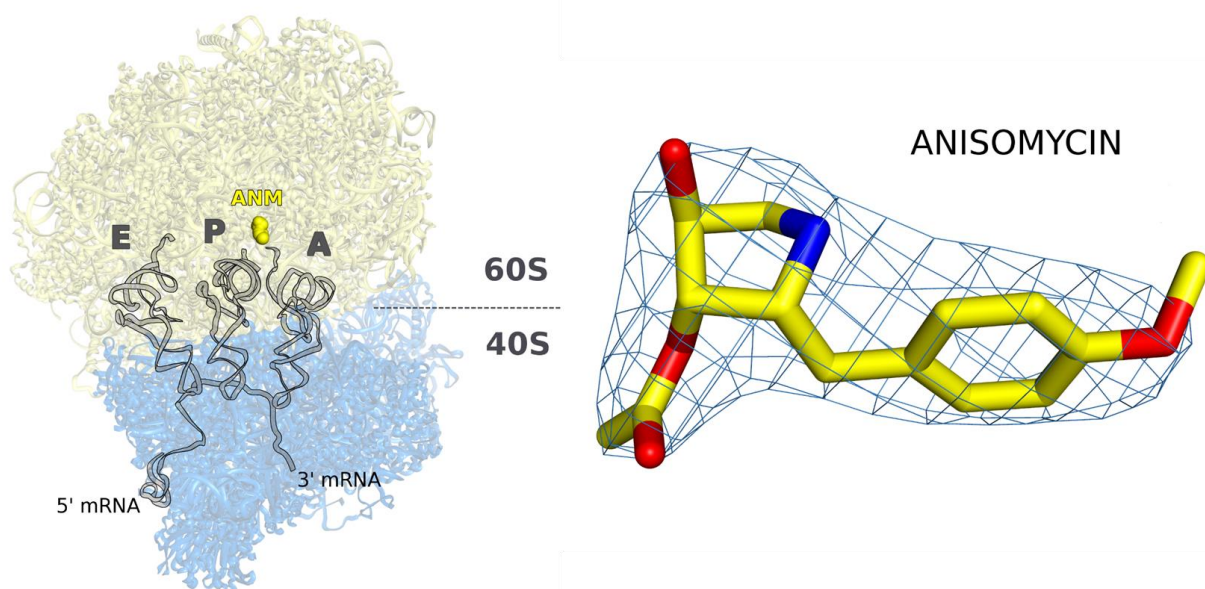
Figure 64 - Overview of the ANM binding site on the 80S *C. albicans* ribosome with the density map for the ANM molecule.

Despite the differences in the translation inhibition in all three species, ANM's binding mechanism is the same. ANM forms a stacking interaction with the C2793 with the hydrogen bond formation between the NH group of the ANM and the base of C2793 (figure 65). Compared with the vacant *C. albicans* ribosome structure, the binding of the compound leads to structural reorganization in the A-site. Residue U2847 undergoes the most drastic change – flipping out of the base. Additionally, the position of the base of C2793 of 25S rRNA is shifted towards ANM, and there is also a slight shift of U2794. These changes were previously described for the *S. cerevisiae* ribosome [76], but in the vacant *C. albicans* ribosome structure, there was no indication for the canonical base pair formation between U2847 and G2924; the U2847 base flipped out in another plane. Comparison with *S. cerevisiae* revealed no differences in nucleotide positions. All these findings confirm that the A-site is highly conserved in higher eukaryotes.
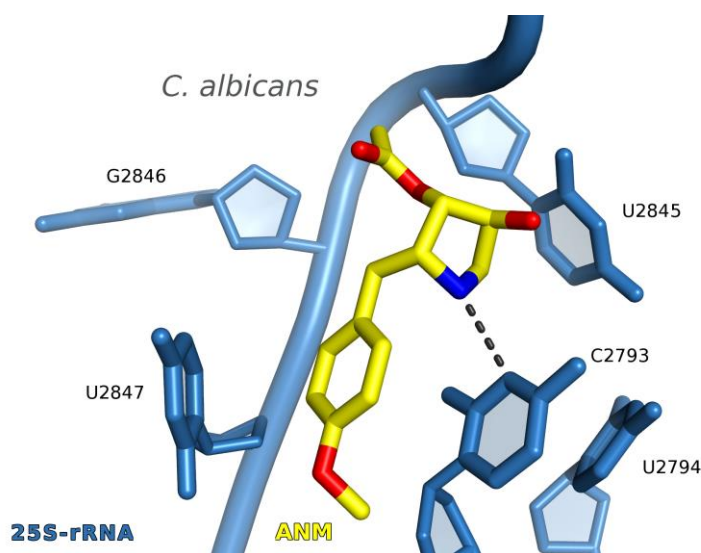
Figure 65 - Close-up views of ANM bound to the A-site of PTC.

## Complex with blasticidin S

The second complex we formed was with the Blasticidin S (BLS), which binds to the P-site of the PTC. The BLS is active not only in the eukaryotes but also against bacteria due to the high similarity of the P-tRNA binding site. Nevertheless, as mentioned above, we found a different conformation of the A2780, which directly interacts with the compound in eukaryotes and bacteria by forming a weak hydrogen bond between the O6 group of blasticidin and the $NH_2$ group of the adenine base. So we decided to check BLS inhibition by cell-free experiments in *C. albicans*, *S. cerevisiae*, and RR. The results are presented in figure 66. The translation inhibition in *S. cerevisiae* and *C. albicans* lysates are similar, indicating that *C. albicans* is sensitive to BLS as yeasts. On the other hand, the RR is more sensitive to the BLS, although there is no difference between mammals and yeast from the structural point of view. The IC50 value for the extracts is the following: ≈0.1 µM for RR, ≈0.6 µM for *S. cerevisiae*, and ≈0.65 µM for *C. albicans*.
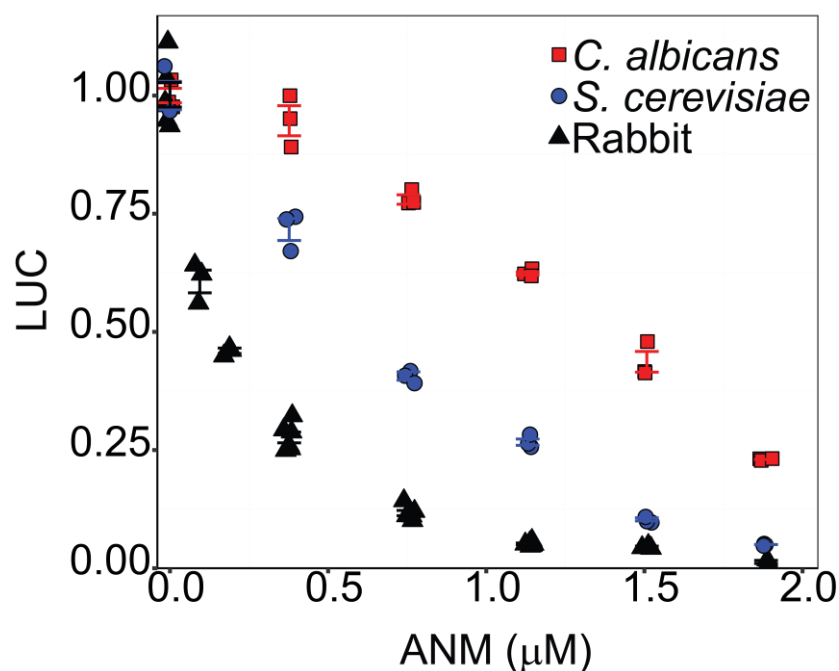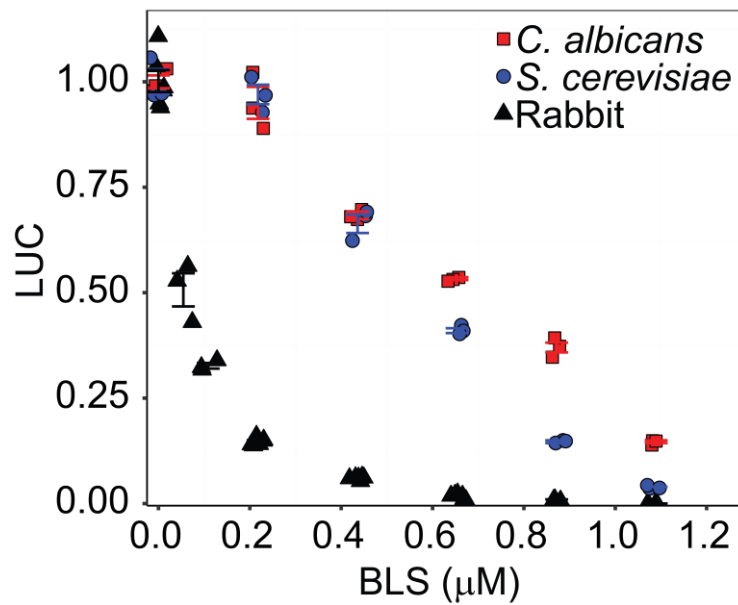
Figure 66 - Inhibition of translation by BLS tested in cell-free systems from *C. albicans*, *S. cerevisiae*, and RR.

Using the data from the cell-free assays, we attempted to make a complex with *C. albicans* 80S ribosome in the same excess as for ANM (250 µM). Finally, we got a 2.67 Å cryo-EM map and reconstructed a complex with the BLS (Fig. S2, S5D, Table S7). During the model inspection, we found a strong density at the P-site of the PTC, which perfectly mimics the BLS molecule (figure 67). Moreover, apart from the extra density in the PTC, we did not find other indications for additional binding sites for BLS, proving the oneness of the BLS binding site.
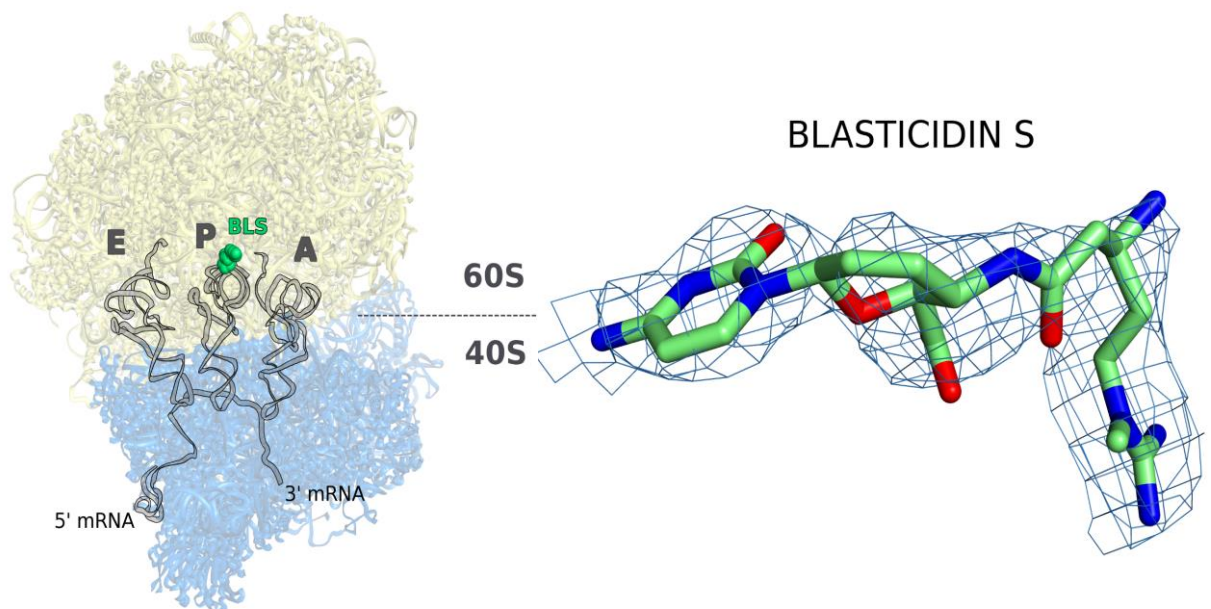


Figure 67 - Overview of the BLS binding site on the 80S *C. albicans* ribosome with the density map for the BLS molecule.

The interaction pattern of the BLS in *C. albicans* is similar to that in *S. cerevisiae* (figure 63). BLS molecule forms a Watson-crick-like base pair with the G2591, BLS ring resembles the cytidine base. From the other end, there are two hydrogen bonds formed, first between the NH group (number) of BLS and the phosphate group of the C2942, and a weak hydrogen bond (4.00 Å) between oxygen O6 of the blasticidin and NH2 group of the base of A2780 (figure 68). Compared with the vacant *C. albicans* ribosome structure, a 28° rotation of A2780 towards the inhibitor was observed. Our results align with observations for higher eukaryotes and some bacterial species [116, 125] that BLS forms a canonical base pair with G2791 preventing the tRNA binding (C75) in the P-site of the PTC. No substantial differences in the binding site geometry and inhibitor interactions were observed when comparing BLS interactions with the *C. albicans* and *S. cerevisiae* ribosomes. Hence it seems that minor structural changes do not affect the binding of the inhibitors in the PTC.
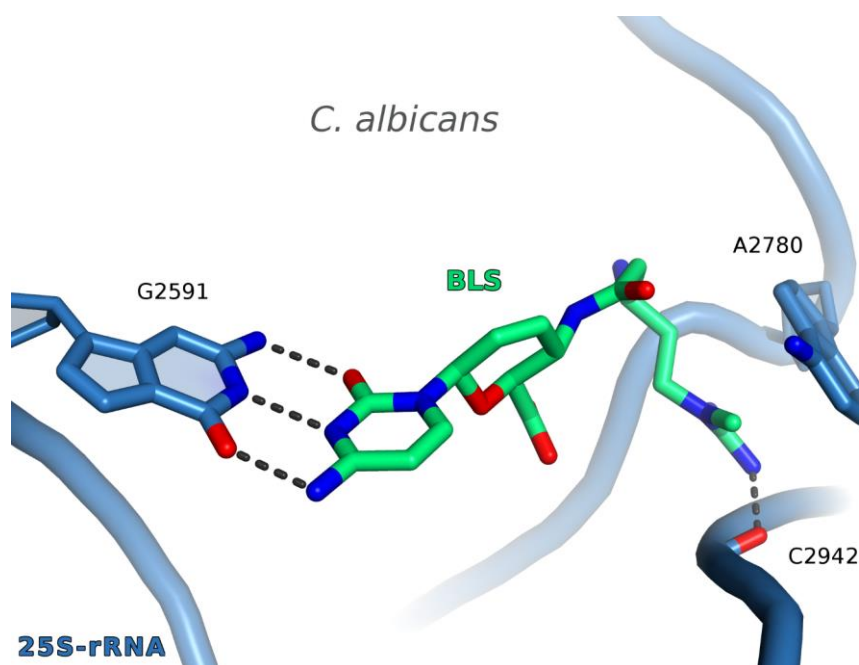


Figure 68 - Close-up views of BLS bound to the P-site of PTC.

## Complex with cycloheximide

According to several functional studies, *C. albicans* is resistant to cycloheximide (CHX), which binds to the ribosomal E-tRNA binding site (E-site). Genetic studies have demonstrated that this resistance is likely caused by a natural substitution, P56Q, in ribosomal protein eL42 (8). Using the vacant *C. albicans* ribosome structure, we proposed a mechanism mentioned above, showing that the clash between the glutamine side chain and glutarimide group of CHX prevents its binding to the E-site at physiological concentration. To get more details on the

resistivity mechanism of *C. albicans,* we firstly made cell-free assays to understand if our particular strain is resistant to CHX and to calculate the IC50 of CHX in *C. albicans* (figure 69). The translation inhibition in *S. cerevisiae* and RR lysates are similar, but the *C. albicans* extract is 1000-fold more resistant to CHX. The IC50 values for the extracts are the following: ≈0.5 µM for RR, ≈0.5 µM for *S. cerevisiae*, and ≈1000 µM (1 mM) for *C. albicans*.
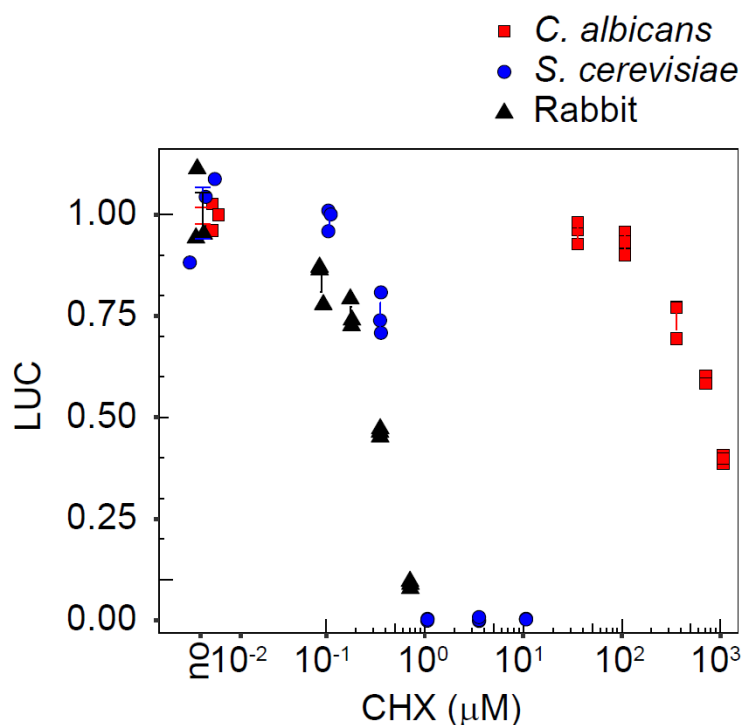


Figure 69 - Inhibition of translation by CHX tested in cell-free systems from *C. albicans*, *S. cerevisiae*, and RR.

We also performed microplate drug inhibition experiments (MIC) to corroborate this finding. Two-fold dilution series of CHX were prepared in fresh YPD medium and distributed into 96-well plates (Falcon, 351177). First, *C. albicans* and *S. cerevisiae* cells from overnight cultures grown in 3 mL YPD medium were collected and resuspended in 500 µl of fresh YPD medium. The number of cells was then determined using a hemocytometer. Next, cell suspensions were diluted with fresh YPD medium to make working suspensions of $2 \times 10^3$ cells per ml and distributed into the drug dilution series (volume ratio 1:1) in the 96-well plates and mixed well. Plates were statically incubated at 30°C for 24 h, and OD600 was measured with a SpectraMax M2e microplate spectrophotometer [126]. In MIC assays, 100% inhibition of *S. cerevisiae* growth was obtained with one µM CHX. In contrast, approximately 67% of *C. albicans* growth was observed with 900 µM CHX, and limited growth was still observed with 7 mM CHX (Fig. 70).
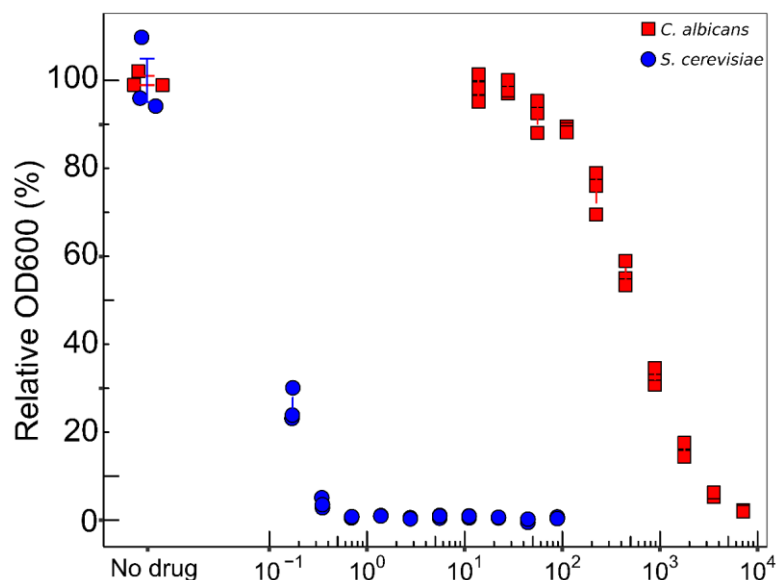
Figure 70 - Drug susceptibility in C. albicans and S. cerevisiae stationary cells.

Based on the results of the cell-free assays, we attempted to form a complex with CHX at non-physiological concentrations (≥1 mM) (Figs. S4-S5A, Table S9). Only at 2 mM concentration did we find a strong density in the E-site perfectly mimicking the CHX molecule (figure 71). The second exciting moment was when we saw density for the part of the CCA-tail of E-site tRNA. C74 and C75 stay at the same position as in the vacant ribosome, although there is no density present for A76. We thought our sample could have different ribosome populations, but different classification strategies finally led us to the same results. So, we suggest that CHX binding to the E-site does not lead to tRNA dissociation. Instead, the high affinity of the E-site tRNA could be connected to the I57L substitution in the eL42 protein, which is directly interacting with the C75. Isoleucine residue is more hydrophobic than leucine, so the interaction between E-site tRNA and eL42 protein is more vital.
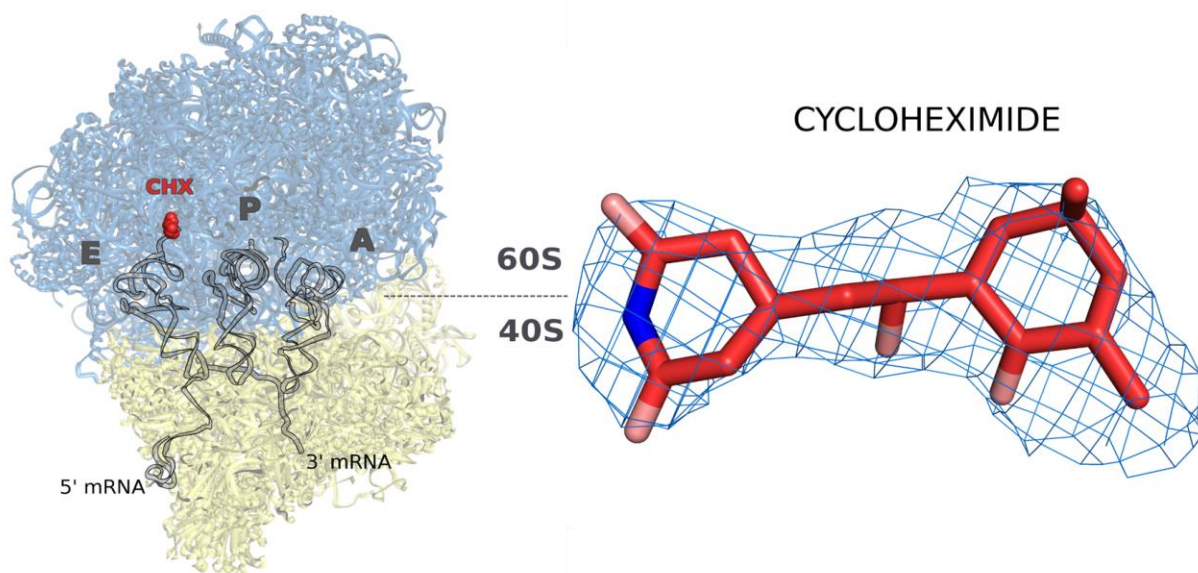
Figure 71 - Overview of the CHX binding site on the 80S *C. albicans* ribosome with the density map for the CHX molecule.

The binding mode of the CHX is different from other structures with CHX. It is not penetrating so deep as in *S. cerevisiae* and *H. sapiens*. Comparing CHX binding with the vacant ribosome with superimposed CHX, a 1 Å shift of the whole CHX molecule was observed (figure 67). To bind to the E-site at a high concentration, the CHX molecule pushes the Q56 side-chain 1.4 Å downwards (figure 72). Consequently, there is a slight shift in positions of the C2736, C2737, and G2766 with a 12° rotation of U2735 compared to the vacant *C. albicans* ribosome structure. Additionally, a slight shift of the eL42 protein backbone is observed. These observations corroborate that there is no high-affinity binding site for CHX in the *C. albicans* ribosome.
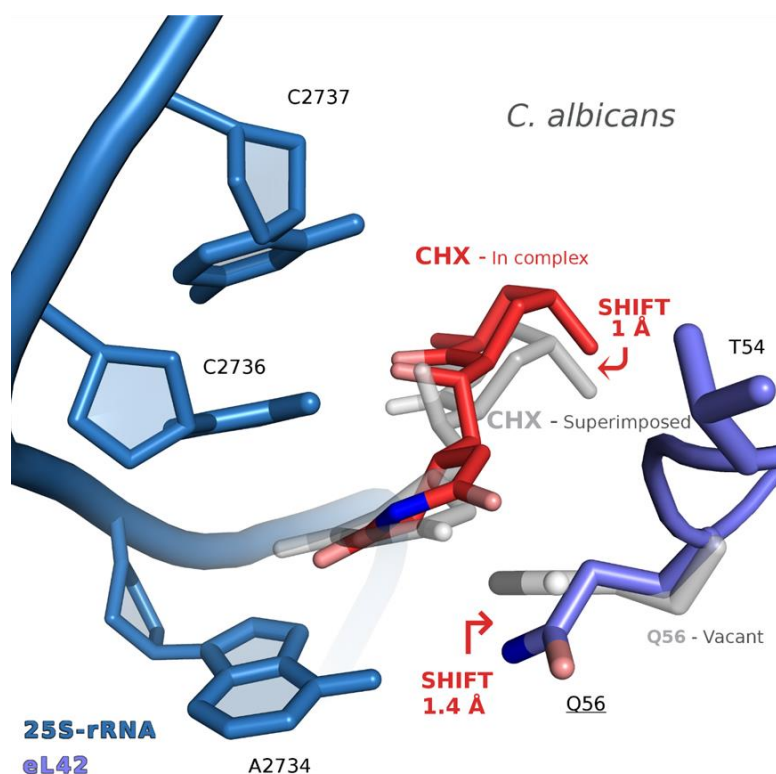
Figure 72 - Close-up views of CHX bound to the E-site of PTC.

## Complex with phyllanthoside

When we elucidated the mechanism of the CHX resistance in *C. albicans,* we started to think about how we could overcome this obstacle and create a specific anti-candida compound targeting the E-site on the 60S subunit. The main problem here is that almost all the E-site inhibitors have the same glutarimide moiety, such as lactimidomycin, so we supposed that they would not be active against *C. albicans*. However, only one inhibitor, called phyllanthoside (PHY), missed the glutarimide group and was shown to bind to the E-site of the *S. cerevisiae* ribosome. To check if PHY is active against *C. albicans*, we performed a cell-free assay in the cell extracts of *C. albicans* and compared the translation inhibition efficiency with other eukaryotes, such as *S. cerevisiae* and RR. Results of the cell-free assays are present in figure 73. Compared to CHX, PHY is active on the same level against *C. albicans*, *S. cerevisiae*, and RR. The IC50 values for the extracts are the following: ≈0.5 μM for RR, ≈2 μM for *S. cerevisiae*, and 2 μM for *C. albicans*. These values indicate that PHY is active against the broad spectrum of eukaryotes at physiological concentrations.

131
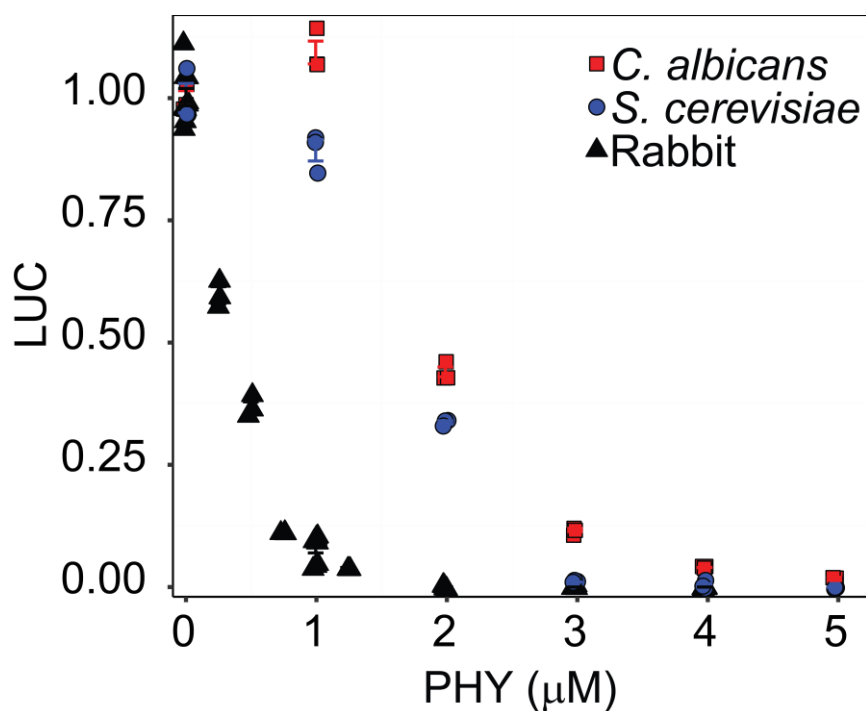
Figure 73 - Inhibition of translation by PHY tested in cell-free systems from *C. albicans*, *S. cerevisiae*, and RR.

Based on the results from the cell-free assays, we were confident that PHY should bind to the E-site of the *C. albicans* ribosome. So, we prepared a complex of the 80S *C. albicans* ribosome with PHY at 150 µM concentration. Using this complex, we collected a 2.64 Å dataset, sufficient to get the molecular details on the inhibitor action (Fig. S3, S5B, Table S8). During the model inspection, we found a firm density corresponding to the PHY molecule. PHY binds to the E-site in a way mimicking the CCA-tail of the tRNA (figure 74).

In contrast to the CHX, PHY binding leads to complete dissociation of the E-site tRNA. The main difference in the PHY binding mode is the presence of 2 stacking interactions: Y43 (eL42 protein) and G2766 (25S rRNA) (figure 75). The conformation of Y43 is changed upon the PHY binding to form a stacking interaction. The second distinct feature of PHY is a covalent bond formation of the epoxide group of PHY and the base of C2736 (figure 75). They are located 2Å apart from each other. The covalent bond formation was previously suggested by studying the effect of the PHY on protein synthesis. It turned out that PHY acts irreversibly on protein biosynthesis, so covalent bond formation was proposed [116, 127]. Also, we found that, with PHY in the E-site, U2735, C2736, G2765, and G2766 slightly changed their conformation compared to the structure of the vacant ribosome. Despite the direct interaction (stacking) with eL42 Y43, PHY causes a 0.65 Å shift of the eL42 backbone (residues K55-K60), similar to what was observed in the *S. cerevisiae* structure (PDB ID 4u4z).
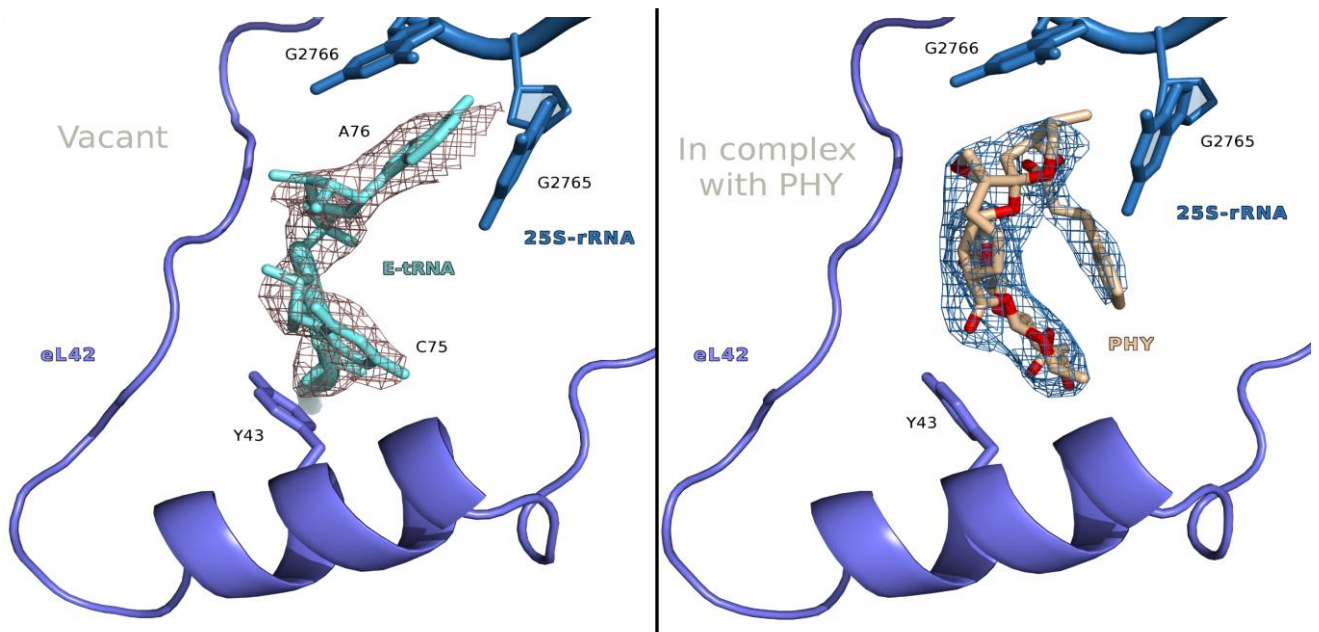
Figure 74 - PHY binds to the E-site in a way mimicking the CCA tail of the E-tRNA.

The binding mechanism of PHY is utterly different from the CHX. The most drastic difference is the interaction with the eL42 protein: PHY does not penetrate so deep into the binding pocket that there is no direct interaction between the two molecules. The closest group of PHY - the epoxide group is located 5.3 Å apart. These structural results suggest that PHY is the only currently known E-site inhibitor of *C. albicans*.
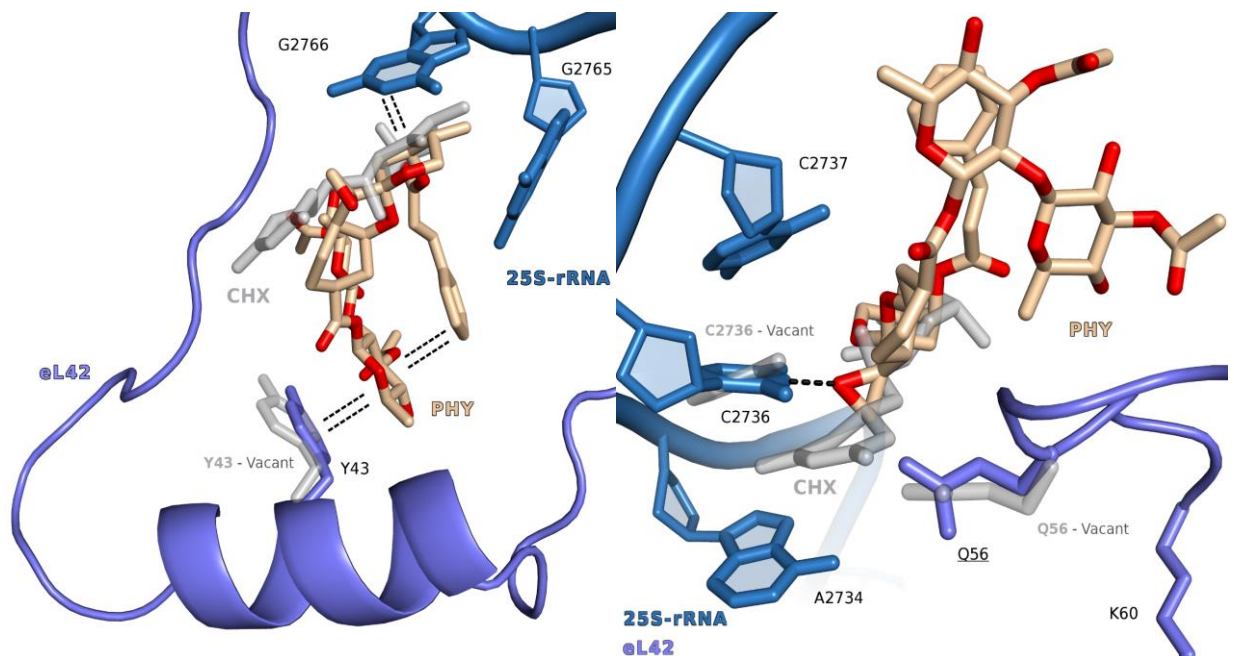


Figure 75 - Comparison of PHY/CHX binding.

To sum up, our results explain the resistance of *C. albicans* to CHX and demonstrate specific features of the *C. albicans* ribosome. Based on structural and cell-free data, we propose that CHX can not bind to the *C. albicans* ribosome due to the clash of the glutarimide group of CHX with the Q56 side chain of eL42 (figure 76A). In contrast to CHX, PHY binds to the E-site of *C. albicans* at a physiologically relevant concentration. Furthermore, due to the lack of glutarimide moiety, PHY adopts an entirely different interaction pattern and does not clash with Q56 (figure 76B).
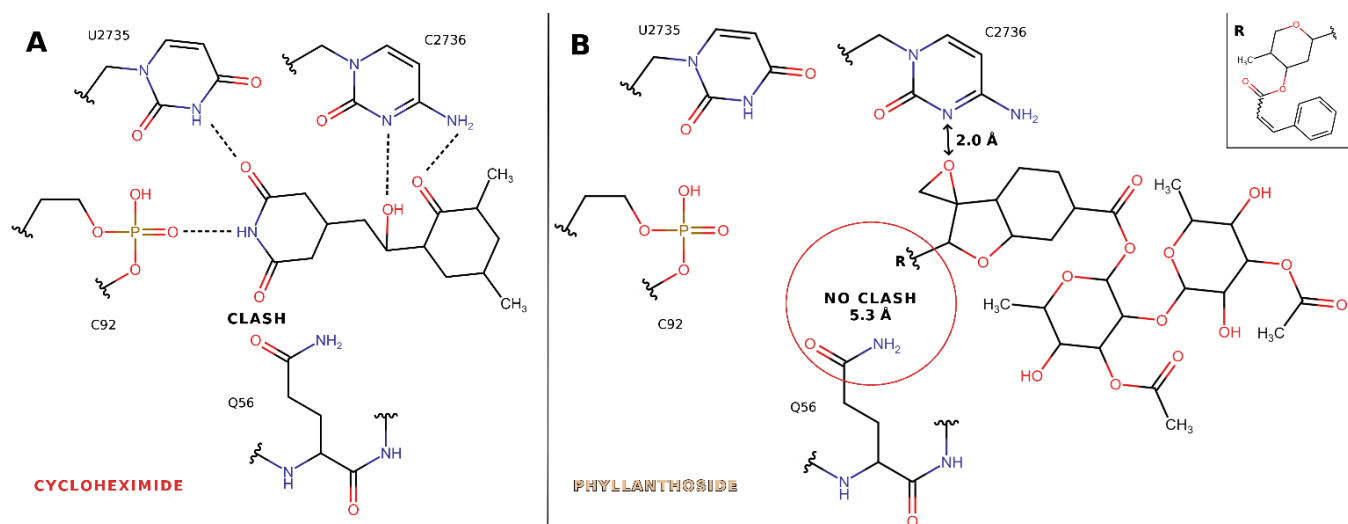


Figure 76 - E-site specificity of the *C. albicans* ribosome

Based on our results, we also suggest some chemical structures of inhibitors that could be specific against *C. albican's* ribosome. We propose to use the cycloheximide molecule as a probe and template for future anti-candida drugs. For example, we suggest we mutate the glutarimide group of CHX in a way replacing oxygen with O6 by the NH group. Instead of the clash, it could create a hydrogen bond with Oε oxygen of the Q56 side chain. We also propose adding oxygen in the fifth place of the glutarimide group (figure 77). We suppose that there is another hydrogen bond that could create a strong interaction between Q56 and novel compound while not being active against other eukaryotes. Cryo-EM, in combination with X-ray, would be a perfect method to test newly synthesized compounds. Our study provides a solid base for the potential future development of anti-Candida drugs with a modified glutarimide moiety which could lead to specific binding to the ribosome of *C. albicans*. Understanding ribosome inhibition will significantly improve the treatment of candidiasis and reduce its mortality.
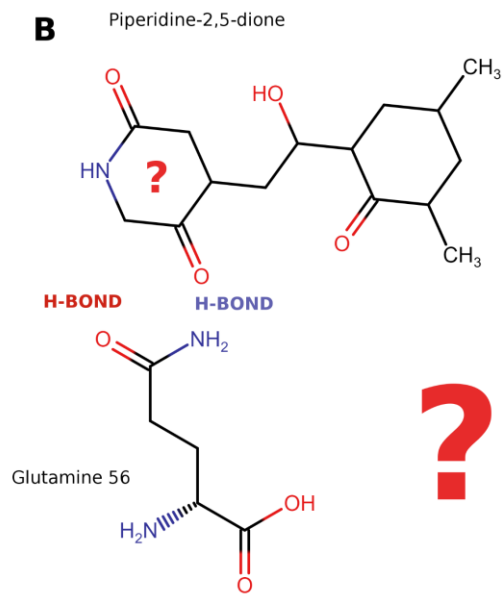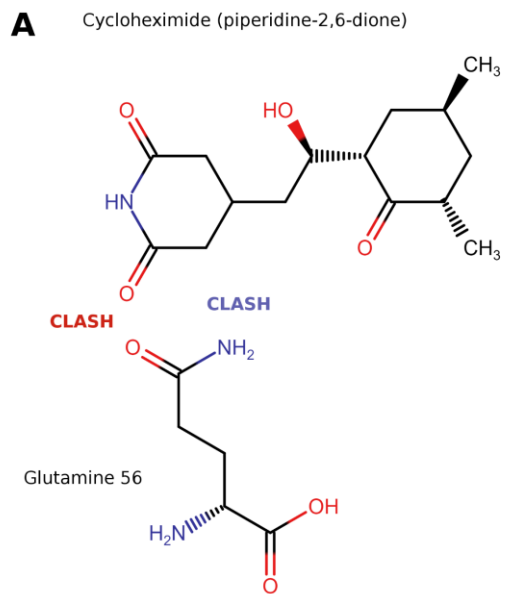
Figure 77 - CHX analogs which could be potent against *C. albicans*

# LIST OF PUBLICATIONS AND COMMUNICATIONS

## List of publications:

1)      E-site drug specificity of the human pathogen Candida albicans ribosome.   **Zgadzay Y**, Kolosova O, Stetsenko A, Wu C, Bruchlen D, Usachev K, Validov S, Jenner L, Rogachev A, Yusupova G, Sachs MS, Guskov A, Yusupov M. Sci Adv. 2022 May 27;8(21):eabn1062. doi: 10.1126/sciadv.abn1062. Epub 2022 May 25. PMID: 35613268; PMCID: PMC9132455.

## List of communications:

1)      E-site specificity of the Candida albicans ribosome, **Zgadzay Y**, Kolosova O, Stetsenko A, Wu C, Bruchlen D, Usachev K, Validov S, Jenner L, Rogachev A, Yusupova G, Sachs MS, Guskov A, Yusupov M., Ribosomes 2022, Bordeaux, 09-14/07/2022 (affiche)

2)      Cryo-EM reconstruction of the Candida albicans 80S ribosome. **Y. Zgadzay**, O. Kolosova, A. Stetsenko, K. Usachev, S. Validov, A. Guskov, M. Yusupov. The 45th FEBS Congress, Ljubljana, 07/2021 (oral)

# BIBLIOGRAPHY

1.      Koehler, P., et al., *Intensive care management of influenza-associated pulmonary aspergillosis.* Clin Microbiol Infect, 2019. **25**(12): p. 1501-1509.

2.      Chung, L.M., et al., *Cancer risk in patients with candidiasis: a nationwide population-based cohort study.* Oncotarget, 2017. **8**(38): p. 63562-63573.

3.      Wilcock, B.C., et al., *C2'-OH of amphotericin B plays an important role in binding the primary sterol of human cells but not yeast cells.* J Am Chem Soc, 2013. **135**(23): p. 8488-91.

4.      Shirai, A., et al., *Methylation of ribosomal protein L42 regulates ribosomal function and stress-adapted cell growth.* J Biol Chem, 2010. **285**(29): p. 22448-60.

5.      Mayer, F.L., D. Wilson, and B. Hube, *Candida albicans pathogenicity mechanisms.* Virulence, 2013. **4**(2): p. 119-28.

6.      Hoyer, L.L., et al., *Candida albicans ALS1: domains related to a Saccharomyces cerevisiae sexual agglutinin separated by a repeating motif.* Mol Microbiol, 1995. **15**(1): p. 39-54.

7.      Lipke, P.N., D. Wojciechowicz, and J. Kurjan, *AG alpha 1 is the structural gene for the Saccharomyces cerevisiae alpha-agglutinin, a cell surface glycoprotein involved in cell-cell interactions during mating.* Mol Cell Biol, 1989. **9**(8): p. 3155-65.

8.      Hoyer, L.L., et al., *Discovering the secrets of the Candida albicans agglutinin-like sequence (ALS) gene family--a sticky pursuit.* Med Mycol, 2008. **46**(1): p. 1-15.

9.      Hoyer, L.L. and E. Cota, *Candida albicans Agglutinin-Like Sequence (Als) Family Vignettes: A Review of Als Protein Structure and Function.* Front Microbiol, 2016. **7**: p. 280.

10.     Sheppard, D.C., et al., *Functional and structural diversity in the Als protein family of Candida albicans.* J Biol Chem, 2004. **279**(29): p. 30480-9.

11.     Salgado, P.S., et al., *Structural basis for the broad specificity to host-cell ligands by the pathogenic fungus Candida albicans.* Proc Natl Acad Sci U S A, 2011. **108**(38): p. 15775-9.

12.     Phan, Q.T., et al., *Als3 is a Candida albicans invasin that binds to cadherins and induces endocytosis by host cells.* PLoS Biol, 2007. **5**(3): p. e64.

13.     Li, F., et al., *Eap1p, an adhesin that mediates Candida albicans biofilm formation in vitro and in vivo.* Eukaryot Cell, 2007. **6**(6): p. 931-9.

14.     Hashash, R., et al., *Characterisation of Pga1, a putative Candida albicans cell wall protein necessary for proper adhesion and biofilm formation.* Mycoses, 2011. **54**(6): p. 491-500.

15.     Ciurea, C.N., et al., *Candida and Candidiasis-Opportunism Versus Pathogenicity: A Review of the Virulence Traits.* Microorganisms, 2020. **8**(6).

16.     Jackson, A.P., et al., *Comparative genomics of the fungal pathogens Candida dubliniensis and Candida albicans.* Genome Res, 2009. **19**(12): p. 2231-44.

17.     Wang, J.M., R.J. Bennett, and M.Z. Anderson, *The Genome of the Human Pathogen Candida albicans Is Shaped by Mutation and Cryptic Sexual Recombination.* mBio, 2018. **9**(5).

18.     Usher, J., *The Mechanisms of Mating in Pathogenic Fungi-A Plastic Trait.* Genes (Basel), 2019. **10**(10).

19.     Sun, Y., et al., *pH Regulates White-Opaque Switching and Sexual Mating in Candida albicans.* Eukaryot Cell, 2015. **14**(11): p. 1127-34.

20.     Mba, I.E., et al., *Genome plasticity in Candida albicans: A cutting-edge strategy for evolution, adaptation, and survival.* Infect Genet Evol, 2022. **99**: p. 105256.

21.     Fan, H. and J.Y. Chu, *A brief review of short tandem repeat mutation.* Genomics Proteomics Bioinformatics, 2007. **5**(1): p. 7-14.

22. Romani, L., *Immunity to fungal infections.* Nat Rev Immunol, 2004. **4**(1): p. 1-23.

23. Gow, N.A., *Fungal morphogenesis: some like it hot.* Curr Biol, 2009. **19**(8): p. R333-4.

24. McKenzie, C.G., et al., *Contribution of Candida albicans cell wall components to recognition by and escape from murine macrophages.* Infect Immun, 2010. **78**(4): p. 1650-8.

25. Dalle, F., et al., *Cellular interactions of Candida albicans with human oral epithelial cells and enterocytes.* Cell Microbiol, 2010. **12**(2): p. 248-71.

26. Richardson, J.P., et al., *Processing of Candida albicans Ece1p Is Critical for Candidalysin Maturation and Fungal Virulence.* mBio, 2018. **9**(1).

27. Pasricha, S. and J.S. Pearson, *Lifting the veil on fungal toxins.* Cell Death Discov, 2016. **2**: p. 16035.

28. Ho, J., et al., *Candidalysin activates innate epithelial immune responses via epidermal growth factor receptor.* Nat Commun, 2019. **10**(1): p. 2297.

29. Velazquez-Salinas, L., et al., *The Role of Interleukin 6 During Viral Infections.* Front Microbiol, 2019. **10**: p. 1057.

30. Bhattacharya, P., et al., *GM-CSF: An immune modulatory cytokine that can suppress autoimmunity.* Cytokine, 2015. **75**(2): p. 261-71.

31. Bergsbaken, T., S.L. Fink, and B.T. Cookson, *Pyroptosis: host cell death and inflammation.* Nat Rev Microbiol, 2009. **7**(2): p. 99-109.

32. Hirota, J.A., et al., *The nucleotide-binding domain and leucine-rich repeat protein-3 inflammasome is not activated in airway smooth muscle upon toll-like receptor-2 ligation.* Am J Respir Cell Mol Biol, 2013. **49**(4): p. 517-24.

33. Eibl, C., et al., *Structural and functional analysis of the NLRP4 pyrin domain.* Biochemistry, 2012. **51**(37): p. 7330-41.

34. Nikou, S.A., et al., *Candida albicans Interactions with Mucosal Surfaces during Health and Disease.* Pathogens, 2019. **8**(2).

35. Talapko, J., et al., *Candida albicans-The Virulence Factors and Clinical Manifestations of Infection.* J Fungi (Basel), 2021. **7**(2).

36. Gulati, M. and C.J. Nobile, *Candida albicans biofilms: development, regulation, and molecular mechanisms.* Microbes Infect, 2016. **18**(5): p. 310-21.

37. Rodriguez-Cerdeira, C., et al., *Pathogenesis and Clinical Relevance of Candida Biofilms in Vulvovaginal Candidiasis.* Front Microbiol, 2020. **11**: p. 544480.

38. Atriwal, T., et al., *Mechanistic Understanding of Candida albicans Biofilm Formation and Approaches for Its Inhibition.* Front Microbiol, 2021. **12**: p. 638609.

39. Cavalheiro, M. and M.C. Teixeira, *Candida Biofilms: Threats, Challenges, and Promising Strategies.* Front Med (Lausanne), 2018. **5**: p. 28.

40. Rudramurthy, S.M., *Candida Infections in Immunocompetent Hosts: Pathogenesis and Diagnosis.* Current Fungal Infection Reports, 2020. **14**: p. 233-245.

41. Gallo, M., et al., *Metabolic Plasticity of Candida albicans in Response to Different Environmental Conditions.* J Fungi (Basel), 2022. **8**(7).

42. Brock, M., *Fungal metabolism in host niches.* Curr Opin Microbiol, 2009. **12**(4): p. 371-6.

43. Fonzi, W.A., *PHR1 and PHR2 of Candida albicans encode putative glycosidases required for proper cross-linking of beta-1,3- and beta-1,6-glucans.* J Bacteriol, 1999. **181**(22): p. 7070-9.

44. Muhlschlegel, F.A. and W.A. Fonzi, *PHR2 of Candida albicans encodes a functional homolog of the pH-regulated gene PHR1 with an inverted pattern of pH-dependent expression.* Mol Cell Biol, 1997. **17**(10): p. 5960-7.

45. Davis, D.A., *How human pathogenic fungi sense and adapt to pH: the link to virulence.* Curr Opin Microbiol, 2009. **12**(4): p. 365-70.

46.  Vylkova, S., et al., *The fungal pathogen Candida albicans autoinduces hyphal morphogenesis by raising extracellular pH.* mBio, 2011. **2**(3): p. e00055-11.

47.  Lindquist, S., *Heat-shock proteins and stress tolerance in microorganisms.* Curr Opin Genet Dev, 1992. **2**(5): p. 748-55.

48.  Lindquist, S., *The heat-shock response.* Annu Rev Biochem, 1986. **55**: p. 1151-91.

49.  Calderone, R.A. and C.J. Clancy, *Candida and candidiasis.* 2nd ed. 2012, Washington, DC: ASM Press. xii, vii, 524 pages.

50.  Wysong, D.R., et al., *Cloning and sequencing of a Candida albicans catalase gene and effects of disruption of this gene.* Infect Immun, 1998. **66**(5): p. 1953-61.

51.  Hromatka, B.S., S.M. Noble, and A.D. Johnson, *Transcriptional response of Candida albicans to nitric oxide and the role of the YHB1 gene in nitrosative stress and virulence.* Mol Biol Cell, 2005. **16**(10): p. 4814-26.

52.  Almeida, R.S., et al., *the hyphal-associated adhesin and invasin Als3 of Candida albicans mediates iron acquisition from host ferritin.* PLoS Pathog, 2008. **4**(11): p. e1000217.

53.  Hood, M.I. and E.P. Skaar, *Nutritional immunity: transition metals at the pathogen-host interface.* Nat Rev Microbiol, 2012. **10**(8): p. 525-37.

54.  Krassowski, T., et al., *Evolutionary instability of CUG-Leu in the genetic code of budding yeasts.* Nat Commun, 2018. **9**(1): p. 1887.

55.  Santos, M.A., V.M. Perreau, and M.F. Tuite, *Transfer RNA structural change is a key element in the reassignment of the CUG codon in Candida albicans.* EMBO J, 1996. **15**(18): p. 5060-8.

56.  Muhlhausen, S., et al., *Proteogenomics analysis of CUG codon translation in the human pathogen Candida albicans.* BMC Biol, 2021. **19**(1): p. 258.

57.  Sarkany, Z., et al., *Ser or Leu: structural snapshots of mistranslation in Candida albicans.* Front Mol Biosci, 2014. **1**: p. 27.

58.  Feketova, Z., et al., *Ambiguous decoding of the CUG codon alters the functionality of the Candida albicans translation initiation factor 4E.* FEMS Yeast Res, 2010. **10**(5): p. 558-69.

59.  Gomes, A.C., et al., *A genetic code alteration generates a proteome of high diversity in the human pathogen Candida albicans.* Genome Biol, 2007. **8**(10): p. R206.

60.  Fleischmann, J. and M.A. Rocha, *Decrease in Ribosomal RNA in Candida albicans Induced by Serum Exposure.* PLoS One, 2015. **10**(5): p. e0124430.

61.  Fleischmann, J. and H. Liu, *Polyadenylation of ribosomal RNA by Candida albicans.* Gene, 2001. **265**(1-2): p. 71-6.

62.  Fleischmann, J., H. Liu, and C.P. Wu, *Polyadenylation of ribosomal RNA by Candida albicans also involves the small subunit.* BMC Mol Biol, 2004. **5**: p. 17.

63.  Callahan, K.P. and J.S. Butler, *TRAMP complex enhances RNA degradation by the nuclear exosome component Rrp6.* J Biol Chem, 2010. **285**(6): p. 3540-3547.

64.  Bernstein, D.A., et al., *Candida albicans Dicer (CaDcr1) is required for efficient ribosomal and spliceosomal RNA maturation.* Proc Natl Acad Sci U S A, 2012. **109**(2): p. 523-8.

65.  Colthurst, D.R., et al., *Efficient translation of synthetic and natural mRNAs in an mRNA-dependent cell-free system from the dimorphic fungus Candida albicans.* J Gen Microbiol, 1991. **137**(4): p. 851-7.

66.  Dehoux, P., J. Davies, and M. Cannon, *Natural cycloheximide resistance in yeast. The role of ribosomal protein L41.* Eur J Biochem, 1993. **213**(2): p. 841-8.

67.  Kawai, S., et al., *Drastic alteration of cycloheximide sensitivity by substitution of one amino acid in the L41 ribosomal protein of yeasts.* J Bacteriol, 1992. **174**(1): p. 254-62.

68.  Melnikov, S., et al., *One core, two shells: bacterial and eukaryotic ribosomes.* Nat Struct Mol Biol, 2012. **19**(6): p. 560-7.

69. Ban, N., et al., *A new system for naming ribosomal proteins.* Curr Opin Struct Biol, 2014. **24**: p. 165-9.

70. Petrov, A.S., et al., *Evolution of the ribosome at atomic resolution.* Proc Natl Acad Sci U S A, 2014. **111**(28): p. 10251-6.

71. Gomez Ramos, L.M., et al., *Eukaryotic Ribosomal Expansion Segments as Antimicrobial Targets.* Biochemistry, 2017. **56**(40): p. 5288-5299.

72. Fujii, K., et al., *Decoding the Function of Expansion Segments in Ribosomes.* Mol Cell, 2018. **72**(6): p. 1013-1020 e6.

73. Giglione, C., S. Fieulaine, and T. Meinnel, *N-terminal protein modifications: Bringing back into play the ribosome.* Biochimie, 2015. **114**: p. 134-46.

74. Jarasch, A., *3D modeling of ribosomal RNA using cryo-electron microscopy density maps.* 2011.

75. Boratyn, G.M., et al., *Domain enhanced lookup time accelerated BLAST.* Biol Direct, 2012. **7**: p. 12.

76. Ben-Shem, A., et al., *The structure of the eukaryotic ribosome at 3.0 A resolution.* Science, 2011. **334**(6062): p. 1524-9.

77. Polacek, N. and A.S. Mankin, *The ribosomal peptidyl transferase center: structure, function, evolution, inhibition.* Crit Rev Biochem Mol Biol, 2005. **40**(5): p. 285-311.

78. Bae, J.H., B.H. Sung, and J.H. Sohn, *Site saturation mutagenesis of ribosomal protein L42 at 56th residue and application as a consecutive selection marker for cycloheximide resistance in yeast.* FEMS Microbiol Lett, 2018. **365**(8).

79. Bruchlen, D., *Candida albicans ribosome: Structure, function and inhibition,.* 2016, Strasbourg University.

80. Ledoigt, G., et al., *[Analysis of ribosomes by polyacrylamide gel electrophoresis (author's transl)].* Biochim Biophys Acta, 1975. **407**(2): p. 222-39.

81. Aranda, P.S., D.M. LaJoie, and C.L. Jorcyk, *Bleach gel: a simple agarose gel for analyzing RNA quality.* Electrophoresis, 2012. **33**(2): p. 366-9.

82. Wang, X., et al., *Use of the novel technique of analytical ultracentrifugation with fluorescence detection system identifies a 77S monosomal translation complex.* Protein Sci, 2012. **21**(9): p. 1253-68.

83. Stetefeld, J., S.A. McKenna, and T.R. Patel, *Dynamic light scattering: a practical guide and applications in biomedical sciences.* Biophys Rev, 2016. **8**(4): p. 409-427.

84. Shen, P. 2022; Available from: https://cryoem101.org/chapter-5/.

85. Punjani, A., et al., *cryoSPARC: algorithms for rapid unsupervised cryo-EM structure determination.* Nat Methods, 2017. **14**(3): p. 290-296.

86. Rubinstein, J.L. and M.A. Brubaker, *Alignment of cryo-EM movies of individual particles by optimization of image translations.* J Struct Biol, 2015. **192**(2): p. 188-95.

87. Punjani, A., H. Zhang, and D.J. Fleet, *Non-uniform refinement: adaptive regularization improves single-particle cryo-EM reconstruction.* Nat Methods, 2020. **17**(12): p. 1214-1221.

88. Zivanov, J., T. Nakane, and S.H.W. Scheres, *Estimation of high-order aberrations and anisotropic magnification from cryo-EM data sets in RELION-3.1.* IUCrJ, 2020. **7**(Pt 2): p. 253-267.

89. Djumagulov, M., et al., *Accuracy mechanism of eukaryotic ribosome translocation.* Nature, 2021. **600**(7889): p. 543-546.

90. Pettersen, E.F., et al., *UCSF Chimera--a visualization system for exploratory research and analysis.* J Comput Chem, 2004. **25**(13): p. 1605-12.

91. Liebschner, D., et al., *Macromolecular structure determination using X-rays, neutrons and electrons: recent developments in Phenix.* Acta Crystallogr D Struct Biol, 2019. **75**(Pt 10): p. 861-877.

92.     Casanal, A., B. Lohkamp, and P. Emsley, *Current developments in Coot for macromolecular model building of Electron Cryo-microscopy and Crystallographic Data.* Protein Sci, 2020. **29**(4): p. 1069-1078.

93.     Hassan, A., et al., *Ratchet, swivel, tilt and roll: A complete description of subunit rotation in the ribosome.* bioRxiv, 2022: p. 2022.06.22.497108.

94.     Nguyen, K. and P.C. Whitford, *Steric interactions lead to collective tilting motion in the ribosome during mRNA-tRNA translocation.* Nat Commun, 2016. **7**: p. 10586.

95.     Abeyrathne, P.D., et al., *Ensemble cryo-EM uncovers inchworm-like translocation of a viral IRES through the ribosome.* Elife, 2016. **5**.

96.     Brown, A., et al., *Structures of translationally inactive mammalian ribosomes.* Elife, 2018. **7**.

97.     Tesina, P., et al., *Molecular mechanism of translational stalling by inhibitory codon combinations and poly(A) tracts.* EMBO J, 2020. **39**(3): p. e103365.

98.     Sun, M., et al., *Dynamical features of the Plasmodium falciparum ribosome during translation.* Nucleic Acids Res, 2015. **43**(21): p. 10515-24.

99.     Prokhorova, I., et al., *Aminoglycoside interactions and impacts on the eukaryotic ribosome.* Proc Natl Acad Sci U S A, 2017. **114**(51): p. E10899-E10908.

100.    Kisonaite, M., et al., *High-resolution structures of a thermophilic eukaryotic 80S ribosome reveal atomistic details of translocation.* Nat Commun, 2022. **13**(1): p. 476.

101.    Natchiar, S.K., et al., *Visualization of chemical modifications in the human 80S ribosome structure.* Nature, 2017. **551**(7681): p. 472-477.

102.    Skrzypek, M.S., J. Binkley, and G. Sherlock, *Using the Candida Genome Database.* Methods Mol Biol, 2018. **1757**: p. 31-47.

103.    Yusupov, M.M., et al., *Crystal structure of the ribosome at 5.5 A resolution.* Science, 2001. **292**(5518): p. 883-96.

104.    Khatter, H., et al., *Structure of the human 80S ribosome.* Nature, 2015. **520**(7549): p. 640-5.

105.    Voorhees, R.M., et al., *Structure of the mammalian ribosome-Sec61 complex to 3.4 A resolution.* Cell, 2014. **157**(7): p. 1632-43.

106.    Krzyzosiak, W., et al., *In vitro synthesis of 16S ribosomal RNA containing single base changes and assembly into a functional 30S ribosome.* Biochemistry, 1987. **26**(8): p. 2353-64.

107.    Coureux, P.D., et al., *Cryo-EM study of an archaeal 30S initiation complex gives insights into evolution of translation initiation.* Commun Biol, 2020. **3**(1): p. 58.

108.    Sloan, K.E., et al., *Tuning the ribosome: The influence of rRNA modification on eukaryotic ribosome biogenesis and function.* RNA Biol, 2017. **14**(9): p. 1138-1152.

109.    Pellegrino, S., et al., *Cryo-EM reconstruction of the human 40S ribosomal subunit at 2.15 Å resolution.* bioRxiv, 2022: p. 2022.01.16.475527.

110.    Arnold, R.J., et al., *The action of N-terminal acetyltransferases on yeast ribosomal proteins.* J Biol Chem, 1999. **274**(52): p. 37035-40.

111.    Pang, C.N., E. Gasteiger, and M.R. Wilkins, *Identification of arginine- and lysine-methylation in the proteome of Saccharomyces cerevisiae and its functional implications.* BMC Genomics, 2010. **11**: p. 92.

112.    Watson, Z.L., et al., *Structure of the bacterial ribosome at 2 A resolution.* Elife, 2020. **9**.

113.    Miao, Z. and Y. Cao, *Quantifying side-chain conformational variations in protein structure.* Sci Rep, 2016. **6**: p. 37024.

114.    Shen, L., et al., *Structure of the translating Neurospora ribosome arrested by cycloheximide.* Proc Natl Acad Sci U S A, 2021. **118**(48).

115.    Buschauer, R., et al., *The Ccr4-Not complex monitors the translating ribosome for codon optimality.* Science, 2020. **368**(6488).

116.   Garreau de Loubresse, N., et al., *Structural basis for the inhibition of the eukaryotic ribosome.* Nature, 2014. **513**(7519): p. 517-22.

117.   Myasnikov, A.G., et al., *Structure-function insights reveal the human ribosome as a cancer target for antibiotics.* Nat Commun, 2016. **7**: p. 12856.

118.   Rozov, A., et al., *Importance of potassium ions for ribosome structure and function revealed by long-wavelength X-ray diffraction.* Nat Commun, 2019. **10**(1): p. 2519.

119.   Pellegrino, S., et al., *Understanding the role of intermolecular interactions between lissoclimides and the eukaryotic ribosome.* Nucleic Acids Res, 2019. **47**(6): p. 3223-3232.

120.   Kammer, P., et al., *Survival Strategies of Pathogenic Candida Species in Human Blood Show Independent and Specific Adaptations.* mBio, 2020. **11**(5).

121.   Pristov, K.E. and M.A. Ghannoum, *Resistance of Candida to azoles and echinocandins worldwide.* Clin Microbiol Infect, 2019. **25**(7): p. 792-798.

122.   Srikantha, T., et al., *The sea pansy Renilla reniformis luciferase serves as a sensitive bioluminescent reporter for differential gene expression in Candida albicans.* J Bacteriol, 1996. **178**(1): p. 121-9.

123.   Wu, C., et al., *The use of fungal in vitro systems for studying translational regulation.* Methods Enzymol, 2007. **429**: p. 203-25.

124.   Wang, Z., P. Fang, and M.S. Sachs, *The evolutionarily conserved eukaryotic arginine attenuator peptide regulates the movement of ribosomes that have translated it.* Mol Cell Biol, 1998. **18**(12): p. 7528-36.

125.   Hansen, J.L., P.B. Moore, and T.A. Steitz, *Structures of five antibiotics bound at the peptidyl transferase center of the large ribosomal subunit.* J Mol Biol, 2003. **330**(5): p. 1061-75.

126.   Liu, C., et al., *cAMP and c-di-GMP synergistically support biofilm maintenance through the direct interaction of their effectors.* Nat Commun, 2022. **13**(1): p. 1493.

127.   Chan, J., et al., *Eukaryotic protein synthesis inhibitors identified by comparison of cytotoxicity profiles.* RNA, 2004. **10**(3): p. 528-43.

# ANNEXES

Table S1. Complete list of intersubunit bridges in *C. albicans* ribosome with interacting residues.

| Bridge | 60S subunit | | 40S subunit | | Comment |
|---|---|---|---|---|---|
| | Component | Residue | Component | Residue | |
| B1a | 25S (H38) | A1021 | uS19 | V75 | |
| | 25S (H38) | A1022 | uS19 | R72 | |
| B1b/c | uL5 | E108 | uS13 | R110 | |
| | uL5 | E88 | uS19 | F12 | |
| B2a | 25S (H69) | A2233 | 18S (h44) | C1631 | |
| | 25S (H69) | A2233 | 18S (h44) | G1744 | |
| | 25S (H69) | A2234 | 18S (h44) | A1742 | |
| | 25S (H69) | C2235 | 18S (h44) | C1633 | |
| | 25S (H69) | U2236 | 18S (h44) | C1633 | |
| | 25S (H69) | A2237 | 18S (h44) | G1632 | |
| | 25S (H69) | A2240 | 18S (h44) | G1767 | |
| | 25S (H69) | C2241 | 18S (h44) | C1746 | |
| B2b | 25S (H68) | C2173 | 18S (h24) | G979 | |
| | 25S (H68) | C2174 | 18S (h24) | A980 | |
| B2c | 25S (H66) | C2129 | 18S (h24) | G969 | Mediated by Mg |
| | 25S (H66) | U2169 | 18S (h27) | C1108 | |
| | 25S (H66) | C2170 | 18S (h24) | U967 | Mediated by Mg |
| B3 | 25S (H64) | A2103 | 18S (h44) | U1657 | stacking |
| | 25S (H71) | C2268 | 18S (h44) | A1733 | |
| | 25S (H71) | A2269 | 18S (h44) | G1732 | |
| | 25S (H71) | A2269 | 18S (h44) | A1642 | |
| | 25S (H71) | U2270 | 18S (h44) | U1643 | |
| | 25S (H71) | U2279 | 18S (h44) | A1642 | |
| | 25S (H71) | G2280 | 18S (h44) | A1642 | |
| | 25S (H71) | G2280 | 18S (h44) | A1733 | Sugar edge bp |
| | 25S (H71) | A2281 | 18S (h44) | G1734 | |
| | 25S (H71) | C2282 | 18S (h44) | G1735 | |
| | 25S (H71) | G2283 | 18S (h44) | G1735 | |
| B4 | 25S (H34) | A842 | 18S (h20) | G626 | stacking |
| | 25S (H34) | A842 | 18S (h20) | U627 | |
| | 25S (H34) | A842 | 18S (h20) | A956 | |
| | 25S (H34) | A842 | 18S (h20) | G957 | |
| | 25S (H34) | A842 | uS15 | H123 | |
| | 25S (H34) | A843 | uS15 | K140 | |
| | 25S (H34) | A843 | 18S (h20) | A958 | |
| | 25S (H34) | A844 | 18S (h20) | A959 | |
| | eL30 | 81-86 | uS15 | 145-151 | |
| B5 | uL14 | R32 | 18S (h44) | U1722 | |
| | uL14 | P97 | 18S (h44) | A1647 | |
| | uL14 | N128 | 18S (h14) | C409 | Mediated by Mg |
| | uL14 | S112 | 18S (h14) | A410 | Mediated by Mg |
| | 25S (H62) | G1931 | 18S (h44) | G1667 | |
| | 25S (H62) | A1932 | 18S (h44) | G1655 | |
| | 25S (H62) | A1932 | 18S (h44) | A1668 | |

| | | | | |
|---|---|---|---|---|
| B6 | Not observed | | | |
| B7a | 25S (H68) | A2186 | 18S (h23) | G898 | stacking |
| | 25S (H68) | G2239 | 18S (h23) | C895 | weak |
| B7b/c | uL2 | K149 | 18S (h24) | G971 | |
| | uL2 | R247 | 18S (h24) | A998 | |
| | uL2 | G248 | 18S (h24) | G972 | |
| | uL2 | T249 | 18S (h24) | G972 | |
| | uL2 | T249 | 18S (h24) | A973 | |
| | eL43 | R24 | 18S (h24) | A967 | |
| | eL43 | K28 | 18S (h24) | A1005 | |
| B8 | Not observed | | | |
| eB8 | eL43 | 78-89 | 18S (h22) | 865-869 | |
| eB11 | 25S (H101) | U3316 | eS8 | K124 | |
| | 25S (H101) | U3316 | eS8 | H129 | |
| | 25S (H101) | U3316 | eS8 | H132 | |
| | 25S (H101) | U3316 | eS8 | R110 | |
| | 25S (H101) | U3316 | eS8 | S168 | |
| | 25S (H101) | U3317 | eS8 | S168 | |
| | 25S (H101) | G3318 | eS8 | R77 | |
| | 25S (H101) | G3318 | eS8 | R170 | |
| eB12 | eL19 | R162 | 18S (h21) | G799 | |
| | eL19 | R163 | 18S (h21) | U797 | |
| | eL19 | R165 | 18S (h21) | A835 | |
| | eL19 | N166 | 18S (h21) | G799 | |
| | eL19 | R170 | 18S (h21) | G800 | |
| | eL19 | R172 | 18S (h21) | U836 | |
| | eL19 | R172 | 18S (h21) | C837 | |
| | eL19 | R173 | 18S (h21) | U839 | |
| | eL19 | R176 | 18S (h21) | C837 | |
| | eL19 | R176 | 18S (h21) | G838 | |
| | eL19 | L184 | eS7 | R35 | |
| | eL19 | L184 | eS7 | P36 | |
| eB13 | eL24 | C-terminal | 18S (h44) | G1699 | weak density |
| eB14 | eL41 | M1 | 18S (h44) | C1628 | |
| | eL41 | R2 | 18S (h45) | C1760 (4AC) | with acetyl group |
| | eL41 | K4 | 18S (h45) | G1761 | |
| | eL41 | K7 | 18S (h45) | U1762 | |
| | eL41 | K8 | 18S (h45) | G1764 | |
| | eL41 | R9 | 18S (h44) | U1630 | |
| | eL41 | R9 | 18S (h45) | A1769 | |
| | eL41 | K14 | 18S (h27) | A1101 | |
| | eL41 | R15 | 18S (h27) | G1111 | |
| | eL41 | R17 | 18S (h45) | A1737 | |
| | eL41 | R18 | 18S (h27) | G1111 | |
| | eL41 | R21 | 18S (h27) | G1103 | |

Table S2. Complete list of 25S rRNA modifications in *C. albicans* ribosome. Specific modifications found in *C. albicans* are highlighted in blue.

| Ribosomal RNA modifications | | |
|---|---|---|
| 25S | | |
| Base | RIbose | Pseudouridines |
| 1MA643 | A2M647 | PSU772 |
| **M7A816** | OMC648 | PSU962 |
| **M7A1053** | OMC661 | PSU982 |
| **7MG1662** | OMG801 | PSU1000 |
| **JMH1702** | OMG863 | PSU1048 |
| 1MA2120 | A2M872 | PSU2111 |
| **7MG2139** | OMU894 | PSU2169 |
| 5MC2256 | OMG904 | PSU2318 |
| 5MC2842 | A2M1129 | PSU2325 |
| | **OMG1430** | PSU2327 |
| | OMC1433 | PSU2329 |
| | A2M1445 | PSU2394 |
| | OMG1446 | PSU2798 |
| | OMU1884 | PSU2837 |
| | OMC2175 | PSU2852 |
| | A2M2198 | PSU2916 |
| | A2M2258 | PSU2947 |
| | A2M2259 | |
| | OMG2266 | |
| | **A2M2304** | |
| | OMC2315 | |
| | OMU2395 | |
| | OMU2399 | |
| | OMG2591 | |
| | A2M2612 | |
| | OMU2696 | |
| | OMU2701 | |
| | OMG2763 | |
| | OMG2765 | |
| | OMG2787 | |
| | **OMC2808** | |
| | OMU2893 | |
| | OMG2894 | |
| | A2M2918 | |
| | **OMG2919** | |
| | OMC2931 | |

Table S3. Complete list of 18S rRNA modification in *C. albicans* ribosome.

| Ribosomal RNA modifications | | |
|---|---|---|
| 18S | | |
| Base | RIbose | Pseudouridines |
| 4AC1760 | A2M28 | PSU120 |
| MA61768 | A2M100 | PSU751 |
| MA61769 | OMC412 | |
| | A2M418 | |
| | A2M434 | |
| | A2M617 | |
| | A2M780 | |
| | A2M959 | |
| | OMC992 | |
| | OMG1111 | |
| | OMU1254 | |
| | OMG1414 | |
| | OMC1626 | |

Table S4. Complete list of residues with double side-chain conformations.

| Proteins with multiple side-chain conformations | | |
|---|---|---|
| **Amino acid** | **Protein** | **Residue** |
| LYSINE | uL2 | 70 |
| | eL6 | 28 |
| | uL5 | 94 |
| | eL18 | 31 |
| | eL32 | 17 |
| | eL33 | 86 |
| | eL33 | 92 |
| | eL34 | 29 |
| | eL34 | 36 |
| | eL34 | 106 |
| | uL29 | 84 |
| | eL36 | 69 |
| | eL38 | 30 |
| | eL42 | 24 |
| ARGININE | uL30 | 143 |
| | eL18 | 113 |
| | eL21 | 5 |
| | uL14 | 128 |
| | eL29 | 14 |
| | eL33 | 48 |
| | eL34 | 91 |
| | eL39 | 21 |
| | eL40 | 30 |
| HISTIDINE | uL3 | 377 |
| | eL20 | 49 |
| | eL42 | 90 |
| GLUTAMIC ACID | eL21 | 118 |
| | eL22 | 31 |
| GLUTAMINE | eL18 | 27 |
| | eL20 | 138 |
| TRYPTOPHAN | eL22 | 95 |
| ASPARAGINE | eL19 | 36 |

Table S5. Complete list of polyamine locations in 80S *C. albicans* ribosome.

| Polyamine | Number (chain) | Interacting parts | Residues |
|---|---|---|---|
| SPERMIDINE | 3 (XX) | uL15 | Q38 |
| | | | H39 |
| | | 25S (H11, H13) | G40 |
| | | | G93 |
| | 6 (XX) | 25S (H50, H53) | 1522 |
| | | | 1602 |
| | 7 (XX) | 25S (H25a, H72) | C636 |
| | | | C2356 |
| | | eL32 | C42 |
| | 8 (XX) | 25S (H37, H39) | U950 |
| | | | G1138 |
| | | eL29 | N11 |
| | 9 (XX) | 25S (H49, H49b) | A485 |
| | | | U836 |
| | 10 (XX) | 25S (H13) | U78 |
| | | eL15 | K192 |
| | 11 (XX) | 25S (H52) | A1542 |
| | | eL15 | R71 |
| | | | T80 |
| | 12 (XX) | 25S (H40, H41) | G1143 |
| | | | G1145 |
| | | | A1166 |
| | | | A1167 |
| | 13 (XX) | uL2 | R6 |
| | | | P197 |
| PUTRESCINE | 5 (XX) | 25S (H26a) | C2332 |
| | | | G2333 |
| | | uL22 | R82 |
| | 14 (XX) | 5.8S (H5) | G42 |
| | | eL37 | R63 |
| SPERMINE | 4 (XX) | 25S (H13, H21) | U279 |
| | | | U280 |
| | | | U282 |
| | | | G90 |

**ANM**

| *Data collection* | |
|---|---|
| *Microscope* | *Talos Arctica with K2-detector* |
| *Voltage* | *200 kV* |
| *Pixel size (Å)* | *1.012* |
| *Micrographs collected (#)* | *2040* |
| *Refinement* | |
| *Particles (#)* | *156 607* |
| *Resolution (Å; at FSC = 0.143)* | *2.77* |
| *CC (model to map fit)* | *0.75* |
| *RMS deviations* | |
| *Bonds (Å)* | *0.004* |
| *Angles ($^0$)* | *0.785* |
| *Chirality ($^0$)* | *0.039* |
| *Planarity ($^0$)* | *0.004* |
| *Validation* | |
| *Clashscore* | *7.16* |
| *Favored rotamers (%)* | *99.67* |
| *Ramachandran favored (%)* | *97.31* |
| *Ramachandran allowed (%)* | *2.65* |
| *Ramachandran outliers (%)* | *0.04* |

Table S6. Data collection parameters and model refinement statistics of the *C. albicans* ribosome complex with anisomycin.

|  | **BLS** |
|---|---|
| ***Data collection*** | |
| *Microscope* | *Titan KRIOS with K3-detector* |
| *Voltage* | *300 kV* |
| *Pixel size (Å)* | *0.836* |
| *Micrographs collected (#)* | *2152* |
| ***Refinement*** | |
| *Particles (#)* | *136 638* |
| *Resolution (Å; at FSC = 0.143)* | *2.67* |
| *CC (model to map fit)* | *0.78* |
| ***RMS deviations*** | |
| *Bonds (Å)* | *0.004* |
| *Angles ($^0$)* | *0.783* |
| *Chirality ($^0$)* | *0.039* |
| *Planarity ($^0$)* | *0.004* |
| ***Validation*** | |
| *Clashscore* | *7.12* |
| *Favored rotamers (%)* | *99.67* |
| *Ramachandran favored (%)* | *97.32* |
| *Ramachandran allowed (%)* | *2.64* |
| *Ramachandran outliers (%)* | *0.04* |

Table S7. Data collection parameters and model refinement statistics of the *C. albicans* ribosome in complex with blasticidin S.

**PHY**

| | |
|---|---|
| ***Data collection*** | |
| *Microscope* | *Titan KRIOS with K3-detector* |
| *Voltage* | *300 kV* |
| *Pixel size (Å)* | *0.836* |
| *Micrographs collected (#)* | *1310* |
| ***Refinement*** | |
| *Particles (#)* | *132 328* |
| *Resolution (Å; at FSC = 0.143)* | *2.64* |
| *CC (model to map fit)* | *0.81* |
| ***RMS deviations*** | |
| *Bonds (Å)* | *0.004* |
| *Angles ($^0$)* | *0.587* |
| *Chirality ($^0$)* | *0.037* |
| *Planarity ($^0$)* | *0.004* |
| ***Validation*** | |
| *Clashscore* | *8.86* |
| *Favored rotamers (%)* | *99.57* |
| *Ramachandran favored (%)* | *97.51* |
| *Ramachandran allowed (%)* | *2.48* |
| *Ramachandran outliers (%)* | *0.01* |

Table S8. Data collection parameters and model refinement statistics of the *C. albicans* ribosome in complex with phyllanthoside.

**CHX**

| Data collection | |
|---|---|
| *Microscope* | *Titan KRIOS with K3-detector* |
| *Voltage* | *300 kV* |
| *Pixel size (Å)* | *0.836* |
| *Micrographs collected (#)* | *3199* |

| Refinement | |
|---|---|
| *Particles (#)* | *180 636* |
| *Resolution (Å; at FSC = 0.143)* | *2.56* |
| *CC (model to map fit)* | *0.86* |

| RMS deviations | |
|---|---|
| *Bonds (Å)* | *0.006* |
| *Angles ($^{0}$)* | *0.807* |
| *Chirality ($^{0}$)* | *0.056* |
| *Planarity ($^{0}$)* | *0.005* |

| Validation | |
|---|---|
| *Clashscore* | *9.88* |
| *Favored rotamers (%)* | *99.50* |
| *Ramachandran favored (%)* | *96.77* |
| *Ramachandran allowed (%)* | *3.21* |
| *Ramachandran outliers (%)* | *0.02* |

Table S9. Data collection parameters and model refinement statistics of the *C. albicans* ribosome in cycloheximide complex.
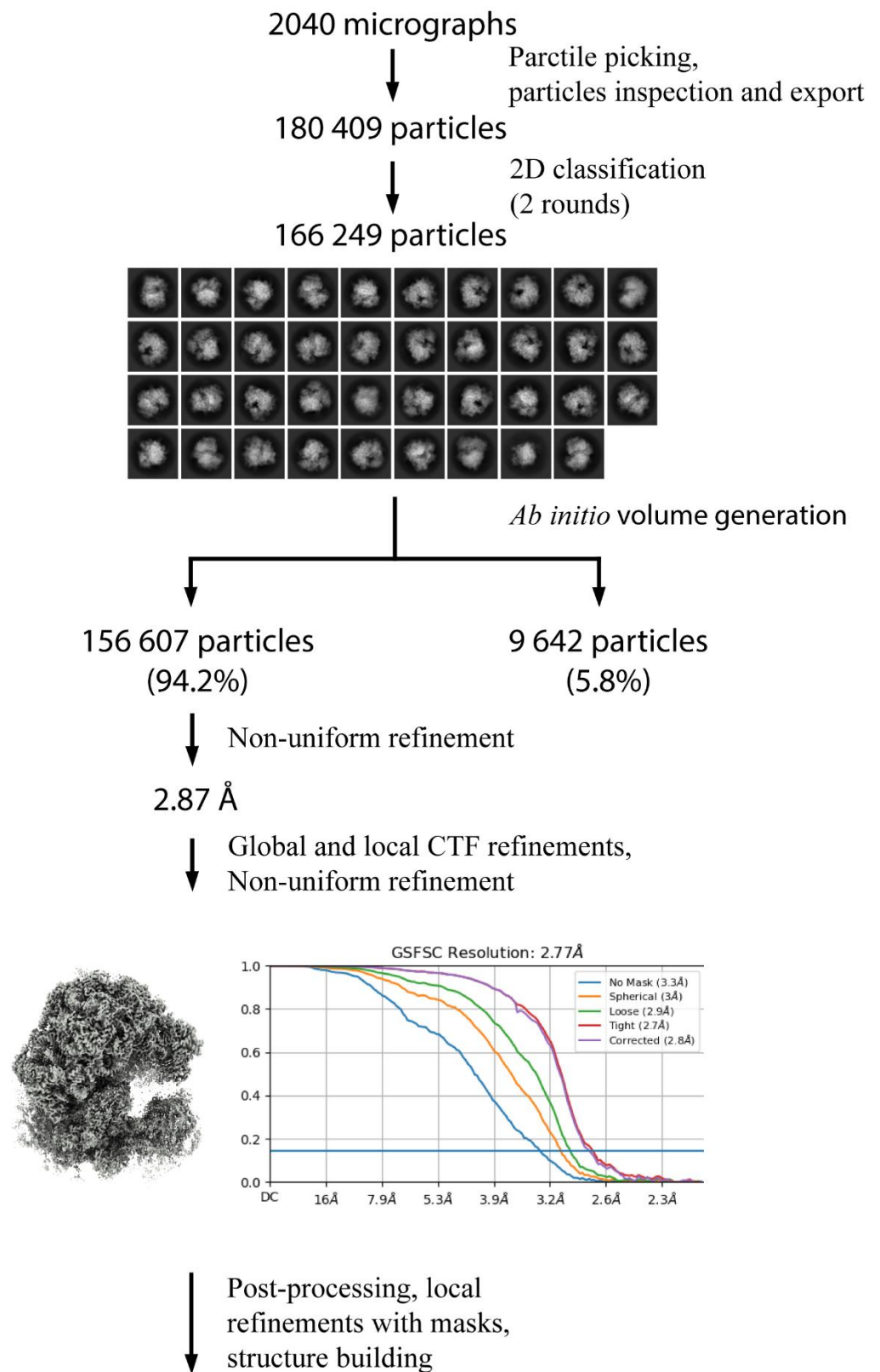
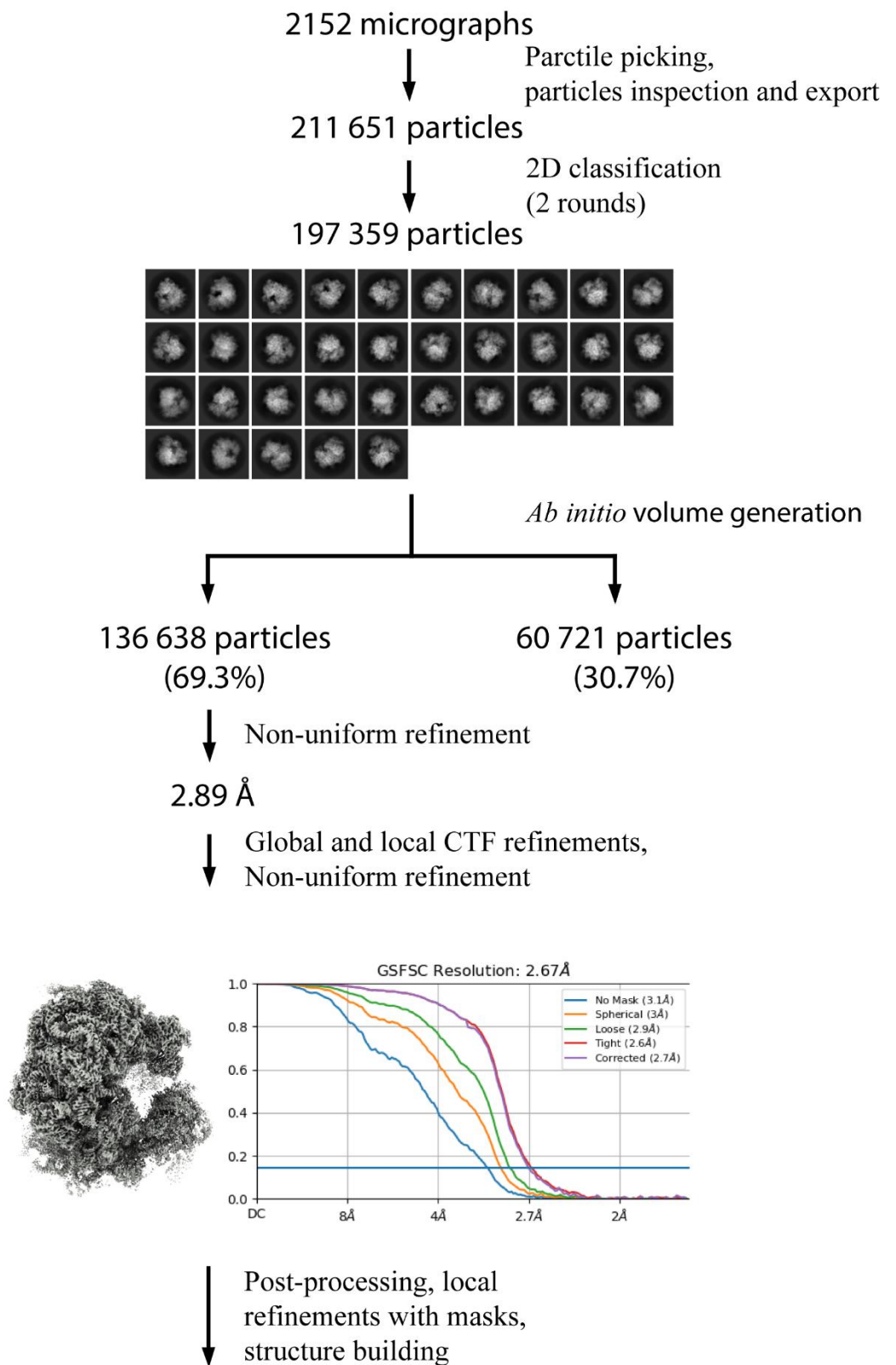Fig. S1. Cryo-EM data processing scheme for the *C. albicans* ribosome complex with aniso-mycin.

Fig. S2. Cryo-EM data processing scheme for the *C. albicans* ribosome in complex with blasti-cidin S.
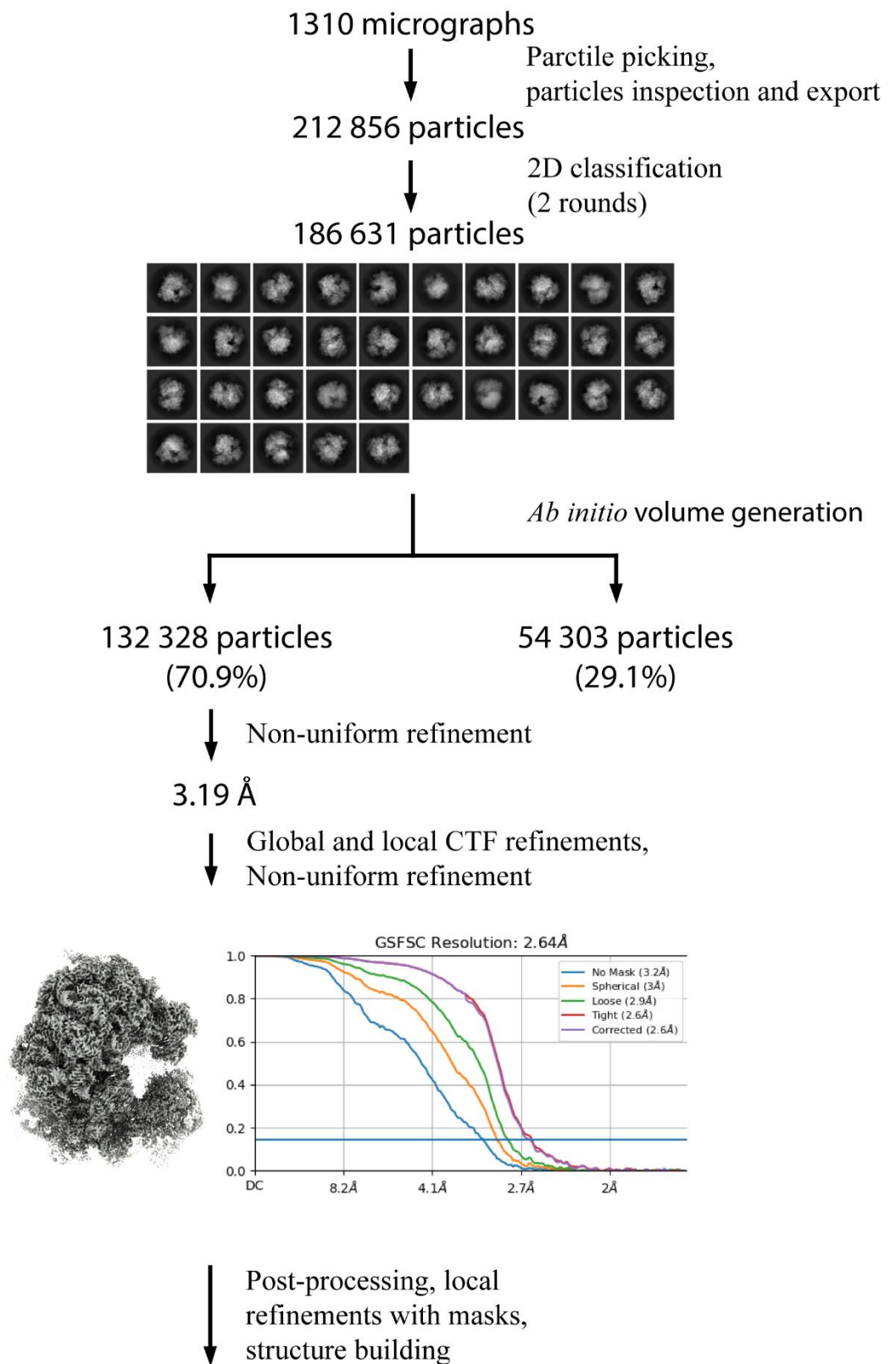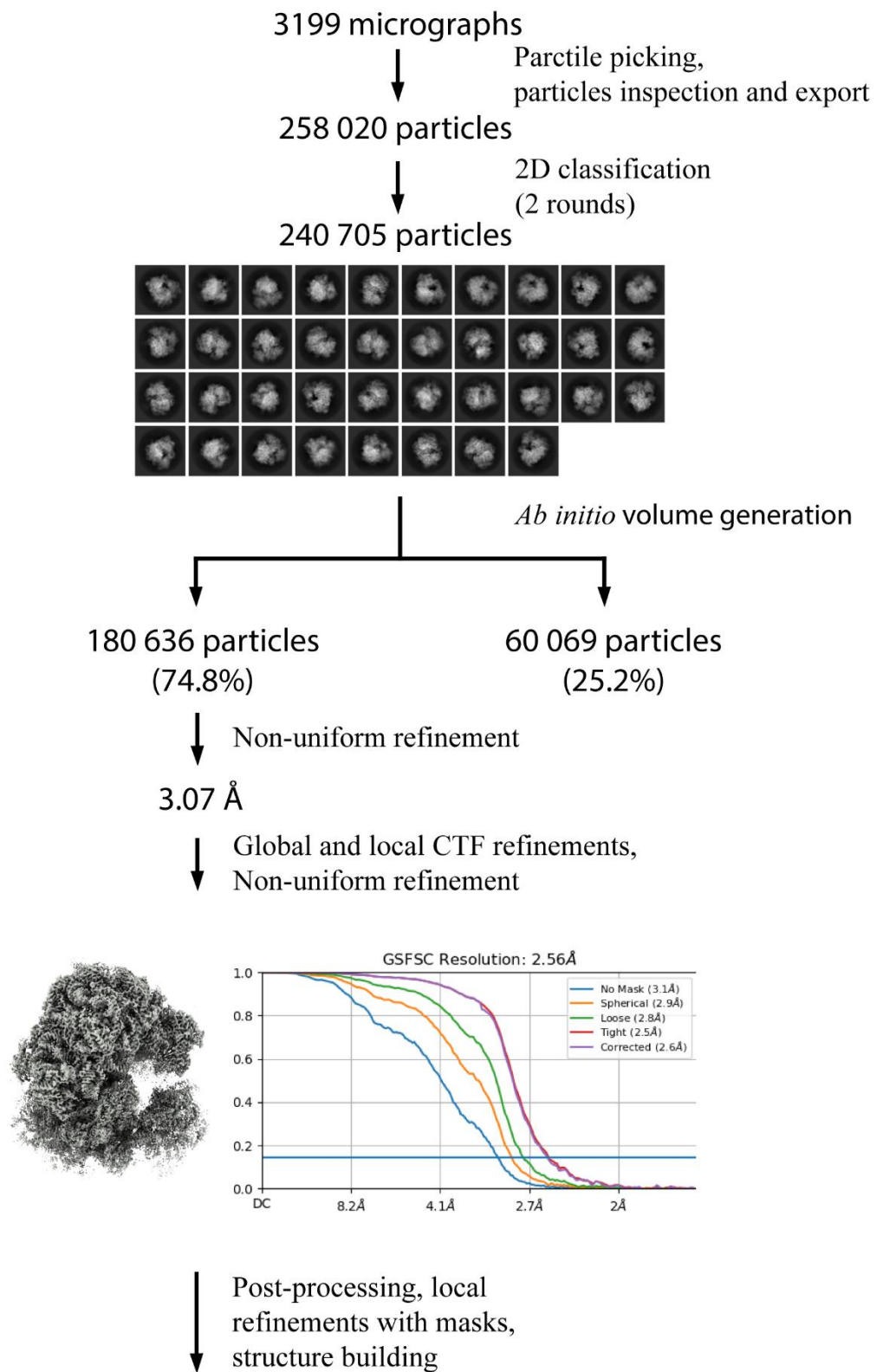
1310 micrographs

↓ Parctile picking,
particles inspection and export

212 856 particles

↓ 2D classification
(2 rounds)

186 631 particles



*Ab initio* volume generation

132 328 particles          54 303 particles
(70.9%)                    (29.1%)

↓ Non-uniform refinement

3.19 Å

↓ Global and local CTF refinements,
Non-uniform refinement



GSFSC Resolution: 2.64Å

No Mask (3.2Å)
Spherical (3Å)
Loose (2.9Å)
Tight (2.6Å)
Corrected (2.6Å)

↓ Post-processing, local
refinements with masks,
structure building

Fig. S3. Cryo-EM data processing scheme for the *C. albicans* ribosome in complex with phyl-lanthoside.

3199 micrographs

$\downarrow$ Parctile picking,
particles inspection and export

258 020 particles

$\downarrow$ 2D classification
(2 rounds)

240 705 particles



*Ab initio* volume generation

180 636 particles          60 069 particles
(74.8%)                    (25.2%)

$\downarrow$ Non-uniform refinement

3.07 Å

$\downarrow$ Global and local CTF refinements,
Non-uniform refinement



$\downarrow$ Post-processing, local
refinements with masks,
structure building

Fig. S4. Cryo-EM data processing scheme for the *C. albicans* ribosome in complex with cyclo-
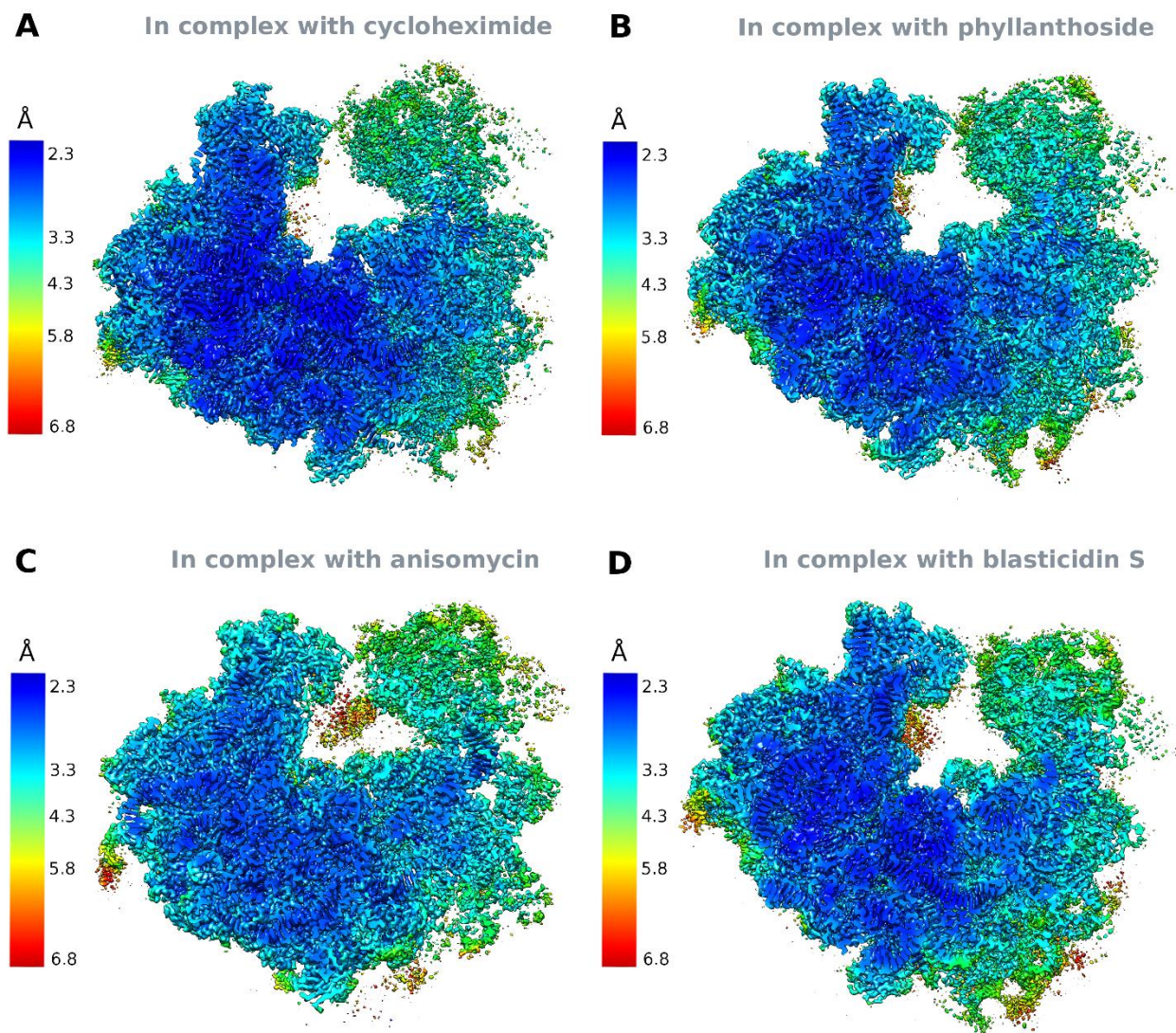heximide.

Fig. S5. Local resolution maps of the *C. albicans* ribosome in complex with cycloheximide (A),
phyllanthoside (B), anisomycin (C), and blasticidin S (D).

STRUCTURAL BIOLOGY

# E-site drug specificity of the human pathogen *Candida albicans* ribosome

Yury Zgadzay[1,2]†, Olga Kolosova[1]†, Artem Stetsenko[3], Cheng Wu[4], David Bruchlen[1], Konstantin Usachev[2,5], Shamil Validov[2,5], Lasse Jenner[1], Andrey Rogachev[6,7], Gulnara Yusupova[1], Matthew S. Sachs[4], Albert Guskov[3,6]*, Marat Yusupov[1,2,5]*

*Candida albicans* is a widespread commensal fungus with substantial pathogenic potential and steadily increasing resistance to current antifungal drugs. It is known to be resistant to cycloheximide (CHX) that binds to the E–transfer RNA binding site of the ribosome. Because of lack of structural information, it is neither possible to understand the nature of the resistance nor to develop novel inhibitors. To overcome this issue, we determined the structure of the vacant *C. albicans* 80*S* ribosome at 2.3 angstroms and its complexes with bound inhibitors at resolutions better than 2.9 angstroms using cryo–electron microscopy. Our structures reveal how a change in a conserved amino acid in ribosomal protein eL42 explains CHX resistance in *C. albicans* and forms a basis for further antifungal drug development.

## INTRODUCTION

*Candida albicans* is a pathogenic yeast that frequently causes potentially lethal infections (*1*). There are several classes of antifungal drugs that combat candidiasis; however, most of them have numerous side effects and are expensive, and there is a steady increase in cases of *C. albicans* infections that are drug resistant (*2*). None of these drugs target the protein synthesis apparatus—the ribosome, which is a very successful route to combat prokaryotic pathogens (*3*). Bioinformatics analysis suggests that the structural organization of functional sites of the *C. albicans* ribosome should be highly similar to the *Saccharomyces cerevisiae* and *Homo sapiens* ribosomes (*4*). Nevertheless, there are several key positions in ribosomal RNA (rRNA) and ribosomal proteins at which nucleotide or amino acid substitutions can modulate specific features of the translation cycle and determine resistance to specific inhibitors (*5*). *C. albicans* is resistant to cycloheximide (CHX) (*6*), which binds to the ribosomal E-tRNA binding site (E-site) (*7*). Genetic studies have demonstrated that this resistance is most likely caused by a natural substitution, P56Q, in ribosomal protein eL42 (*8*). However, the mechanistic basis for this has not been determined by direct structural methods.

For the rational design of drugs targeting the *C. albicans* ribosome but not human ribosomes, an understanding of drug-target interactions in the context of the structure of the *C. albicans* ribosome is indispensable. Therefore, we investigated the structural determinants of ribosomal functional sites, including the E-site and the peptidyl transferase center (PTC), of the *C. albicans* ribosome as potential targets for antifungal drug development. Here, we present cryo–electron microscopy (cryo-EM) structures of the vacant *C. albicans* ribosome and its complexes with four known eukaryotic

inhibitors, namely, CHX, phyllanthoside (PHY), anisomycin (ANM), and blasticidin S (BLS). These studies reveal structural differences in the *C. albicans* E-site compared to the *S. cerevisiae* and *H. sapiens* ribosomes that affect CHX binding, which we propose could be exploited for the development of selective translational inhibitors.

## RESULTS AND DISCUSSION

Previously, we have studied the structural organization of the E-site of the 60*S* subunit of *S. cerevisiae* ribosome by determining complexes with a CCA-end analog of tRNA and E-site inhibitors (*9*). It was shown that the rRNA in this pocket is highly conserved between yeasts and humans and is responsible for most interactions with inhibitors. Along with rRNA in the E-site, eukaryote-specific ribosomal protein eL42 interacts with some inhibitors and stabilizes them in the binding pocket (*10*). Here, in the determined structure of the vacant *C. albicans* ribosome, a strong density for a domain of the E-site tRNA was observed, although it was not introduced exogenously (fig. S1F). The presence of endogenous E-site tRNA is not a unique feature of the *C. albicans* ribosome but has been observed for isolation of ribosomes from many other species. Further comparison of the vacant *C. albicans* ribosome with the ribosomes from *S. cerevisiae* and from *H. sapiens* revealed that in the E-site of *C. albicans* ribosome, there is a P56Q alteration in ribosomal protein eL42 (fig. S1A). This is the only difference found in the organization of the functional sites between *C. albicans*, *S. cerevisiae*, and *H. sapiens* (table S1).

The eL42 P56Q substitution decreases the volume of the binding pocket. To establish whether the reduction of the pocket volume affects the binding of inhibitors, we compared the *S. cerevisiae* ribosome [Protein Data Bank (PDB) 4U3U] and *H. sapiens* (PDB 5LKS) ribosome in complex with CHX (fig. S3A) to the vacant *C. albicans* ribosome (at 2.3 Å) with a superimposed CHX molecule. CHX binds to the 60*S* subunit in the E-site, preventing translocation of tRNA from P- to E-site (Fig. 1A). In *S. cerevisiae*, CHX forms five hydrogen bonds with 25*S* rRNA specifically with G92, C93, U2763, and C2764 (*C. albicans* G91, C92, U2735, and C2736). The main difference between the two species concerning CHX binding is the lack of interaction of CHX with P56 of eL42 in *S. cerevisiae*, where

[1]Department of Integrated Structural Biology, Institute of Genetics and Molecular and Cellular Biology, University of Strasbourg, Illkirch, France. [2]Laboratory of Structural Biology, Institute of Fundamental Medicine and Biology, Kazan Federal University, Kazan, Russia. [3]Groningen Biomolecular Sciences and Biotechnology Institute (GBB), University of Groningen, Groningen, Netherlands. [4]Department of Biology, Texas A&M University, College Station, TX, USA. [5]Federal Research Center "Kazan Scientific Center of Russian Academy of Sciences", Kazan, Russia. [6]Moscow Institute of Physics and Technology, Dolgoprudny, Russia. [7]The Joint Institute for Nuclear Research, Dubna, Russia.
*Corresponding author. Email: a.guskov@rug.nl (A.G.); marat@igbmc.fr (M.Y.)
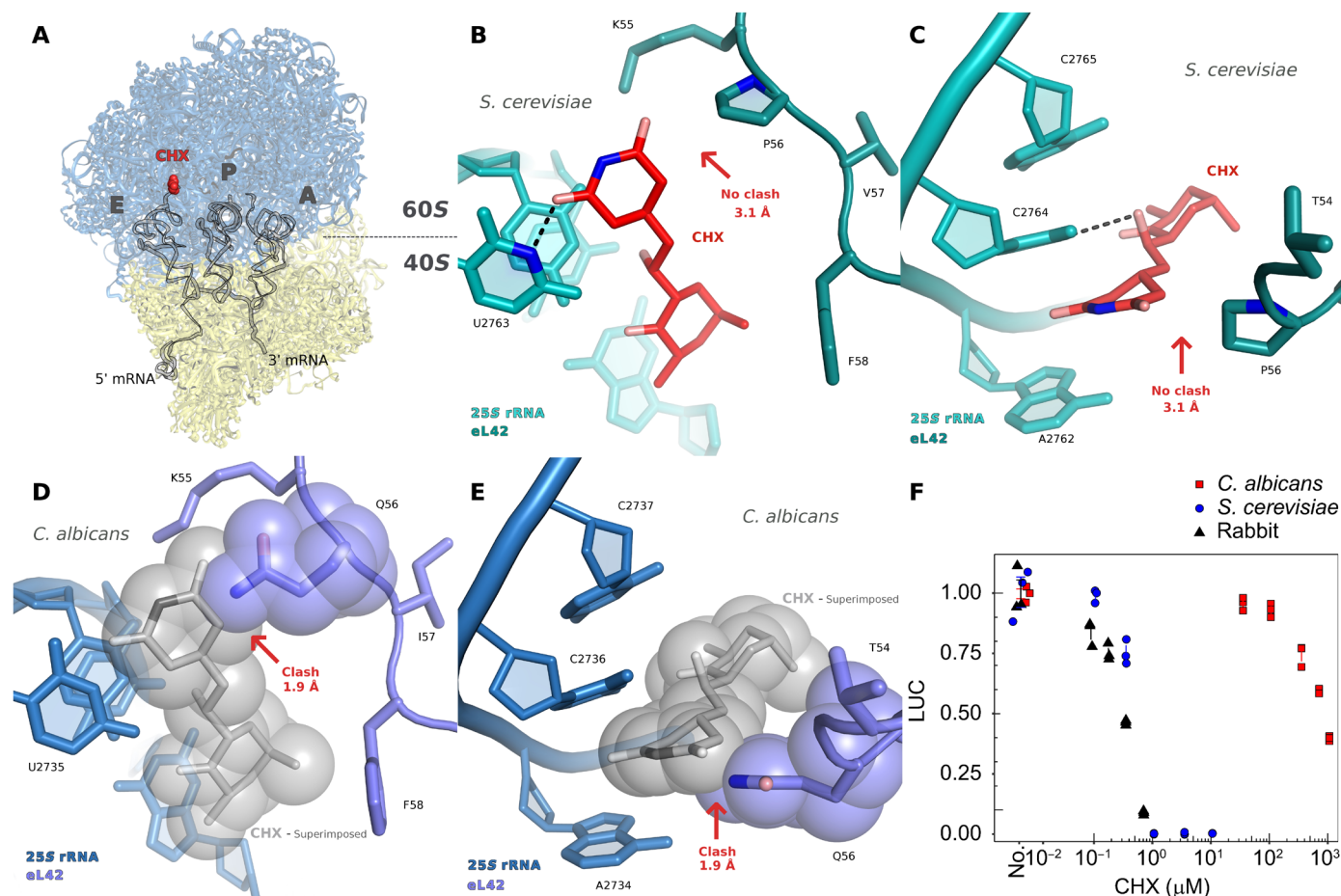†These authors contributed equally to this work.

**Fig. 1. Q56 prevents binding of CHX to the *C. albicans* ribosome.** (**A**) Overview of the CHX binding site (red) in the *C. albicans* 80S ribosome. The 40S subunit is shown in yellow, the 60S subunit is shown in blue, and mRNA and tRNA are shown in gray. The CHX molecule was superimposed from *S. cerevisiae* ribosome (PDB 4U3U), and mRNA and tRNAs were superimposed from the *Thermus thermophilus* (PDB 4V4Y). (**B** and **C**) Binding of CHX to the *S. cerevisiae* ribosome shown in two orientations (PDB 4U3U) (*9*). (**D** and **E**) Close-up views of the *C. albicans* CHX binding site in two orientations. The glutarimide group of CHX clashes with the side chain of Q56 preventing CHX from binding to the ribosome of *C. albicans*. (**F**) Inhibition of translation by CHX in cell-free translation extracts (CFTSs) from *C. albicans*, *S. cerevisiae*, and rabbit reticulocytes. Cell-free experiments were performed twice using independent technical triplicates; the results of one set of triplicates are shown. The root mean square deviation of luciferase (LUC) activity was 2 to 5%.

the CHX molecule is 3.1 Å distant from the proline side chain (Fig. 1, B and C). Superimposing CHX into the vacant *C. albicans* ribosome creates a clash between the Q56 side chain and the glutarimide group of CHX (Fig. 1, D and E). Our findings suggest that electrostatic repulsion between Oε oxygen of the glutamine side chain and O6 oxygen of CHX occludes its binding to the *C. albicans* ribosome.

Cell-free assays and microplate drug inhibition (MIC) experiments corroborated this finding. Translation of sea pansy luciferase (spLUC) in the *C. albicans* cell-free translation extract (CFTS) is approximately 1000-fold more resistant to CHX than the *S. cerevisiae* and the rabbit reticulocyte CFTSs (Fig. 1F). In MIC assays, 100% inhibition of *S. cerevisiae* growth was obtained with 1 μM CHX. In contrast, approximately 67% inhibition of *C. albicans* growth was observed with 900 μM CHX, and limited growth was still observed with 7 mM CHX (fig. S2).

On the basis of CFTS assays, we attempted to bind CHX at high excess in nonphysiological conditions (≥1 mM) to understand possible rearrangements in the E-site upon the inhibitor binding.

Only at 1 mM was density for CHX observed in the E-site (fig. S3B). The quality of the map allowed for visualization of the ribosome structural rearrangement upon CHX binding (Fig. 2A). We found that, in *C. albicans*, the CHX molecule adopts a different conformation, not penetrating so deep as in *S. cerevisiae* and in *H. sapiens*. By comparing CHX binding with the vacant ribosome with superimposed CHX, a 1-Å shift of the whole CHX molecule was observed (Fig. 2B). To bind to the E-site at a high concentration, the CHX molecule pushes the Q56 side chain 1.4 Å downward (Fig. 2C). Consequently, there is a slight shift in positions of the C2736, C2737, and G2766 with a 12° rotation of U2735 in comparison to the vacant *C. albicans* ribosome structure. In addition, a slight shift of the eL42 protein backbone is observed. These observations corroborate that there is no high-affinity binding site for CHX in the *C. albicans* ribosome.

While many inhibitors that target the E-site are known, most of them have a glutarimide group, which prevents their binding to the *C. albicans* ribosome at physiological concentrations (*4*). Only one known E-site inhibitor, PHY (fig. S3C), does not have a glutarimide
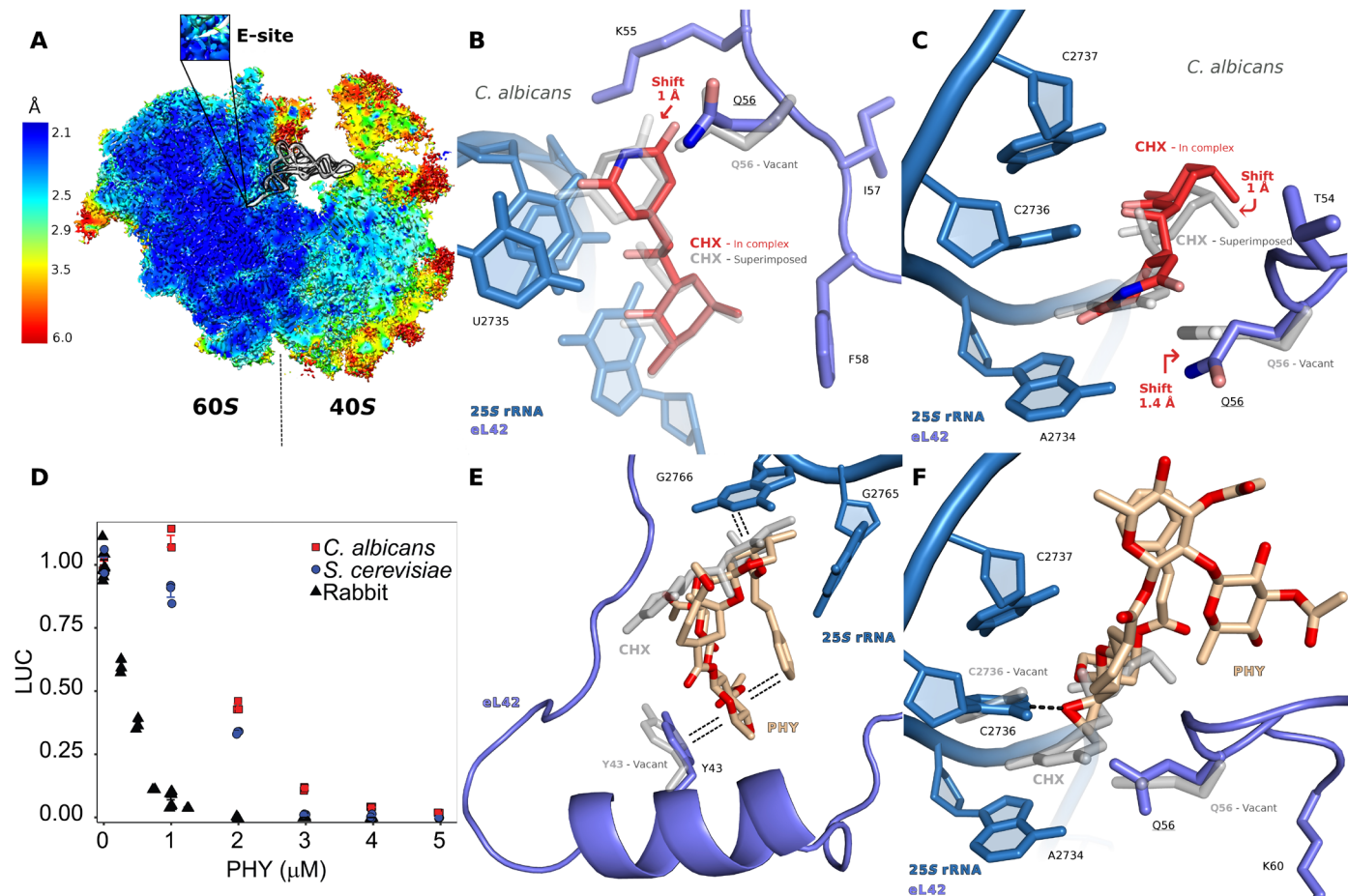
**Fig. 2. CHX and PHY binding to the *C. albicans* ribosome.** (**A**) Local resolution map of the *C. albicans* ribosome with the close-up view onto the E-site. (**B** and **C**) CHX adopts a different conformation in comparison with the superimposed molecule. Low-affinity binding of CHX leads to movement of the Q56 side chain. (**D**) Effect of PHY on translation in cell-free systems from *C. albicans*, *S. cerevisiae*, and rabbit reticulocytes. Cell-free experiments were performed twice using independent technical triplicates; the results of one set of triplicates is shown. The root mean square deviation of LUC activity was 2 to 5%. (**E** and **F**) Overview of PHY binding site. PHY interacts with Y43 of the eL42 and with 25S rRNA forming a hydrogen bond with C1736.

moiety and thus could be active against *C. albicans*. To test this hypothesis, we performed cell-free translation experiments in the presence of PHY. In notable contrast to CHX, translation of spLUC in all three species was similarly sensitive to PHY (Fig. 2D). To corroborate this finding, we determined the cryo-EM structure of the *C. albicans* ribosome in complex with PHY (100 μM concentration) at 2.6-Å resolution. The obtained map revealed a strong density in the E-site that corresponds to PHY (fig. S3D), which binds in a manner resembling the tRNA CCA-end. It forms two stacking interactions with G2766 of 25S rRNA and Y43 of eL42 (Fig. 2E). Because of the lack of a glutarimide group, PHY does not clash with Q56, in contrast to the situation with CHX (Fig. 2F). The epoxide group of PHY, which is the closest to Q56, is located 5.3 Å away from that residue. However, this group is very close to C2735 (2 Å) and has previously been suggested to form a covalent bond with C2736 (C2764 in *S. cerevisiae*), which results in an irreversible inhibitory effect on protein synthesis (*9*). In addition, we found that, with PHY in the E-site, U2735, C2736, G2765, and G2766 slightly changed their conformation compared to the structure of the vacant ribosome (Fig. 2F). Despite the direct interaction (stacking) with eL42 Y43 (Fig. 2E), PHY causes a 0.65-Å shift of the eL42

backbone (residues K55 to K60; Fig. 2F) similar to what was observed in the *S. cerevisiae* structure (PDB 4u4z). In addition, density for the E-site tRNA was not detected, indicating that PHY's binding prevents tRNA entry into the E-site (fig. S4). These structural results suggest that PHY is the only currently known E-site inhibitor of *C. albicans*. Although this inhibitor cannot discriminate between *C. albicans* and other eukaryotic ribosomes, it can serve as a starting point for the rational drug design of a specific inhibitor.

In addition, we found a strong density for a spermidine molecule in the E-site close to uL15, although spermidine was not introduced exogenously. This has previously been observed in *Neurospora crassa* (*11*) and in *S. cerevisiae* (*12*), but, here, we propose a structural role of spermidine for the E-site pocket formation. The spermidine molecule interacts with Q38 and H39, stabilizing the E-site binding pocket, although no hydrogen bonds are formed (fig. S5). We suggest that spermidine is the key factor to explain CHX resistance arising from mutations at residues Q38 and H39 of ribosomal protein uL15 (see Supplementary Text and fig. S5).

Additional differences of interest arising from the comparison between *C. albicans* and *S. cerevisiae* were also found. These differences could potentially be important for drug specificity at other
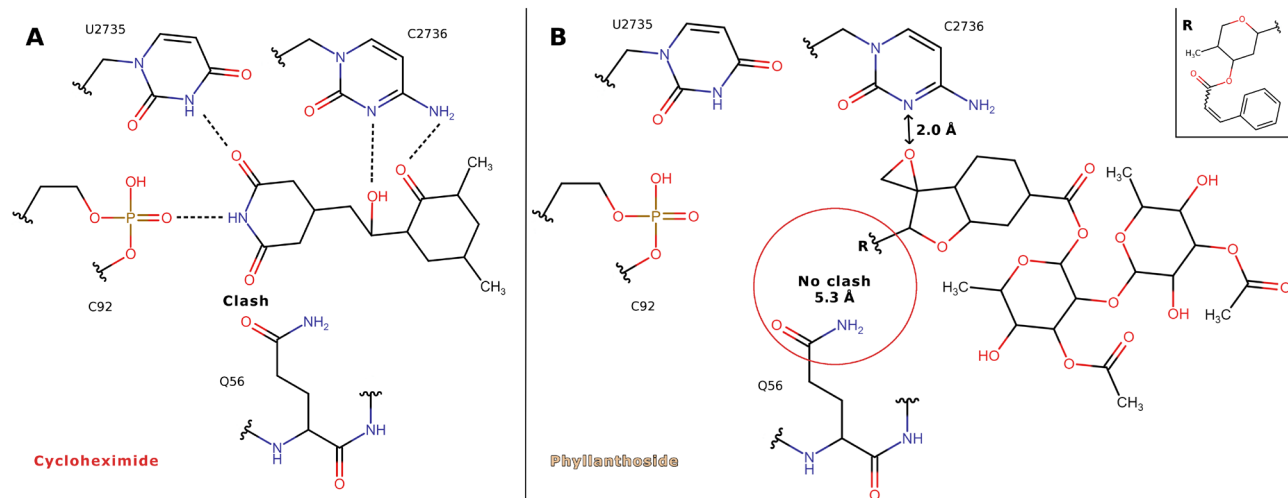
**Fig. 3. E-site specificity of the *C. albicans* ribosome.** (**A**) Schematic interaction of CHX binding to the E-site. CHX could not bind to the E-site of *C. albicans* due to the clash between the glutarimide group of CHX and Q56 side chain. (**B**) Schematic interaction of PHY binding to the E-site. PHY is the only E-site inhibitor that binds to *C. albicans* ribosome at physiological concentration. Because of the lack of glutarimide moiety, PHY does not clash with the Q56 located 5.3 Å apart.

functional sites of the ribosome. The PTC nucleotide composition of *C. albicans*, *S. cerevisiae*, and *H. sapiens* is identical (table S1). Nevertheless, in the *C. albicans* vacant ribosome, we found that 2793C and U2847 adopt different conformations compared to the vacant yeast ribosome (PDB 4v88). To understand whether these differences play any physiological role or might arise from differences in sample analyses (single particles versus crystal), structures of the *C. albicans* ribosome with an added ANM and BLS were determined (see Supplementary Text and figs. S3, E to H, and S6). No substantial differences in the binding site geometry and inhibitor interactions were observed when comparing ANM and BLS interactions with *C. albicans* and *S. cerevisiae* ribosomes. Consistent with the observed similarity of the binding of the A-site inhibitor ANM and the P-site inhibitor BLS to the *C. albicans* and *S. cerevisiae* ribosomes, inhibition of translation by these compounds was also similar in translation extracts from these two yeasts (fig. S6, C and E). Hence, it seems that the minor structural changes do not affect the binding or action of these inhibitors in the PTC.

In addition to the structural features of the PTC (fig. S1B), a high-quality map enabled us to find different conformations and modifications of proteins and rRNAs. About 60 amino acids with multiple side-chain conformations were observed, as well as three amino acids (lysines) with side-chain monomethylation, and 138 possible rRNA modifications (116 in 25*S* and 22 in 18*S* rRNAs) (fig. S1, C to E). While eL41 is not currently annotated in *Candida* species, eL41 protein was evident in the experimental density. A conserved DNA sequence in the genome of *C. albicans* SC5314 between orf19.1676 and orf19.1677 was identified with the help of curators at the Candida Genome Database (*13*) that specifies a 25-residue polypeptide similar to *S. cerevisiae* eL41 that fits into the density and therefore appears to be *C. albicans* eL41 (fig. S7).

A 2.32-Å [at FSC (Fourier shell correlation) = 0.143] high-resolution ribosome structure of one of the most pathogenic fungi, *C. albicans*, is reported. Our results explain the resistance of *C. albicans* to CHX and demonstrate specific features of the *C. albicans* ribosome. On the basis of structural and cell-free translation data, we propose that CHX cannot bind to the *C. albicans*

ribosome due to the clash of the glutarimide group of CHX with the Q56 side chain of eL42 (Fig. 3A). In contrast to CHX, PHY binds to the E-site of *C. albicans* at a physiologically relevant concentration. Because of the lack of the glutarimide moiety, PHY adopts an entirely different interaction pattern and does not clash with Q56 (Fig. 3B). Our study provides a solid base for potential future development of anti-*Candida* drugs without a glutarimide moiety that could lead to specific binding to the ribosome of *C. albicans*. Understanding ribosome inhibition will significantly improve the treatment of candidiasis and reduce the mortality associated with it.

## MATERIALS AND METHODS
### Materials
ANM, BLS, and CHX were purchased from Sigma-Aldrich. These compounds were dissolved in water because of their sufficient solubility at low concentrations (5 to 10 mM). PHY was provided by the National Institutes of Health Development Therapeutics Program and dissolved in dimethyl sulfoxide (54 mM).

### Ribosome purification
80*S* ribosomes from *C. albicans* SC5314 were purified as described earlier, with minor changes (*4*). The *C. albicans* SC5314 strain was provided by S. Znaidi (Institut Pasteur, Paris, France). Candida cells grew in flasks to an $OD_{600}$ (optical density at 600 nm) of 1.0 in yeast extract–peptone–dextrose (YPD) medium at 30°C. Cells were pelleted by centrifugation, resuspended with YP, and incubated in flasks with vigorous shaking (250 rpm) for 10.5 min. Cells were precipitated and washed three times in buffer M [30 mM Hepes-KOH (pH 7.5) at room temperature, 50 mM KCl, 10 mM $MgCl_2$, 8.5% mannitol, 2 mM dithiothreitol (DTT), and 0.5 mM EDTA]. Following the final centrifugation (3450*g* for 10 min), the pellet was weighed. Typically, we obtained 5.5 g of cells from 4 liters of cell culture.

For 5.5 g of cells, the pellet was resuspended in 8 ml of buffer M and supplemented with additional 1500 µl from a solution of one complete protease inhibitor tablet (without EDTA, Roche) dissolved in 2 ml of buffer M, 250 µl of RNasin (Promega), 300 µl of

100 mM Pefabloc, 80 μl of heparin (100 mg/ml), 30 μl of 1 M DTT, and 650 μl of 2 M KCl (concentration adjusted to 130 mM to precipitate lipids after breaking cells). The cell suspension was transferred to a round-bottom 50-ml tube (Nalgene) with 16.5 g of glass beads (Sigma-Aldrich). Cells were mechanically disrupted nine times on a vortex at a frequency of 40 Hz for 1 min with 1-min breaks on ice between each shake.

Beads were removed by short centrifugation (20,000$g$ for 2 min), and the lysate was further clarified by a longer centrifugation (30,000$g$ for 9 min). Polyethylene glycol (PEG) 20,000 was then added from a 30% (w/v) stock (Hampton Research) to a final concentration of 4.5% (w/v), and the solution was left to stand for 5 min on ice. The solution was clarified by centrifugation (20,000$g$ for 5 min), and the supernatant was transferred to a new tube. Then, PEG 20,000 concentrations were adjusted to 8.5%, and the solution was left to stand for 10 min on ice. Ribosomes were precipitated (17,500$g$ for 10 min), the supernatant was discarded, and residual solution was removed by a short spin of the pellet (14,500$g$ for 1 min). Ribosomes were suspended (8 to 10 mg/ml) in buffer M+ (buffer M with KCl concentration adjusted to 150 mM and supplemented with protease inhibitors and heparin).

Ribosomes were further purified by a 10 to 30% sucrose gradient in buffer S [20 mM Hepes-KOH (pH 7.5), 120 mM KCl, 8.3 mM MgCl$_2$, 2 mM DTT, and 0.3 mM EDTA] using the SW28 rotor (18,000 rpm for 15 hours). The appropriate fractions were collected; KCl and MgCl$_2$ concentrations were adjusted to 150 and 10 mM, respectively; PEG 20,000 was then added to a final concentration of 7% (w/v); and the solution was left to stand 10 min on ice. Ribosomes were precipitated (17,500$g$ for 10 min), the supernatant was discarded, and residual solution was removed by a short spin of the pellet (17,500$g$ for 1 min). Ribosomes were suspended (25 mg/ml) in buffer G [10 mM Hepes-KOH (pH 7.5), 50 mM KOAc, 10 mM NH$_4$OAc, 2 mM DTT, and 5 mM Mg(OAc)$_2$]. Typically, 14 to 16 mg of pure ribosomes were obtained from 5.5 g of cells.

### Complex formation, grid freezing, and image processing

The purified ribosome sample (in buffer G) was filtered (0.22-μm centrifugal filters, Millipore) and concentrated to a final concentration of ~1 to 2 mg/ml. Antibiotics were added at the following concentrations: 250 μM for ANM and BLS, 100 μM for PHY, and 1 mM for CHX. Aliquots of 2.7 μl were applied to a freshly glow-discharged holey carbon grids (Quantifoil Cu R1.2/1.3 with ultrathin carbon support, 200 mesh), excess liquid was blotted away for 3 to 5 s using a FEI Vitrobot Mark IV (Thermo Fisher Scientific), and the samples were plunge-frozen in liquid ethane. Prepared grids were transferred into a Titan Krios 300-keV microscope (Thermo Fisher Scientific), equipped with a K3 direct electron detector or a Talos Arctica 200-keV microscope (Thermo Fisher Scientific), equipped with a K2 direct electron detector. Zero-loss images were recorded semiautomatically, using the UCSF Image script (14). The GIF Quantum energy filter was adjusted to a slit width of 20 eV. Images were collected at a various nominal magnification, yielding pixel sizes from 0.413 to 1.012 Å, and with a defocus range of −0.5 to −3.0 μm. Movie images were collected with 24 frames dose-fractionated over 18 s. In total, we collected 9807, 2040, 2152, 1310, and 3199 micrographs for the vacant *C. albicans* ribosome or in complex with ANM, BLS, PHY, and CHX, respectively.

Motion correction, CTF (contrast transfer function) estimation, manual- and template-based particles picking, two-dimensional (2D) classification, ab initio volume generation, CTF global and local refinements, and nonuniform 3D refinement were performed using cryoSPARC (v 3.1) (15). Maps were sharpened using Autosharpen Map procedure in Phenix (16). The separate masks for the focused refinement were generated for 60$S$ and 40$S$ subunits using Chimera. The cryo-EM data processing schemes for the vacant *C. albicans* ribosome and in complex with investigated inhibitors are presented in figs. S8 to S12, and local resolution maps are presented in fig. S13.

### Modeling

The structure of the *S. cerevisiae* 80$S$ ribosome (17) was used as a template for model building. Model-to-map alignment was performed in Chimera (18). The 60$S$ and 40$S$ subunits were refined separately into their respective focused refined maps using the Phenix real-space refinement (16). The protein and rRNA chains were visually checked in Coot (19) and manually adjusted where necessary. All investigated inhibitors were manually docked into the experimental density, followed by real-space refinement in Phenix (16). The 40$S$ subunit of *C. albicans* follows a classic division into the head, body, and shoulder consisting of 1787 nucleotides (nt) in 18$S$ rRNA and 32 ribosomal proteins. The 18$S$ rRNA is 13 and 82 nt shorter than the 18$S$ rRNA of *S. cerevisiae* and *H. sapiens*, respectively. The large subunit (LSU) contains an active peptidyl transferase site that catalyzes the formation of peptide bonds during protein synthesis. In *C. albicans*, this 60$S$ subunit includes 25$S$ rRNA (3361 nt), 5.8$S$ rRNA (157 nt), 5$S$ rRNA (121 nt), and 45 proteins. The 25$S$ rRNA is 35 nt shorter than the 25$S$ rRNA of *S. cerevisiae* and 1716 nt shorter than the 28S rRNA of *H. sapiens*. 5.8$S$ rRNA and 5$S$ rRNA are almost identical to that in *S. cerevisiae* and *H. sapiens* (only 5.8$S$ is 1 nt shorter). The ribosomal proteins of the LSU of the *C. albicans* ribosome are highly identical (82%) to those in *S. cerevisiae* and *H. sapiens*. The exception is the eL40 protein that is more than twice as short [52 amino acids instead of 128 amino acids in *S. cerevisiae*]. The only unmodeled regions are the L1-stalk and the P-stalk. In addition, because of disordered density and high flexibility, the expansion segments and some protein loops were only partially built in our structures. Overall, the *C. albicans* ribosome model includes 95% of amino acids and 92% of RNA residues from the entire sequence. The model quality statistics are presented in tables S2 to S6.

### Inhibition of cell-free translation by CHX, PHY, ANM, and BLS

We prepared CFTSs from the *C. albicans* and *S. cerevisiae* strains used for structural analyses. These CFTSs were programmed with LUC mRNA, and then their capacity to produce the enzyme in the presence of increasing concentrations of CHX was examined. *C. albicans* belongs to a subclade in which the "universal" genetic code is altered; in this "CTG-clade," the CUG codon is translated as Ser, not Leu (20, 21). Therefore, spLUC was used as the translational reporter because the coding region for this enzyme lacks CUG codons and functions as a reporter in *C. albicans* (22). Translation of spLUC RNA using CFTSs from these yeasts can thus be directly compared without concern for their use of different genetic codes.

*C. albicans* and *S. cerevisiae* CFTSs were prepared using the method 1 protocol for *S. cerevisiae*, and translation reactions were assayed for LUC activity, as described in (23). Rabbit reticulocyte lysate (RRL) was obtained from Promega (L4960). Capped and polyadenylated spLUC mRNA was prepared by T7 transcription of

EcoRI-linearized plasmid pQQ101 encoding spLUC (*24*). For quantification, triplicate-independent CFTSs (10 μl each) programmed with 60 ng of spLUC RNA and RRLs programmed with 6 ng of spLUC RNA were incubated at 26°C in the absence or presence of different concentrations of inhibitors for 30 min and the activity of spLUC then measured by luminometry.

## Drug susceptibility assay

Drug susceptibility was determined as previously described with modifications (*25*). Briefly, twofold dilution series of CHX were prepared in fresh YPD medium and distributed into 96-well plates (Falcon, 351177). *C. albicans* and *S. cerevisiae* cells from overnight cultures grown in 3 ml of YPD medium were collected and resuspended in 500 μl of fresh YPD medium. The numbers of cells were then determined using a hemocytometer. Cell suspensions were diluted with fresh YPD medium to make working suspensions of $2 \times 10^3$ cells per ml and distributed into the drug dilution series (volume ratio, 1:1) in the 96-well plates and mixed well. Plates were statically incubated at 30°C for 24 hours, and $OD_{600}$ was measured with a SpectraMax M2$^e$ microplate spectrophotometer.

## Figure preparation

Cryo-EM maps were manually inspected in Coot (*19*). Panels of figures showing structural models were prepared using PyMOL and Gimp. The sequence of logo drawings was made using WebLogo 3.7.4 (*26*).

## Data deposition

The final models and associated maps are deposited with the PDB and Electron Microscopy Data Bank (EMDB) with the following accession codes: 7PZY and EMD-13737 for the vacant *C. albicans* ribosome, 7Q0P and EMD-13749 for complex with ANM, 7Q0R and EMD-13750 for complex with BLS, 7Q0F and EMD-13744 for complex with PHY, and 7Q08 and EMD-13741 for complex with CHX, respectively.

## SUPPLEMENTARY MATERIALS

Supplementary material for this article is available at https://science.org/doi/10.1126/sciadv.abn1062

View/request a protocol for this paper from *Bio-protocol*.

## REFERENCES AND NOTES

1. F. L. Mayer, D. Wilson, B. Hube, *Candida albicans* pathogenicity mechanisms. *Virulence* **4**, 119–128 (2013).
2. G. C. de Oliveira Santos, C. C. Vasconcelos, A. J. O. Lopes, M. d. S. de Sousa Cartágenes, A. K. D. B. Filho, F. R. F. do Nascimento, R. M. Ramos, E. R. R. B. Pires, M. S. de Andrade, F. M. G. Rocha, C. de Andrade Monteiro, Candida infections and therapeutic strategies: Mechanisms of action for traditional and alternative agents. *Front. Microbiol.* **9**, 1351 (2018).
3. D. N. Wilson, The A-Z of bacterial translation inhibitors. *Crit. Rev. Biochem. Mol. Biol.* **44**, 393–433 (2009).
4. D. Bruchlen, "*Candida albicans* ribosome: Structure, function and inhibition," thesis, Strasbourg University, Strasbourg (2016).
5. J. H. Bae, B. H. Sung, J. H. Sohn, Site saturation mutagenesis of ribosomal protein L42 at 56th residue and application as a consecutive selection marker for cycloheximide resistance in yeast. *FEMS Microbiol. Lett.* **365**, fny066 (2018).
6. P. Dehoux, J. Davies, M. Cannon, Natural cycloheximide resistance in yeast. The role of ribosomal protein L41. *Eur. J. Biochem.* **213**, 841–848 (1993).
7. R. Ben-Yaacov, S. Knoller, G. A. Caldwell, J. M. Becker, Y. Koltin, *Candida albicans* gene encoding resistance to benomyl and methotrexate is a multidrug resistance gene. *Antimicrob. Agents Chemother.* **38**, 648–652 (1994).
8. S. Kawai, S. Murao, M. Mochizuki, I. Shibuya, K. Yano, M. Takagi, Drastic alteration of cycloheximide sensitivity by substitution of one amino acid in the L41 ribosomal protein of yeasts. *J. Bacteriol.* **174**, 254–262 (1992).
9. N. Garreau de Loubresse, I. Prokhorova, W. Holtkamp, M. V. Rodnina, G. Yusupova, M. Yusupov, Structural basis for the inhibition of the eukaryotic ribosome. *Nature* **513**, 517–522 (2014).
10. S. Pellegrino, M. Meyer, Z. A. Könst, M. Holm, V. K. Voora, D. Kashinskaya, C. Zanette, D. L. Mobley, G. Yusupova, C. D. Vanderwal, S. C. Blanchard, M. Yusupov, Understanding the role of intermolecular interactions between lissoclimides and the eukaryotic ribosome. *Nucleic Acids Res.* **47**, 3223–3232 (2019).
11. L. Shen, K. Yang, C. Wu, T. Becker, D. Bell-Pedersen, J. Zhang, M. S. Sachs, Structure of the translating *Neurospora* ribosome arrested by cycloheximide. *Proc. Natl. Acad. Sci. U.S.A.* **118**, e2111862118 (2021).
12. R. Buschauer, Y. Matsuo, T. Sugiyama, Y. H. Chen, N. Alhusaini, T. Sweet, K. Ikeuchi, J. Cheng, Y. Matsuki, R. Nobuta, A. Gilmozzi, O. Berninghausen, P. Tesina, T. Becker, J. Coller, T. Inada, R. Beckmann, The Ccr4-Not complex monitors the translating ribosome for codon optimality. *Science* **368**, eaay6912 (2020).
13. M. S. Skrzypek, J. Binkley, G. Sherlock, Using the Candida Genome Database. *Methods Mol. Biol.* **1757**, 31–47 (2018).
14. X. Li, S. Zheng, D. A. Agard, Y. Cheng, Asynchronous data acquisition and on-the-fly analysis of dose fractionated cryoEM images by UCSFImage. *J. Struct. Biol.* **192**, 174–178 (2015).
15. A. Punjani, J. L. Rubinstein, D. J. Fleet, M. A. Brubaker, cryoSPARC: Algorithms for rapid unsupervised cryo-EM structure determination. *Nat. Methods* **14**, 290–296 (2017).
16. D. Liebschner, P. V. Afonine, M. L. Baker, G. Bunkóczi, V. B. Chen, T. I. Croll, B. Hintze, L. W. Hung, S. Jain, A. J. McCoy, N. W. Moriarty, R. D. Oeffner, B. K. Poon, M. G. Prisant, R. J. Read, J. S. Richardson, D. C. Richardson, M. D. Sammito, O. V. Sobolev, D. H. Stockwell, T. C. Terwilliger, A. G. Urzhumtsev, L. L. Videau, C. J. Williams, P. D. Adams, Macromolecular structure determination using x-rays, neutrons and electrons: Recent developments in Phenix. *Acta Crystallogr. D Struct. Biol.* **75**, 861–877 (2019).
17. A. Ben-Shem, N. Garreau de Loubresse, S. Melnikov, L. Jenner, G. Yusupova, M. Yusupov, The structure of the eukaryotic ribosome at 3.0 Å resolution. *Science* **334**, 1524–1529 (2011).
18. E. F. Pettersen, T. D. Goddard, C. C. Huang, G. S. Couch, D. M. Greenblatt, E. C. Meng, T. E. Ferrin, UCSF Chimera—A visualization system for exploratory research and analysis. *J. Comput. Chem.* **25**, 1605–1612 (2004).
19. A. Casanal, B. Lohkamp, P. Emsley, Current developments in Coot for macromolecular model building of electron cryo-microscopy and crystallographic data. *Protein Sci.* **29**, 1069–1078 (2020).
20. P. Kammer, S. McNamara, T. Wolf, T. Conrad, S. Allert, F. Gerwien, K. Hünniger, O. Kurzai, R. Guthke, B. Hube, J. Linde, S. Brunke, Survival strategies of pathogenic *Candida* species in human blood show independent and specific adaptations. *MBio* **11**, e02435-20 (2020).
21. K. E. Pristov, M. A. Ghannoum, Resistance of Candida to azoles and echinocandins worldwide. *Clin. Microbiol. Infect.* **25**, 792–798 (2019).
22. T. Srikantha, A. Klapach, W. W. Lorenz, L. K. Tsai, L. A. Laughlin, J. A. Gorman, D. R. Soll, The sea pansy Renilla reniformis luciferase serves as a sensitive bioluminescent reporter for differential gene expression in *Candida albicans*. *J. Bacteriol.* **178**, 121–129 (1996).
23. C. Wu, N. Amrani, A. Jacobson, M. S. Sachs, The use of fungal in vitro systems for studying translational regulation. *Methods Enzymol.* **429**, 203–225 (2007).
24. Z. Wang, P. Fang, M. S. Sachs, The evolutionarily conserved eukaryotic arginine attenuator peptide regulates the movement of ribosomes that have translated it. *Mol. Cell. Biol.* **18**, 7528–7536 (1998).
25. Subcommittee on Antifungal Susceptibility Testing (AFST) of the ESCMID European Committee for Antimicrobial Susceptibility Testing (EUCAST), EUCAST definitive document EDef 7.1: Method for the determination of broth dilution MICs of antifungal agents for fermentative yeasts. *Clin. Microbiol. Infect.* **14**, 398–405 (2008).
26. G. E. Crooks, G. Hon, J. M. Chandonia, S. E. Brenner, WebLogo: A sequence logo generator. *Genome Res.* **14**, 1188–1190 (2004).
27. W. H. Mager, R. J. Planta, J. G. Ballesta, J. C. Lee, K. Mizuta, K. Suzuki, J. R. Warner, J. Woolford, A new nomenclature for the cytoplasmic ribosomal proteins of *Saccharomyces cerevisiae*. *Nucleic Acids Res.* **25**, 4872–4875 (1997).
28. N. F. Kaufer, H. M. Fried, W. F. Schwindinger, M. Jasin, J. R. Warner, Cycloheximide resistance in yeast: The gene and its protein. *Nucleic Acids Res.* **11**, 3123–3135 (1983).
29. Z. Huang, K. Chen, J. Zhang, Y. Li, H. Wang, D. Cui, J. Tang, Y. Liu, X. Shi, W. Li, D. Liu, R. Chen, R. S. Sucgang, X. Pan, A functional variomics tool for discovering drug-resistance genes and drug targets. *Cell Rep.* **3**, 577–585 (2013).
30. J. L. Hansen, P. B. Moore, T. A. Steitz, Structures of five antibiotics bound at the peptidyl transferase center of the large ribosomal subunit. *J. Mol. Biol.* **330**, 1061–1075 (2003).

**Yury ZGADZAY**

UNIVERSITÉ DE STRASBOURG

igbmc
institut de génétique et de
biologie moléculaire et cellulaire

# Structural basis of protein synthesis apparatus of *Candida albicans* studied by Cryo-EM

## Résumé

Candida albicans est l'espèce responsable de la grande majorité des candidoses et un pathogène dangereux pour les patients immunodéprimés. Ce serait une grande percée de trouver de nouveaux agents capables d'inhiber un agent pathogène aussi nocif responsable d'infections disséminées, souvent mortelles. Il existe plusieurs médicaments antifongiques actifs contre *C. albicans* mais ils ont beaucoup d'effets secondaires et n'impactent pas l'une des voies les plus prometteuses - la synthèse des protéines. Le ribosome est, dans cette perspective, une cible majeure. Il existe de nombreux composés qui peuvent bloquer spécifiquement le ribosome eucaryote, mais le principal défi est de trouver un inhibiteur hautement spécifique, qui agira uniquement contre la cible choisie, comme le ribosome de *C. albicans*. Cette espèce est connue empiriquement dans les hôpitaux pour être résistante au cycloheximide. Cette drogue se lie sur le site E du ribosome cela n'a jamais été démontré de manière structurelle. Au cours de mes travaux, j'ai obtenu pour la première fois une structure à haute résolution (2,4 Å) du ribosome vacant de *C. albicans* par Cryo-EM. J'ai démontré que la mutation de la protéine L42 peut conduire à une résistance au cycloheximide de *C. albicans*. Mes résultats actuels constituent une base solide pour la conception ultérieure de médicaments potentiels qui se lieront spécifiquement au ribosome de *C. albicans*.

Mots-clés : Ribosome, Candida albicans, cryo-EM, E-site, inhibition de la traduction

## Résumé en anglais

Most infections caused by *C. albicans* - the most common fungal pathogen - are associated with very toxic and expensive treatments. Finding new agents to inhibit such a harmful pathogen responsible for disseminated, often deadly, infections would be a breakthrough. Currently, there are several antifungal drugs effective against *C. albicans* available. However, they have many side effects and do not affect one of the most promising pathways - protein synthesis. A significant target on this pathway is the ribosome. Many compounds can specifically block the eukaryotic ribosome. However, the main challenge is finding specific inhibitors that only act against the chosen target, such as the *C. albicans* ribosome. *C. albicans* has been empirically observed in hospitals to be resistant to cycloheximide, which binds to the E-site; however, it had never been demonstrated structurally. In my study, I obtained the high-resolution (2.4 Å) structure of the vacant C. albicans ribosome for the first time by Cryo-EM microscopy. Furthermore, I demonstrated that mutation in the eL42 protein could lead to the cycloheximide resistance of *C. albicans*. My current results offer a solid basis for the potential future development of drugs that specifically bind to the *C. albicans* ribosome.

Keywords: Ribosome, Candida albicans, cryo-EM, E-site, translation inhibition